

*Stimuli-Controlled Manipulation of  
Synthetic Discrete Micrometre Sized  
“Vehicles”*

Wayne Francis, B.Sc

Thesis submitted for the Degree of Doctor of Philosophy

Principal Supervisor: Prof. Dermot Diamond

Dr. Larisa Florea

Secondary Supervisor: Dr. Aoife Morrin

The Insight Centre for Data Analytics, National Centre for Sensor Research, School of  
Chemical Sciences, Dublin City University, Dublin, Ireland

Dublin City University

August 2017



## **Declaration**

I hereby certify that this material, which I now submit for assessment on the programme of study leading to the award of Doctor of Philosophy is entirely my own work, and that I have exercised reasonable care to ensure that the work is original, and does not, to the best of my knowledge, breach any law of copyright, and has not been taken from the work of others save and to the extent that such work has been cited and acknowledged within the text of my work.

Signed: \_\_\_\_\_  
(Wayne Francis)

ID No.: \_\_\_\_\_

Date: \_\_\_\_\_

## Acknowledgements

First of all I would like to thank Prof. D. Diamond for giving me this amazing opportunity and chance to work in his research group. Growing up in Coolock I never dreamed I would get to experience all the wonderful adventures I have been involved in over the last four years. Thank you for all the scientific help, for encouraging me, for believing in me, for reminding me how important it is to have fun during your research and most importantly for being such a great mentor.

I would also like to thank Dr. Larisa Florea for the constant encouragement and help during my research. I would have not made it this far without you. Thank you for all always being there, being enthusiastic, for the incredible amount of knowledge and experience you bring and for putting up with my terrible grammar. Most importantly thank you for building up my confidence, making me believe in myself, for being my supervisor and such a fantastic friend.

I also wish to thank all the other academics, mentors, supervisors and friends who have helped me to become a researcher, including Dr. S Coleman, Dr. C Fay, Prof R Forester, Dr. A Morrin, Dr. B White, Dr. P O'Mahony and Dr. M. Kitching. I would like to especially like to thank Dr. Colm Delaney for all the help, encouragement and laughs we shared over the last two years, even if he prefers red to blue.

A big Thanks to Prof. D. Officer, Prof. G. Wallace, Dr. Klaudia Wagner and Dr. Pawel Wagner, for all their scientific help, their kindness and for taking care of me during my research visit to Australia.

Thanks to Jen, Aishling, Alex and Danielle for being my travel companions and such great friends during my PhD, I will never forget the experiences and trials we faced together during our time in SG07 and abroad. I would also like to thank Simon G, Deidre, Kevin, Giusy, John, Connor, Tom, and all the people within Insight and NCSR who have helped me.

I would especially like to thank my parents, my mother Patricia, who always was and always will be my greatest inspiration, thank you for always putting me onto the right path for success and believing in me (even when I did not believe in myself) and my father Victor, for always being my biggest fan, teaching me how to enjoy life and always trying to ensure I was

happy. Thank you both for the unconditional love and support that you have always shown me. I would also like to thank my two younger brothers, Sam and Charlie; you have always giving me a reason to work hard and could always make me smile after a hard day. I would also like to thank my extended family members, growing up in such a large, close family meant I always had support, guidance and an abundance of inspiration from my aunts and uncles, Liz, Cloe, Ann, Angie , Sandra, Sharon, Derrick, Shay, Paul and Ken. It also meant I had an army of cousin, who have always been my closest friends, while I could never name them all, I would particularly like to thank John, Josh, Dean, Greg, Brian, Aaron, Jackson, Jack, Gary, Danielle, Bernice, Kenzie, Zareana and Erin.

Thanks to my two closet friends Stephen and Grace. Thanks to Grace for sharing in the trials and tribulations of our undergraduate degree, I never would have made it through without you. Thanks to Stephen for always being there for me, for always checking up on me and for sharing a dream of bettering ourselves and building toward a future outside of Coolock, I will see you at the lake.

Finally I wish to thank Claire and Aiden. Thank you for being my partner and my son. Thank you for all the love you have shown me, for always being there for me (through the good times and the bad), for given me a future and goal to work towards, for all the encouragement and believe, for being my best friend and for sharing this life with me.

## List of Publications:

### Peer-reviewed Articles

1. **“Self-propelled chemotactic ionic liquid droplets”**, W. Francis, C. Fay, L. Florea\*, D. Diamond, *Chemical communications*, **51**, 2342 – 2344, 2015.
2. **“Electrotactic ionic liquid droplets”**, W. Francis, K. Wagner, S. Beirne, D. Officer, G. Wallace, L. Florea\* and D. Diamond, *Sensors and Actuators B. Chemical*, **239**, 1069-1075, 2017.
3. **“Spiropyran Based Hydrogels Actuators - Walking in the Light”**, W. Francis, A. Dunne, C. Delaney, L. Florea\* and D. Diamond, *Sensors and Actuators B. Chemical*, **250**, 608–616, 2017.
4. **“Multi-functional chemotactic ionic liquid droplets”**, W. Francis, C. Delaney, H. Breen, M. Kitching, L. Florea\* and D. Diamond, *Lab on a Chip*, submitted.

### Peer-reviewed Book Chapters

1. **“Stimuli-controlled fluid control and microvehicle movement in microfluidic channels”**, A. Dunne, W. Francis, C. Delaney, L. Florea\*, D. Diamond. *The Reference Module in Materials Science and Materials Engineering*, 2017, accepted.
2. **“Application of Ionic Liquid Materials in Microfluidic Devices”**, *T. Akyazi, J. Saez, A. Tudor, C. Delaney, W. Francis, D. Diamond, L. Basabe-Desmonts, L. Florea\*, F. Benito-Lopez\**, *Ionic liquid devices*, 978-1-78801-181-5, 2017, in press.

### Conference Presentations

#### Peer-Reviewed Conference Proceedings

1. **“Self-propelled chemotactic ionic liquid droplets”**, W. Francis, L. Florea\* and D. Diamond, *18th International Conference on Miniaturized Systems for Chemistry and Life Sciences October 26-30, 2014, San Antonio, Texas, USA*.

2. **“Electro-tactic ionic liquid droplets,”** W. Francis, K. Wagner, S. Beirne, D. Officer, G. Wallace, L. Florea\* and D. Diamond, *19th International Conference on Miniaturized Systems for Chemistry and Life Sciences October 25-29, 2015, Gyeongju, Korea.*
3. **“Self-powered micro-droplets for biomimetic microfluidics”,** W. Francis, C. Delaney, L. Florea\* and D. Diamond, *20th International Conference on Miniaturized Systems for Chemistry and Life Sciences October 9-13, 2016, Dublin, Ireland.*

## Conference Contributions

\* indicates presenting author

## Oral Presentations

1. **“Droplets with life-like Behavior”** W. Francis\*, C. Delaney, L. Florea and D. Diamond, 2<sup>nd</sup> Annual Chemistry Day, DCU, May 12<sup>th</sup>, 2017.
2. **“Chemotactic ionic liquid droplets: striving to mimic nature”,** C. Delaney\*, W. Francis, L. Florea and D. Diamond, Analytical and Nanoanalytical Methods for Biomedical and Environmental Sciences” IC-ANMBES 2016”, 29 Jun - 1 Jul 2016, Brasov, Romania.
3. **“Stimuli-responsive materials for self-reporting micro-fluidic devices”,** L. Florea\*, A. Dunne, W. Francis, D. Bruen, A. Tudor, D. Diamond, IC-ANMBES 2016, 29 Jun - 1 Jul 2016 , Brasov, Romania.
4. **“From finger prick sampling to on-body and ultimately implantable chem/bio-sensors: The key role of active fluidics in realising the long-term functional platforms of the future”,** L. Florea, D. Bruen, W. Francis, A. Dunne, S. Coleman, A. Azouz, D. Diamond\*, CIMTEC2016, 5-10 Jun 2016, Perugia, Italy.
5. **“Signaler and Seeker Droplets”,** W. Francis\*, C. Delaney, L. Florea and D. Diamond, 8<sup>th</sup> Conference on Analytical Sciences Ireland (CASI) 2016, 14<sup>th</sup> and 15<sup>th</sup> April, 2016, The Helix, DCU.
6. **“From ‘Devices’ to ‘Self-Aware, Bioinspired MicroSystems’: What does the future hold for optical sensing? ”,** L. Florea, W. Francis, A. Azouz, S. Coleman and D. Diamond\*, EUROPTRODE XIII, 20-23 Mar 2016, University of Graz, Graz, Austria.

7. **“Electro-Guided Self-Propelled Ionic Liquid Droplets as Vessels for Chemical Reactions”**, W. Francis\*, K. Wagner, S. Beirne, D. Officer, G. Wallace, L. Florea and D. Diamond, Advanced Materials World Congress 2015, Viking Line, Stockholm, Sweden, 23-26 August, 2015.
8. **“Chemical sensing based on biomimetic principles”**, L. Florea, W. Francis and D. Diamond\*, 4th International Symposium on Sensor Science (I3S 2015), Basel, Switzerland, 13-15 July 2015.
9. **“Biomimetic microfluidics and stimuli-responsive materials: the key to realising chemical sensing platforms with revolutionary capabilities”**, L. Florea, W. Francis, A. Dunne, A. Tudor and D. Diamond\*, Royal Society of Chemistry Analytical Research Forum 2015, London, UK, 3<sup>rd</sup> July 2015
10. **“Bio-inspired active fluidic systems based on stimuli-responsive materials”**, D. Diamond\*, L. Florea, W. Francis, A. Tudor and D. Bruen, 67th Irish Universities Chemistry Research Colloquium, Maynooth University, Ireland, 25-26 June 2015.
11. **“Chemotactic and Electrotactic Self-Propelled Ionic Liquid Droplets”**, W. Francis\*, L. Florea and D. Diamond, 67th Irish Universities Chemistry Research Colloquium, Maynooth University, Ireland, 25-26 June 2015.
12. **“The exciting potential of stimuli-responsive materials and biomimetic microfluidics”**, D. Diamond\*, L. Florea, W. Francis, S. Coleman and A. Dunne, EuroNanoForum Sensors Workshop, Riga, Latvia, 10-12 June 2015.
13. **“Stimuli-responsive materials and biomimetic fluidics: key building blocks of futuristic autonomous chem/bio-sensing platforms”**, D. Diamond\*, L. Florea, W. Francis, S. Coleman and A. Dunne, Invited Seminar, University of Pisa, 27 May 2015,
14. **“Biomimetic microfluidic systems incorporating photoswitchable building blocks”**, D. Diamond\*, L. Florea, W. Francis and A. Dunne, COST Action MP 1205 Advances in Optofluidics: Integration of Optical Control and Photonics with Microfluidics, Porto, Portugal, 7-8 May 2015.
15. **“Electro-Guided Self-Propelled Droplets”**, W. Francis\*, K. Wagner, S. Beirne, D. Officer, G. Wallace, L. Florea and D. Diamond, XIV International Symposium on Polymer Electrolytes (ISPE-14), Geelong, Australia, 24-29 Sept 2014. (1 out of 16 people selected to give flash presentation about poster)
16. **“Using molecular photoswitches to build functionality for microfluidic systems”**, D. Diamond\*, L. Florea, W. Francis and A. Dunne, COST Action MP 1205 Advances

in Optofluidics: Integration of Optical Control and Photonics with Microfluidics, Dublin Institute of Technology, 24-25 Apr 2014.

## Poster Presentations

1. **“Self-powered micro-droplets for biomimetic microfluidics”**, W. Francis\*, C. Delaney, L. Florea and D. Diamond *20th International Conference on Miniaturized Systems for Chemistry and Life Sciences October 9-13, 2016, Dublin, Ireland.*
2. **“Signaler and Seeker Droplets,”** W. Francis\*, C. Delaney, L. Florea and D. Diamond, *8<sup>th</sup> conference on analytical sciences Ireland (CASI) 2016, 14<sup>th</sup> and 15<sup>th</sup> April, 2016, The Helix, DCU.*
3. **“Electro-tactic ionic liquid droplets”**, W. Francis\*, K. Wagner, S. Beirne, D. Officer, G. Wallace, L. Florea and D. Diamond, *19th International Conference on Miniaturized Systems for Chemistry and Life Sciences October 25-29, 2015, Gyeongju, Korea.*
4. **“Chemotactic movement of ionic liquid droplets”**, W. Francis\*, L. Florea and D. Diamond, *1st Brazil Ireland Science Week, Dublin Castle, Ireland, 23-26 Feb 2015.*
5. **“Self-propelled chemotactic droplets”**, W. Francis\*, C. Fay, L. Florea and D. Diamond, *MicroTAS 2014, San Antonio, Texas, USA, 26-30 Oct 2014. (Short listed for best poster)*
6. **“Biocompatible, reversible photo-actuated hydrogels, operative in neutral environments, for micro-valve applications in microfluidic device”**, L. Florea\*, W. Francis, A. Dunne, F. Benito-Lopez and D. Diamond, *MicroTAS 2014, San Antonio, Texas, USA, 26-30 Oct 2014.*
7. **“Electro-guided self-propelled droplets”**, W. Francis\*, K. Wagner, S. Beirne, D. Officer, G. Wallace, L. Florea\* and D. Diamond, *XIV International Symposium on Polymer Electrolytes (ISPE-14), Geelong, Australia, 24-29 Sept 2014.*
8. **“Self-propelled ionic liquid droplets”**, W. Francis, L. Florea\* and D. Diamond, *Insight Student Conference 2014, UCD, Dublin, Ireland, 12 Sept 2014.*
9. **“Stimuli-controlled movement of droplets and polymeric “vehicles”**, W. Francis\*, L. Florea and D. Diamond, *CIMTEC 2014 – 6th Forum on New Materials, Montecatini Terme, Italy, 15-19 June 2014.*

10. **“Stimuli-controlled fluid movement at the microscale”**, A. Dunne\*, W. Francis\*, L. Florea and D. Diamond, COST Action MP 1205 Advances in Optofluidics: Integration of Optical Control and Photonics with Microfluidics, Dublin Institute of Technology, 24-25 Apr 2014.

## **Awards**

1. **Best poster presentation** at the 8<sup>th</sup> Conference on Analytical Sciences Ireland (CASI) 2016, 14<sup>th</sup> and 15<sup>th</sup> April, 2016, The Helix, DCU.
2. **The Intel prize for best physical chemistry presentation** at the 67<sup>th</sup> Irish University Chemistry Research Colloquium, Maynooth University, June 2015.
3. **CBMS student/young researcher travel grant** for attending MicroTAS 2015 in Gyeongju, South Korea, 23-29<sup>th</sup> October 2015.
4. **Short-listed for best poster presentation** at 2014 MicroTAS conference in San Antonio, Texas, 26 - 30<sup>th</sup> October 2014.

## **Overall Aim and Thesis Structure**

### ***Overall Aim***

The aim of this thesis was to explore the concept of stimuli-responsive micro-vehicles by developing stimuli-responsive ionic liquid droplets and polymeric materials based on spiropyran. The movement mechanism and means for generating chemical gradient required for droplet movement are presented in Chapter 4 and 5 of this thesis. Various roles and applications for these droplets are discussed in Chapter 6 and finally the movement mechanism and synthesis of the bipedal hydrogel walker, based on p(*N*-isopropylacrylamide-*co*-acrylated spiropyran-*co*-acrylic acid), is presented in Chapter 7.

### ***Selected Publications and Author Contribution***

This thesis includes one literature survey chapter (Chapter 1), two published book chapters (Chapter 2 and 3), three original papers published in peer reviewed journals (Chapter 4, 5 and 7), one submitted publication (Chapter 6) and one future work chapter (Chapter 8). The core theme of the thesis is the development of stimuli-responsive droplets and soft robotics. The ideas, development and writing up of all the papers in the thesis were the principal responsibility of myself, the candidate, working within The Insight Centre for Data Analytics, National Centre for Sensor Research, School of Chemical Sciences, Dublin City University under the supervision of Professor Dermot Diamond and Dr. Larisa Florea.

The inclusion of co-authors reflects the fact that part of the work came from active collaboration between researchers and acknowledges input into team-based research.

In the case of Chapters 2 to 7, my contribution to the work was as detailed in the next table.

| <b>Thesis Chapter</b> | <b>Publication title</b>   | <b>Publication status*</b>  | <b>Nature and extent of candidate's contribution</b>  |
|-----------------------|--|---|---|
| 2                     | <b>Stimuli-controlled fluid control and microvehicle movement in microfluidic channels</b> | Published.<br><i>The Reference Module in Materials Science and Materials Engineering</i> , 2017 | Author, manuscript development and writing up.  |
| 3                     | <b>Application of Ionic Liquid Materials in Microfluidic Devices</b>                       | Published<br><i>Ionic liquid devices</i> , 978-1-78801-181-5, 2017                              | Author and writing up.  |
| 4                     | <b>Self-propelled chemotactic ionic liquid droplets</b>                                    | Published.<br><i>Chemical communications</i> , 51, 2342 – 2344, 2015                            | Main-author, key ideas, experimental design, data collection and analysis, manuscript development and writing up. |
| 5                     | <b>Electrotactic ionic liquid droplets</b>   | Published.<br><i>Sensors and Actuators B. Chemical</i> , 239, 1069-1075, 2017                   | Main-author, key ideas, experimental design, data collection and analysis, manuscript development and writing up. |
| 6                     | <b>Spiropyran Based Hydrogels Actuators - Walking in the Light</b>                         | Published.<br><i>Sensors and Actuators B. Chemical</i> , 250, 608–616, 2017                     | Shared first author, key ideas, data collection and analysis, manuscript development and writing up.              |
| 7                     | <b>Multi-functional chemotactic ionic liquid droplets</b>                                  | Submitted.<br><i>Lab on a chip</i>  | Main-author, key ideas, experimental design, data collection and analysis, manuscript development and writing up. |

Signed: .....  
(Candidate)

.....  
(Principal Supervisor)

.....  
(Principal Supervisor)

.....  
Date

---

\* For example, 'published'/'in press'/'accepted'/'returned for revision'/'submitted'

## ***Chapter Overview***

A detailed overview of each chapter, together with particular contributions from research collaborators (where applicable), are given below:

### **Chapter 1: Literature Survey**

This introduction chapter gives a detailed overview of the themes common to all papers included in the thesis and sets the following chapters in the context of existing literature. Important topics including: micro-fluidics, droplet micro-fluidics, segmented flow micro-fluidics, digital microfluidics, actuation of synthetic droplet through localised changes in wettability, surfactants and surface tensions, actuation of synthetic droplets through controlled release of surfactants, ionic liquids and adaptive polymeric materials, are extensively discussed in order to inform the reader on the concepts that will be further used in the experimental chapters (Chapter 4 to 7). Moreover, this chapter presents the context in which the experimental chapters below contribute to the scientific advancement of the research area.

### **Chapter 2: Stimuli-Controlled Fluid Control and Microvehicle Movement in Microfluidic Channels**

This published book chapter discusses the most recent examples of droplet movement using various mechanisms for actuation, including segmented flow micro fluidics, digital micro fluidics, movement through localised changes in wettability and movement via controlled release of surfactant. This chapter's role is to identify and compare the similarities and underlying mechanisms employed in the current state of the art research in stimuli-controlled micro-vehicle movement. It also endeavours to propose possible directions for the evolution of this area of research.

### **Chapter 3: Application of Ionic Liquid Materials in Microfluidic Devices**

This published book chapter examines the various uses for ionic liquids within microfluidic devices and discusses the benefits ionic liquids can provide to microfluidics field. Ionic liquids for actuation, sensing and reagent storage in microfluidics together with their usage in segmented flow regimes will be addressed.

#### **Chapter 4: Self-Propelled Chemotactic Ionic Liquid Droplets**

This work, published as an original article, focuses on the spontaneous chemotactic movement of ionic liquid droplets at the aqueous-air interface. These single component droplets are self-propelling and can be guided to specific destinations in open fluidic channels through the use of chemoattractants such as hydrochloric acid. The movement mechanism, methods for creating the chemical gradients required for droplet movement and analysis of droplets speeds are discussed.

#### **Chapter 5: Electrotactic Ionic liquid Droplets**

This work, published as an original article, describes the development of electrotactic ionic liquid droplets. These droplets function similar to the droplets described in Chapter 3; however the gradients are developed electrochemically. This approach of generating gradients allows for longer and reversible movements of the ionic liquid droplets. The design and fabrication of 3D printed channels and electrodes, movement mechanism and applications for such droplets is described. This work was completed in collaboration with the Intelligent Polymer Research Institute, University of Wollongong.

#### **Chapter 6: Multi-Functional Chemotactic Ionic Liquid Droplets**

In this work, submitted as an original article to *Lab on a Chip* journal, key applications for chemotactic ionic liquid droplets are described. Six applications are established which demonstrate the versatile nature of these ILs. These applications include reversible chemotactic movement, two forms of decision making (finding the highest concentration of the same chemoattractant and choosing between different halides of the same concentration), signalling and seeking (droplets which can find and merge with a stationary droplet), sensing and reporting (droplets which can sense the solution they are traversing across), and finally finding of damage and repair (droplets which can sense and constrain a leak within a fluidic system).

#### **Chapter 7: Spiropyran Based Hydrogels Actuators - Walking in the Light**

This work, published as an original article, describes synthesis of a bipedal hydrogel walker, based on poly(*N*-isopropylacrylamide-*co*-acrylated spiropyran-*co*-acrylic acid), p(NIPAAm-*co*-SP-*co*-AA). Due to the presence of the photochromic spiropyran molecule in the polymer structure, these hydrogels reversibly shrink and swell in aqueous environments when exposed to different light conditions. When placed onto a ratcheted surface, the actuation of the

bipedal gel produces a walking motion by taking a series of steps in a given direction, as determined by the optimised design of the ratchet scaffold. This work was completed in collaboration with Aishling Dunne, from the Insight Centre of Data Analytics, who was responsible with the synthesis of the spiropyran monomer and the mechanical analysis of the hydrogel walkers.

## Chapter 8: **Future Work and Perspectives**

This chapter suggests possible following paths of the work presented in this thesis. Several new strategies for the development of novel applications for chemotactic ionic liquid droplets are suggested.

## Table of Contents

|  |           |
|--|-----------|
| LIST OF FIGURES  | 1         |
| LIST OF TABLES   | 6         |
| LIST OF ABBREVIATIONS  | 7         |
| THESIS ABSTRACT  | 9         |
| <b>CHAPTER 1 – LITERATURE SURVEY</b>   | <b>10</b> |
| <b>1.1 MICROFLUIDICS</b>   | <b>12</b> |
| <b>1.2 DROPLET MICROFLUIDICS</b>   | <b>14</b> |
| <i>1.2.1 SEGMENTED FLOW MICROFLUIDICS</i>  | 15        |
| <i>1.2.2 DIGITAL MICROFLUIDICS</i>   | 21        |
| <i>1.2.1 DROPLET ACTUATION THROUGH LOCALISED CHANGES IN WETTABILITY</i>                                | 22        |
| <i>1.2.1 DROPLET ACTUATION THROUGH LOCALISED CHANGES IN SURFACE TENSION</i>                            | 22        |
| <b>1.3 IONIC LIQUIDS</b>   | <b>23</b> |
| <i>1.3.1 OVERVIEW</i>  | 23        |
| <i>1.3.2 SYNTHESIS</i>   | 25        |
| <i>1.3.3 IONIC LIQUIDS AS SURFACTANTS</i>  | 27        |
| <i>1.3.4 IONIC LIQUIDS AS ELECTROLYTES</i>   | 29        |
| <i>1.3.5 IONIC LIQUIDS AS SOLVENTS</i>   | 31        |
| <b>1.4 SOFT ROBOTICS AND SOFT ACTUATORS</b>  | <b>33</b> |
| <i>1.4.1 OVERVIEW</i>  | 33        |
| <i>1.4.2 HYDROGELS</i>   | 37        |
| <i>1.4.3 THERMO-RESPONSIVE HYDROGELS</i>   | 37        |
| <i>1.4.4 PH-RESPONSIVE HYDROGELS</i>   | 40        |
| <i>1.4.5 ELECTRO-ACTUATED HYDROGELS</i>  | 42        |
| <i>1.4.6 PHOTO-RESPONSIVE HYDROGELS</i>  | 45        |
| <b>1.5 AIMS OF THIS WORK</b>   | <b>49</b> |
| <b>1.6 REFERENCES</b>  | <b>50</b> |
| <b>CHAPTER 2 – STIMULI-CONTROLLED FLUID CONTROL AND MICROVEHICLE MOVEMENT IN MICROFLUIDIC CHANNELS</b> | <b>59</b> |
| <b>2.1 ABSTRACT</b>  | <b>61</b> |
| <b>2.2 INTRODUCTION</b>  | <b>61</b> |
| <b>2.3 STIMULI-CONTROLLED MANIPULATION OF SYNTHETIC DISCRETE MICROMETER-SIZED “VEHICLES”</b>           | <b>62</b> |
| <i>2.3.1 ACTUATION THROUGH LOCALISED CHANGES IN WETTABILITY</i>  | 64        |
| 2.3.1.1 DIGITAL MICROFLUIDICS  | 64        |
| 2.3.1.2 ELECTROWETTING ON DIELECTRIC   | 64        |
| 2.3.1.3 DIELECTROPHORESIS  | 66        |

|  |                   |
|--|-------------------|
| <b>2.3.2 ALTERNATIVE METHODS FOR DROPLET ACTUATION</b>                           | <b>66</b>         |
| 2.3.2.1 PHOTO-INDUCED ACTUATION  | 66                |
| 2.3.2.2 THERMO-INDUCED ACTUATION   | 69                |
| 2.3.2.3 MAGNETIC-INDUCED ACTUATION   | 69                |
| 2.3.2.4 SURFACE ACOUSTIC WAVES   | 70                |
| <b>2.5 ACTUATION THROUGH LOCALISED CHANGES IN SURFACE TENSION</b>                | <b>70</b>         |
| 2.5.1 SURFACTANT SATURATED SYSTEMS   | 72                |
| 2.5.2 "VEHICLE" CONTAINED SURFACTANTS  | 77                |
| <b>2.5 CONCLUSIONS AND OUTLOOK</b>   | <b>91</b>         |
| <b>2.6 REFERENCES</b>  | <b>91</b>         |
| <br>   |                   |
| <b><u>CHAPTER 3 – APPLICATIONS OF IONICS LIQUIDS IN MICROFLUIDIC DEVICES</u></b> | <b><u>96</u></b>  |
| 3.1 ABSTRACT   | 98                |
| 3.2 INTRODUCTION   | 98                |
| 3.3 IONIC LIQUIDS FOR ACTUATORS  | 101               |
| 3.4 IONIC LIQUIDS FOR SENSING  | 108               |
| 3.5 IONIC LIQUIDS FOR REAGENT STORAGE  | 114               |
| 3.6 IONIC LIQUIDS IN SEGEMENTED FLOW MICROFLUIDCS                                | 115               |
| 3.6.1 ELECTROWETTING ON DIELECTRIC BASED MICROFLUIDICS                           | 115               |
| 3.6.2 CHEMOTACTIC IONIC LIQUIDS  | 118               |
| 3.6.3 IONIC LIQUIDS AS MICROREACTORS   | 122               |
| 3.7 CONCLUSIONS  | 124               |
| 3.8 AKNOWLEGMENTS  | 125               |
| 3.9 REFERENCES   | 125               |
| <br>   |                   |
| <b><u>CHAPTER 4 – SELF-PROPELLED CHEMOTACTIC IONIC LIQUID DROPLETS</u></b>       | <b><u>131</u></b> |
| 4.1 ABSTRACT   | 133               |
| 4.2 INTRODUCTION   | 133               |
| 4.3 EXPERIMENTAL   | 135               |
| 4.3.1 MATERIALS AND METHODS  | 135               |
| 4.3.2 MICRO-CHANNEL FABRICATION  | 136               |
| 4.3.3 SURFACE TENSION MEASUREMENTS   | 136               |
| 4.3.4 VIDEO PROCESS ANALYSIS   | 137               |
| 4.4 RESULTS AND DISCUSSION   | 139               |
| 4.4.1 <sup>31</sup> P AND <sup>1</sup> H SPECTROSCOPY                            | 139               |
| 4.4.2 PROPULSION MECHANISM   | 140               |
| 4.4.3 DROPLET TRACKING AND GRADIENT ANALYSIS                                     | 143               |
| 4.5 CONCLUSIONS  | 146               |
| 4.6 REFERENCES   | 147               |

|   |            |
|---|------------|
| <b>CHAPTER 5 – ELECTROTACTIC IONIC LIQUID DROPLETS</b>                        | <b>149</b> |
| <b>5.1 ABSTRACT</b>   | <b>151</b> |
| <b>5.2 INTRODUCTION</b>   | <b>151</b> |
| <b>5.3 EXPERIMENTAL</b>   | <b>155</b> |
| <b>5.3.1 MATERIALS</b>  | <b>155</b> |
| <b>5.3.2 MICRO-CHANNEL AND ELECTRODES FABRICATION</b>                         | <b>155</b> |
| <b>5.3.3 METHODS</b>  | <b>157</b> |
| <b>5.4 RESULTS AND DISCUSSION</b>   | <b>158</b> |
| <b>5.4.1 DROPLET MOVEMENT</b>   | <b>158</b> |
| <b>5.4.2 CHANNEL CURRENT STUDY</b>  | <b>161</b> |
| <b>5.4.3 Cl<sup>-</sup> CONCENTRATION GRADIENT VISUALISATION</b>              | <b>163</b> |
| <b>5.5 CONCLUSIONS</b>  | <b>165</b> |
| <b>5.6 AKNOWLEGMENTS</b>  | <b>165</b> |
| <b>5.7 REFERENCES</b>   | <b>165</b> |
| <b>CHAPTER 6 – MULTI-FUNCTIONAL CHEMOTACTIC DROPLETS</b>                      | <b>169</b> |
| <b>6.1 ABSTRACT</b>   | <b>171</b> |
| <b>6.2 INTRODUCTION</b>   | <b>171</b> |
| <b>6.3 EXPERIMENTAL</b>   | <b>173</b> |
| <b>6.3.1 MATERIALS</b>  | <b>173</b> |
| <b>6.3.2 METHODS</b>  | <b>174</b> |
| 6.3.2.1 MICRO-CHANNEL FABRICATION   | 174        |
| 6.3.2.2 ABSORBANCE MEASUREMENTS   | 174        |
| 6.3.2.3 EXPERIMENTAL SETUPS   | 175        |
| <b>6.4 RESULTS AND DISCUSSION</b>   | <b>175</b> |
| <b>6.4.1 DROPLET MOVEMENT</b>   | <b>175</b> |
| <b>6.4.2 SIGNAL AND SEEKING DROPLETS</b>                                      | <b>175</b> |
| <b>6.4.3 DROPLETS MAKING DECISIONS</b>  | <b>178</b> |
| <b>6.4.4 SENSING AND REPORTING</b>  | <b>179</b> |
| <b>6.4.5 DETECTION AND REPAIR OF DAMAGE</b>                                   | <b>181</b> |
| <b>6.5 CONCLUSIONS</b>  | <b>182</b> |
| <b>6.6 AKNOWLEGMENTS</b>  | <b>183</b> |
| <b>6.7 REFERENCES</b>   | <b>183</b> |
| <b>CHAPTER 7 – SPIROPYRAN BASED HYDROGEL ACTUATORS – WALKING IN THE LIGHT</b> | <b>186</b> |
| <b>7.1 ABSTRACT</b>   | <b>188</b> |
| <b>7.2 INTRODUCTION</b>   | <b>188</b> |
| <b>7.3 EXPERIMENTAL</b>   | <b>191</b> |
| <b>7.3.1 MATERIALS</b>  | <b>191</b> |
| <b>7.3.2 GEL PREPARATION</b>  | <b>191</b> |
| <b>7.3.3 PHOTO-MASK FABRICATION</b>   | <b>192</b> |
| <b>7.3.4 RATCHETED CHANNEL FABRICATION</b>                                    | <b>192</b> |

|  |            |
|--|------------|
| 7.3.5 <i>HYDROGEL WALKER RELATIVE AREA AND RELATIVE LEG DISTANCE ANALYSIS</i>                                    | 193        |
| 7.3.6 <i>RHEOLOGY</i>  | 194        |
| 7.3.7 <i>HYDROGEL WALKER ACTUATION</i>   | 194        |
| 7.4 <b>RESULTS AND DISCUSSION</b>  | 195        |
| 7.4.1 <i>HYDROGEL WALKER</i>   | 195        |
| 7.4.2 <i>MECHANICAL PROPERTIES</i>   | 198        |
| 7.4.3 <i>RELATIVE AREA AND RELATIVE LEG DISTANCE ANALYSIS</i>  | 200        |
| 7.5 <b>CONCLUSIONS</b>   | 204        |
| 7.6 <b>AKNOWLEGMENTS</b>   | 204        |
| 7.7 <b>REFERENCES</b>  | 204        |
| <br>   |            |
| <b>CHAPTER 8 – FUTURE WORK</b>   | <b>208</b> |
| <hr/>  |            |
| 8.1 <b>MICRO-SIZED IONIC LIQUID DROPLETS AS MICRO-VESSELS FOR CHEMICAL REACTIONS AT PRE-DETERMINED LOCATIONS</b> | 210        |
| 8.1.1 <i>INTRODUCTION</i>  | 210        |
| 8.1.2 <i>POLYMERISATIONS AT PRE-DETERMINED LOCATIONS</i>   | 215        |
| 8.2 <b>CHEMOTACTIC DROPLETS IN NON-GEOMETRICALLY CONFINED ENVIRONMENTS</b>                                       | 218        |
| 8.2.1 <i>INTRODUCTION</i>  | 218        |
| 8.2.2 <i>AUTONOMOUS LEAK DETECTION AND REPAIR</i>  | 219        |
| 8.2.3 <i>CONTROLLING THE CHEMOTACTIC SIGNAL IN OPEN SYSTEMS</i>  | 221        |
| 8.2.4 <i>MICRO-VESSELS FOR CHEMICAL SYNTHESIS IN OPEN SYSTEMS</i>  | 224        |
| 8.3 <b>FUTURE PROSPECTS</b>  | 227        |
| 8.4 <b>REFERENCES</b>  | 228        |
| <br>   |            |
| <b>APPENDIX A</b>  | <b>230</b> |
| <hr/>  |            |
| A.1 <b>EXAMPLES OF DROPLET CHEMOTAXIS</b>  | 231        |
| <br>   |            |
| <b>APPENDIX B</b>  | <b>232</b> |
| <hr/>  |            |
| B.1 <b>ELECTROTACTIC IONIC LIQUID DROPLET VIDEO</b>  | 233        |
| B.2 <b>GRADIENT ANALYSIS VIDEO</b>   | 233        |
| <br>   |            |
| <b>APPENDIX C</b>  | <b>234</b> |
| <hr/>  |            |
| C.1 <b>SIGNALLING AND SEEKING DROPLETS</b>   | 235        |
| C.2 <b>DECISION MAKING DROPLETS</b>  | 236        |
| C.1.1 <i>FINDING THE HIGHEST CONCENTRATION OF CHEMOATTRACTANT</i>  | 236        |
| C.2.2 <i>CHOOSING BETWEEN DIFFERENT HALIDE SALTS</i>   | 237        |
| C.3 <b>CARGO TRANSPORT, SENSING AND REPORTING</b>  | 238        |
| C.4 <b>DAMAGE FIND AND REPAIR</b>  | 242        |
| C.5 <b>VIDEOS</b>  | 244        |
| <br>   |            |
| <b>APPENDIX D</b>  | <b>247</b> |
| <hr/>  |            |
| D.1 <b>FIGURES</b>   | 248        |
| D.2 <b>VIDEOS</b>  | 249        |

## List of Figures

|   |    |
|---|----|
| Figure 1.1 Cartoon displaying the difference between the fluid layers of a laminar flow (top) and a turbulent flow (bottom).....  | 13 |
| Figure 1.2 Typical schematic of a T-junction channel with given dimensions (top) and snapshot of the formation of monodispersed droplets using a T-junction channel (bottom) .....  | 16 |
| Figure 1.3 Example of a flow focuser used to create monodisperse droplets in a microfluidic device.....   | 17 |
| Figure 1.4 Microfluidic device used for cells encapsulation. Image on the right shows droplets containing single cells, which have been fluorescently marked.....   | 18 |
| Figure 1.5 Microfluidic device used to generate drug loaded biodegradable polymers. ....  | 19 |
| Figure 1.6 (a) Cartoon representation of the microfluidic device used to generate Janus and ternary polymer particles;.....   | 20 |
| Figure 1.7 Example of typical IL cations. ....  | 25 |
| Figure 1.8 Typical reaction scheme for the preparation of ILs.....  | 26 |
| Figure 1.9 General structure of the imidazole based ionic liquids with appended fluororous tails. ....  | 28 |
| Figure 1.10 Anions and cations of the ILs used in the electrochemical window study,.....  | 30 |
| Figure 1.11 Snapshots showing movement of soft robot. 1 shows movement via undulation; (A) shows the start of the experiment when no PNs are pressurised. (B) shows the hind legs being pressurised. (C) shows the spine being pressurised which lifts the robot and anchors it. (D) shows the front legs receiving pressure followed by depressurisation of the hind legs (E). (F) shows the forward motion of the robot. (G) shows further forward motion by depressurization of front legs. 2 shows movement via crawling motion. (A) shows pressurisation of the spine PN. (B) shows actuation of the right hind leg. (C) shows actuation of the front left leg and depressurisation of the right hind leg resulting in forward movement. (D) shows actuation of left hind leg. (E) shows actuation of the front right leg and depressurisation of the left hind leg resulting in forward movement. (F) shows process beginning again. .... | 35 |
| Figure 1.12 Snapshots showing soft robotic tentacle arm picking up a spanner. ....  | 36 |
| Figure 1.13 Series of snapshots which show the 4 stages of transition of poly(N-isopropylacrylamide-co-acrylamide) micro-gels. A (< 22 °C) – gels are in a swollen semi translucent state; B (36 °C) – gels form a flow-able clear solution; C (> 36 °C < 40 °C) – suspensions becomes cloudy. D (40 °C) – formation of semi solid shrunken gels..  | 39 |
| Figure 1.14 Experimental snapshots of the micro grippers while being subjected to different temperatures and B is a cartoon showing this response. ....   | 39 |
| Figure 1.15 Thermo-response of the bilayer semi-IPN hydrogel structure. Below 25°C, the structure is closed with the PDMS layer on the inside. When the temperature was raised above the LCST (40°C) the structure bends in the opposite direction with the PDMS layer on the outside. ....   | 41 |
| Figure 1.16 pH response of the hydrogel gripper. A shows the hydrogels which had pDADMAC trapped within the gel network. At pH 3 the hydrogels were swollen and the gripper was closed with the PDMS layer on the inside. When the pH is raised to 6.5 the hydrogel layer shrinks and the gripper closes with the PDMS layer on the outside. B shows the gels which excluded pDADMAC. At pH 6.5 the gripper was closed with the PDMS layer on the inside. At pH 3 the gels expelled water and the structure opened flat. ....   | 42 |
| Figure 1.17 Actuation mechanism and snapshots of the of electro-actuated hydrogel walkers while submerged in a solution of 0.1 M NaCl with an applied potential of 5 V. i) no potential is applied; ii) 5 V is applied resulting in the anionic leg (right leg) bending toward the anode and the cationic leg (left leg) bending towards the cathode; in this position the anodic leg has a greater area in contact with the surface and thus pulls the cathodic leg to the right; iii) the potential is reversed, resulting in both legs bending in the opposite direction; in this position the cathodic leg now has a greater area in contact with the surface and pushes the anodic leg to the right; iv – ix) shows that repeated cycling of the applied potential results in the forward motion of the hydrogel walker..  | 44 |
| Figure 1.18 Series of snapshots showing the locomotion of the hydrogels walkers carrying varying weights of cargo (25 m <sub>0</sub> , 50 m <sub>0</sub> , 75 m <sub>0</sub> , 100 m <sub>0</sub> and 125m <sub>0</sub> , respectively, where m <sub>0</sub> =is the weight of the walker in the dried state ) while submerged in a solution of 0.01M NaCl with an applied voltage of 25V. At time 0 no voltage is applied, meaning that the gel is in a relaxed expanded state. When the voltage is applied (time=10s) the gels bend towards the electrode (above the ratchet). Due to the design of the ratchet, only one leg of the gel can move upon stimulation. This results in the gel being pulled when bending (voltage on) and being pushed during relaxation (voltage off). Repeated cycles of contraction and relaxation of the gel resulted in a walking motion.   | 45 |
| Figure 1.19 Spiropyran-merocyanine structure in equilibrium under UV-visible light irradiation. When exposed to UV radiation, spirocyan (left) undergoes a reversible conformational change to the merocyanine form (right). The reverse reaction is possible under white light irradiation .....   | 46 |
| Figure 1.20 Chemical structure of p(NIPAAm-co-SP-co-AA) hydrogel under various irradiation conditions. The AA co-monomer acts as an internal acidic source for the protonation of SP to the more hydrophilic MC-H <sup>+</sup> form; this switch induce a hydrophobicity change resulting in the absorption of water from the external environment into the gel. When irradiated with white light (λ <sub>max</sub> = 422 nm) MC-H <sup>+</sup> is deprotonated, resulting in the isomerisation back to the more hydrophobic SP form. Inside the p(NIPAAm-co-SP-co-AA) hydrogel, this isomerisation results in an expulsion of water and reduction of the gel's volume. ....  | 47 |
| Figure 1.21 Snapshots showing the area decrease of p(NIPAAm-co-SP-co-AA) hydrogels while submerged in DI water and irradiated with light for 5 minutes (top) and the subsequent area increase when left in the dark for further 11 minutes (bottom). ....   | 48 |

|  |     |
|--|-----|
| Figure 2.1 (a) Closed/two plate DMF system. (b) Open/one plate DMF system. (c) basic DMF operations.....   | 65  |
| Figure 2.2 Schematic of (a) conventional EWOD and (b) an OEW device. The major difference between the two systems is the photoconductive layer inserted between the electrode and insulating layer in an OEW device. ..  | 67  |
| Figure 2.3 Representation of the net forces in water. ....   | 71  |
| Figure 2.4 Photo-induced confirmation change of AzoTAB between its two isomers: from trans (high $\gamma$ ) and to cis (low $\gamma$ ). ....   | 72  |
| Figure 2.5 Cartoon illustrating the photoreversible fragmentation of a two phase (aqueous/oil) liquid flow from a continuous flow (no UV light applied) to a segmented flow (UV light applied). ....   | 74  |
| Figure 2.6 (a) Illustration of reaction happening on the exterior of the droplet and (b) fluorescent images of the droplet in motion. ....   | 75  |
| Figure 2.7 Illustration representing the reversible chemotactic movement of decanol droplets in NaCl gradients. ....   | 76  |
| Figure 2.8 Snapshots showing that the decanol droplets were attracted by the stronger NaCl source. ....  | 77  |
| Figure 2.9 Distribution of HDA and DA <sup>-</sup> around a droplet in a pH gradient. ....   | 78  |
| Figure 2.10 Schematic of micro-boat which contains the ethanol soaked ionogel. ....  | 79  |
| Figure 2.11 Mechanism for the depolymerisation of the polymer PECA.....  | 80  |
| Figure 2.12 Schematic of actuation of PECA loaded vehicle.....   | 81  |
| Figure 2.13 Structure of DEPHA surfactant and mechanism of movement of the oil droplet. Movement is due to the deprotonation of the DEPHA, which results in Marangoni convection within the droplet. This was maintained due to the replenishment of protonated DEPHA at the droplet/liquid interface. ....  | 82  |
| Figure 2.14 Photo-chemopropulsion of a micro droplet which is resting on an aqueous solution containing the photochromic molecule, spiropyran. A – depicts the droplet before white light irradiation and B – depicts the droplet after white light irradiation. After the introduction of the light source, the cationic surfactant Cl-H <sup>+</sup> is released, breaking the surface tension symmetry of the solution around the droplet and creating Marangoni like flows which drive the droplet away from the white light source. Reproduced from [76].....   | 84  |
| Figure 2.15 Structural change of the SP-SO <sub>3</sub> H photochromic molecule when dissolved in an aqueous solution under different illumination conditions. ....  | 85  |
| Figure 2.16 Diagram showing composition and relative solubility of [P <sub>6,6,6,14</sub> ][Cl] in solutions of 10 <sup>-2</sup> M NaOH and 10 <sup>-2</sup> M HCl.....  | 85  |
| Figure 2.17 Schematic representation showing the chemotactic movement of Ionic liquid droplets in open fluidic channels (left) and sequence of video frames showing the chemotactic movement of multiple Ionic liquid droplets in an open fluidic channel (right). A– Depicts the creation of Cl <sup>-</sup> gradient, the channels were initially filled with a solution of 10 <sup>-2</sup> M NaOH, at the desired destination a few drops of a 10 <sup>-2</sup> M solution of HCl was placed. B– Shows the initial placement of the Ionic liquid droplet(s). C – The droplet(s) are propelled towards the highest area of surface tension. D – The droplet arrives at the desired destination. ....  | 86  |
| Figure 2.18 Sequence of snapshots showing the electro-tactic movement of an Ionic liquid droplet. The channels are filled with a 10 <sup>-3</sup> M solution of NaCl and a potential difference of 9 V is applied across selected electrodes A – The droplet is introduced B – D The droplet is propelled from cathode (3) to anode (1). E – The polarity of electrodes (3) and (1) is reversed and the droplet begins to move to electrode (3). F – As the droplet approaches the junction, the potential difference is applied between electrodes (2) and (4) and removed from electrodes (3) and (1). The droplet then begins to migrate toward anode (2). G – Upon arriving at anode (2) the polarity of electrode (2) and (4) is reversed and the droplet moves towards the new anode (4). H – Upon returning at anode (4) the potential is again reversed and using a similar method to sequence F the droplet is returned to the starting position. I – L shows the process repeated in the same run.. .... | 88  |
| Figure 2.19 Condensation reaction between octylaniline and the catalytic aldehyde producing a catalytic imine.....   | 89  |
| Figure 2.20 Schematic of the self-reproducing oil droplets.. ....  | 90  |
| Figure 2.21 Reaction between octylaniline and the membrane precursor which produces the vesicular membrane molecule.....   | 90  |
| Figure 3.1 Image of the microfluidic manifold showing the performance of the ionogel microfluidic valves: (a) all microvalves are closed under the applied vacuum. White light is applied for the time specified in each picture (b) Hydrogel (no IL present) valve is first to actuate followed by ionogels incorporating [DCA]- (c), [Tos]- (d), [DBSA]- (e), [NTf2]- (f). Numbers and arrows indicate when the channel is filled with the dye due to microvalve actuation. Reproduced from Benito-Lopez et al. [30] with permission from The Royal Society of Chemistry.....  | 102 |
| Figure 3.2 Microscope images of ionogel discs made of: (a) [P <sub>6,6,6,14</sub> ][NTf2], (b) [P <sub>6,6,6,14</sub> ][DCA] and (c) [P <sub>6,6,6,14</sub> ][Cl] after photopolymerisation (left); swelling in 1mM HCl solution for 2h (middle) and shrinking upon white light irradiation (right). Reproduced from Czugala et. al [31]. Copyright © 2014 Elsevier B.V. All rights reserved. ....   | 104 |
| Figure 3.3 Picture of the microfluidic device fabricated in PMMA: PSA polymer by CO <sub>2</sub> laser ablation (left). Schematic (top) and images (bottom) of the photoresponsive microvalve in closed (middle) and opened (right) state.....   | 105 |
| Figure 3.4 Flow profile during three full actuation cycles (left) and photo of the microfluidic device containing the thermo-actuated valve and the microfluidic holder with integrated heaters at the bottom. High flow spikes are due to the stabilisation of the microflow sensor after opening of the valve. ....  | 106 |
| Figure 3.5 (a) BGA bending motion as a result of ion transfer between layers; direction of bending can be reversed by changing the polarity of the applied potential; (b) BGA strip bended (10 V, 0.1 Hcolor); (c) Base part and (d) 3D view of the flow regulator assembly. ....  | 108 |
| Figure 3.6 (a) Chemical structure of [P <sub>1,4,4,4</sub> ][Tos]. (b) Schematic of the OECT. (c) Image of the OECT with a drop of glucose solution added. ....  | 109 |

|   |     |
|---|-----|
| Figure 3.7 a) Normalised response vs. lactate concentration for the OECT and b) Flexible OECT on the forearm. ..  | 110 |
| Figure 3.8 Chemical structures of A) N-Isopropyl-acrylamide and N,N-methylene-bis(acrylamide) crosslinked polymer; (B) ionic liquid tetrabutylphosphonium dicyanamide [P <sub>4,4,4,4</sub> ][DCA] and (C) Bromocresol Purple, showing colour changes in acidic and basic environments. ....  | 111 |
| Figure 3.9 (a) Calibration curve of the sensing area of the microfluidic device using pH buffer solutions; (b) Image of the CD platform with the sensing area. ....   | 112 |
| Figure 3.10 (a) Chemical structures of the pH sensitive dyes: Bromophenyl Blue (BPB), Bromocresol Green (BCG), Bromocresol Purple (BCP) and Bromothymol Blue (BTB); (b) Fabricated micro-fluidic device; (c) Smartphone application imaging on-body device.....   | 113 |
| Figure 3.11 A) Ink-jet printed ionogel microarray in the microfluidic device and representation of the composition of the ionogel spots; B) Fluorescence images of biotin-647 inside an ionogel-based microarray. ....  | 114 |
| Figure 3.12 Illustration of ILs electrowetting and retraction behaviour in the presence (top) and absence (bottom) of a DC potential of 120V. ....  | 116 |
| Figure 3.13 Cartoon illustration of the ionic liquid micro-gripper.....   | 118 |
| Figure 3.14 Cartoon illustrating the composition and relative solubility of [P <sub>6,6,6,14</sub> ][Cl] in solutions of 10 <sup>-2</sup> M NaOH and 10 <sup>-2</sup> M HCl. ....   | 119 |
| Figure 3.15 Illustration showing the chemotactic movement of ionic liquid droplets across the liquid-air interface (left) and sequence of snapshots showing the chemotactic movement of multiple Ionic liquid droplets in an open fluidic channel (right). A – Depicts the creation of Cl <sup>-</sup> gradient; the channels were initially filled with a solution of 10 <sup>-2</sup> M NaOH and at the desired destination a few drops of a 10 <sup>-2</sup> M solution of HCl were placed. B– Shows the initial placement of the Ionic liquid droplet(s). C – The droplet(s) are propelled towards the highest area of surface tension. D – The droplet arrives at the desired destination. ....  | 120 |
| Figure 3.16 Series of snapshots which demonstrate the electrotactic movement of IL droplets. Initially the open fluidic channels are filled with a 10 <sup>-3</sup> M solution of NaCl and a potential difference of 9 V is applied across selected electrodes A –introduction of the IL droplet B – D droplet moves away from cathode (3) to anode (1). E – The polarity of electrodes (3) and (1) is reversed and the droplet begins to move to electrode (3). F – As the droplet approaches the junction, the potential difference is applied between electrodes (2) and (4) and removed from electrodes (3) and (1). The droplet then begins to migrate toward anode (2). G – Upon arriving at anode (2) the polarity of electrode (2) and (4) is reversed and the droplet moves towards the new anode (4). H – Upon arriving at anode (4) the potential is again reversed and using a similar method to sequence F the droplet is returned to the starting position. I – L shows the process repeated in the same run..... | 122 |
| Figure 3.17 Reaction scheme for the synthesis of tetrahydroquinoline. ....  | 123 |
| Figure 3.18 Reaction scheme for the synthesis of fluorescent 1,2,3-triazole.....  | 124 |
| Figure 4.1 Diagram showing the relative solubility of [P <sub>6,6,6,14</sub> ][Cl] droplet in solutions of 10 <sup>-2</sup> M NaOH (left) and solutions of 10 <sup>-2</sup> M HCl (right). ....   | 135 |
| Figure 4.2 Example of a captured image from Video 4.1 (left) with processed mask image (right). The droplet position is ringed in both images. ....   | 138 |
| Figure 4.3 <sup>31</sup> P spectra of the cleaned [P <sub>6,6,6,14</sub> ][Cl] before (blue) and after extraction (red). ....   | 139 |
| Figure 4.4 <sup>1</sup> H NMR spectrum of a sample of cleaned [P <sub>6,6,6,14</sub> ][Cl], after extraction study.....   | 140 |
| Figure 4.5 Schematic representation showing the movement of the [P <sub>6,6,6,14</sub> ][Cl] droplet in open fluidic channels. A – Depicts the creation of the Cl <sup>-</sup> gradient. The channel was initially filled with NaOH 10 <sup>-2</sup> M solution. Then at the desired destination two or three drops of HCl 10 <sup>-2</sup> M solution were added (right); B – The IL droplet was placed at the NaOH end of the channel causing surfactant to diffuse into the solution, thus breaking the surface tension symmetry around the droplet; C – Droplet is propelled towards areas of highest surface tension; D – Droplet arrives at the desired destination. ....   | 141 |
| Figure 4.6 Sequence of video frames showing multiple droplets travelling towards the source of chemoattractant (100-200 μl of 10 <sup>-2</sup> M HCl). A – The channels were filled with a solution of 10 <sup>-2</sup> M NaOH and the chemoattractant (100-200 μl of 10 <sup>-2</sup> M HCl) was added at the desired destination; B – Placement of first three droplets. C – First two droplets moving towards the chemoattractant source; D – Placement of final three droplets; E – Movement of all droplets toward chemoattractant source; F – All droplets arrive at destination and merge.....   | 142 |
| Figure 4.7 Tracking of the droplet’s distance from its point of entry (t <sub>0</sub> ) towards its end position/source of chemoattractant (X). Grey line – full dataset at every video frame. Black squares – down sampled data points from full dataset (every 35 <sup>th</sup> point).....   | 144 |
| Figure 4.8 Fluidic network diagram showing the locations where each solution was introduced. (X) Chemoattractant, (a) Droplet a, (b) Droplet b, (c) Droplet c, (d) Droplet d, (e) Droplet e, (f) Droplet f. ....  | 144 |
| Figure 4.9 Tracking of all 6 droplets in Video 4.4 introduced in the sequence presented in table 4.2. (A) Droplet a, (B) Droplet b, (C) Droplet c, (D) Droplet d, (E) Droplet e, (F) Droplet f, (X) Cl <sup>-</sup> source and end location of each droplet movement.....   | 145 |
| Figure 5.1 3D printed titanium mesh electrodes. ....  | 155 |
| Figure 5.2 Channels for electro-stimulation of droplets showing embedded 3D printed titanium electrodes; A) Cross-shape 3D printed channels in ABS Polyjet Photopolymer (Stratasys) based on acrylic monomers B) Laser cut PMMA channel.....  | 156 |
| Figure 5.3 Diagram which depicts the relative release of the [P <sub>6,6,6,14</sub> ] <sup>+</sup> surfactant from the [P <sub>6,6,6,14</sub> ][Cl] droplet in lower Cl <sup>-</sup> concentration (at the cathode, left) and in higher Cl <sup>-</sup> concentration (at the anode, right) when 9 V is applied to a solution of 10 <sup>-3</sup> M NaCl. ....  | 159 |

|  |     |
|--|-----|
| Figure 5.4 Sequence of video frames demonstrating controlled movement of the [P6, 6,6,14][Cl] droplet using potential differences applied across pairs of electrodes 1-4. The channels are filled with a solution of 10 <sup>-3</sup> M NaCl and a 9 V potential difference is applied across selected electrode pairs. A – Introduction of the droplet onto the aqueous solution; B – C - The droplet is propelled from the initial cathode (3) towards the opposite anode (1); D – The droplet arrives at electrode (1); E – The polarity of the electrodes is then reversed and the droplet moves back towards electrode (3); F – As the droplet approaches the centre point, the potential difference is applied across electrodes (2 - cathode) and (4 - anode) and the droplet is diverted into the cross channel; G – Upon arrival at electrode (2) the polarity is reversed, and the droplet moves towards electrode (4); H – Using a similar approach, the droplet is made to return to the original starting position. I – L The process is repeated, showing that the droplet can be moved to each electrode multiple times. (For full video see Appendix B, video 5.1) ..... | 160 |
| Figure 5.5 Current generated when the applied voltage was varied over the range 1 – 10 V for 10 <sup>-2</sup> M and 10 <sup>-3</sup> M NaCl solutions, respectively. Error bars are standard deviations for n = 3 replicate measurements. Unidirectional movement was first observed at 5 V for all of the solutions. Visible gas generation was first observed at the electrodes at 7 V for 10 <sup>-2</sup> M solutions and at 10 V for the 10 <sup>-3</sup> M solutions.....  | 162 |
| Figure 5.6 Snapshots showing the fluorescent gradient due to quenching of the lucigenin dye by Cl <sup>-</sup> anions in the case when a solution of 10 <sup>-3</sup> M NaCl containing 10 <sup>-4</sup> M lucigenin was used. A) The fluorescence of the solution when no voltage is applied. B) The fluorescence of the solution when 9 V was applied for 30 minutes. ....   | 164 |
| Figure 6.1 Diagram showing the different functionalities of the IL droplets demonstrated in this study. Inset depicts the movement of the [P6,6,6,14][Cl] IL droplet due to the asymmetric release of [P6,6,6,14] <sup>+</sup> from the droplet in the aqueous solution. ....  | 173 |
| Figure 6.2 Diagram showing the movement behaviour of the signaller (10 <sup>-2</sup> M Cu(NO <sub>3</sub> ) <sub>2</sub> or 10 <sup>-2</sup> M Co(NO <sub>3</sub> ) <sub>2</sub> in [P <sub>6,6,6,14</sub> ][DCA]) and seeker (10 <sup>-2</sup> M PADAP in [P <sub>6,6,6,14</sub> ][Cl]) droplets. Once the signaller (green) droplet was placed, Cu(NO <sub>3</sub> ) <sub>2</sub> or Co(NO <sub>3</sub> ) <sub>2</sub> diffused from the droplet into the aqueous phase, generating an ionic strength gradient. This gradient enabled the seeker droplet (red) to chemotactically find and merge with the signaller droplet. ....  | 177 |
| Figure 6.3 A) Absorbance spectra of three IL droplets ([PADAP][Co] in IL, PADAP in [P <sub>6,6,6,14</sub> ][Cl] and Co <sup>2+</sup> in [P <sub>6,6,6,14</sub> ][DCA]) showing Co <sup>2+</sup> detection; B) Absorbance spectra of three IL droplets ([PADAP][Cu] in IL, PADAP in [P <sub>6,6,6,14</sub> ][Cl] and Cu <sup>2+</sup> in [P <sub>6,6,6,14</sub> ][DCA]) showing Cu <sup>2+</sup> detection. ....  | 177 |
| Figure 6.4 Diagram showing the sensing ability of the IL droplets. The sensing droplets were composed of bromothymol blue (4% w/v) in [P <sub>6,6,6,14</sub> ][Cl]. The channels were filled with a solution of 10 <sup>-2</sup> M NaOH and a solution of 0.001M KBr was used as a chemoattractant. It was observed that as the IL droplet moved spontaneously towards the KBr source, it could sense and report the pH of the solution through which it was traversing (Video 6.4-6.6). As the droplet neared the chemoattractant source an ion exchange within the IL droplet resulted in a more permeable droplet/water interface. As the Br <sup>-</sup> ions entered the droplet, it is likely that OH <sup>-</sup> ions were also taken up, resulting in the colour change of the droplet containing Bromothymol blue from yellow (pH<7) to blue (pH>7).....   | 180 |
| Figure 6.5 Absorbance spectra of the [P <sub>6,6,6,14</sub> ][Cl] droplet containing bromothymol blue vs. time, reflecting the change in maximum absorbance as the droplet migrated across the NaOH solution (10 <sup>-2</sup> M) when 70µl of 0.005M KBr solution was used as chemoattractant (left). Microscope images showing the Marangoni-like flows and the influx of OH <sup>-</sup> ions into the droplet upon reaching the destination. Scale bar represents 1 mm (right).181   | 181 |
| Figure 6.6 Diagram showing the CaCl <sub>2</sub> containing droplet migrating across the liquid/air interface of a solution of 10 <sup>-2</sup> M NaOH towards the source of “damage”, upon the addition of the chemoattractant solution (60 µl aliquot composed of 1:1 (V:V) 10 <sup>-2</sup> M HCl: 0.05M KBr solution containing 0.5% w/v sodium alginate). Upon reaching the damage area, the repair functionality starts by creating a crosslinked gel composed of calcium alginate, that seals the damage. ....  | 182 |
| Figure 7.1 Side view of in-house made cell for gel polymerisation; insets show the photomask including specific measurements of a single arc-shaped walker. ....   | 192 |
| Figure 7.2 A) Schematic diagram showing the individual components of the ratcheted channel: glass slide, ratcheted channel bottom with side walls in black PMMA and PMMA back layer; Cartoon showing side (B) and front (C) views of the channel after assembly and D) Photo of the real ratcheted channel. ....   | 193 |
| Figure 7.3 Chemical structure of the p(NIPAAm-co-SP-co-AA) hydrogel walkers under different illumination conditions and the physical effect it has on the gel morphology. The AA co-polymer acted as an internal acidic source for the protonation of SP to the more hydrophilic MC-H <sup>+</sup> form, this switch induced hydrophobicity changes resulting in the absorption of water from the external environment into the gel. When irradiated with white light (λ <sub>max</sub> = 422 nm) MC-H <sup>+</sup> was deprotonated, resulting in the isomerisation back to the more hydrophobic SP form. Inside the p(NIPAAm-co-SP-co-AA) hydrogel, this isomerization resulted in an expulsion of water and reduction of the gel’s volume Therefore when left in the dark the gel expanded, because of the design of the ratchet only one leg can move and thus the gel was pushed forward. When white light is introduced the gel shrank, again due to the design of the ratchet this resulted in the gel being pulled forward by the trapped leg. ....  | 196 |
| Figure 7.4 Series of snapshots showing the effect of light irradiation on the hydrogel walker. A) Light irradiation is initiated; B-D) Gradual reduction of inter-leg distance results in the trailing leg (right) being “dragged” over the bevel of the ratchet step. ....  | 197 |
| Figure 7.5 Series of snapshots showing the walking behaviour of the hydrogel (Video 7.1). A – B shows contraction of the trailing leg. C – Swelling in the dark results in the forward leg being pushed over the ratchet. D – E The sequence is repeated which results in the gel achieving a unidirectional walking motion (right to left).....   | 198 |

|   |     |
|---|-----|
| Figure 7.6 Photo-curing of hydrogels produced under different light irradiation times (40s, 45s and 50 s, respectively). White light polymerisation was initiated at $t=60$ s. ....   | 199 |
| Figure 7.7 Three photo-actuation cycles of hydrogel walkers produced after 40s, 45s and 50s of light irradiation, respectively, showing the relative changes in walker area when exposed to different illumination conditions. The measurements have been done in triplicate and the error bars represent standard deviations. ....   | 201 |
| Figure 7.8 Three photo-actuation cycles of hydrogel walkers produced after 40s, 45s and 50s of light irradiation, respectively, showing the relative changes in legs distance when exposed to different illumination conditions. ....   | 202 |
| Figure 7.9 Three photo-actuation cycles of hydrogel walkers produced after 40s, 45s and 50s of light irradiation, respectively, showing the relative changes in legs distance when exposed to different illumination conditions. ....   | 203 |
| Figure 8.1 Schematic representation of the DMF chip used for the merging of the three droplets in the toxicology assay. ....  | 211 |
| Figure 8.2 Schematic representation of the microfluidic device used for the high-throughput screening of a single cell. A – Droplets containing cells and dye are introduced to the device; B – Droplets are electronically merged; C – Contents of the two droplets are mixed together; D – Delay lane where droplets are incubated for 15 minutes; E – Detection module for detecting live and dead cells. ....   | 212 |
| Figure 8.3 Series of snap shots showing droplet mixing using the DMF device. Firstly two heterogeneous droplets are drawn together (A); the merged droplet is then rapidly mixed by shuttling the droplet back and forth across the array of electrodes (B, C) in order to achieve full mixing (D). ....  | 214 |
| Figure 8.4 Schematic of microfluidic reactor used for the multistep polymerisation reactions within droplets. ....  | 216 |
| Figure 8.5 Polymerisation scheme of $[P_{4,4,4,6}][SPA]$ for the formation of a soft polymer gel consisting of a crosslinked $poly([P_{4,4,4,6}][SPA])$ network dispersed through the $[P_{6,6,6,14}][CI]$ IL droplet. ....   | 218 |
| Figure 8.6 Diagram of the two dimensional movement of a chemotactic IL droplet in a petri dish. A – Droplet is resting on the surface of the aqueous solution (10-2 M NaOH), no directional movement is observed; B – Introduction of chemoattractant (100 – 200 $\mu$ l of a solution of 10-2 M HCl) through the central tubing; C - Droplet senses the introduction of the chemoattractant and begins to move toward the source of the chemoattractant; D – Droplet arrives at the chemoattractant source and more chemoattractant is introduced through the next tubing (top left); E – The introduction of fresh chemoattractant creates a stronger gradient; F – Droplet arrives at the second chemoattractant source and fresh chemoattractant is added at a new location (third tubing, top right); G – The droplet moves towards the last source of chemoattractant; H – Droplet arrives at final destination. .... | 220 |
| Figure 8.7 Snapshots showing the self-propelled movement of an IL droplet to three separate locations within a petri dish upon sequential introduction of chemoattractant. A – Droplet is placed onto the $10^{-2}$ M NaOH solution within the petri dish prior to chemoattractant addition; B – Chemoattractant (100 – 200 $\mu$ l $10^{-2}$ M HCl) is introduced to the system via the first tube; C – Once the Cl <sup>-</sup> gradient is established the droplet migrates towards the chemoattractant source; D – Droplet arrives at first chemoattractant source; E – Further chemoattractant is added via the second tube; F – Droplet migrates towards second tube; G – chemoattractant is added via the third tube; H – Droplet arrives at the third chemoattractant source. Bromocresol purple was added to the HCl solution for a better visualisation of the introduction of chemoattractant. ....              | 221 |
| Figure 8.8 Snapshots showing control over the chemotactic signal. A – droplet 1 (2M Benzoyl chloride in $[P_{6,6,6,14}][CI]$ ) and droplet 2 (2M Benzoyl droplets in $[P_{6,6,6,14}][CI]$ ) sitting on a solution of $10^{-2}$ M NaOH for 40s. B – droplet 3 (0.5M octylamine in $[P_{6,6,6,14}][CI]$ ) is added, causing a change in contact angle of droplet 1 and droplet 2. C – Droplet 1 and 2 are pushed away from droplet 3. D – Droplet 1 is attracted towards droplet 2. E – Droplet 1 and 2 merge to create droplet 4. F – droplet 3 is attracted by droplet 4. ....  | 223 |
| Figure 8.9 Snapshots showing chemical synthesis using chemotactic droplets in a petri dish. A – The two reactive droplets (1) 2M Benzoyl chloride in $[P_{6,6,6,14}][CI]$ and (2) 2M 4-Nitroaniline in $[P_{6,6,6,14}][DCA]$ sitting on a solution of $10^{-2}$ M NaOH. B – “signaler” droplet is added, followed by a change in morphology of the original droplets. C – Droplets are pushed away from signaler droplet. D – $[P_{6,6,6,14}][DCA]$ droplet is attracted recruited to the $[P_{6,6,6,14}][CI]$ droplet. E – Droplets merge. F – Reaction occurring inside the merged droplet. ....  | 225 |
| Figure 8.10 Reaction scheme between 4-nitroaniline and benzoyl chloride resulting in the formation of n-(4-nitrophenyl)benzamide. ....  | 225 |
| Figure 8.11. <sup>1</sup> H NMR spectra of the (1) two hour reaction droplet, (2) the twenty minute reaction droplet, (3) pure n-(4-nitrophenyl)benzamide, (4) 4-nitroaniline in $[P_{6,6,6,14}][DCA]$ and (5) benzoyl chloride in $[P_{6,6,6,14}][CI]$ . ....  | 226 |
| Figure C.1 Sequence of snaps shots from video S1, which show an example of signalling and seeking droplets. A – depicts the preparation of the gradient, with the signalling droplet placed at the destination; B – The seeker droplet is introduced into the system; C – The seeker droplet migrates toward the signaller droplet; D – Seeker droplet arrived at the destination; E – Seeker droplet merged with signaller droplet; F – Colour change indicating the formation of $Cu^{2+}$ – PADAP complex begins to occur. ....  | 235 |
| Figure C.2 Custom-made holder (left: open; right: closed) used for absorbance measurements of the droplets in this study. ....  | 236 |
| Figure C.3 Diagram showing a $[P_{6,6,6,14}][CI]$ droplet finding the highest concentration of HCl chemoattractant when subject simultaneously to two chemical gradients of different concentrations. ....  | 237 |
| Figure C.4 Absorbance spectra of $[P_{6,6,6,14}][CI]$ containing 4% (w/v) bromothymol blue (left) and 4 % (w/v) phenol red (right), before and after being introduced in the channel containing $10^{-2}$ M NaOH solution in the presence of 70 $\mu$ l of 0.005 M KBr. The spectra represents the colour of the $[P_{6,6,6,14}][CI]$ droplet containing the pH dye at the start and destination. ....  | 238 |
| Figure C.5 Selection of sequential snapshots from Video S7 showing the colour change of the phenol red containing $[P_{6,6,6,14}][CI]$ droplet upon reaching the source of KBr chemoattractant. The channels were filled with 0.01 M  |     |

NaOH and 70  $\mu$ l of 0.005 M KBr solution was placed at the desired destination. Marangoni like flows can be clearly observed inside the droplet..... 239

Figure C.6 Sequential snapshots showing the colour change of the phenol red containing [P<sub>6,6,6,14</sub>][Cl]droplet when subject to 0.01 M NaOH solution in the absence of any chemoattractant. Photos were taken after A) 1 min; B) 2 min; C) 3 min; D) 4min; E) 5 min; F) 6 min; G) 7 min; H) 8 min; I) 9 min; J) 10 min; K) 11 min; L) 12 min; M) 13 min; N) 14 min; O) 15 min; P) 16 min; Q) 17 min; R) 18 min; S) 19 min; T) 20 min; U) 21min; V) 22 min; W) 23 min; and X) 24 min. .... 240

Figure C.7 Sequential snapshots showing the colour change of the bromothymol blue containing [P<sub>6,6,6,14</sub>][Cl] droplet when subjected to a 0.01 M NaOH solution in the absence of any chemoattractant. Photos were taken after A) 1 min; B) 2 min; C) 3 min; D) 4 min; E) 5 min; F) 6 min; G) 7 min; H) 8 min; I) 9 min; J) 10 min; K) 11 min; L) 12 min; M) 13 min; N) 14 min; O) 15 min; P) 16 min; Q) 17 min; R) 18 min; S) 19 min; T) 20 min; U) 21 min; V) 22 min; W) 23 min; and X) 24 min. .... 241

Figure C.8: Sequential snapshots showing the colour change of the bromothymol blue containing [P<sub>6,6,6,14</sub>][Cl] droplet when 70  $\mu$ l of 0.005M KBr solution was added to a 0.01M NaOH solution prior to droplet addition. Photos were taken after A) 1 min; B) 2 min; C) 3 min; D) 4 min; E) 5 min; F) 6 min; and G) 7 min. .... 242

Figure C.9 Series of snapshots which demonstrate the IL droplet’s ability to chemotactically find a damaged section of a channel and repair it. A – Depicts the introduction of the repairing droplet; B – Droplet migrating to source of damage; C – Droplet attaches itself to the walls of the channel; D – Droplet gels and forms a seal to repair the damage..... 243

Figure C.10 Reaction scheme showing the crosslinking of sodium alginate chains by the Ca<sup>2+</sup> ions..... 243

Figure C.11 Absorbance (at 700 nm) increase over time of the [P<sub>6,6,6,14</sub>][Cl] droplet (containing 4 % w/v CaCl<sub>2</sub>) resting on a 10<sup>-2</sup> M NaOH solution after the addition of the chemoattractant (60  $\mu$ l aliquot of a 10<sup>-2</sup> M HCl solution which contained 1 % w/v sodium alginate and 50 % v/v 0.05 M KBr)..... 244

Figure D.1 Storage moduli versus shear stress of the hydrated hydrogels polymerised during 40s, 45s and 50s of white light irradiation, respectively, using a strain amplitude sweep with a normal force of 1 N. .... 248

Figure D.2 Series of snapshots showing the walking behaviour of the hydrogel (Video 7.2); A - shows the initial position of the hydrogel before any white irradiation; B, D and F show the contraction of the trailing leg during respective white light irradiation phases. C and E show how the swelling in the dark (after the respective white light irradiation phases) results in the forward leg being pushed over the ratchet..... 249

## List of Tables

Table 3.1 Ionic liquid names and abbreviations.....100

Table 4.1 Surface tension measurements of solutions used in the study, with and without the IL surfactant added..137

Table 4.2Time and location of addition of HCl solution and droplets, as in Video 4; see Figure 2.7 for location correlation.....145

Table 6.1Halide pairs included in each test and the destination the droplet chose in each case.....179

Table C.1 Table indicating HCl concentrations included in each test and final destination of the droplet in each case.....237

## List of abbreviations

|                                |  |
|--------------------------------|--|
| ATR-FTIR                       | Attenuated Total Reflectance - Fourier Transform Infrared spectroscopy |
| ACN                            | Acetonitrile   |
| APS                            | Ammonium persulfate  |
| ATRP                           | Atom Transfer Radical Polymerisation                                   |
| C1                             | Chromoionophore 1  |
| CMC                            | Critical micelle concentration   |
| DCM                            | Dichloromethane  |
| DEP                            | Dielectrophoresis  |
| DMAP                           | 4-(Dimethylamino)pyridine  |
| DMF                            | Digital microfluidics  |
| [EMIM][NTf <sub>2</sub> ]      | 1-Ethyl-3-methylimidazolium<br>bis(trifluoromethylsulfonyl)amide       |
| [EtMeIm][BF <sub>4</sub> ]     | 1-butyl-3-methylimidazolium tetrafluoroborate                          |
| EWOD                           | Electrowetting on dielectric   |
| EOF                            | Electroosmotic flow  |
| EtOH                           | Ethanol  |
| FTIR                           | Fourier Transform Infrared spectroscopy                                |
| Fe <sub>3</sub> O <sub>4</sub> | Iron(III) oxide  |
| HDA                            | 2-Hexyldecanoic acid   |
| HOMO                           | Highest occupied molecular orbital                                     |
| HPLC                           | High Performance Liquid Chromatography                                 |
| HCl                            | Hydrochloric acid  |
| IL                             | Ionic Liquid   |
| IPA                            | Isopropyl alcohol  |
| IR                             | Infrared   |
| LED                            | Light-emitting diode   |
| LCST                           | Lower critical solution temperature                                    |
| LOC                            | Lab-on-a-chip  |
| LUMO                           | Lowest unoccupied molecular orbital                                    |
| MC                             | Merocyanine form   |
| MC-H <sup>+</sup>              | Protonated merocyanine form  |

|  |  |
|--|--|
| MeOH                                       | Methanol   |
| NaCl                                       | Sodium Chloride  |
| NaOH                                       | Sodium Hydroxide   |
| NIPAAm                                     | <i>N</i> -isopropyl acrylamide   |
| NMR  | Nuclear magnetic resonance   |
| [N <sub>6,2,2,2</sub> ][NTf <sub>2</sub> ] | <i>n</i> -hexyltriethylammonium bis(trifluoromethylsulfonyl)-<br>imide                     |
| OEW  | Optoelectrowetting   |
| PDMS                                       | Polydimethylsiloxane   |
| PCR  | Polymerase chain reactions   |
| PMMA                                       | Polymethylmethacrylate   |
| pSPNIPAAm                                  | Copolymer of an acrylated SP and poly( <i>N</i> - isopropyl-<br>acrylamide)                |
| SAWS                                       | Surface acoustic wave  |
| SP   | Spiropyran form  |
| SP-SO <sub>3</sub> H                       | Spiropyran-sulfonic acid derivative  |
| THF  | Tetrahydrofuran  |
| [P <sub>6,6,6,14</sub> ][FAP]              | tris( <i>n</i> -hexyl)tetradecylphosphonium, trifluorotris-<br>(pentafluoroethyl)phosphate |
| [P <sub>1,4,4,4</sub> ][Tos]               | triisobutyl(methyl) phosphonium tosylate   |
| [P <sub>6,6,6,14</sub> ][Cl]               | Trihexyl(tetradecyl)phosphonium chloride   |
| [P <sub>6,6,6,14</sub> ][DCA]              | trihexyl(tetradecyl)phosphonium dicyanamide  |
| μTAS                                       | Micro-Total Analysis Systems   |
| UV   | Ultraviolet  |
| Vis  | Visible  |

# *Stimuli-Controlled Manipulation of Synthetic Discrete Micrometre Sized “Vehicles”*

*Wayne Francis*

## *Thesis abstract:*

Research in the microfluidic sector has seen serious growth since the 1980s and much progress has been made towards the realisation of true lab on a chip (LOC) devices. However, despite the amount of work put into the design and applications of these chips, there has been a noticeable lack of innovation into the control of flow inside these microfluidic platforms. Conventionally flow is controlled via external pumps and solenoid valves which hinder the scalability of the system. Stimuli-controlled manipulation of discrete micro-sized “vehicles” offers a novel method for controlling flow inside fluidic platforms, while also offering many unique advantages. These include external manipulation of individual or multiple droplets simultaneously while also opening the possibility of using these droplets as micro-vessels for chemical reactions, cargo transport to desired destinations, dynamic sensing, leak detection and drug delivery. Two novel methods for stimuli-controlled movement of micro-sized droplets are presented in the following chapters of this thesis that include chemotaxis and electrotaxis. These single component droplets are self-propelling and are guided to specific destinations through chemically generated  $\text{Cl}^-$  gradients. The droplets consist solely of the ionic liquid (IL) Trihexyl(tetradecyl)phosphonium chloride ( $[\text{P}_{6,6,6,14}][\text{Cl}]$ ). The movement of the droplets is controlled by the triggered release of the  $[\text{P}_{6,6,6,14}]^+$ , a very efficient cationic surfactant, which is a constituent of the IL droplet. Several applications are explored for these droplets. Additionally, polymeric hydrogel walkers containing photochromic spiropyran molecules are studied for their ability to achieve photo-controlled movement at the liquid-solid interface.

# **Chapter 1: Literature Survey**

## **Stimuli-Controlled Manipulation of Synthetic Discrete Micrometre Sized “Vehicles”**

### **1.1 Microfluidics**

#### **1.2 Droplet Microfluidics**

##### **1.2.1 Segmented Flow**

##### **1.2.2 Digital Microfluidics**

##### **1.2.3 Droplet Actuation through Localised Changes in Wettability**

##### **1.2.4 Droplet Actuation through Localised Changes in Surface Tension**

### **1.3 Ionic Liquids**

#### **1.3.1 Overview**

#### **1.3.2 Synthesis**

#### **1.3.3 Ionic Liquids as Surfactants**

#### **1.3.4 Ionic Liquids as Electrolytes**

#### **1.3.5 Ionic Liquids as Solvents**

### **1.4 Soft Robotics and Soft Actuators**

#### **1.4.1 Overview**

#### **1.4.2 Hydrogels**

#### **1.4.3 Thermo-Responsive Hydrogels**

#### **1.4.4 pH-Responsive Hydrogels**

#### **1.4.5 Electro-Actuated Hydrogels**

#### **1.4.6 Photo-Responsive Hydrogels**

### **1.5 Aims of this Work**

### **1.6 References**

# Chapter 1

---

## Literature Survey

---

### **Stimuli-Controlled Manipulation of Synthetic Discrete Micrometre Sized “Vehicles”**

## 1.1 Microfluidics

Microfluidics is the science and technology that deals with the manipulation of small amounts of fluids, commonly in the range of microliters ( $\mu\text{L}$ ) to picoliters (pL), which are geometrically constrained within micro-fabricated integrated circuits of fluidic channels (generally referred to as a “chip”) with dimensions in the order of micrometres ( $\mu\text{m}$ ). Microfluidic devices offer many benefits, the most obvious being the reduction in size allowing for reduced reagent and sample use (compared to conventional laboratory techniques) which can result in shorter experimental times and ultimately can lead to reduced cost of experiments and applications; additionally laminar flow and high surface to volume ratio characteristic for microfluidic devices, can improve the precision of experiments, increase resolution of separations and lower the limits of detection in chem/bio analysis [1]. The design and development of microfluidic devices is generally aimed for the realisation of a true “Lab on a Chip” device. Lab-on-a-chip (LAOC) is a device meant to miniaturise and integrate one or several laboratory applications on a single mm or cm sized platform. Initially microfluidic devices only found success in chemical and biological analysis, owing to the high sensitivity and resolutions offered by such devices [1]. More recently, due to advancements in the areas of micro-fabrication and fluid handling, microfluidics have seen applications in a broad spectrum of fields including cell sorting and separation [2,3], organs on a chip [4,5], drug discovery [6-8], synthesis [9-11] and even 3D printing [12].

The flow within these devices is characterised by low Reynolds numbers. The Reynolds number is a unitless measure used to predict when a fluid flow will transition from a laminar flow to a turbulent flow. Below a Reynolds number of 2000, the fluid will have a laminar regime, where viscous forces dominate and the fluid flows in parallel layers. At these Reynolds numbers there is no lateral mixing between the layers, no eddies, swirls or cross currents (Figure 1.1). Above a Reynolds number of 2000 the flow starts to become turbulent, where inertial forces dominate and whirlpools, eddies and various flow instabilities begin to form. Due to the small dimensions of the channels and low flow rates, typically microfluidic devices have very small Reynolds numbers, usually less than 1 [13]. As such, a defining characteristic of microfluidics is the laminar flow [14].

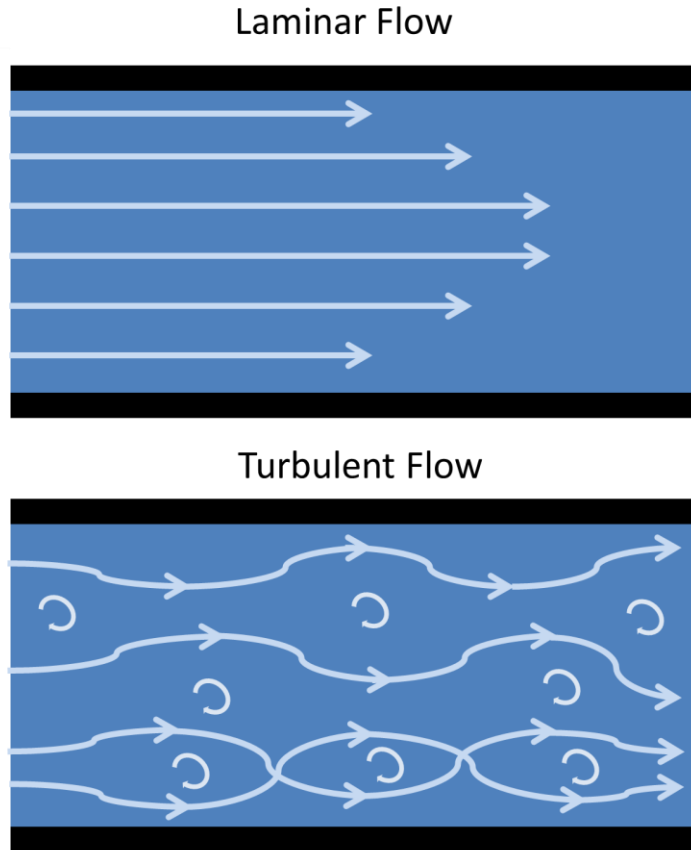


*Figure 1.1 Cartoon displaying the difference between the fluid layers of a laminar flow (top\_ and a turbulent flow (bottom).*

The fluids within microfluidics devices are typically pumped through the chip as either a continuous flow or a segmented flow, both of which retain a laminar regime. A microfluidic device which uses a continuous flow regime involves the uninterrupted flow of one or more streams through a microfluidic device. The flow is generally controlled through external or integrated mechanical pumps or via capillary [15], centrifugal [16] or electrokinetic forces [17]. In general continuous flows are easier to implement and are very useful for tasks such as chemical/biological separation or analysis [18,19]. In a typical microfluidic device, two or more fluids are introduced into the device via separate channels. At a desired location these channels will converge, and since the flows are laminar, mixing will only occur via diffusion. Therefore, exchange of materials between the two flows is a relatively slow process; because of this the rate of mixing (if at all) can be controlled via the design of the channels within the device. For example, channels with a serpentine shape can increase the rate of diffusion thus increasing the rate of mixing. A microfluidic device which has a segmented flow uses two immiscible fluids; at a

convergent point, one fluid disperses within the other to form two separate phases, the dispersed phase (droplet phase) and the continuous phase (fluid which contains the dispersed phase). Segmented flows are better suited for applications that require a higher degree of fluid manipulation or flexibility. Scaling up the number of reactions on a microfluidic chip which use continuous flows can be difficult, as the size of the device must also increase with the number of experiments being carried out (in order to accommodate the additional channels required). However, because segmented flow microfluidics involves the manipulation of discrete individual droplets, these devices do not need to increase in size in order to run additional experiments, as essentially each droplet becomes a micro-reactor. As such, these devices are typically more suited than continuous flow based microfluidics for applications which require high throughput analysis [20].

## 1.2 Droplet Microfluidics

A sub category within the microfluidics sector is segmented flow microfluidics, also known as droplet microfluidics. Unlike continuous flow systems, which focus on a continuous stream of a single volume of fluid, droplet microfluidics generates individual discrete volumes of liquids. This field is further specialised by the manner in which these droplets are generated or transported through the chip. The main approach to this is termed continuous flow droplet microfluidics or more commonly referred to as *segmented flow microfluidics*. In these types of devices, two flows of immiscible fluids are merged together to form two phases, where one phase becomes a droplet phase and the second a continuous phase, which contains the droplets. Typically this is achieved by merging an aqueous based stream and an oil based stream. These droplets are then transported through the device by the continuous phase which is controlled by various means (mechanical pumps, capillary, centrifugal or electrokinetic forces). Another form of manipulation of droplets in microfluidics is known as *digital microfluidics* (DMF). In DMF discrete droplets are generated from a bulk source and individually transported across an array of electrodes via manipulation of interfacial tension by applying a potential across neighbouring electrodes [21]. Finally a new and exciting method for droplet control involves the transportation of  $\mu\text{L}$  sized droplets across the liquid/air interface through the generation of surface tensions gradients [22].

### **1.2.1 Segmented Flow Microfluidics**

As the microfluidics sector grows so does the complexity of the applications that these devices are being used for. As such new and innovative methods for controlling fluid flow are needed if the full potential of microfluidics is to be harnessed. Microfluidic devices which use a simple continuous flow regime suffer from the need for relatively long channel lengths, interactions of fluids with surfaces, cross contamination of flows, dispersion and dilution of reagents [23]. These issues can potentially be addressed via compartmentalisation of reagents into discrete monodispersed droplets. These droplets essentially become individual micro-reactors and through careful design of the device high throughput assays can be achieved.

The formation of droplets within these devices has been an area of extensive research [24,25]. However, the main method for generating droplets is by using two main channel types, either T-Junctions [26-28] or flow focusing [29-31]. In a T-junction configuration the channel containing the dispersive fluid, which is to become the droplets, perpendicularly intersects the channel that contains the continuous flow (or carrier fluid). This results in the formation of an interface forming at the junction between the two phases. When the dispersive phase enters into the main channel, the shear forces generated by the continuous flow and the resulting pressure gradient causes the tip of the disperse fluid to elongate and eventually break into individual droplets [32] (Figure 1.2).

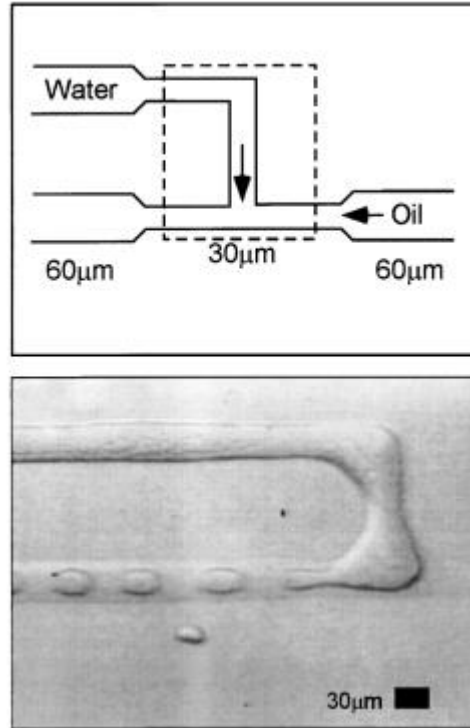


Figure 1.2 Typical schematic of a T-junction channel with given dimensions (top) and snapshot of the formation of monodispersed droplets using a T-junction channel (bottom). Reprinted with permission from [32].

In a flow focusing geometry three channels are used to generate droplets; a centre channel, which contains the fluid that will become dispersed, and two flanking channels that contain the continuous phase. All three channels converge at an orifice (Figure 1.3 **D**). As the fluid from the central channel enters the orifice, pressure is exerted on it from the flanking channels (continuous phase). This pressure elongates the fluid (from the central channel) and eventually splits it to form droplets [33]. Both of these configurations routinely use surfactants to control the interface tension between the immiscible liquids which is an important parameter of droplet formation as it controls how much elongation the solution can withstand before it breaks to form a droplet.

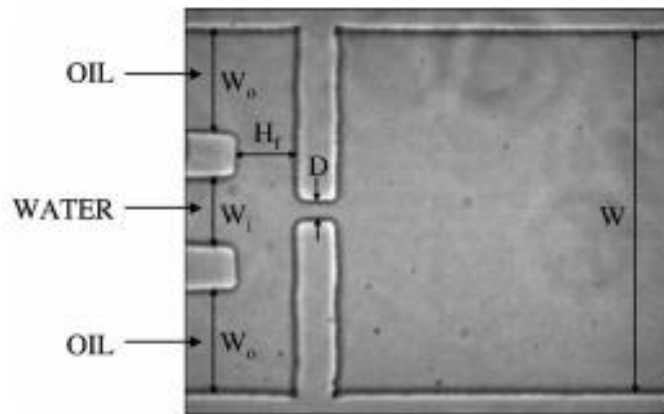


Figure 1.3 Example of a flow focuser used to create monodisperse droplets in a microfluidic device. Reprinted with permission from [33].

These methods can produce droplets in the range of nanoliter to microliter and at rates of thousands per second [34]. Therefore, these types of devices have found great success in biological based applications due to high throughput of droplets and the ability to perform multiple experiments simultaneously [35]. Each monodisperse droplet can be analysed separately, which allows for the collection of data on a large-scale population. Individual cells can be captured in droplets and each droplet (out of thousands) can be analysed. Since the droplets generated can have extremely small volumes (nL), it is possible to screen thousands at a time, which allows for large screening of biological samples and collection/trapping of rare cells (such as circulating tumour cells (CTCs) [35]). Examples of applications include single-cell analysis [36-38], polymerase chain reactions (PCR) [27,39,40], proteomics [38,41,42] and biological assays [43-45].

Clausell-Tormos *et al.* [46] reported droplet-based microfluidic devices which can be used to capture and analyse mammalian cells. In this study the group designed a microfluidic device that could be used to encapsulate cells within a droplet which was surrounded by perfluorocarbon oils. Perfluorocarbon oils were suitable for cell encapsulation as they facilitated gas delivery into the encapsulated cells, and allowed for optical analysis since they are transparent. The microfluidic device itself used a flow focuser to capture the cells; three inlets were used (Figure 1.4). In the main middle channel one inlet fed in cells and the second inlet provided the cell media. A second inlet provided the oil to the outer channels. To regulate the number of cells per droplet, on-chip dilution was performed to control the cell density at the inlet nozzle. High cell densities

meant that the probability of encapsulation of multiple cells was probable, while low cells densities meant that capture of more than one cell per droplet was unlikely.

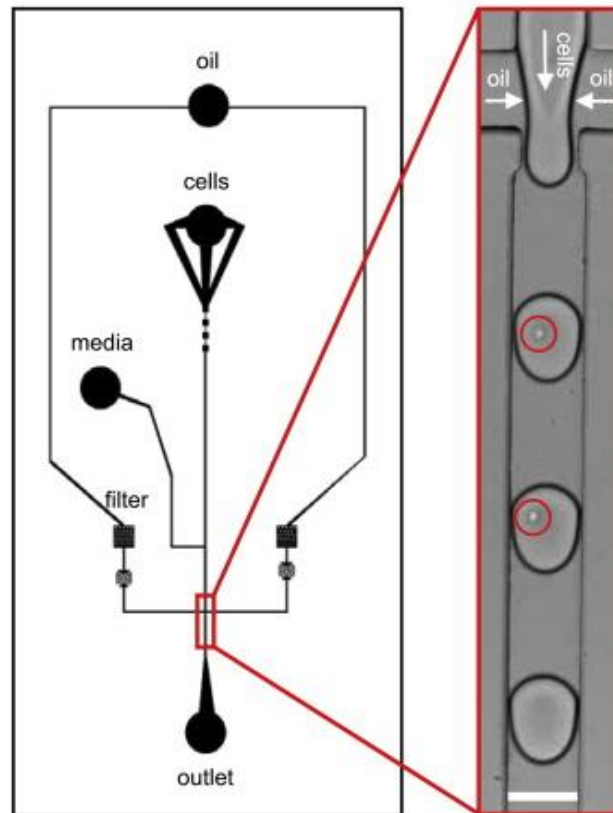
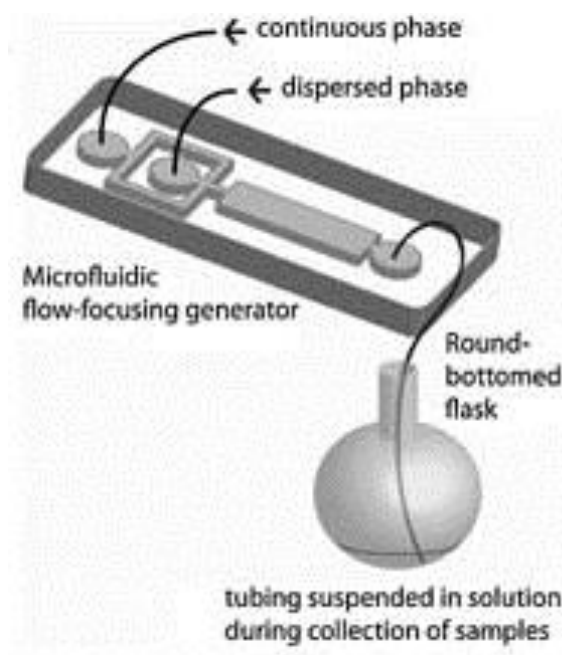


Figure 1.4 Microfluidic device used for cells encapsulation. Image on the right shows droplets containing single cells, which have been fluorescently marked. Reprinted with permission from [46].

After the cells were encapsulated into the droplets, they were collected as an emulsion and incubated. After incubation the droplets were reintroduced to the chip where analysis of individual droplets was performed. During preparation, the cells were tagged with fluorescent markers so that fluorometric analysis could be performed. It was determined that the number of cells per droplet could be controlled and that the cells trapped inside the droplets could grow and survive for several days in these conditions. By simply changing channel dimensions and flow rates, the droplet volumes can be controlled and thus the micro-reactors can be adjusted to host required cells.

Xu *et al* [30] have developed a microfluidic device which uses a flow focuser to create monodispersed biodegradable polymers for drug delivery. Figure 1.5 shows the microfluidic platform used in the synthesis of the drug-loaded poly (lactic-co-glycolic

acid) (PLGA). The polymer was loaded with bupivacaine, a local anaesthetic and the solvent was removed via evaporation.



*Figure 1.5 Microfluidic device used to generate drug loaded biodegradable polymers. Reproduced with permission from [30].*

The continuous phase used was 1% poly(vinyl alcohol)poly (PVA) aqueous solution and was flowed through the outer channels. The inner channel contained the disperse phase, a solution PLGA/bupivacaine dissolved in dichloromethane (DCM). The stream of PLGA/DCM split into uniform droplets as it existed the convergent point between the three channels. The PVA acted as a surfactant which prevented the droplets from coalescing once in the collection point (round bottomed flask). The round-bottomed flask contained buffer solution, which diluted the droplets of PLGA/DCM. The buffer helped to minimise aggregation and the high pH prevented leaching of the drug. Once collected, the DCM was removed via rotary evaporation. The kinetic studies performed showed that drug was released from the polymer slower compared to when they were prepared via conventional methods. The polymers prepared using this device also allowed for the release of the drug more uniformly when compared to biodegradable polymers of similar sizes synthesised by conventional methods. The improved kinetics was attributed to the uniform distribution of the drug inside of the polymers, which was controlled by finely controlling flow rates in the microfluidic device.

Nie *et al* [47] also developed a microfluidic device which used a flow focuser to continuously produce Janus and ternary polymer particles, with sizes which ranged from 40 to 100  $\mu\text{m}$ . Two monomer solutions were used to produce the particles, namely methacryloxypropyl dimethylsiloxane (M1) and a mixture of pentaerythritol triacrylate, poly(ethylene glycol) diacrylate and acrylic acid (M2). These two solutions acted as the disperse phase, which flowed through the central channel. An aqueous solution of sodium dodecylsulfate (W) was employed as the continuous phase and flowed through the two flanking channels (Figure 1.6). A photoinitiator was also included in both solutions of M1 and M2.

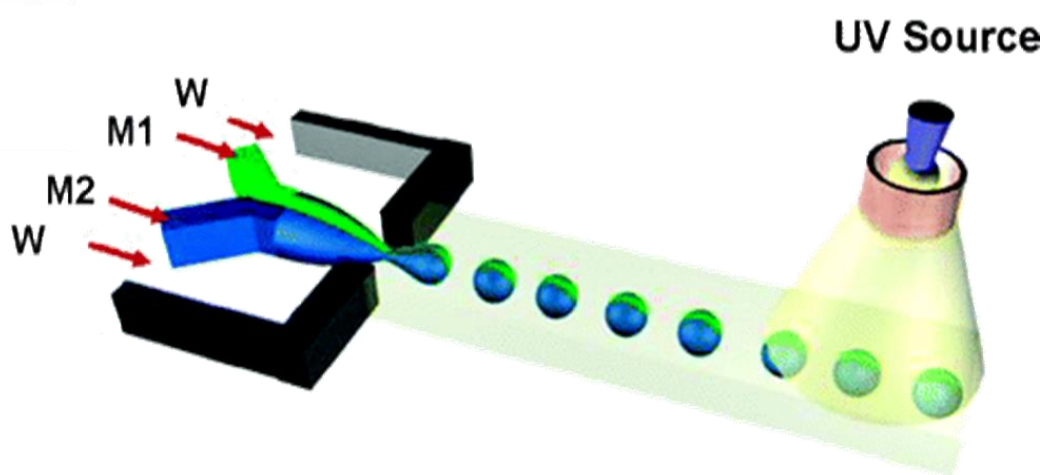


Figure 1.6 (a) Cartoon representation of the microfluidic device used to generate Janus and ternary polymer particles; Reprinted with permission from [47]. Copyright (2006) American Chemical Society.

As the mixture of M1 and M2 passed through the orifice, the pressure applied by the continuous phase split the solution into monodispersed droplets. As the droplets travelled down the adjoining channel they pass under a UV light source upon which they are polymerised. The properties of the produced particles could be fine-tuned by varying the ratio of the M1 and M2 solutions and by controlling the flow rates. Introduction of an additional central channel between M1 and M2 channels allowed for the production of ternary particles (comprised of either 2 parts M1 or 1 part M2 and vice versa).

The versatile nature and fine control over droplet sizes has allowed segmented flow microfluidic devices to be used for a broad range of applications including drug

discovery [6], material synthesis [48,49], parallel chemical reactions [50] and electrochemical analysis [51].

### **1.2.2 Digital Microfluidics**

A sub sector of droplet microfluidics is a field known as digital microfluidics (DMF). In DMF individual discrete droplets are transported across an array of electrodes by generating a wettability gradient by applying electrical potentials between neighbouring electrodes. In this manner droplets can be moved from electrode to electrode in the direction determined by the user. In most cases the movement is completely reversible and it is possible to move multiple droplets at a time. Droplets are created from reservoirs which are most often included on the device, thus allowing for droplets with multiple different compositions to be present on the chip. This type of movement allows for merging, mixing and splitting of droplets, which in turn allows for complex and multi-step reactions. DMF allows for fine control over the movement of the droplet, unlike in segmented flow microfluidics, where droplets must follow a path predefined by the design of the device. Since the droplets move across a solid substrate, there is no cross contamination between phases, which can occur in segmented flow microfluidic devices. An in-depth discussion on DMF can be found in Chapter 2 of this thesis, with a detailed description of the various mechanisms for droplet movement, device design and some brief examples of applications that utilize these devices. Understanding the movement of droplets through changes of interfacial tension is pivotal for the development of droplets which can move across the liquid/air interface, which is the basis of the movement mechanism for droplets described in Chapter 4, 5 and 6.

### **1.2.3 Droplet Actuation through Localised Changes in Wettability**

Control over the interfacial energy of a substrate is not solely achieved by applying voltages across an array of electrodes. Many research groups have looked to harness other forms of stimulation to control the wettability of substrates. These include droplet movement through photo-, thermo-, or magnetic-induced actuation and surface acoustic

waves (SAWS). A brief discussion on the mechanism for each of these methods is described in Chapter 2, along with examples and applications.

#### **1.2.4 Droplet Actuation through Localised Changes in Surface Tension**

This section describes droplets which are moved across the liquid/air interface through the generation of surface tension gradients. This is a relatively new concept for droplet movement used in microfluidics and it is still in its infancy compared to segmented flow microfluidics or DMF.

The cohesive forces between liquid molecules are responsible for the phenomenon known as surface tension ( $\gamma$ ). The contractile layer formed at the liquid/air interface is due to the fact that the molecules at the surface experience a greater attraction to their neighbouring molecules compared to molecules in the bulk of the solution. This is because in the bulk of a liquid, the attractive forces between molecules are shared by all neighbouring molecules, and no net force is felt as the forces cancel each other out. However, molecules at the interface (liquid/gas, liquid/liquid) have no attractive forces being exerted from above, therefore, they exhibit stronger forces between the nearest neighbouring molecules at the surface. This causes the molecules at the liquid/air interface to contract forming an elastic layer. When the surface tension of a liquid is interrupted, for example by the addition of a surfactant, it causes the molecules to pull away from the source of the interruption. In this fashion a flow is created, that goes from areas of low surface tension to areas of high surface tension. This phenomenon is known as the Marangoni effect [52]. The Marangoni effect describes the mass transfer along an interface between two fluids due to a surface tension gradient [53]. This creates convective flows in the bulk of a solution as well as inside of an immiscible liquid resting on the surface of the solution. Any object resting on the solution surface when the flow is created will also be carried towards the areas of greatest surface tension. Surfactant molecules have special properties whereby they can imbed themselves at the liquid/ air interface and interrupt the elastic layer reducing the local surface tension. The term surfactant comes from surface-active agents. Surfactants are molecules which are generally long chained amphiphiles which have a hydrophilic “head” and a hydrophobic tail. In an aqueous solution (below a certain concentration known as the critical micelle concentration (CMC)) the surfactant’s polar head will interact with the polar molecules at the surface and the tails will stick out of the solution. This interaction will interrupt

neighbouring attractive forces and lower the surface tension of the solution, thus creating the Marangoni like flows.

This phenomenon constitutes the basis for droplet movement discussed in Chapter 4, 5 and 6. A detailed discussion on the mechanism, various methods of generating surface gradients and several examples where on-demand surface tension changes have been used to move droplets to pre-determined locations can be found in Chapter 2 - **“Droplet actuation through localized changes in surface tension”**.

## 1.3 Ionic Liquids

### 1.3.1 Overview

Ionic liquids (IL) describe salts that are comprised solely of ions which, by definition, have a melting point below the boiling point of water (100°C) [54]. Some of the most common ILs contain ammonium, phosphonium, pyridinium or imidazolium cations. Variation of the anions within organic salts can reduce cation-anion Coulombic interactions which disrupts the ion-ion packing. This ultimately affects the melting point and lattice energies [55] which allows for salts to be molten at relatively low temperatures (below 100°C) when compared to the relatively high melting point of common salts such as sodium chloride (NaCl) which has a melting point of 801°C. To this end it is theorized that nearly all organic salts could potentially become ILs via substitution and variation of the cation-anion pairs. Seddon [56] estimates that over  $10^{18}$  salts could have their melting point reduced below 100°C and thus could become ILs and this statement refers only to salts which contain imidazolium and pyridinium cations.

The melting point of a compound describes the temperature at which the ions within the molecular structure receive enough energy to fall out of their crystal lattice and become disordered liquids. For ILs, this phase transition is governed by intermolecular forces (Van der Waals forces) and electrostatic interactions between the ion pairs [57]. Although these intermolecular forces have a large effect on the melting point of ILs, *i.e* they can determine if an IL is a room temperature liquid or a high temperature IL, the main reason ILs have melting points below 100°C is due to the large unsymmetrical ions which have a high degree of conformational flexibility. The steric hindrance caused by these bulky ions reduces the Coulombic interactions between the ion pairs and ultimately affects the ion-ion packing enough that the ions can flow freely. The average Coulombic

bond energy between the ions in an IL is in the region of 300 – 400 kJ/mol [58], significantly higher compared to that of water (~ 20 kJ [59]) but significantly lower than that of a typical salt (NaCl 545 kJ mol<sup>-1</sup>). This reduction in Coulombic bond energy allows for ILs to be molten salts but the intermolecular attractions are still strong enough that ILs have negligible vapour pressures and a high decomposition temperature [60]. In general, the melting point of ILs decreases with an increase of the alkyl chain length in the cation and increases with increasing degrees of symmetry in the cation.

Van der Waals forces also play a role in the viscosity of ILs - as a rule of thumb, ILs are more viscous than aqueous or organic based solvents, due to the Coulombic interactions within the cation-anion pair [61]. ILs have negligible vapour pressure, high thermal stability and have been shown to make excellent solvents [62], making them suitable for replacing conventional organic solvents in many areas [63]. Through variation of the anion-cation pair, the properties of the IL can be significantly altered such as viscosity, polarity and ionic conductivity. Dramatic variation in IL properties can be achieved even by changing only one of the ions; for example, tetradecyl(tributyl)phosphonium chloride is solid at room temperature and hydrophilic, while tetradecyl(tributyl)phosphonium dodecylsulfonate is liquid at room temperature and hydrophobic [62]. The differences in properties and the vast range of possible ion pairs, has led to ILs being referred to as “designer solvents” [64]. Many ILs have long chain hydrophobic “tails” and charged hydrophilic heads, which makes them surfactants of interest.

### 1.3.2 Synthesis

Generally the synthesis of ILs involves two main steps. The first step is the formation of the desired cation, typically through the quaternization of amines or phosphines (list of typical cations can be seen in Figure 1.7), followed by (in cases where the desired product is not formed through the quaternization reaction) anion exchange reactions in order to produce the desired IL product [65].

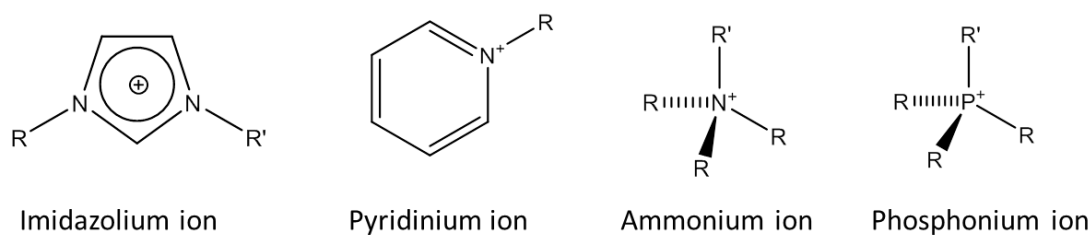


Figure 1.7 Example of typical IL cations. Reproduced from [66].

A typical scheme for the preparation of ILs can be seen in Figure 1.8. In this scheme, an amine ( $\text{NR}_3$ ) undergoes a quaternization reaction to form the desired cation ( $[\text{R}'\text{R}_3\text{N}]^+$ ). From there the cation can undergo two different anion exchange steps to produce different ILs. In step 2a the cation is treated with a Lewis acid  $[\text{MX}_y]$  to produce an IL in the form  $[\text{R}'\text{R}_3\text{N}]^+[\text{MX}_{y+1}]^-$  and in the alternative step (2b) it undergoes anion metathesis, which itself has three steps. First step involves treatment with a metal salt ( $\text{M}^+[\text{A}]^-$ ), which is then removed through precipitation ( $-\text{MX}$ ). The second step involves the addition of a Bronsted acid ( $\text{H}^+[\text{A}]^-$ ) followed by removal of the by-product ( $-\text{HX}$ ). Finally ion exchange resins are used to produce an IL in the form  $[\text{R}'\text{R}_3\text{N}]^+[\text{A}]^-$  [66].

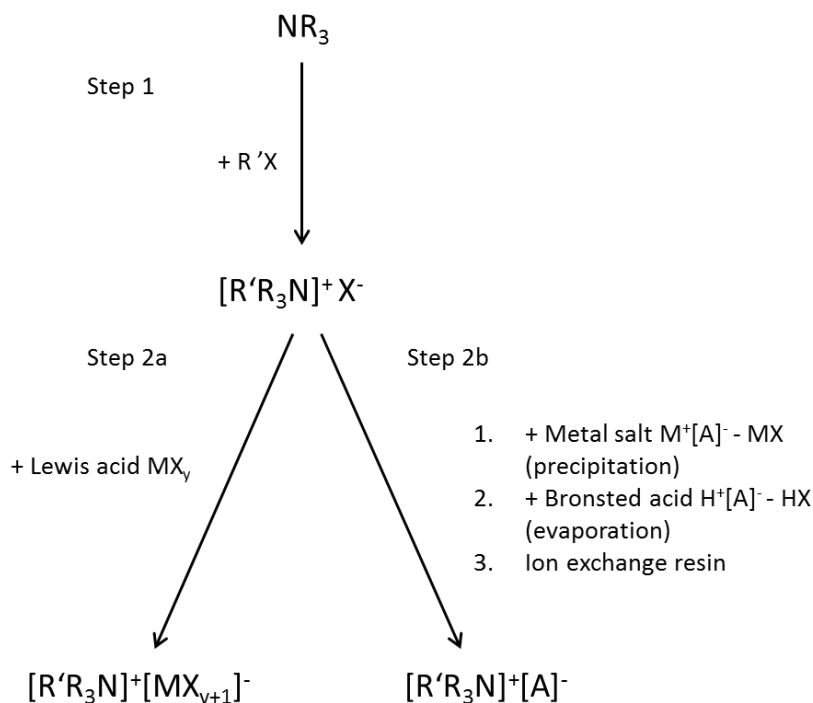


Figure 1.8 Typical reaction scheme for the preparation of ILs. Reproduced from [66].

Quaternization is a relatively simple method as it involves mixing of an amine or phosphine with the desired haloalkane, which is then stirred and heated. The quaternization of 1-alkylimidazoles produces the most common starting materials. In these reactions the temperature and reaction time are dependent on the haloalkane used. For example, reacting chloroalkanes with 1-methylimidazole requires temperatures of 80°C and mixing for three days in order to achieve high yields while reactions with bromoalkanes usually take 24 hours and temperatures of 50°C [65].

Treatment of a halide salt with a Lewis acid involves the mixture of the acid with halide salt. These reactions are generally exothermic. Without care the build-up of heat can result in the decomposition or decolouration of the IL. This type of reactions can generally result in the formation of more than one anion species. For example, in the reaction of 1-ethyl-3-methylimidazolium chloride ([EMIM][Cl]) with aluminium chloride (AlCl<sub>3</sub>) a series of equilibrium reactions 1.1 – 1.3 can occur. When [EMIM][Cl] is in molar excess over the AlCl<sub>3</sub>, equation 1.1 is dominant with the formation of a basic IL ([EMIM]<sup>+</sup>[AlCl<sub>4</sub>]<sup>-</sup>). In contrary, if [EMIM][Cl] is in excess over AlCl<sub>3</sub>, equation 1.2 and 1.3 dominate the equilibrium, resulting in the formation of acidic ILs. Lewis acid based ILs generally tend to be prepared in this manner [65].



Anion Metathesis is another approach that can be used to produce the desired IL. The first anion metathesis which produced stable ILs was based on 1,3-dialkylmethylimidazolium cation [67]. This reaction involved the mixture of [EMIM]I with silver salts in methanol solutions. The low solubility of silver iodide allowed relatively simple separation through filtration. Finally, through the removal of the solvent this procedure resulted in high purity ILs. This technique remains the most popular synthesis for ILs of this type, however, it is limited due to the expensive nature of silver salts [65].

### 1.3.3 Ionic Liquids Surfactants

As mentioned previously, ILs are composed of anion-cation pairs. In most cases, the cation is a large bulky ion while the anion is considerably smaller. Many of these bulky cations have surfactant properties. They often have multiple branching long chained alkyl tails (which are hydrophobic) and a localised positive charge, which is due to the inclusion of particularly electronegative atom (which acts as hydrophilic “head” section). For example trihexyl tetradecyl phosphonium chloride ([P<sub>6,6,6,14</sub>][Cl]) is an efficient cationic surfactant, due to the four long chained alkyl chains and a localised positive charge on the phosphonium atom [68]. By varying the alkyl chain substituents on the cation or by changing the counter anion, the surface activity of the IL can be controlled. This allows for a high degree of flexibility when designing ILs with surfactant-like properties [69].

Merrigan *et al.* [70] reported the synthesis of new perfluorinated (fluorous) ILs which can function as surfactants when added to other room-temperature ionic liquids. These ILs were formulated from imidazole cations which have appended fluoride substituted tails, allowing the molecule to act as a surfactant (Fig 1.9).

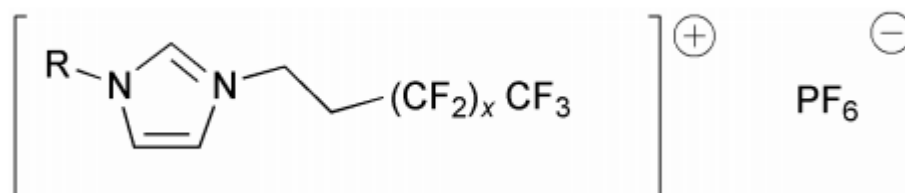


Figure 1.9 General structure of the imidazole based ionic liquids with appended fluoruous tails. Reproduced from [70].

These novel ILs promoted the formation and stabilization of dispersions of perfluorocarbons in conventional ILs. The authors showed that the surface tension of 1-hexyl-3-methylimidazolium hexafluorophosphate ([HMIM][PF<sub>6</sub>]) was 10-15 % lower when saturated with the perfluorocarbons compared to [HMIM][PF<sub>6</sub>] without the perfluorocarbons.

Yan *et al.* [71] have also reported synthesis of surfactants which are based on imidazolium ILs. These ILs had an imidazolium cation polar group, with long chain hydrophobic tails. Some of the novel ILs included polymerizable and reactive surfactants.

Polymerization of these ILs in microemulsions, stabilized the system and allowed for the production of polymers particles, gels and open-cell microporous materials.

Flieger *et al.* [72] demonstrated the use of ILs surfactants in micellar liquid chromatography (MLC). The IL surfactants used were 1-dodecyl-3-methyl-imidazolium chloride [DMIM][Cl] and dodecyltrimethylammonium chloride [DTMA][Cl]. By using [DTMA][Cl] successful separation of polar organic compounds was achieved. These ILs were the first to be used in HPLC.

Trivedi *et al.* [73] reported biodegradable ionic liquid surfactants based on amino acids. The ILs were based on the natural amino acids L-glycine, L-alanine, L-valine, L-glutamic acid and L-proline, respectively. The amino acids allowed for variations in their side chains. Through esterification of the amino group the IL melting point was decreased and biodegradability of the IL was greatly increased. These novel amino acid based ILs have shown to have better surface activity than several conventional surfactants including 1-dodecyl-3-methylimidazolium chloride, sodium dodecyl sulfate and dodecyl trimethyl ammonium chloride while also being highly biodegradable. Moreover, amino acid based IL surfactants could have potential applications in the mitigation of harmful algal blooms for sea water and could be used for nanomaterial synthesis.

Although there are a vast number of papers presenting the possible application and synthesis of IL surfactants, no other research groups have explored the use of IL surfactants as “fuel” for micro-vehicle movement. However, previous research on IL surfactants clearly shows that there is a vast number of ILs that are surface active. Coupled with their “designer solvent” properties, surfactant ILs offer an exciting opportunity for the development of new methods for micro-vehicle movement.

#### **1.3.4 Ionic Liquids as Electrolytes**

Due to their high thermal and electrochemical stability, ILs are useful for many electrochemical processes [74-78], such as electrolytes for carbon nanotube electrodes [79], batteries [80] capillary electrophoresis [81] and electromechanical actuator systems [82]. One of the most important parameters when choosing an electrolyte is the electrochemical window. Electrochemical windows are defined as the potential interval between the cathodic and anodic potential limits at which reduction and oxidation reactions of electrolytes occur at the electrodes. Ionic liquids have been known to exhibit large electrochemical windows [57,83-85]. For ionic liquids, the reduction potential of

cation and the oxidation of anion depend on their respective counter-ions. The most common stability range for ILs is -4.5 to 4.5 V [74] Buzzeo *et al.* [85] studied the electrochemical window of several ILs, namely (1-ethyl-3-methylimidazolium bis(trifluoromethylsulfonyl)imide ([C<sub>2</sub>mim][NTf<sub>2</sub>]), *n*-hexyltriethylammonium bis(trifluoromethylsulfonyl)-imide ([N<sub>6,2,2,2</sub>][NTf<sub>2</sub>]), 1-hexyl-3-methylimidazolium trifluorotris-(pentafluoroethyl)phosphate ([C<sub>6</sub>mim][FAP]) and tris(*n*-hexyl)tetradecylphosphonium trifluorotris-(pentafluoroethyl)phosphate ([P<sub>6,6,6,14</sub>][FAP])) (Figure 1.10) using cyclic voltammetry at gold and platinum electrodes. The results showed that for [P<sub>6,6,6,14</sub>][FAP] no redox activity occurred between -5 V to 5 V at the gold electrode, and no redox activity in the range of -4 to 4 V at the platinum electrode. This window could potentially be extended as this represents the maximum window achieved in these experimental conditions.

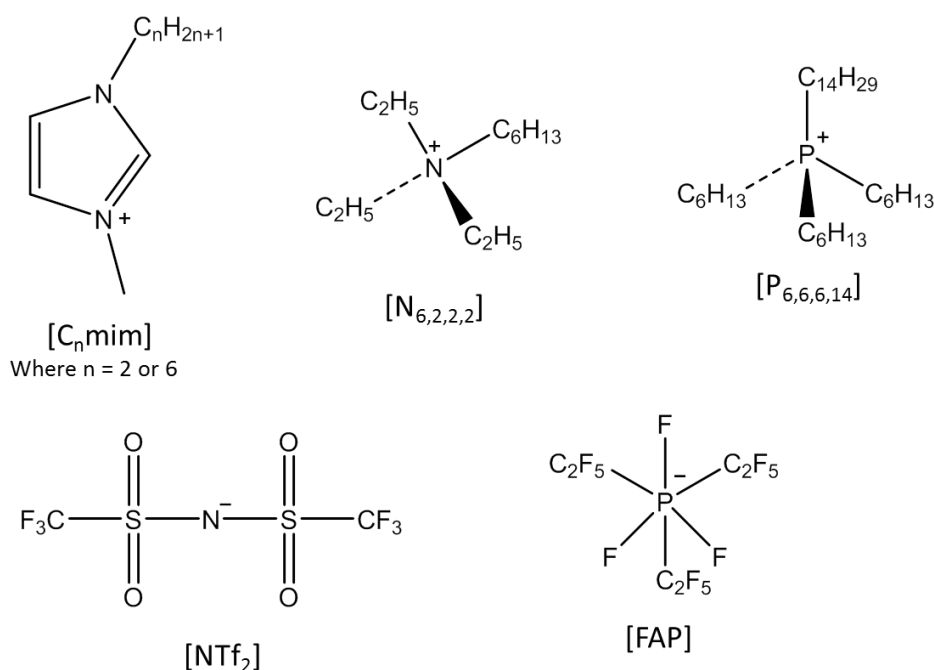


Figure 1.10 Anions and cations of the ILs used in the electrochemical window study, reproduced from [85].

For [N<sub>6,2,2,2</sub>][NTf<sub>2</sub>] no redox activity was observed between -4 V and 4 V for both electrodes and no activity was shown for both [C<sub>2</sub>mim][NTf<sub>2</sub>] and [C<sub>6</sub>mim][FAP] between -2 V and 2V (at both electrodes). This is one of many studies showing that ILs have extended electrochemical windows, when compared to typical electrolytes such as

water and lithium nitrate, which have oxidation potentials of 1.23 V and 2.3 V, respectively [86], and are suitable for use in many electrochemical processes.

The conductivity of a material is the degree to which it conducts electricity, and is calculated as a ratio of the current density of the material vs the applied electric field. In liquids conductivity is linked to the mobility of the ions within the solution. Thus conductivity is related to viscosity. A liquid with a low viscosity will have ions of higher mobility compared to a liquid with a high viscosity. Therefore, ILs with a lower viscosity will have higher conductivities. Other parameters which determine the ionic conductivity of ILs include the ion pairs weights, densities and atomic radii [57]. Temperature affects the intermolecular forces within a molecule. For room temperature ILs a higher temperature reduces these forces resulting in a less viscous liquid. Therefore, temperature directly affects the viscosity of ILs, which means it indirectly influences the conductivity. Due to the customizable nature of ILs and the very large (and ever growing) library available there is a broad scope of conductivities. The average range for ILs is between 0.1–18 mS/cm. Imidazolium based ILs usually have conductivities in the order of 10 mS/cm and pyridinium and ammonium based ILs have much lower conductivities in the range of 0.1–5 mS/cm [74]. When compared with typical electrolytes such as acidic solutions used in batteries (*i.e.* Sulfuric acid ca. 730 mS/cm [74]) they are considerably lower, however, these solutions often react with the electrodes after a period of time and therefore, limit the lifetime of the batteries, while ILs are electrochemically stable and have negligible vapour pressure. The conductivity of ILs can be improved by mixing the neat IL with organic solvents. This improves the conductivity by separating the ion pairs by non-charged molecules. For example, neat 1-butyl-3-methylimidazolium tetrafluoroborate ([EtMeIm][BF<sub>4</sub>]) has a conductivity of 14 mS/cm, while a 2M solution of [EtMeIm][BF<sub>4</sub>] in acetonitrile increases the conductivity to 47 mS/cm [74]. Due to these properties, many groups have looked at replacing acidic and organic electrolytes with ILs for batteries [87-89]. For example, Kuboki *et al* [80] developed a lithium-air battery which uses the hydrophobic IL 1-Ethyl-3-methylimidazolium bis(trifluoromethylsulfonyl)amide ([EMIM][NTf<sub>2</sub>]). [EMIM][NTf<sub>2</sub>] is highly conductive and immiscible with water, which is important in lithium-air batteries as moisture contains oxidative agents (such as carbon dioxide) which degrade the lithium anodes and decrease performance. A non-aqueous based electrolyte results in a battery with discharge capacity of 1600 mAhg<sup>-1</sup>. However, lithium oxide and lithium dioxide (side products of cathodic discharge) can build up on the cathode, which reduces performance

of the battery by interrupting catalytic oxygen reduction. Inclusion of conductive carbon into these batteries has improved the discharge capacity up to 2120 mAhg<sup>-1</sup>. However, when left in air these capacity values drop to 944 mAhg<sup>-1</sup> due to solvent evaporation and anodic hydrolysis. Inclusion of the IL [EMIM][N(Tf)<sub>2</sub>] greatly improved the capacity to 5360 mAhg<sup>-1</sup> and the battery lifetime (56 days).

### 1.3.5 Ionic Liquids as Solvents

One of the primary driving forces behind the research into ILs is in the desire to replace traditionally used organic solvents with ionic non-volatile alternatives. Typically volatile organic compounds (VOCs) are used as solvents in industrial processes; however, VOCs are a major source of environmental pollution. ILs offer a promising alternative to VOCs; although not all ILs can be termed as green solvents, they can be designed to be environmentally friendly while maintaining the properties which make them excellent solvents [64,90,91]. One of the biggest advantages they have over traditional solvents is that they possess negligible vapour pressure, therefore, cannot contribute to gaseous environmental pollution, and can be used in high vacuum processes. Another advantage is the staggering breath of potential ILs; for example approx. a million binary ionic liquids, and 1018 ternary ionic liquids, are theoretically possible [56], while only 600 solvents are typically used in industry today [63]. By substituting either the anion or cation control over many of the IL properties can be achieved including their polarity, thermal properties, biocompatibility, toxicological properties, hydrophobicity profile and their solution behaviours [92-94]. More specially, ILs can be designed to interact or to solvate nearly any analyte [95]. This customizable nature has led to ILs being referred to as “designer solvents” and as a result they have seen heavy use in extractions and separation experiments [96,97]. As mentioned IL liquids are also generally electrochemically stable and can be used as solvents in electrochemical applications. The most common property used to classify solvents is solvent polarity, typically measured using Reichardt’s dye [98]. Measuring the absorption band of this dye when dissolved can give information on the solvents polarity, hydrogen bonding, and Lewis acidity and can be used to determine the solvent’s relative polarity ( $E_T(30)$ ). For example, the relative polarity of alkylammonium nitrate, are between ca. 0.95- 1.01 which is similar to that of water (1.00), while ammonium sulfonates have lower values, 0.45-0.65, which are typical of polar organic solvents [99,100]. In general ionic liquids are classified as polar solvents,

with their solvation properties being directly related to the IL's ability to act as hydrogen bond donors and/or acceptors and the degree of charge localisation on the anions. Increasing the chain of alkyl groups leads to an increase in hydrophobicity, while inclusion of fluoride groups interrupts the salts ability to hydrogen bond [101]. Due to the large unsymmetrical nature of the cation within most ILs, they have the potential to be highly polar solvents while being non-coordinating. Finally ILs can form a two phase system with both organic and polar solvents; therefore, they can be used as a non-aqueous polar phase with organic solvents and hydrophobic ILs can be used as an immiscible polar phase with water based systems [102]. Examples of some common reactions in which ILs have successfully replaced organic solvents include Diels-Alder reactions [103] and Heck reactions [104].

Due to the importance and relevance of this topic in regards to Chapters 4 – 6 of this thesis, this subject has been additionally discussed in Chapter 3 of this thesis where ILs are explored for their use as solvents in microfluidics.

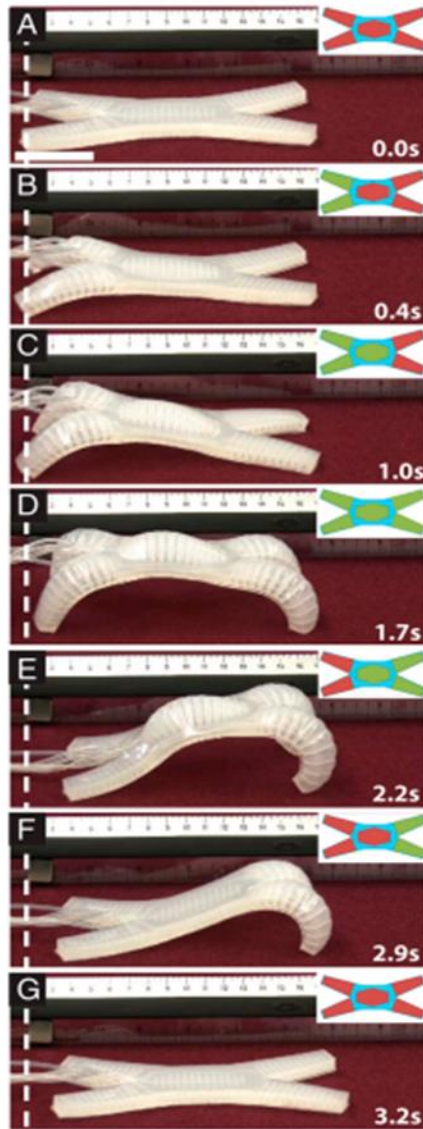
## **1.4 Soft Actuators and Soft Robotics**

### **1.4.1 Overview**

Soft robotics is a new and emerging field of robotics which looks to nature for inspiration. The field looks at the development of non-rigid robots which are synthesised with soft and deformable materials. To date the hard robotics field has failed to reproduce functionalities offered by biology, such as flexibility, adaptability and self-repair, which can be performed by the simplest living organisms (*e.g.* cells, bacteria, jellyfish and worms). To solve these issues scientists have begun to look to nature for inspiration and begun to develop synthetic analogues of some simple organisms. For example the earthworm is one of the most widely imitated forms of locomotion [105-107]. Whitesides was one of the first research groups to use soft material to fabricate bio-inspired soft robotics, mainly using elastomers. Robots designed using elastomeric polymers work via anisotropic contraction and expansion. This is achieved through pressure from a network of pneumatic chambers which are connected via channels within the polymers structure [108]. This type of movement has a number of advantages over hard robotics. Firstly it allows for more complex movements than a conventional hard robots, which have restricted movement due to the rigid nature of the material used in their construction

[109,110]. Secondly owing to the soft nature of the material used to fabricate these new types of robots, they can interact with more delicate objects [111,112], such as fruits and vegetables, which can often be damaged by hard robotics. Finally robots designed using elastomeric polymers can withstand severe bending or blunt force impacts better than robots fabricated using rigid material [108]. For example, Martinez *et al.* [113] developed a robot which was capable of taking multiple gaits by either crawling or through undulation. The robot was fabricated from two layers, where the top layer was an elastomer (Ecoflex) and the bottom was a layer of PDMS (Figure 1.11). The extensible elastomeric polymer contained a network of embedded pneumatic chambers connected via channels. The elastomer layer was then bonded to an inextensible layer of PDMS. The overall device was termed a pneu-net (PN). The pneumatic chambers act like balloons and inflate during actuation, creating a strain within the elastomer layer (Figure 1.11). The pressure difference between the two layers would cause the PN bending. The force and direction of bending could be tuned by adjusting the material of layers and the number, size and orientation of the pneumatic chambers. For example if the chambers were aligned orthogonally to a single axis, during actuation, the PN would curl along this axis. The soft robot developed in this study had four legs, where each leg could be individually controlled and lifted while the other three remained stationary. Each limb and the spine of the robot contained independent PN networks. Each PN network could be pressurized via external compressed air source. The compressed air source was connected to robot through a central hub which was attached to one end of the robot and each PN could be supplied with air via a network of solenoid valves. To achieve robot movement, each PN was actuated in sequence, with an applied pressure of 7 psi, which took only one second to complete. To achieve actuation through undulation the hind legs were first actuated, followed by actuation of the spine. This anchored the robot and stopped the hind legs from slipping. Pressurizing the forelegs, followed by depressurising the back legs and spine caused the robot to be pulled forward. Since there was an anisotropy frictional difference between the front and back of the robot (due to only one half of the robot being in contact with the surface), depressurisation of the front legs resulted in another forward movement of the robot (Figure 1.11(1)).

1



2

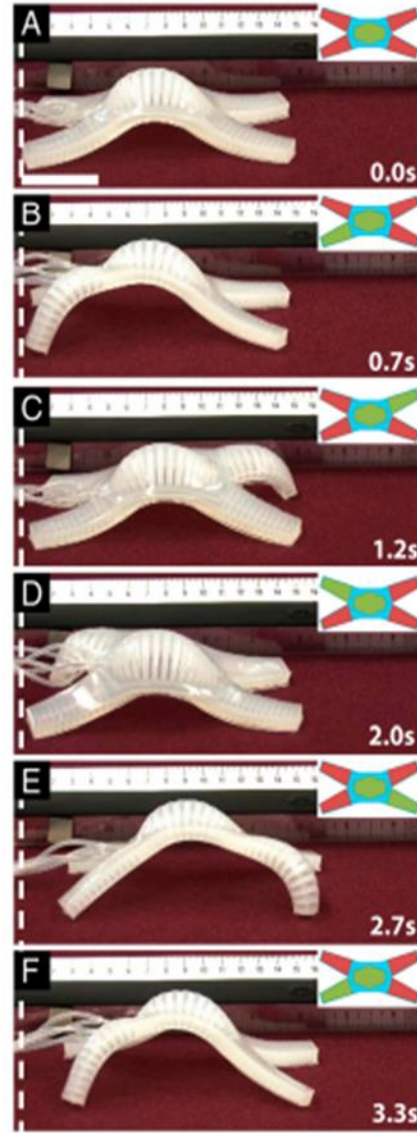
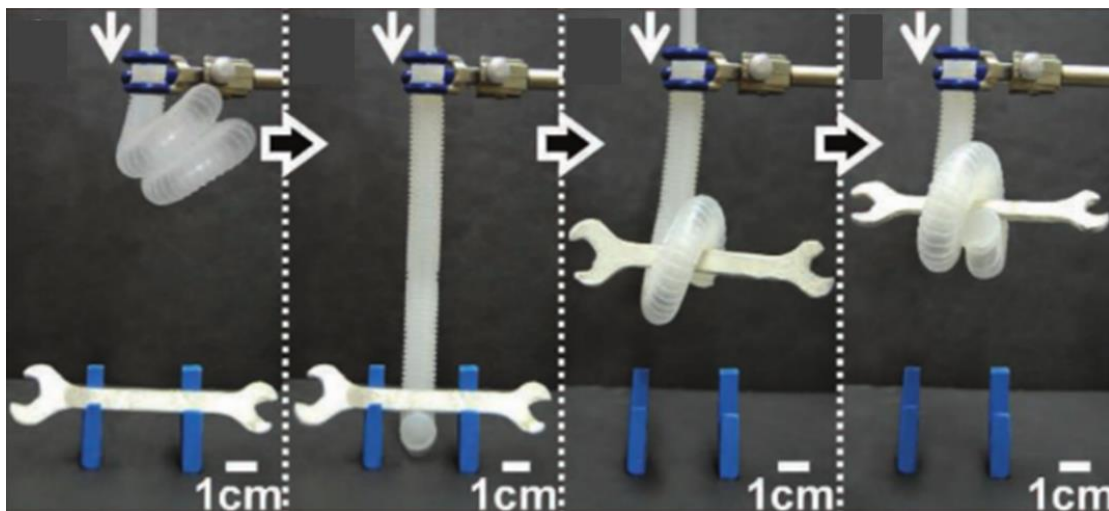


Figure 1.11 Snapshots showing movement of soft robot. 1 shows movement via undulation; (A) shows the start of the experiment when no PNs are pressurised. (B) shows the hind legs being pressurised. (C) shows the spine being pressurised which lifts the robot and anchors it. (D) shows the front legs receiving pressure followed by depressurisation of the hind legs (E). (F) shows the forward motion of the robot. (G) shows further forward motion by depressurization of front legs. 2 shows movement via crawling motion. (A) shows pressurisation of the spine PN. (B) shows actuation of the right hind leg. (C) shows actuation of the front left leg and depressurisation of the right hind leg resulting in forward movement. (D) shows actuation of left hind leg. (E) shows actuation of the front right leg and depressurisation of the left hind leg resulting in forward movement. (F) shows process beginning again. Reproduced with permission from [113].

To achieve a crawling motion five steps were performed. Initially the spine was pressurised, which lifted the body of the robot off the surface. Pressurising the right hind-leg pulled it (the leg) forward. Pressurising the left front-leg and simultaneously depressurising the right hind-leg resulted in a forward motion of the whole robot. Pressurising the left hind-leg, while depressurising the left front-leg, pulled the left rear-leg forward. Actuating the right-front leg, while removing the pressure from the left hind-leg resulted in another forward motion of the whole robot (Figure 1.9(2)). The same group later developed robotic tentacles which had three dimensional mobility [114]. These tentacles worked via three PN networks which work similarly to previous example. However, in the later case each PN controlled a section of the tentacle and could be individually actuated. This allowed the tentacle to interact with and manipulate objects (Figure 1.12). Introduction of functional components to the tentacle allowed for it to perform advanced tasks, such as a needle for delivering fluids, a camera for recording and a suction cup for lifting object.



*Figure 1.12 Snapshots showing soft robotic tentacle arm picking up a spanner. Reproduced with permission from [114].*

Recently there has been great interest in developing soft robotics based on hydrogels [115]. This is because stimuli-responsive hydrogels can undergo large deformations when actuated. In this manner the robot can be made to interact with its environment via external control. Of particular interest is the development of hydrogels with biomimetic properties [116,117] such as the ability to walk [118].

## 1.4.2 Hydrogels

Hydrogels are comprised of a broad range of polymeric materials which due to their hydrophilic nature are capable of storing vast quantities of water. Hydrogels can be actuated via the expulsion and absorption water. In this manner they can undergo radical volume changes, up to 90% in some cases [119]. A method of controlling the gels hydrophilic profile is via the integration of stimuli-responsive compounds into the gels structure. In this fashion the gel's volume and shape can be externally controlled by applying the correct stimulus. Upon actuation the gel will either expel or absorb water from its surrounding environment. A large number of stimuli-responsive gels have been reported, including thermal [120,121], pH [122], magnetic [123], glucose [124], antigen [125], electro- [126], photo- [127], and even multi-responsive hydrogels [128,129].

## 1.4.3 Thermo-Responsive Hydrogels

poly(*N*-isopropylacrylamide) (pNIPAAm) is one of the best known thermo-responsive polymers. When the pNIPAAm chains are crosslinked they form a hydrogel that undergoes a low critical solution temperature (LCST) (32 - 34°C) [130]. The LCST of a material is the critical temperature, at which point the components of the material undergo a drastic physical and chemical change, usually resulting in a solubility alteration in a given solvent. For pNIPAAm hydrogels, the LCST temperature determines the hydrophobicity of the gel. Below the LCST the gel can be described as hydrophilic. Absorption of water at low temperatures is thermodynamically favored due to the formation of hydrogen bonds between water molecules and the amide groups on the polymer chains. This leads to a negative enthalpy and the absorption of water into the gel matrix leads to a large increase in compositional entropy. However, water molecules which are hydrogen bonded to the polymer acquire low orientational entropy. In this phase the gel will actively absorb water molecules and will be swollen. Increasing the temperature destabilizes the hydrogen bonding between water molecules and polymer chains, induced by the presence of hydrophobic isopropyl group of pNIPAAm. Above the LCST temperature phase separation occurs as the energy of free water molecules is greater than the low orientational entropy gained from hydrogen bonding [130]. Therefore, when a pNIPAAm gel is heated above its LCST, there is a

collapse of the polymer network, causing an expulsion of water from the gel into the external environment and resulting in the gel shrinking.

The LCST of pNIPAAm can be manipulated by copolymerization of NIPAAm with other hydrophilic or hydrophobic monomers. For example, Wang *et al.* [119] copolymerized NIPAAm with acrylamide in order to study the temperature-sensitive properties, phase transition and drug release profiles of solutions of aqueous poly(N-isopropylacrylamide-co-acrylamide) and interpenetrating polymer network nanoparticles consisting of poly(NIPAAm) and polyacrylic acid. These systems had a thermo-reversible response and were flow-able suspensions at room temperature which underwent gelation above the LCST. Six different hydrogels were prepared using different crosslinking densities. Gels which consisted of lower than 5 mol% crosslinker had abrupt volume change in the range of 35 – 40 °C, while gels which had a greater concentration (above 5 mol% crosslinker) did not. For example, a gel which had less than 5 mol% crosslinker underwent 4 phase transitions. A suspension (9% wt) of this micro gel was prepared in a phosphate buffered solution (Figure 1.13). At stage one (< 22 °C) the gels were semi translucent, swollen, and had maximum volume of water stored. When the temperature was increased from 22 °C to 36 °C the gel became a clear flow-able suspension (stage two). At this stage the hydrogen bonds between the amide groups and water molecules had become destabilized and water was being expelled from the gel. This is known as the gelling temperature (GT). With a further increase of temperature (> 36 °C < 40 °C) the gel suspension entered stage 3 and became cloudy, due to the further break down of the polymer-water hydrogen bonds and the formation of interpolymer and hydrophobic interactions between side-chains in poly(NIPAAm). This increased the hydrophobicity of the gel resulting in further collapse of the gel structure and more expulsion of water. This temperature is known as the cloud point temperature (CPT). Finally when heated to a temperature higher than what is known as the gel shrinkage temperature (ST, ca 40 °C), the gel entered its final stage and became a semi solid shrunken gel. This was due to the strong hydrophobic interactions between the gel particles. This resulted in the expulsion of the majority of water from the gel and further collapse of the gels structure.

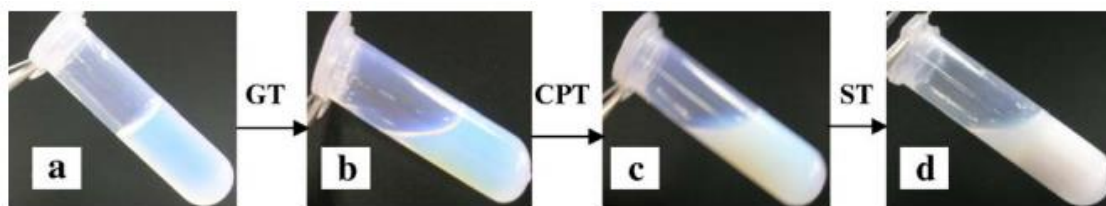


Figure 1.13 series of snapshots which show the 4 stages of transition of poly(N-isopropylacrylamide-co-acrylamide) micro-gels. A ( $< 22\text{ }^{\circ}\text{C}$ ) – gels are in a swollen semi translucent state; B ( $36\text{ }^{\circ}\text{C}$ ) – gels form a flow-able clear solution; C ( $> 36\text{ }^{\circ}\text{C} < 40\text{ }^{\circ}\text{C}$ ) – suspensions becomes cloudy. D ( $40\text{ }^{\circ}\text{C}$ ) – formation of semi solid shrunken gels. Reproduced with permission from [119].

Breger et al [131] have reported on self-folding thermo responsive soft micro-grippers. These micro-grippers were fabricated using soft lithography and were based on a cross-linked poly(N-isopropylacrylamide-co-acrylamide) soft-hydrogel attached to a nonswellable, stiff polypropylene fumarate (PPF) polymer. The polymeric grippers shown in Figure 1.14 were thermo-responsive and were able to self-fold in opposite directions. The center of the gripper comprised of the stiff PPF polymer and the grippers were made of the thermo-responsive pNIPAAm gel.

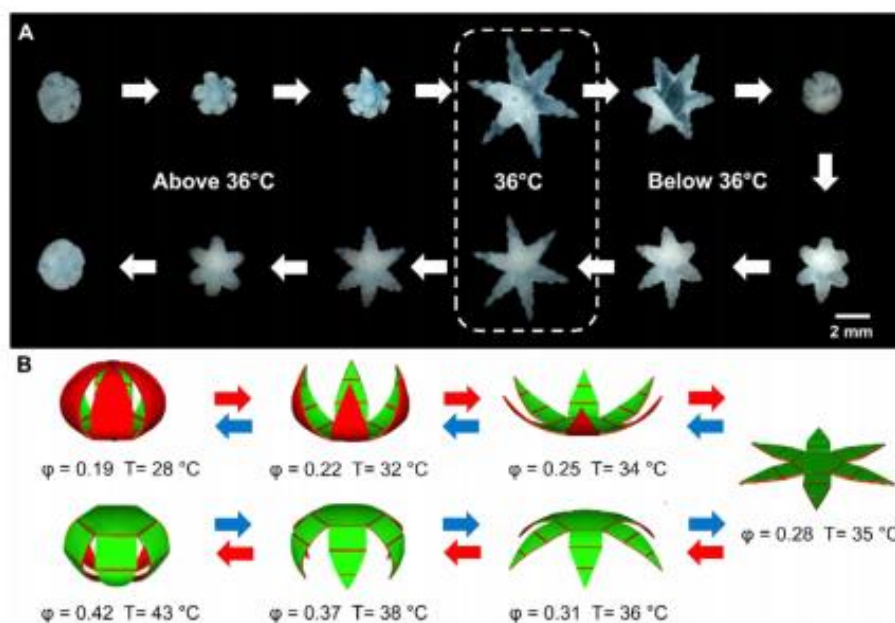


Figure 1.14 shows Experimental snapshots of the micro grippers while being subjected to different temperatures and B is a cartoon showing this response.

The LCST value for the structure produced in this study was 36 °C. When heated above this temperature, the pNIPAAm based grippers underwent a phase transition to a more hydrophobic state. In this state water was expelled from the gels and they began to fold with the PPF segments visible on the outside of the structure. When the polymer chains of pNIPAM-AAc gels began to collapse they became opaque, therefore, this transition was monitored by microscopy. When the temperature was cooled below 36 °C, the gels became more hydrophilic, thus absorbing water, swelling and opening. Raising the temperature again resulted in the grippers folding in the opposite direction with the PPF segments on the inside (Figure 1.13). This cycle could be repeated up to 50 times without any observable degradation of the gel. Introduction of iron nanoparticles into the porous structure of the pNIPAM-AAc gels also allowed for the structure to be manipulated through externally applied magnetic fields.

#### 1.4.4 pH Responsive Hydrogels

pH is a biologically relevant signal, and plays a particularly important role in drug delivery [132]. Incorporation of pH-responsive materials allows for the development of pH-responsive hydrogels. Polymers which undergo ionisation within the pKa range of 3–10 are favourable contenders for a pH-responsive hydrogel. Typically weak acids and bases show this ionisation state when introduced to different pH solutions. If such groups undergo ionisation while bonded to the polymer structure of a hydrogel, this results in a change in the hydrophobic/hydrophilic character of the gel. This means that the shape and volume can be controlled via altering the pH of solution that they are submerged in. Examples of commonly used pH responsive materials include polymers of and copolymers of acrylic acid, methacrylic acid, maleic anhydride, N,N-dimethylaminoethyl methacrylate and phosphoric acid derivatives [133].

Li *et al.* [134] have reported on the synthesis of a thermo- and pH responsive hydrogel. The semi-interpenetrating (semi-IPN) hydrogel was based on a bilayer of pNIPAAm which had a positively charged polyelectrolyte poly(diallyldimethylammonium chloride (pDADMAC) trapped within the gels network, and a layer of gold-coated PDMS (non-swellable rigid layer). A gripper structure was developed (similar to the example described previously, Figure 1.12). The thermo-response of these bilayers was due to the pNIPAAm/pDADMAC hydrogel layer. At low temperatures (25 °C) the hydrogel was fully swollen, resulting in the bilayer structure

bending towards the PDMS layer. This caused the gripper to close with the PDMS layer on the inside. When the temperature was raised to 40°C (LCST) the pNIPAAm layer shrank (due to water expulsion); this resulted in the bilayer structure bending towards the hydrogel layer causing the gripper to close in the opposite direction, with the PDMS layer on the outside (Figure 1.15).

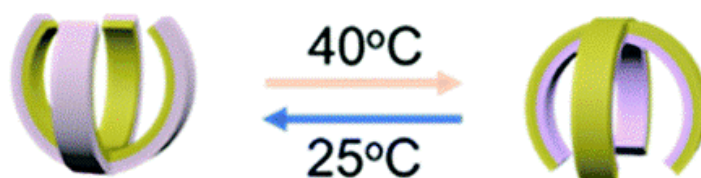


*Figure 1.15 Thermo-response of the bilayer semi-IPN hydrogel structure. Below 25°C, the structure is closed with the PDMS layer on the inside. When the temperature was raised above the LCST (40°C) the structure bends in the opposite direction with the PDMS layer on the outside. Reproduced with permission from [134].*

The pH response of the gel was obtained by copolymerising poly(acrylic acid) (AA) into the hydrogel structure. This was done with and without pDADMAC. At pH 6.5 the gels which included pDADMAC were in the hydrophobic state and water was expelled from the gel. This results in the gripper folding towards the hydrogel layer with the PDMS on the outside. At this pH AA (which is part of the hydrogel structure) was deprotonated and negatively charged and had strong electrostatic interaction with the positively charged pDADMAC (poly electrolyte which is physically trapped inside the hydrogel network). This interaction restricted the pDADMAC from absorbing water and created small pores within the gel. When the pH was lowered to pH 3.0 AA was neutralised, thus releasing the pDADMAC and allowing it to readily absorb water, while also increasing pore sizes within the gel. This resulted in the gel swelling, causing the bilayer to bend towards the PDMS layer and causing the gripper to close with the PDMS layer on the inside (Figure 1.16.) This process was repeatable and the gripper could be made to close in opposite directions multiple times by simply switching the pH of the solution from 3.0 to 6.5.

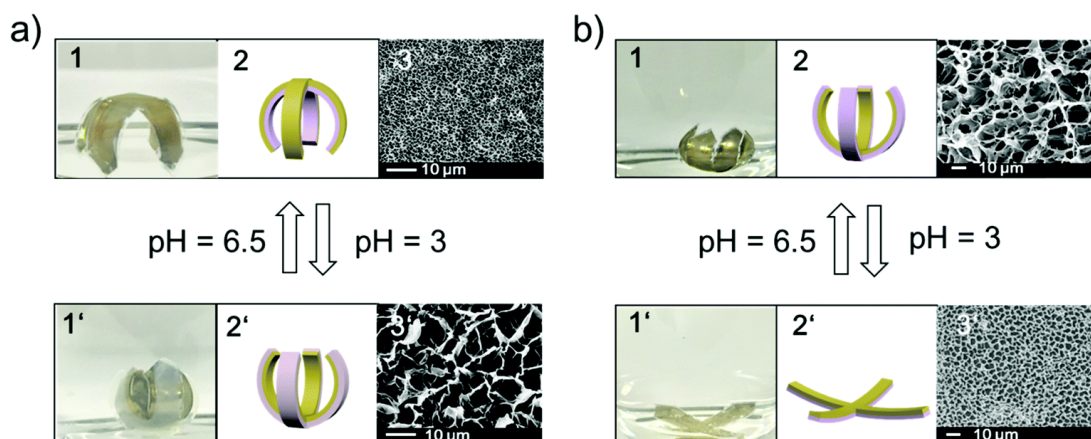


Figure 1.16 pH response of the hydrogel gripper. A shows the hydrogels which had pDADMAC trapped within the gel network. At pH 3 the hydrogels were swollen and the gripper was closed with the PDMS layer on the inside. When the pH is raised to 6.5 the hydrogel layer shrinks and the gripper closes with the PDMS layer on the outside. B shows the gels which excluded pDADMAC. At pH 6.5 the gripper was closed with the PDMS layer on the inside. At pH 3 the gels expelled water and the structure opened flat. Reproduced with permission from [134]

This effect was reversed for gels which did not have pDADMAC trapped within the hydrogel structure. At pH 6.5 the charged AAc made the hydrogel hydrophilic. This resulted in large pore sizes and the high osmotic pressure (due to the gel swelling) generated resulted in the gel bending towards the PDMS layer. When the pH was dropped to 3, the AAc was neutralised and the gel became hydrophobic. This reduced the pore size and caused the expulsion of water from the gel causing it to open flat (Figure 1.16 b). All the pH experiments were performed at 25°C which indicated that bending was solely due to the inclusion of AAc. Both the thermo- and pH response of these gels was repeatable and the degree to which the bilayers would bend (and direction) could be modulated by tuning the composition of the hydrogel layer. These grippers could also be used for controlled delivery of molecular cargo, making them highly useful for biomedical devices.

### 1.4.5 Electro-Actuated Hydrogels

Electro-actuated polyelectrolyte hydrogels are particularly interesting as they have the ability to transform electrochemical energy into mechanical movement via application of external electrical potentials. When a voltage is applied across an aqueous electrolyte

solution, this results in migration and redistribution of the mobile ions within the system. This process is highly controllable and repeatable. Morales *et al.* [118] have synthesised a polyelectrolyte-doped bipedal hydrogel. The gels legs were comprised of different material. One leg, termed “cationic leg” was based on copolymer networks of acrylamide/sodium acrylate; this polymer network had a negative charge and mobile counter cations. The second leg, termed “anionic leg” was synthesised from acrylamide quaternized dimethylaminoethyl methacrylate and had a positively charged backbone and thus mobile counter anions. When submerged in an aqueous electrolyte solution (0.01 M NaCl) and subjected to an applied potential (5 V) the mobile ions within the gel would distribute asymmetrically. The cations within the cationic leg would migrate towards the side of the gel facing the cathode and the anions within the anionic leg would migrate towards the side of the gel facing the anode. This mass transfer of ions creates an osmotic difference within the gel causing it deform and swell. By placing the gels onto a PDMS surface and applying (and reversing) potentials the gels can be made to walk in a direction dictated by the design of the walker. The sequence of applying the voltages is important in controlling the motion of the hydrogel. Initially the potential is applied with the cationic leg facing the cathode and the anionic leg facing the anode, this result in the legs bending towards one another. Since the anionic leg (right leg, Figure 1.11) has a greater surface area in contact with the PDMS, it pulls the gel to the right. Reversing the applied electrical field causes the anionic leg to stretch towards the cathode. Since the cation now had a greater surface area in contact with the PDMS it pushed the gel to the right. Repeated cycles of this process enabled unidirectional movement of the gels on flat surfaces (Figure 1.17).

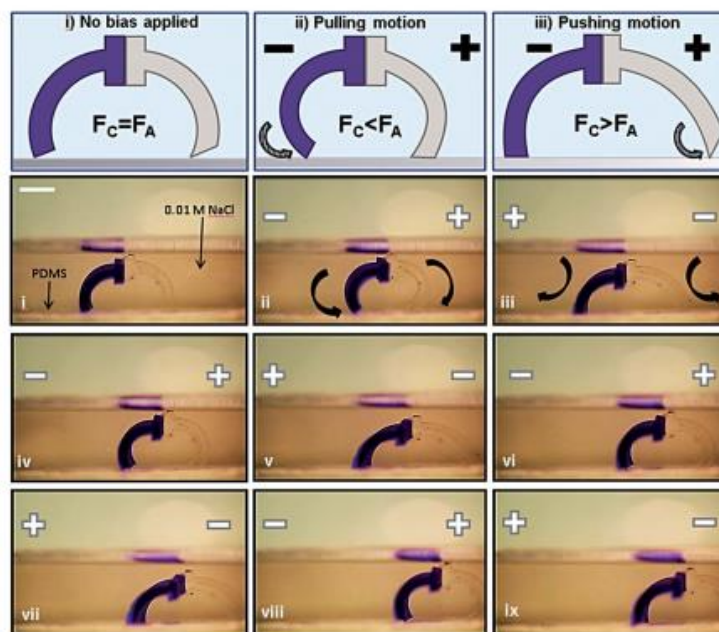


Figure 1.17 Actuation mechanism and snapshots of the of electro-actuated hydrogel walkers while submerged in a solution of 0.1 M NaCl with an applied potential of 5 V. i) no potential is applied; ii) 5 V is applied resulting in the anionic leg (right leg) bending toward the anode and the cationic leg (left leg) bending towards the cathode; in this position the anodic leg has a greater area in contact with the surface and thus pulls the cathodic leg to the right; iii) the potential is reversed, resulting in both legs bending in the opposite direction; in this position the cathodic leg now has a greater area in contact with the surface and pushes the anodic leg to the right; iv – ix) shows that repeated cycling of the applied potential results in the forward motion of the hydrogel walker. Reproduced with permission from [118].

Yang *et al.* [135] have also demonstrated the walking behaviour of an arc shaped hydrogel based on poly(2-acrylamido-2-methylpropanesulfonic acid-*co*-acrylamide) (poly(AMPS-*co*-AAm)). When placed onto a ratcheted surface under electro-stimulation the resultant contraction and relaxation of the gel, resulted in gel locomotion in the direction dictated by the design of the ratchet. The polymeric network of the gel contains negatively charged sulfonic groups. When submerged in NaCl solution with an applied voltage, the free ions of the NaCl electrolyte move towards their respective counter electrodes. However, within the gel network only the counter ions of the bound sulfonic group can move. The resulting influx of ions results in a bending motion of the gel. This is a reversible process and can be controlled by turning on and off the voltage applied to the aqueous solution. Due to the design of the ratchet, only one leg of the gel can move upon stimulation. This results in the gel being pulled when bending (voltage on) and

being pushed during relaxation (voltage off). Repeated cycles of contraction and relaxation of the gel resulted in a walking motion, molecular cargo could be incorporated on the walker which enabled them to be used as vehicles for molecular transport (Figure 1.18).

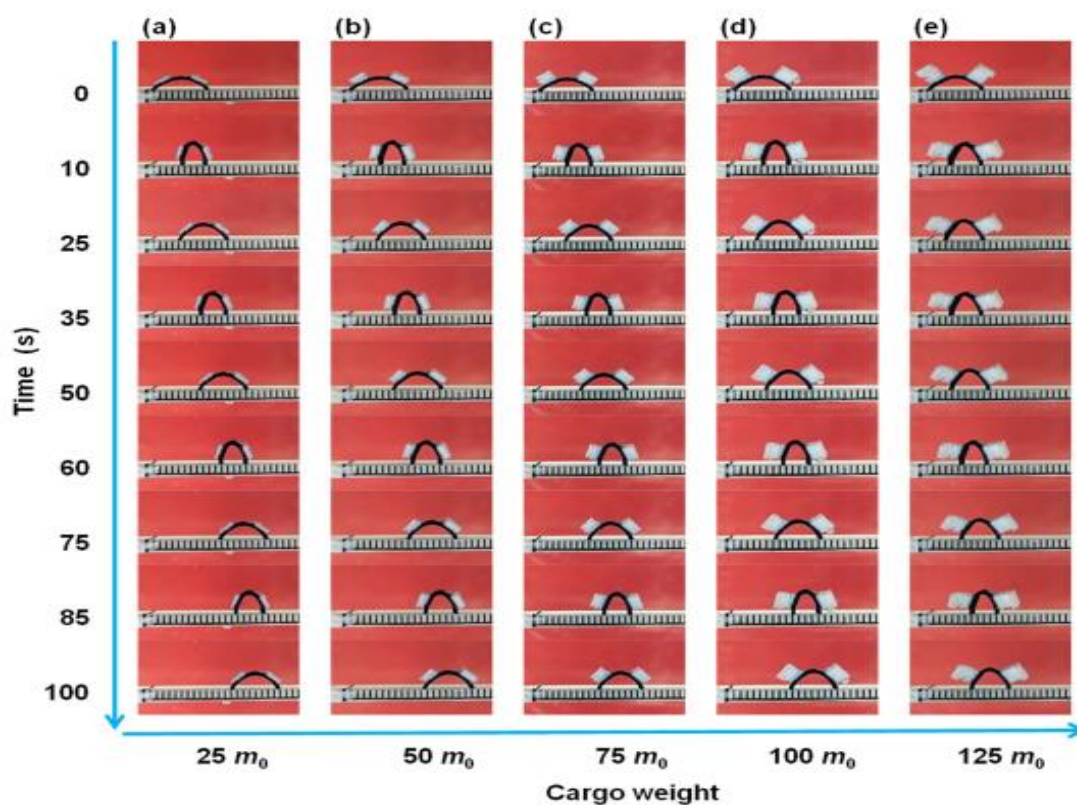
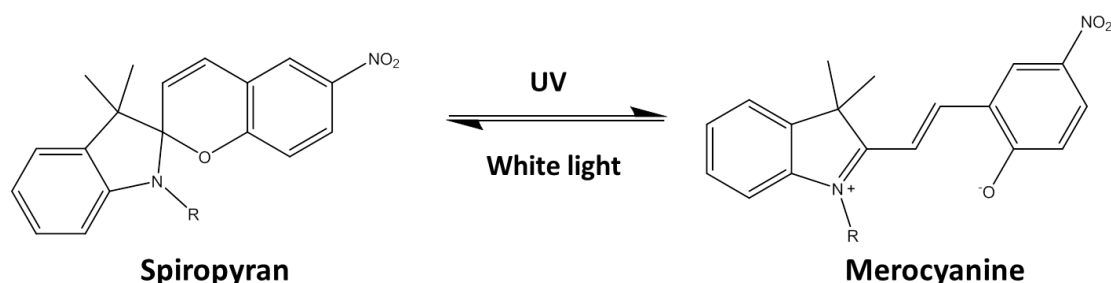


Figure 1.18 Series of snapshots showing the locomotion of the hydrogels walkers carrying varying weights of cargo ( $25 m_0$ ,  $50 m_0$ ,  $75 m_0$ ,  $100 m_0$  and  $125 m_0$ , respectively, where  $m_0$  is the weight of the walker in the dried state ) while submerged in a solution of  $0.01M$  NaCl with an applied voltage of  $25V$ . At time  $0$  no voltage is applied, meaning that the gel is in a relaxed expanded state. When the voltage is applied (time= $10s$ ) the gels bend towards the electrode (above the ratchet). Due to the design of the ratchet, only one leg of the gel can move upon stimulation. This results in the gel being pulled when bending (voltage on) and being pushed during relaxation (voltage off). Repeated cycles of contraction and relaxation of the gel resulted in a walking motion. Reproduced with permission from [135].

#### 1.4.6 Photo-Responsive Hydrogels

Light as a stimulus is one of the easiest to control and can be applied externally in a non-invasive manner. Photochromism is the reversible conformation change of a compound

through the absorption of electromagnetic radiation. Each confirmation has a different absorbance spectrum. The isomers of certain photochromic compounds can have different chemical properties, such as polarity or hydrophobicity. If these photochromic groups are integrated into the backbone of a hydrogel, the gel's volume and shape can be modulated by irradiation with specific wavelengths of light [136]. Some of the most common and notable photochromic families include diarylethenes [137], azobenzenes [138], spirooxazines [139] naphthopyran [140] and spiro-benzopyrans [127]. When these compounds absorb electromagnetic radiation, they undergo a reversible conformational change. These properties have led to the development of various optically activated devices such as light responsive spectacles [141], 3D optical memory devices [126] and optical sensing platforms [142-144]. Spiro-benzopyrans are perhaps one of the most used and widely studied photo responsive compounds [145-147]. When subjected to various illumination conditions, spiro-benzopyrans undergo a rapid switching between two isomers. Spiro-benzopyrans can be rapidly switched from a closed ring spiropyran (SP) form to an open ring merocyanine (MC) form (polar) via irradiation with ultra violet (UV) light. Irradiation of MC with white light (or blue light) will switch the MC back to the SP form (Figure 1.19).



*Figure 1.19 Spiropyran-merocyanine structures in equilibrium under UV-visible light irradiation. When exposed to UV radiation, spiropyran (left) undergoes a reversible conformational change to the merocyanine form (right). The reverse reaction is possible under white light irradiation.*

Incorporation of SP compounds into hydrogels has been widely reported, as it not only provides photochromism but it can also add sensitivity to pH, solvent polarity and metal ions [148-150]. While in the open MC form, spiropyrans also show solvatochromism, and have been reported as efficient chelators for the binding of various metal ions [142,151]. It has been previously demonstrated that incorporation of spiropyrans into hydrogels [152] and ionogels [153,154] can be used for the fabrication of



Using this formulation Dunne *et al.* [152] have synthesised photo-actuator hydrogels based on p(NIPAAm-co-SP-co-AA) copolymer, in 100–1–5 mole ratio. This study focused on the relationship between the polymerisation solvent and pore sizes within the hydrogels. The pore size is an important factor as it determines the kinetics of water expulsion and absorption after isomerisation of the SP compound and thus the rate at which the gels can shrink and swell. In the study, the highest shrinking was observed when a solvent mixture comprised of a ratio of 4 : 1 acetone to deionised water was used during polymerisation. The hydrogel produced from this solvent had a 40% reduction in volume after four minutes of white irradiation and swelled back to roughly 62 % of its original size after 11 minutes in the dark. Using a solvent ratio of 1:1 tetrahydrofuran to deionised water resulted in a hydrogel with the best swelling capabilities; after shrinking the gel was able to swell back to 92 % of its original volume after 11 minutes in the dark (Figure 1.21).

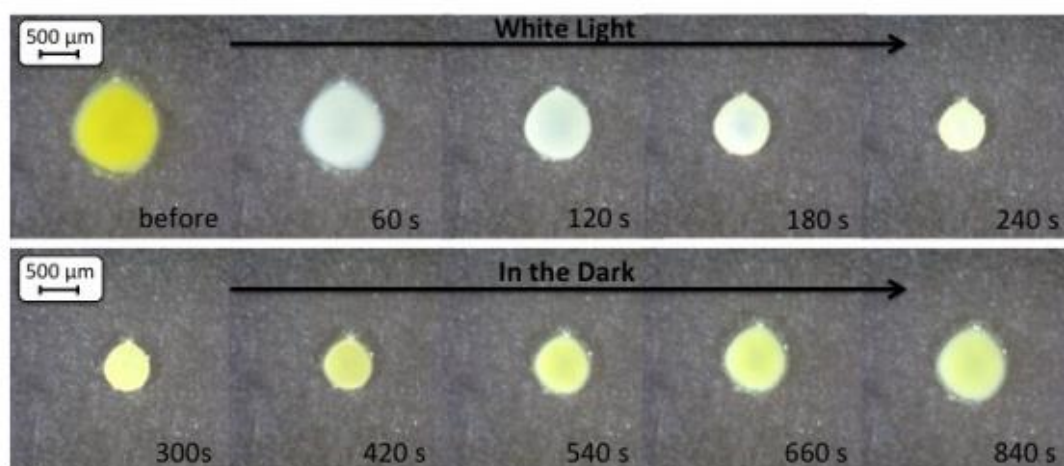


Figure 1.21 Snapshots showing the area decrease of p(NIPAAm-co-SP-co-AA) hydrogels while submerged in DI water and irradiated with light for 5 minutes (top) and the subsequent area increase when left in the dark for further 11 minutes (bottom). Reproduced from [152] with permission from the author.

At the time of publication this was the largest reported photo-induced area change for SP hydrogels which are self-protonating. Swelling and shrinking of the gel could be performed in DI water (due to the internal acidic source, AA) and no degradation of the gel was observed over three cycles of white light illumination. Continuing on from this work, the possibility of using similar materials for the development of photo-controlled bipedal hydrogel walkers will be explored in Chapter 7 of this thesis.

## 1.5 Aims of this Work

The aim of this work was to realise stimuli-controlled manipulation of synthetic micrometre sized “vehicles”. This was achieved by developing self-propelled IL droplets which moved through the triggered release of cationic surfactant which was a component of the IL. Two methods for controlling droplet movement were analysed. Chapter 4 describes the development of chemotactic IL droplets which travelled spontaneously towards a source of a chemoattractant while Chapter 5 describes electrotactic droplets that move in response to an electro-chemically generated chloride gradient. Chapter 6 of this thesis aims to introduce functionality to these droplet systems and demonstrate several applications that they can perform. Chapter 7 looks at the development of a different type of micro-vehicle and describes the synthesis of a bipedal hydrogel walker, based on poly(*N*-isopropylacrylamide-*co*-acrylated spiropyran-*co*-acrylic acid), p(NIPAAm-*co*-SP-*co*-AA). Due to the presence of spiropyran in the polymer structure, these hydrogels reversibly shrink and swell in aqueous environments when exposed to different light conditions. When these gels are placed onto a ratcheted surface, the actuation of the bipedal gel produces a walking motion by taking a series of steps in a given direction, as determined by the optimised design of the ratchet scaffold.

The following chapters include two book chapters (published) which explore in detail some of the literature previously published on droplet work (Chapter 2) and the use of ILs in the microfluidic sector (Chapter 3), followed by 4 experimental chapters which illustrate the progress I have made thus far in the development of *Stimuli-Controlled Synthetic Discrete Micrometre Sized “Vehicles”* and will hopefully give the reader some insight into the exciting potential of this research.

## 1.6 References

1. Whitesides, G.M. The origins and the future of microfluidics. *Nature* **2006**, *442*, 368-373.
2. Krüger, J.; Singh, K.; O'Neill, A.; Jackson, C.; Morrison, A.; O'Brien, P. Development of a microfluidic device for fluorescence activated cell sorting. *Journal of micromechanics and microengineering* **2002**, *12*, 486.
3. Bhagat, A.A.S.; Bow, H.; Hou, H.W.; Tan, S.J.; Han, J.; Lim, C.T. Microfluidics for cell separation. *Med Biol Eng Comput* **2010**, *48*, 999-1014.

4. Moraes, C.; Mehta, G.; Leshner-Perez, S.C.; Takayama, S. Organs-on-a-chip: A focus on compartmentalized microdevices. *Ann. Biomed. Eng.* **2012**, *40*, 1211-1227.
5. Wikswo, J.P.; Curtis, E.L.; Eagleton, Z.E.; Evans, B.C.; Kole, A.; Hofmeister, L.H.; Matloff, W.J. Scaling and systems biology for integrating multiple organs-on-a-chip. *Lab on a Chip* **2013**, *13*, 3496-3511.
6. Dittrich, P.S.; Manz, A. Lab-on-a-chip: Microfluidics in drug discovery. *Nature Reviews Drug Discovery* **2006**, *5*, 210-218.
7. Kang, L.; Chung, B.G.; Langer, R.; Khademhosseini, A. Microfluidics for drug discovery and development: From target selection to product lifecycle management. *Drug Discovery Today* **2008**, *13*, 1-13.
8. Neuzi, P.; Giselsbrecht, S.; Länge, K.; Huang, T.J.; Manz, A. Revisiting lab-on-a-chip technology for drug discovery. *Nature reviews Drug discovery* **2012**, *11*, 620-632.
9. Hakimi, N.; Tsai, S.S.; Cheng, C.H.; Hwang, D.K. One-step two-dimensional microfluidics-based synthesis of three-dimensional particles. *Adv. Mater.* **2014**, *26*, 1393-1398.
10. Jebrail, M.J.; Ng, A.H.; Rai, V.; Hili, R.; Yudin, A.K.; Wheeler, A.R. Synchronized synthesis of peptide-based macrocycles by digital microfluidics. *Angew. Chem. Int. Ed.* **2010**, *49*, 8625-8629.
11. Liu, Y.; Tian, M.; Zhang, H. Microfluidics for synthesis of peptide-based pet tracers. *BioMed research international* **2013**, *2013*.
12. Hardin, J.O.; Ober, T.J.; Valentine, A.D.; Lewis, J.A. Microfluidic printheads for multimaterial 3d printing of viscoelastic inks. *Adv. Mater.* **2015**, *27*, 3279-3284.
13. Stone, H.A.; Kim, S. Microfluidics: Basic issues, applications, and challenges. *AIChE J.* **2001**, *47*, 1250-1254.
14. Mark, D.; Haeberle, S.; Roth, G.; von Stetten, F.; Zengerle, R. Microfluidic lab-on-a-chip platforms: Requirements, characteristics and applications. *Chem. Soc. Rev.* **2010**, *39*, 1153-1182.
15. Atencia, J.; Beebe, D.J. Controlled microfluidic interfaces. *Nature* **2005**, *437*, 648-655.
16. Duffy, D.C.; Gillis, H.L.; Lin, J.; Sheppard, N.F.; Kellogg, G.J. Microfabricated centrifugal microfluidic systems: Characterization and multiple enzymatic assays. *Anal. Chem.* **1999**, *71*, 4669-4678.
17. Chang, H.-C.; Yeo, L.Y. *Electrokinetically driven microfluidics and nanofluidics*. Cambridge University Press Cambridge, UK.: 2010.
18. Kamholz, A.E.; Weigl, B.H.; Finlayson, B.A.; Yager, P. Quantitative analysis of molecular interaction in a microfluidic channel: The t-sensor. *Anal. Chem.* **1999**, *71*, 5340-5347.
19. Kopp, M.U.; De Mello, A.J.; Manz, A. Chemical amplification: Continuous-flow pcr on a chip. *Science* **1998**, *280*, 1046-1048.
20. Teh, S.-Y.; Lin, R.; Hung, L.-H.; Lee, A.P. Droplet microfluidics. *Lab on a Chip* **2008**, *8*, 198-220.
21. Fair, R.B. Digital microfluidics: Is a true lab-on-a-chip possible? *Microfluid. Nanofluid.* **2007**, *3*, 245-281.
22. Lagzi, I.; Soh, S.; Wesson, P.; Browne, K.; Grzybowski, B. Maze solving by chemotactic droplets. *J. Am. Chem. Soc.* **2010**, *132*, 1198-1199.
23. Stanley, C.E.; Wootton, R.C.; deMello, A.J. Continuous and segmented flow microfluidics: Applications in high-throughput chemistry and biology. *CHIMIA International Journal for Chemistry* **2012**, *66*, 88-98.

24. Song, H.; Chen, D.L.; Ismagilov, R.F. Reactions in droplets in microfluidic channels. *Angew. Chem. Int. Ed.* **2006**, *45*, 7336-7356.
25. Garstecki, P.; Ganan-Calvo, A.; Whitesides, G. Formation of bubbles and droplets in microfluidic systems. *Technical sciences* **2005**, *53*.
26. Dendukuri, D.; Tsoi, K.; Hatton, T.A.; Doyle, P.S. Controlled synthesis of nonspherical microparticles using microfluidics. *Langmuir* **2005**, *21*, 2113-2116.
27. Guo, M.T.; Rotem, A.; Heyman, J.A.; Weitz, D.A. Droplet microfluidics for high-throughput biological assays. *Lab on a Chip* **2012**, *12*, 2146-2155.
28. Wang, J.T.; Wang, J.; Han, J.J. Fabrication of advanced particles and particle-based materials assisted by droplet-based microfluidics. *small* **2011**, *7*, 1728-1754.
29. Garstecki, P.; Gitlin, I.; DiLuzio, W.; Whitesides, G.M.; Kumacheva, E.; Stone, H.A. Formation of monodisperse bubbles in a microfluidic flow-focusing device. *Appl. Phys. Lett.* **2004**, *85*, 2649-2651.
30. Xu, Q.; Hashimoto, M.; Dang, T.T.; Hoare, T.; Kohane, D.S.; Whitesides, G.M.; Langer, R.; Anderson, D.G. Preparation of monodisperse biodegradable polymer microparticles using a microfluidic flow-focusing device for controlled drug delivery. *Small* **2009**, *5*, 1575-1581.
31. Ward, T.; Faivre, M.; Abkarian, M.; Stone, H.A. Microfluidic flow focusing: Drop size and scaling in pressure versus flow-rate-driven pumping. *Electrophoresis* **2005**, *26*, 3716-3724.
32. Thorsen, T.; Roberts, R.W.; Arnold, F.H.; Quake, S.R. Dynamic pattern formation in a vesicle-generating microfluidic device. *Phys. Rev. Lett.* **2001**, *86*, 4163.
33. Anna, S.L.; Bontoux, N.; Stone, H.A. Formation of dispersions using “flow focusing” in microchannels. *Appl. Phys. Lett.* **2003**, *82*, 364-366.
34. Kobayashi, I.; Takano, T.; Maeda, R.; Wada, Y.; Uemura, K.; Nakajima, M. Straight-through microchannel devices for generating monodisperse emulsion droplets several microns in size. *Microfluid. Nanofluid.* **2008**, *4*, 167-177.
35. Theberge, A.B.; Courtois, F.; Schaerli, Y.; Fischlechner, M.; Abell, C.; Hollfelder, F.; Huck, W.T. Microdroplets in microfluidics: An evolving platform for discoveries in chemistry and biology. *Angew. Chem. Int. Ed.* **2010**, *49*, 5846-5868.
36. Joensson, H.N.; Andersson Svahn, H. Droplet microfluidics—a tool for single-cell analysis. *Angew. Chem. Int. Ed.* **2012**, *51*, 12176-12192.
37. Brouzes, E.; Medkova, M.; Savenelli, N.; Marran, D.; Twardowski, M.; Hutchison, J.B.; Rothberg, J.M.; Link, D.R.; Perrimon, N.; Samuels, M.L. Droplet microfluidic technology for single-cell high-throughput screening. *Proceedings of the National Academy of Sciences* **2009**, *106*, 14195-14200.
38. Huebner, A.; Srisa-Art, M.; Holt, D.; Abell, C.; Hollfelder, F.; Edel, J. Quantitative detection of protein expression in single cells using droplet microfluidics. *Chem. Commun.* **2007**, 1218-1220.
39. Hindson, B.J.; Ness, K.D.; Masquelier, D.A.; Belgrader, P.; Heredia, N.J.; Makarewicz, A.J.; Bright, I.J.; Lucero, M.Y.; Hiddessen, A.L.; Legler, T.C. High-throughput droplet digital pcr system for absolute quantitation of DNA copy number. *Anal. Chem.* **2011**, *83*, 8604-8610.
40. Leng, X.; Zhang, W.; Wang, C.; Cui, L.; Yang, C.J. Agarose droplet microfluidics for highly parallel and efficient single molecule emulsion pcr. *Lab on a Chip* **2010**, *10*, 2841-2843.
41. Zheng, B.; Roach, L.S.; Ismagilov, R.F. Screening of protein crystallization conditions on a microfluidic chip using nanoliter-size droplets. *J. Am. Chem. Soc.* **2003**, *125*, 11170-11171.

42. Zheng, B.; Tice, J.D.; Roach, L.S.; Ismagilov, R.F. A droplet-based, composite pdms/glass capillary microfluidic system for evaluating protein crystallization conditions by microbatch and vapor-diffusion methods with on-chip x-ray diffraction. *Angew. Chem. Int. Ed.* **2004**, *43*, 2508-2511.
43. Shi, W.; Qin, J.; Ye, N.; Lin, B. Droplet-based microfluidic system for individual caenorhabditis elegans assay. *Lab on a Chip* **2008**, *8*, 1432-1435.
44. Huebner, A.; Bratton, D.; Whyte, G.; Yang, M.; Abell, C.; Hollfelder, F. Static microdroplet arrays: A microfluidic device for droplet trapping, incubation and release for enzymatic and cell-based assays. *Lab on a Chip* **2009**, *9*, 692-698.
45. Kintses, B.; Hein, C.; Mohamed, M.F.; Fischlechner, M.; Courtois, F.; Lainé, C.; Hollfelder, F. Picoliter cell lysate assays in microfluidic droplet compartments for directed enzyme evolution. *Chem. Biol.* **2012**, *19*, 1001-1009.
46. Clausell-Tormos, J.; Lieber, D.; Baret, J.-C.; El-Harrak, A.; Miller, O.J.; Frenz, L.; Blouwolff, J.; Humphry, K.J.; Köster, S.; Duan, H. Droplet-based microfluidic platforms for the encapsulation and screening of mammalian cells and multicellular organisms. *Chem. Biol.* **2008**, *15*, 427-437.
47. Nie, Z.; Li, W.; Seo, M.; Xu, S.; Kumacheva, E. Janus and ternary particles generated by microfluidic synthesis: Design, synthesis, and self-assembly. *J. Am. Chem. Soc.* **2006**, *128*, 9408-9412.
48. Günther, A.; Jensen, K.F. Multiphase microfluidics: From flow characteristics to chemical and materials synthesis. *Lab on a Chip* **2006**, *6*, 1487-1503.
49. Sebastian Cabeza, V.; Kuhn, S.; Kulkarni, A.A.; Jensen, K.F. Size-controlled flow synthesis of gold nanoparticles using a segmented flow microfluidic platform. *Langmuir* **2012**, *28*, 7007-7013.
50. Song, H.; Tice, J.D.; Ismagilov, R.F. A microfluidic system for controlling reaction networks in time. *Angew. Chem.* **2003**, *115*, 792-796.
51. Wang, M.; Roman, G.T.; Perry, M.L.; Kennedy, R.T. Microfluidic chip for high efficiency electrophoretic analysis of segmented flow from a microdialysis probe and in vivo chemical monitoring. *Anal. Chem.* **2009**, *81*, 9072.
52. Sternling, C.; Scriven, L. Interfacial turbulence: Hydrodynamic instability and the marangoni effect. *AIChE J.* **1959**, *5*, 514-523.
53. Velarde, M.; Rednikov, A.Y.; Ryazantsev, Y.S. Drop motions and interfacial instability. *J. Phys.: Condens. Matter* **1996**, *8*, 9233.
54. Davis Jr, J.H.; Fox, P.A. From curiosities to commodities: Ionic liquids begin the transition. *Chem. Commun.* **2003**, 1209-1212.
55. Rogers, R.D.; Seddon, K.R.; Industrial, A.C.S.D.o.; Chemistry, E.; Meeting, A.C.S. *Ionic liquids as green solvents: Progress and prospects*. American Chemical Society: 2003.
56. Seddon, K. The international george papatheodorou symposium: Proceedings. *Boghosian, S*, 131-135.
57. Zhang, S.; Sun, N.; He, X.; Lu, X.; Zhang, X. Physical properties of ionic liquids: Database and evaluation. *J. Phys. Chem. Ref. Data* **2006**, *35*, 1475-1517.
58. Zahn, S.; Uhlig, F.; Thar, J.; Spickermann, C.; Kirchner, B. Intermolecular forces in an ionic liquid ([mmim][cl]) versus those in a typical salt (nacl). *Angew. Chem. Int. Ed.* **2008**, *47*, 3639-3641.
59. Zahn, S.; Bruns, G.; Thar, J.; Kirchner, B. What keeps ionic liquids in flow? *PCCP* **2008**, *10*, 6921-6924.
60. Wasserscheid, P.; Keim, W. Ionic liquids—new “solutions” for transition metal catalysis. *Angew. Chem. Int. Ed.* **2000**, *39*, 3772-3789.

61. Bonhote, P.; Dias, A.-P.; Papageorgiou, N.; Kalyanasundaram, K.; Grätzel, M. Hydrophobic, highly conductive ambient-temperature molten salts. *Inorg. Chem.* **1996**, *35*, 1168-1178.
62. Fraser, K.J.; MacFarlane, D.R. Phosphonium-based ionic liquids: An overview. *Aust. J. Chem.* **2009**, *62*, 309-321.
63. Rogers, R.D.; Seddon, K.R. Ionic liquids--solvents of the future? *Science* **2003**, *302*, 792-793.
64. Earle, M.J.; Seddon, K.R. Ionic liquids. Green solvents for the future. *Pure Appl. Chem.* **2000**, *72*, 1391-1398.
65. Wasserscheid, P.; Welton, T. *Ionic liquids in synthesis*. Wiley Online Library: 2008; Vol. 1.
66. Wasserscheid, P.; Keim, W. Ionic liquids-new " solutions" for transition metal catalysis. *Angew. Chem.* **2000**, *39*, 3772-3789.
67. Wilkes, J.S.; Zaworotko, M.J. Air and water stable 1-ethyl-3-methylimidazolium based ionic liquids. *J. Chem. Soc., Chem. Commun.* **1992**, 965-967.
68. Thompson, D.; Coleman, S.; Diamond, D.; Byrne, R. Electronic structure calculations and physicochemical experiments quantify the competitive liquid ion association and probe stabilisation effects for nitrobenzospiropyran in phosphonium-based ionic liquids. *PCCP* **2011**, *13*, 6156-6168.
69. Asadov, Z.; Akhmedova, G.; Aga-Zadeh, A.; Nasibova, S.M.; Zarbalieva, I.; Bagirova, A.; Ragimov, R. Ionic liquid surfactants. *Russ. J. Gen. Chem.* **2012**, *82*, 1916-1927.
70. Merrigan, T.L.; Bates, E.D.; Dorman, S.C.; Davis Jr, J.H. New fluoros ionic liquids function as surfactants in conventional room-temperature ionic liquids. *Chem. Commun.* **2000**, 2051-2052.
71. Yan, F.; Texter, J. Surfactant ionic liquid-based microemulsions for polymerization. *Chem. Commun.* **2006**, 2696-2698.
72. Flieger, J.; Siwek, A.; Pizoń, M.; Czajkowska-Żelazko, A. Ionic liquids as surfactants in micellar liquid chromatography. *J. Sep. Sci.* **2013**, *36*, 1530-1536.
73. Trivedi, T.J.; Rao, K.S.; Singh, T.; Mandal, S.K.; Sutradhar, N.; Panda, A.B.; Kumar, A. Task-specific, biodegradable amino acid ionic liquid surfactants. *ChemSusChem* **2011**, *4*, 604-608.
74. Galiński, M.; Lewandowski, A.; Stępnia, I. Ionic liquids as electrolytes. *Electrochim. Acta* **2006**, *51*, 5567-5580.
75. Ye, Y.-S.; Rick, J.; Hwang, B.-J. Ionic liquid polymer electrolytes. *Journal of Materials Chemistry A* **2013**, *1*, 2719-2743.
76. Lewandowski, A.; Świdarska-Mocek, A. Ionic liquids as electrolytes for li-ion batteries—an overview of electrochemical studies. *J. Power Sources* **2009**, *194*, 601-609.
77. Fuller, J.; Breda, A.C.; Carlin, R.T. Ionic liquid-polymer gel electrolytes from hydrophilic and hydrophobic ionic liquids. *J. Electroanal. Chem.* **1998**, *459*, 29-34.
78. Noda, A.; Susan, M.A.B.H.; Kudo, K.; Mitsushima, S.; Hayamizu, K.; Watanabe, M. Brønsted acid-base ionic liquids as proton-conducting nonaqueous electrolytes. *The Journal of Physical Chemistry B* **2003**, *107*, 4024-4033.
79. Barisci, J.; Wallace, G.; MacFarlane, D.; Baughman, R. Investigation of ionic liquids as electrolytes for carbon nanotube electrodes. *Electrochem. Commun.* **2004**, *6*, 22-27.

80. Kuboki, T.; Okuyama, T.; Ohsaki, T.; Takami, N. Lithium-air batteries using hydrophobic room temperature ionic liquid electrolyte. *J. Power Sources* **2005**, *146*, 766-769.
81. Kaljurand, M. Ionic liquids as electrolytes for nonaqueous capillary electrophoresis. *Electrophoresis* **2002**, *23*, 426-430.
82. Ding, J.; Zhou, D.; Spinks, G.; Wallace, G.; Forsyth, S.; Forsyth, M.; MacFarlane, D. Use of ionic liquids as electrolytes in electromechanical actuator systems based on inherently conducting polymers. *Chem. Mater.* **2003**, *15*, 2392-2398.
83. Ong, S.P.; Andreussi, O.; Wu, Y.; Marzari, N.; Ceder, G. Electrochemical windows of room-temperature ionic liquids from molecular dynamics and density functional theory calculations. *Chem. Mater.* **2011**, *23*, 2979-2986.
84. Vaughan, J.; Dreisinger, D. Electrodeposition of aluminum from aluminum chloride-trihexyl (tetradecyl) phosphonium chloride. *J. Electrochem. Soc.* **2008**, *155*, D68-D72.
85. Buzzeo, M.C.; Hardacre, C.; Compton, R.G. Extended electrochemical windows made accessible by room temperature ionic liquid/organic solvent electrolyte systems. *Chemphyschem* **2006**, *7*, 176-180.
86. Wessells, C.; Ruffo, R.; Huggins, R.A.; Cui, Y. Investigations of the electrochemical stability of aqueous electrolytes for lithium battery applications. *Electrochem. Solid-State Lett.* **2010**, *13*, A59-A61.
87. Zhao, L.; Hu, Y.S.; Li, H.; Wang, Z.; Chen, L. Porous  $\text{Li}_4\text{Ti}_5\text{O}_{12}$  coated with n-doped carbon from ionic liquids for li-ion batteries. *Adv. Mater.* **2011**, *23*, 1385-1388.
88. Armand, M.; Tarascon, J.-M. Building better batteries. *Nature* **2008**, *451*, 652-657.
89. Sakaebe, H.; Matsumoto, H.; Tatsumi, K. Application of room temperature ionic liquids to li batteries. *Electrochim. Acta* **2007**, *53*, 1048-1054.
90. Fields, M.; Hutson, G.V.; Seddon, K.R.; Gordon, C.M. Ionic liquids as solvents. Google Patents: 2002.
91. Kubisa, P. Application of ionic liquids as solvents for polymerization processes. *Prog. Polym. Sci.* **2004**, *29*, 3-12.
92. Deetlefs, M.; Seddon, K.R.; Shara, M. Predicting physical properties of ionic liquids. *PCCP* **2006**, *8*, 642-649.
93. Earle, M.J.; Katdare, S.P.; Seddon, K.R. Paradigm confirmed: The first use of ionic liquids to dramatically influence the outcome of chemical reactions. *Org. Lett.* **2004**, *6*, 707-710.
94. Rebelo, L.P.N.; Lopes, J.N.C.; Esperanca, J.M.; Guedes, H.J.; Łachwa, J.; Najdanovic-Visak, V.; Visak, Z.P. Accounting for the unique, doubly dual nature of ionic liquids from a molecular thermodynamic and modeling standpoint. *Acc. Chem. Res.* **2007**, *40*, 1114-1121.
95. Kunz, W.; Häckl, K. The hype with ionic liquids as solvents. *Chem. Phys. Lett.* **2016**, *661*, 6-12.
96. Petkovic, M.; Seddon, K.R.; Rebelo, L.P.N.; Pereira, C.S. Ionic liquids: A pathway to environmental acceptability. *Chem. Soc. Rev.* **2011**, *40*, 1383-1403.
97. Zhang, S.; Dong, K. *Structures and interactions of ionic liquids*. Springer: 2013; Vol. 151.
98. Reichardt, C. Solvatochromic dyes as solvent polarity indicators. *Chem. Rev.* **1994**, *94*, 2319-2358.

99. Shetty, P.H.; Youngberg, P.J.; Kersten, B.R.; Poole, C.F. Solvent properties of liquid organic salts used as mobile phases in microcolumn reversed-phase liquid chromatography. *J. Chromatogr. A* **1987**, *411*, 61-79.
100. Poole, S.K.; Shetty, P.H.; Poole, C.F. Chromatographic and spectroscopic studies of the solvent properties of a new series of room-temperature liquid tetraalkylammonium sulfonates. *Anal. Chim. Acta* **1989**, *218*, 241-264.
101. Furton, K.G.; Morales, R. Effect of anion chain length on the solvent properties of liquid tetrabutylammonium alkylsulfonate salts studied by gas—liquid chromatography. *Anal. Chim. Acta* **1991**, *246*, 171-179.
102. Welton, T. Room-temperature ionic liquids. Solvents for synthesis and catalysis. *Chem. Rev.* **1999**, *99*, 2071-2084.
103. Jaeger, D.A.; Tucker, C.E. Diels-alder reactions in ethylammonium nitrate, a low-melting fused salt. *Tetrahedron Lett.* **1989**, *30*, 1785-1788.
104. Kaufmann, D.E.; Nouroozian, M.; Henze, H. Molten salts as an efficient medium for palladium catalyzed cc coupling reactions. *Synlett* **1996**, *1996*, 1091-1092.
105. Quillin, K. Ontogenetic scaling of hydrostatic skeletons: Geometric, static stress and dynamic stress scaling of the earthworm lumbricus terrestris. *J. Exp. Biol.* **1998**, *201*, 1871-1883.
106. Menciassi, A.; Gorini, S.; Pernorio, G.; Dario, P. In *A sma actuated artificial earthworm*, Robotics and Automation, 2004. Proceedings. ICRA'04. 2004 IEEE International Conference on, 2004; IEEE: pp 3282-3287.
107. Murakami, Y.; Uchiyama, H.; Kurata, J.; Maeda, M. In *Dynamical locomotion analysis and a model for the peristaltic motion of earthworms*, 2006 SICE-ICASE International Joint Conference, 2006; IEEE: pp 4224-4229.
108. Martinez, R.V.; Glavan, A.C.; Keplinger, C.; Oyetibo, A.I.; Whitesides, G.M. Soft actuators and robots that are resistant to mechanical damage. *Adv. Funct. Mater.* **2014**, *24*, 3003-3010.
109. Tahara, K.; Arimoto, S.; Yoshida, M. In *Dynamic object manipulation using a virtual frame by a triple soft-fingered robotic hand*, Robotics and Automation (ICRA), 2010 IEEE International Conference on, 2010; IEEE: pp 4322-4327.
110. She, Y.; Li, C.; Cleary, J.; Su, H.-J. Design and fabrication of a soft robotic hand with embedded actuators and sensors. *Journal of Mechanisms and Robotics* **2015**, *7*, 021007.
111. Bogue, R.; Bogue, R. Flexible and soft robotic grippers: The key to new markets? *Industrial Robot: An International Journal* **2016**, *43*, 258-263.
112. Krahn, J.; Fabbro, F.; Menon, C. A soft-touch gripper for grasping delicate objects. *IEEE/ASME Transactions on Mechatronics* **2017**.
113. Shepherd, R.F.; Ilievski, F.; Choi, W.; Morin, S.A.; Stokes, A.A.; Mazzeo, A.D.; Chen, X.; Wang, M.; Whitesides, G.M. Multigait soft robot. *Proceedings of the National Academy of Sciences* **2011**, *108*, 20400-20403.
114. Martinez, R.V.; Branch, J.L.; Fish, C.R.; Jin, L.; Shepherd, R.F.; Nunes, R.; Suo, Z.; Whitesides, G.M. Robotic tentacles with three-dimensional mobility based on flexible elastomers. *Adv. Mater.* **2013**, *25*, 205-212.
115. Kim, S.; Laschi, C.; Trimmer, B. Soft robotics: A bioinspired evolution in robotics. *Trends Biotechnol.* **2013**, *31*, 287-294.
116. Moon, J.J.; Saik, J.E.; Poche, R.A.; Leslie-Barbick, J.E.; Lee, S.-H.; Smith, A.A.; Dickinson, M.E.; West, J.L. Biomimetic hydrogels with pro-angiogenic properties. *Biomaterials* **2010**, *31*, 3840-3847.

117. Venkatesh, S.; Sizemore, S.P.; Byrne, M.E. Biomimetic hydrogels for enhanced loading and extended release of ocular therapeutics. *Biomaterials* **2007**, *28*, 717-724.
118. Morales, D.; Palleau, E.; Dickey, M.D.; Velev, O.D. Electro-actuated hydrogel walkers with dual responsive legs. *Soft Matter* **2014**, *10*, 1337-1348.
119. Wang, Q.; Zhao, Y.; Yang, Y.; Xu, H.; Yang, X. Thermosensitive phase behavior and drug release of in situ gelable poly (n-isopropylacrylamide-co-acrylamide) microgels. *Colloid. Polym. Sci.* **2007**, *285*, 515-521.
120. Kim, J.H.; Randall Lee, T. Discrete thermally responsive hydrogel-coated gold nanoparticles for use as drug-delivery vehicles. *Drug Dev. Res.* **2006**, *67*, 61-69.
121. Weng, H.; Zhou, J.; Tang, L.; Hu, Z. Tissue responses to thermally-responsive hydrogel nanoparticles. *J. Biomater. Sci. Polym. Ed.* **2004**, *15*, 1167-1180.
122. Kim, J.-H.; Lee, T.R. Thermo- and pH-responsive hydrogel-coated gold nanoparticles. *Chem. Mater.* **2004**, *16*, 3647-3651.
123. Ozay, O.; Ekici, S.; Baran, Y.; Aktas, N.; Sahiner, N. Removal of toxic metal ions with magnetic hydrogels. *Water Res.* **2009**, *43*, 4403-4411.
124. Peppas, N.A.; Bures, C.D. Glucose-responsive hydrogels. *Encyclopedia of Biomaterials and Biomedical Engineering*, DOI **2006**, *10*.
125. Miyata, T.; Asami, N.; Uragami, T. A reversibly antigen-responsive hydrogel. *Nature* **1999**, *399*, 766-769.
126. Murdan, S. Electro-responsive drug delivery from hydrogels. *J. Controlled Release* **2003**, *92*, 1-17.
127. Ziółkowski, B.; Florea, L.; Theobald, J.; Benito-Lopez, F.; Diamond, D. Self-protonating spiropyran-co-nipam-co-acrylic acid hydrogel photoactuators. *Soft Matter* **2013**, *9*, 8754-8760.
128. Dumitriu, R.P.; Mitchell, G.R.; Vasile, C. Multi-responsive hydrogels based on n-isopropylacrylamide and sodium alginate. *Polym. Int.* **2011**, *60*, 222-233.
129. Tudor, A.; Florea, L.; Gallagher, S.; Burns, J.; Diamond, D. Poly (ionic liquid) semi-interpenetrating network multi-responsive hydrogels. *Sensors* **2016**, *16*, 219.
130. Costa, R.O.; Freitas, R.F. Phase behavior of poly (n-isopropylacrylamide) in binary aqueous solutions. *Polymer* **2002**, *43*, 5879-5885.
131. Breger, J.C.; Yoon, C.; Xiao, R.; Kwag, H.R.; Wang, M.O.; Fisher, J.P.; Nguyen, T.D.; Gracias, D.H. Self-folding thermo-magnetically responsive soft microgrippers. *ACS applied materials & interfaces* **2015**, *7*, 3398-3405.
132. Gupta, P.; Vermani, K.; Garg, S. Hydrogels: From controlled release to pH-responsive drug delivery. *Drug Discovery Today* **2002**, *7*, 569-579.
133. Schmaljohann, D. Thermo- and pH-responsive polymers in drug delivery. *Adv. Drug Del. Rev.* **2006**, *58*, 1655-1670.
134. Li, X.; Cai, X.; Gao, Y.; Serpe, M.J. Reversible bidirectional bending of hydrogel-based bilayer actuators. *Journal of Materials Chemistry B* **2017**, *5*, 2804-2812.
135. Yang, C.; Wang, W.; Yao, C.; Xie, R.; Ju, X.-J.; Liu, Z.; Chu, L.-Y. Hydrogel walkers with electro-driven motility for cargo transport. *Sci. Rep.* **2015**, *5*.
136. Byrne, R.; Benito-Lopez, F.; Diamond, D. Materials science and the sensor revolution. *Mater. Today* **2010**, *13*, 9-16.
137. Irie, M.; Uchida, K. Synthesis and properties of photochromic diarylethenes with heterocyclic aryl groups. *Bull. Chem. Soc. Jpn.* **1998**, *71*, 985-996.
138. Diguët, A.; Guillermic, R.-M.; Magome, N.; Saint-Jalmes, A.; Chen, Y.; Yoshikawa, K.; Baigl, D. Photomanipulation of a droplet by the chromocapillary effect. *Angewandte Chemie (International ed. in English)* **2009**, *48*, 9281-9284.

139. it Bandyopadhyay, S. The syntheses and properties of photochromic systems based on dimethyldihydropyrenes. University of Victoria, 2004.
140. Yassar, A.; Garnier, F.; Jaafari, H.; Rebiere-Galy, N.; Frigoli, M.; Moustrou, C.; Samat, A.; Guglielmetti, R. Light-triggered molecular devices based on photochromic oligothiophene substituted chromenes. *Appl. Phys. Lett.* **2002**, *80*, 4297-4299.
141. Crano, J.C.; Flood, T.; Knowles, D.; Kumar, A.; VanGemert, B. Photochromic compounds: Chemistry and application in ophthalmic lenses. *Pure and Applied Chemistry* **1996**, *68*, 1395-1398.
142. Fries, K.H.; Driskell, J.D.; Samanta, S.; Locklin, J. Spectroscopic analysis of metal ion binding in spiropyran containing copolymer thin films. *Anal. Chem.* **2010**, *82*, 3306-3314.
143. Fries, K.H.; Driskell, J.D.; Sheppard, G.R.; Locklin, J. Fabrication of spiropyran-containing thin film sensors used for the simultaneous identification of multiple metal ions. *Langmuir* **2011**, *27*, 12253-12260.
144. Benito-Lopez, F.; Scarmagnani, S.; Walsh, Z.; Paull, B.; Macka, M.; Diamond, D. Spiropyran modified micro-fluidic chip channels as photonically controlled self-indicating system for metal ion accumulation and release. *Sens. Actuators, B* **2009**, *140*, 295-303.
145. Minkin, V.I. Photo-, thermo-, solvato-, and electrochromic spiroheterocyclic compounds. *Chem. Rev.* **2004**, *104*, 2751-2776.
146. Anastasiadis, S.H.; Lygeraki, M.I.; Athanassiou, A.; Farsari, M.; Pisignano, D. Reversibly photo-responsive polymer surfaces for controlled wettability. *J. Adhes. Sci. Technol.* **2008**, *22*, 1853-1868.
147. Gorner, H. Photochromism of nitrospiropyrans: Effects of structure, solvent and temperature. *Physical Chemistry Chemical Physics* **2001**, *3*, 416-423.
148. Florea, L.; Diamond, D.; Benito-Lopez, F. Photo-responsive polymeric structures based on spiropyran. *Macromolecular Materials and Engineering* **2012**, *297*, 1148-1159.
149. Rosario, R.; Gust, D.; Hayes, M.; Jahnke, F.; Springer, J.; Garcia, A.A. Photon-modulated wettability changes on spiropyran-coated surfaces. *Langmuir* **2002**, *18*, 8062-8069.
150. Shao, N.; Jin, J.; Wang, H.; Zheng, J.; Yang, R.; Chan, W.; Abliz, Z. Design of bis-spiropyran ligands as dipolar molecule receptors and application to in vivo glutathione fluorescent probes. *J. Am. Chem. Soc.* **2009**, *132*, 725-736.
151. Rosario, R.; Gust, D.; Hayes, M.; Springer, J.; Garcia, A.A. Solvatochromic study of the microenvironment of surface-bound spiropyrans. *Langmuir* **2003**, *19*, 8801-8806.
152. Dunne, A.; Delaney, C.; Florea, L.; Diamond, D. Solvato-morphologically controlled, reversible nipaam hydrogel photoactuators. *RSC Advances* **2016**, *6*, 83296-83302.
153. Benito-Lopez, F.; Antoñana-Díez, M.; Curto, V.F.; Diamond, D.; Castro-López, V. Modular microfluidic valve structures based on reversible thermoresponsive ionogel actuators. *Lab on a Chip* **2014**, *14*, 3530-3538.
154. Czugala, M.; O'Connell, C.; Blin, C.; Fischer, P.; Fraser, K.J.; Benito-Lopez, F.; Diamond, D. Swelling and shrinking behaviour of photoresponsive phosphonium-based ionogel microstructures. *Sensors Actuators B: Chem.* **2014**, *194*, 105-113.
155. Benito-Lopez, F.; Byrne, R.; Răduță, A.M.; Vrana, N.E.; McGuinness, G.; Diamond, D. Ionogel-based light-actuated valves for controlling liquid flow in micro-fluidic manifolds. *Lab on a Chip* **2010**, *10*, 195-201.

156. ter Schiphorst, J.; Coleman, S.; Stumpel, J.E.; Ben Azouz, A.; Diamond, D.; Schenning, A.P. Molecular design of light-responsive hydrogels, for in situ generation of fast and reversible valves for microfluidic applications. *Chem. Mater.* **2015**, *27*, 5925-5931.
157. Stumpel, J.E.; Ziółkowski, B.; Florea, L.; Diamond, D.; Broer, D.J.; Schenning, A.P. Photoswitchable ratchet surface topographies based on self-protonating spiropyran–nipaam hydrogels. *ACS applied materials & interfaces* **2014**, *6*, 7268-7274.

## **Chapter 2:**

### **Stimuli-Controlled Fluid Control and Microvehicle Movement in Microfluidic Channels**

#### **2.1 Abstract**

#### **2.2 Introduction**

#### **2.3 Stimuli-Controlled Manipulation of Synthetic Discrete Micrometre-Sized “Vehicles”**

##### **2.3.1 Actuation through Localised Changes in Wettability**

###### 2.3.1.1 Digital Microfluidics

###### 2.3.1.2 Electrowetting on Dielectric

###### 2.3.1.3 Dielectrophoresis

##### **2.3.2 Alternative Methods for Droplet Actuation**

###### 2.3.2.1 Photo-Induced Actuation

###### 2.3.2.2 Thermo-Induced Actuation

###### 2.3.2.3 Magnetic-Induced Actuation

###### 2.3.2.4 Surface Acoustic Waves

#### **2.4 Actuation through Localised Changes in Surface Tension**

##### **2.4.1 Surfactant Saturated Systems**

##### **2.4.2 “Vehicle” Contained Surfactants**

#### **2.5 Conclusions and Outlook**

#### **2.6 References**

## Chapter 2

---

# Stimuli-Controlled Fluid Control and Microvehicle Movement in Microfluidic Channels\*

---

\*Stimuli-controlled fluid control and microvehicle movement in microfluidic channels, A. Dunne, **W. Francis**, C. Delaney, L. Florea, D. Diamond. *The Reference Module in Materials Science and Materials Engineering*, 2017

## 2.1 Abstract

Integration of stimuli-responsive materials into microfluidic systems provides a means to locally manipulate flow at the microscale, in a non-invasive manner, while also reducing system complexity. In recent years, several modes of stimulation have been applied, including electrical, magnetic, light and temperature, among others. To achieve remote control of flow in microfluidics using external stimulation, stimuli-controlled manipulation of discrete micrometer-sized “vehicles” (droplets, beads, Janus particles, *etc.*) through localized induced changes in wettability or surface tension has emerged in the recent years. The focus of this chapter will be to identify and compare the similarities and underlying mechanisms employed in the current state of the art research in stimuli-controlled micro-vehicle movement. It will also endeavor to propose possible directions for the evolution of this area of research.

## 2.2 Introduction

Since the onset of research into microfluidics during the 1990s, there has been much progress made in the generation and control of flow in micrometre-sized devices [1,2]. The aim of these tiny devices is to perform complex biological and chemical tasks on a single chip [3]. Advantages of this approach include a significant reduction in reactant volume (down to microlitres or even picolitres), parallel processing of multiple analytes, portability,[4] multistage automation [5], single cell sampling [6] and manipulation [7]. Therefore, the potential for microfluidic devices is tremendous. Nevertheless, the microfluidics field is still very much in its infancy and a number of areas are constantly under investigation, including micro-fabrication, component integration, device generalisation and fluid flow and control [8]. Despite considerable advances in recent years, fluid handling on microfluidic chips still relies, in many cases, on macroscopic external control boxes containing power supplies, high power sources, sensing elements and complicated control systems based on external computers and/or electronics [9] . While there are still many challenges facing this field, there have been a number of revolutionary approaches, one of the most exciting of which is the incorporation of stimuli-responsive actuators within the fluidics, to achieve integrated fluid handling on-chip. This approach can result in flow control [10,11], mixing [12], flow sorting [13], pumping [14] and even sensing components fully integrated into the microfluidics chip

[15]. Recent developments in stimuli-responsive materials, and particularly stimuli responsive polymers and surfaces make microfluidics a great platform for demonstrating the capabilities and highlighting the functionality of these materials [16,17]. Indeed, the microfluidic platform generally enhances the functionality of smart materials by offering faster kinetics and shorter reaction times due to increased surface to volume ratios; improved interfacial and chemical interactions; dominant surface tension and capillarity effects and efficient absorption of electro-magnetic radiation.

To date, one of the main approaches to achieve flow control in microfluidic devices involves using stimuli-responsive materials, including discrete micrometre-sized droplets which are externally manipulated through stimuli-induced changes in wettability or surface tension. This chapter will focus on these particular approaches for microvehicle movement, with the motivation of identifying and comparing current state of the art methodologies and offering the reader an up-to-date view of this exciting research area.

### **2.3 Stimuli-Controlled Manipulation of Synthetic Discrete Micrometer-Sized “Vehicles”**

Controlled movement of micro “vehicles” offers many intriguing and beneficial opportunities in the microfluidics field. For example, in droplet based microfluidic devices, the high surface area to volume ratio results in high heat and mass transfer rates. Also, most droplet microfluidic chips allow for control over individual droplets, thus allowing them to act as micro-vessels which can be mixed or merged with other droplets, moved to desired destinations or even individually analysed. These properties allow the droplets to have a diverse range of applications including micro-vessels for chemical reactions, dynamic sensing, cargo transport and potential drug delivery units [18,19]. This section will focus on the most popular actuation methods employed thus far for stimuli controlled-movement of synthetic “vehicles” (*e.g.* droplets, beads, gels). Although the majority of the actuation methods described to date were not explored in microfluidics, the same concepts could be applied to work within a microfluidic system. These “vehicles” could also be used to mimic biological vesicles, which transport nutrients in and out of cells through highly regulated pathways, for drug transport and targeted delivery.

Actuation of liquids in the form of synthetic “vehicles” offers many advantages over conventional laminar flow microfluidic systems, which rely upon the use of pumps and valves to control and direct flow, while stimuli-controlled droplet microfluidic systems allow for external manipulation of individual or multiple droplets simultaneously. These “vehicles” can act as micro-reactors, cargo-carriers, and can be used to transport or store volumes of reagents down to the picoliter range [20,21].

Actuation of droplets can be categorised based on two main mechanisms. The first mechanism (and the most widely used) involves control over the wettability of a substrate, such as polymeric plastics (*e.g.* polydimethylsiloxane (PDMS), poly(methyl methacrylate) (PMMA)), glass and silicon wafers, which allows for unidirectional movement of droplets over the substrate. One of the most popular droplet actuation methods based on this principle is known as digital microfluidics (DMF). In DMF small discrete droplets are transported across an array of individually addressable electrodes, by controlling the displacement of the droplet through localised control of surface polarisation and wettability. Additionally, many research groups have explored the use of different alternative stimuli such as light [22-27], temperature [28-33] and magnetic stimuli [34-39] for wettability control.

The second mechanism involves manipulation of the surface tension of a liquid. This allows controllable movement of droplets or other “vehicles” at the liquid/air interface. To control the surface tension of a liquid, surfactants are used. Through the asymmetrical release or alteration of the surface activity of stimuli-responsive surfactants, surface tension gradients can be created around the droplet. This in turn results in Marangoni flows, through which liquid spontaneously moves from areas of low surface tension towards areas of high surface tension. Thus, through contactless control over the surface tension of an aqueous solution, unidirectional movement of a droplet resting at the liquid/air interface can be achieved. This type of surfactant driven movement can be broken down into two main actuation mechanisms, either by addition of the surfactant to the aqueous medium or inclusion of the surfactant in the ‘vehicle’. In the first approach, with stimuli-responsive surfactants dispersed in the aqueous solution, application of an appropriate stimulus to the surfactant alters its surface activity, which results in a change in the local surface tension. This in turn causes a flow of liquid towards areas of higher surface tension; any droplet or “vehicle” resting on the surface of the liquid will be consequently transported in the direction of the flow. In the second approach, the surfactant is contained within the “vehicle” itself and its asymmetric release is externally

controlled, resulting in a surface tension gradient around the droplet, which triggers unidirectional droplet movement.

### **2.3.1 Actuation through Localised Changes in Wettability**

This concept involves moving droplets on a substrate to targeted areas, through changes in the wettability of the substrate. Numerous reviews and articles have been published in this area in the past decade which provide comprehensive overviews of the topic [19,40,41]. This section will focus on the “vehicle” movement mechanism and the different means for achieving “vehicle” actuation. Several applications will be mentioned and discussed.

#### **2.3.1.1 Digital Microfluidics**

In DMF, droplets are actuated on an array of electrodes which are individually addressable. Using this array of electrodes, a wettability gradient can be generated on the substrate by applying different voltages between adjacent electrodes. The droplet can be then moved along this electro-generated wettability gradient to a desired destination by continually altering the potential difference between neighbouring electrodes. The droplets are produced from reservoirs within the chip and they can be split, mixed with other droplets or simply used to transport cargo inside the chip [40]. There are two types of actuation mechanisms required for this mechanism; the first involves the initial generation of the droplets from a reservoir and the second is needed for movement of the droplets through the system. The two main methods of electro-chemical control over droplet formation and movement in DMF systems are dielectrophoresis (DEP) and electrowetting on dielectric (EWOD). Alternative actuation for DMF utilizes thermocapillary transport, surface acoustic wave transport (SAWS) and optical forces and magnetic forces [40,41].

Applications of DMF systems include bio-assays [42], DNA applications, such as polymerase chain reactions (PCR) [43,44], separation and analysis of aminoacids, peptides and other biological molecules [45], cell based assays [46], proteomics [47], and adaptive cooling of integrated circuits systems [48].

### 2.3.1.2 Electrowetting on Dielectric

The phenomenon termed electrowetting on dielectric (EWOD) is one of the main forms of actuation associated with DMF. In EWOD the interfacial tension between an aqueous droplet and electrode is electrically altered in such a manner as to actuate the droplets across a series of electrodes. When a voltage is applied, the interfacial energy between the droplet and electrode surface is lowered, changing the wettability of the substrate [19,40]. Voltage range varies greatly depending on the application, but typically the values lie between 0 – 200 V [49-51]. For example a micro-sized droplet was split into two daughter droplets by applying a potential difference of 25 V between adjacent electrodes [49]. Interfacial energy directly affects the contact angle; by lowering the contact angle between the droplet and the surface, an interfacial energy gradient is created which actuates the droplet. By applying voltages to individual electrodes an interfacial energy gradient will be formed which the droplet follows [52]. In EWOD there are generally two possible set-ups, namely a single plate or a two-plate system. In a single plate (or open plate) system the droplet sits on a substrate, which contains both actuation and ground electrodes. The two-plate configuration is a closed system in which the droplet is held between two substrates. The top substrate contains a continuous ground electrode while the bottom layer houses the actuation electrodes. Figure 2.1 is a representation of a typical a) closed, b) open and c) operation of both open plate (single) and closed plate (double) DMF systems. In both cases the layer containing the actuation electrodes must be insulated and covered by a layer of hydrophobic material. The hydrophobic material ensures that the aqueous solutions do not wet the surface and thus form droplets; it also ensures that the droplets have a high contact angle with the substrate. Using the actuation electrodes this contact angle can be altered which can result in unidirectional movement of the droplet [52].

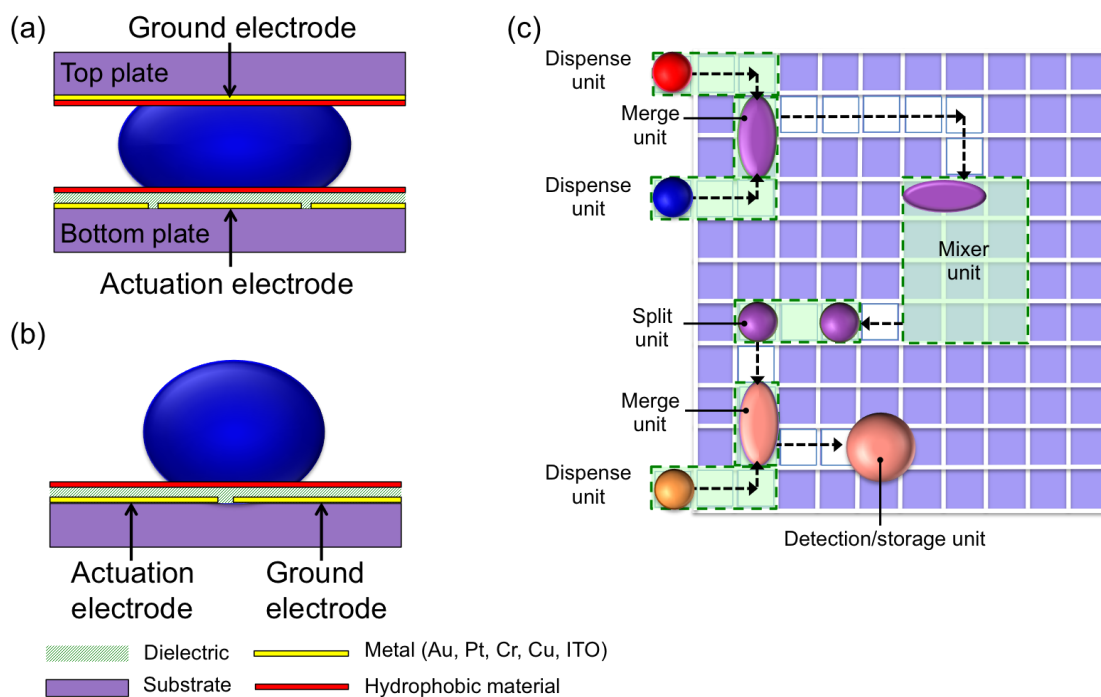


Figure 2.1 (a) Closed/two plate DMF system. (b) Open/one plate DMF system. (c) basic DMF operations. Adapted from [52] with permission from The Royal Society of Chemistry.

### 2.3.1.3 Dielectrophoresis

Dielectrophoresis (DEP) is one of the most popular techniques for the manipulation of droplets in DMF. DEP works by pulling (positive DEP) or pushing (negative DEP) a dielectric particle away from the actuation electrode. In a DEP driven system the particle does not necessarily need to have a charge, as all particles will exhibit electrostatic properties when introduced to an electric field. Typical frequencies for DEP driven systems are between 100 Hz – 10 MHz [53,54]. In DEP the particles are subjected to a non-uniform electric field, creating a dipole moment on the particle, that causes the droplet to be electrostatically pulled towards the actuated electrode. The size and uniformity of the droplets being formed in this manner depends on the magnitude and frequency of the applied voltage [55].

### 2.3.2. Alternative Methods for Substrate Droplet Actuation

Many research groups have explored alternative methods for achieving droplet actuation on a solid substrate. Although DMF is a great tool for the manipulation of discrete volumes of liquids in microfluidics, the chip designs are complicated and energy is required to move the droplets. The following sections will focus on alternative methods which use various types of stimuli for moving droplets on a solid substrate.

### 2.3.2.1 Photo-Induced Actuation

Optoelectrowetting (OEW) has a similar mechanism to EWOD, however, in OEW a photoconductive layer (generally amorphous silicon) is inserted between the dielectric layer and the electrodes layer. Droplet actuation is achieved when a voltage is applied across the insulating layer of the device. In darkness, the resistance of the photoconductive layer is high, resulting in the insulating layer receiving no voltage, meaning that the contact angle between the droplet and the substrate remains unchanged and therefore, no actuation is achieved. Upon illumination, the conductivity of the photoconductive layer increases. This results in the insulating layer receiving the applied voltage. In this fashion the contact angle of the droplet can be controlled with light and actuation can be achieved [24]. When an optical beam is used to irradiate on one end of the droplet, the contact angle is reduced in such a way that the pressure difference between both ends causes the droplet to follow the light beam. This was firstly demonstrated by Chiou *et al.* [24] in 2003 when a droplet was successfully actuated using a 525 nm laser with intensity of  $65 \text{ mW/cm}^2$ . The difference between an OEW device and a conventional EWOD device can be seen in Figure 2.2.

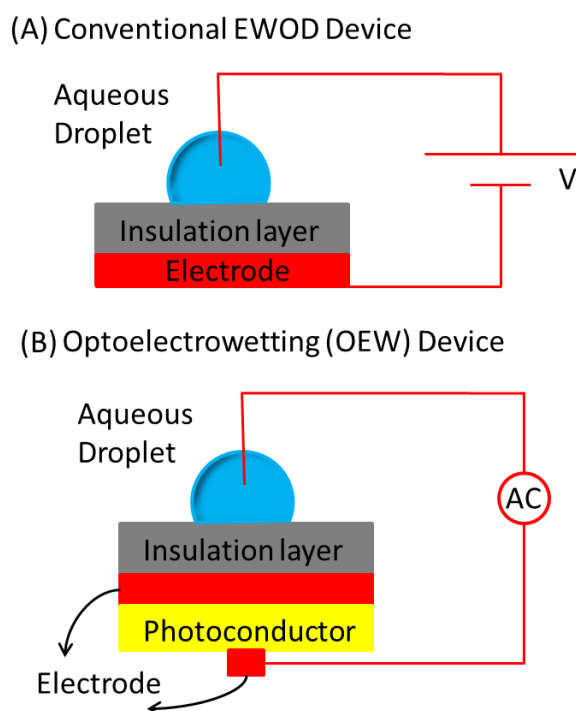


Figure 2.2 Schematic of (a) conventional EWOD and (b) an OEW device. The major difference between the two systems is the photoconductive layer inserted between the electrode and insulating layer in an OEW device. Adapted from [24].

Since Chiou and co-workers [24] successfully demonstrated photo-induced droplet actuation by using a photoconductive layer, many research groups have explored various means of photo-actuating droplets. Wereley *et al.* [25] developed a novel open-Optoelectrowetting (o-OEW) system which used a 670 nm laser with an intensity of 15 mW/cm<sup>2</sup>. Wereley's OEW system actuates droplets through photo-induced electrowetting of a substrate using a photoconductive layer, much like Chiou's device. However, in the chip designed by Wereley, all the electrodes needed for droplet actuation are contained within a single substrate. This open fluidic chip allows easier integration with additional components or chip extension.

Photo-induced actuation of droplets can also be achieved by creating photo-responsive surfaces. In this manner the hydrophobicity of the surface can be controlled through photo-stimulation. Various photo-responsive surfaces have been created by functionalising glass or polymeric surfaces with photo-sensitive units. Examples of widely used photo-sensitive molecules include spiropyrans and azobenzenes [27]. Under photo-irradiation these photo-responsive materials are reversibly switched between two isomers of different hydrophobic character and surface activities. When immobilised on surfaces, switching between the different isomers directly affects the wettability of the substrate allowing for photo-controlled droplet actuation. Rosario *et al.* [56] demonstrated actuation of water droplets across a rough and flat silicone surface coated with hydrophobic monolayers which contained photochromic spiropyrans. Under visible light, the spiropyran molecule was in its closed spiropyran (SP) hydrophobic state however, upon UV light (366 nm) irradiation, the SP isomer was switched to the more hydrophilic merocyanine (MC) form, reducing the contact angle between the water droplets and the surface. Therefore, unidirectional movement of the droplets was achieved through the use of UV/visible light generated wettability gradients.

Azobenzenes are another popular photochromic group, due to their reversible photoisomerization between *cis* and *trans* isomers. Azobenzenes were first used to control the wettability of a substrate by Siewierski *et al.* [57] in 1996. The paper describes two methods for preparing silicon surfaces coated with azobenzene monolayers. Irradiation of the monolayers with light of 354 nm resulted in the isomerisation of the azobenzene

within the monolayer to the *cis* conformation. This resulted in a decrease in the contact angle between water and the substrate. The contact angle difference in the case of all the monolayers were in the range of 2°-9° and the results were repeatable. The greatest photo-induced contact angle change was observed for a film prepared by acylation and had pentyl terminal groups. Under ambient laboratory conditions (in *trans* configuration) the azobenzene monolayer film had a contact angle with water of 85° while after UV irradiation (*cis* configuration) the contact angle was lowered to 76°. Since 1996 there has been much interest in azobenzenes and many research groups have used them for photo-actuation. Oh *et al.* [58] achieved photo-controlled directional movement of an oil droplet on an azobenzene-terminated monolayer modified silica substrate. This was realised by photo-isomerizing the azobenzene unit from the *cis* (contact angle of 11°) to *trans* (contact angle of 24°) conformation through asymmetrical blue light (436 nm) irradiation. Movement of the light source allowed for continuous droplet movement. The direction and speed of the droplet was dependent on the steepness and intensity of the light gradient.

### **2.3.2.2 Thermo-Induced Actuation**

Thermo-induced actuation provides an alternative method for controlling droplet movement on a substrate without chemical surface functionalization. This type of movement is known as thermocapillary transport of droplets. Droplet actuation is induced from the temperature variation which arises at the liquid/gas interface of the droplet, when placed on a solid substrate which has a temperature gradient. The temperature variation between the liquid/gas interfaces creates a surface tension ( $\delta$ ) gradient around the droplet from the warm (low  $\delta$ ) to the cool side (high  $\delta$ ). This asymmetrical gradient creates a flow within the droplet which applies a hydrodynamic force on the substrate. Since the solid surface is held in a fixed position it produces an equal and opposite force which actuates the droplet driving it to the cooler region [59]. Darhuber *et al.* [33] demonstrated that thermocapillary actuation can be used for droplet formation as well as moving droplets.

### **2.3.2.3 Magnetic-Induced Actuation**

Magnetic-induced actuation of droplets is achieved through the use of magnetic materials in various forms. A popular approach is to use liquid marbles, which are aqueous droplets that are rendered completely non-wetting by coating with magnetic hydrophobic powders. Since the powders are hydrophobic they are immiscible with the droplet and therefore, adhere to the exterior of the droplet. This results in a liquid droplet which does not stick to smooth substrates and can be manipulated using magnetic fields. Many research groups used iron or iron oxides micro-particles (due to their ferromagnetic properties) as the hydrophobic powders in order to create the liquid marble [34]. Zhao *et al* [36] demonstrated magnetic manipulation of a liquid marble on a glass substrate by coating their droplet with highly hydrophobic Iron(III) oxide ( $\text{Fe}_3\text{O}_4$ ) and placing a magnetic bar at one end of a glass substrate. Droplet actuation was achieved by slowly moving the magnet towards the droplet until this began to move. The droplet could then be made to follow the magnetic bar (by slowly moving the bar away from the droplet) across the glass substrate. Zhao and co-workers also demonstrated that the marble particles could be pulled from the liquid by placing a strong magnet directly under the droplet on the glass slide. To prove this, the group coated a water droplet containing a blue dye with  $\text{Fe}_3\text{O}_4$ . Once the droplet was coated, the dye was not visible. When the magnet was placed below, the droplet's coating was attracted to the bottom of the droplet, hence showing the dye. When the magnet was removed, the  $\text{Fe}_3\text{O}_4$  nanoparticles quickly moved back to the exposed liquid to reform the liquid marble.

#### **2.3.2.4 Surface Acoustic Waves**

Actuation of droplets can also be realised using surface acoustic waves (SAWs). In this case, actuation is achieved by producing acoustic radiation pressure on the surface of the substrate. This leads to an internal flow within the droplet and to eventual droplet actuation [60]. Wixforth *et al* [60] demonstrated actuation of a droplet across a piezoelectric chip through the use of SAW pumps. The chip was designed to have virtual beakers and channels which confined the liquid to the surface. Since the acoustic waves were electronically addressable they were able to act as programmable nanopumps. Another example of using SAWs to move droplets across a substrate was demonstrated by Guttenberg *et al.* [61]. Guttenberg developed a planar chip for polymerase chain reactions (PCR) and hybridization which utilizes SAWs for the movement of micro-droplets. The microfluidic device used had a planar piezoelectric Lithium niobate

(LiNbO<sub>3</sub>) substrate. The chip was chemically modified to produce high contact angles between the substrate and the droplet thus ensuring that the droplet movement was controlled through the SAW pump. The chip also contained thin film resistance heaters which provided the energy needed for the PCR reactions.

## **2.4 Actuation through Localised Changes in Surface Tension**

This type of actuation in the microfluidic sector is a relatively new concept compared to actuation through changes in wettability and involves generation and transport of droplets across liquid environments.

To achieve actuation through localised changes of surface tension at the liquid/liquid, liquid/gas interface, surfactants have been used as these have the unique property of modifying the surface tension of a liquid [62]. Although many stimuli-responsive surfactants have been synthesised, only a small number have been used for actuation of droplets or other micro-vehicles [63].

In the bulk of a liquid, the attractive forces between molecules are shared by all neighbouring molecules and no net force is felt as they cancel each other out. However, molecules at the interface (liquid/gas, liquid/liquid) have no attractive forces been exerted from above, therefore, they exhibit stronger forces between the nearest neighbouring molecules at the surface. This causes the molecules at the interface to contract forming a contractile layer (Figure 2.3). This contractile layer at the surface is known as the surface tension ( $\gamma$ ).

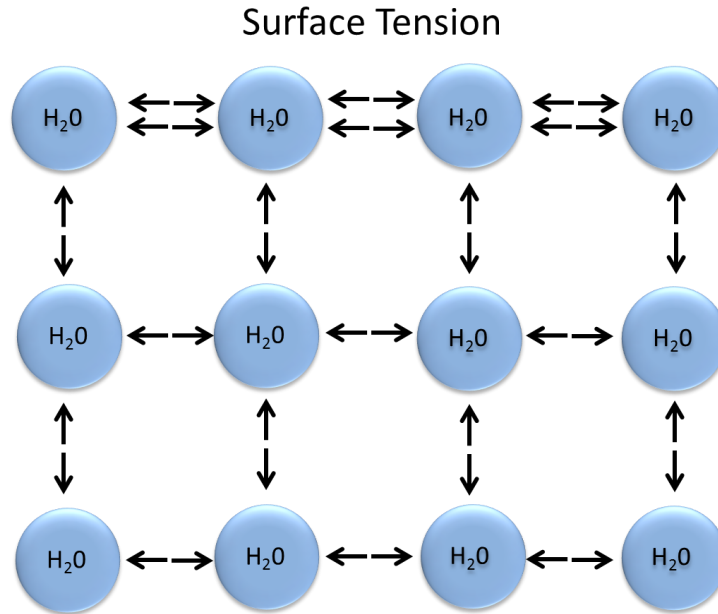


*Figure 2.3 Representation of the net forces in water.*

Certain molecules have special properties whereby they can imbed themselves at the interface and interrupt this elastic layer reducing the local surface tension. These molecules are known as surfactants. The term surfactant comes from surface active agents. Surfactants are molecules which are generally long chained amphiphiles which have a polar “head” and a non-polar tail. In an aqueous solution (below a certain concentration known as the critical micelle concentration (CMC)) the surfactant’s polar head will interact with the polar molecules at the surface. This interaction will interrupt neighbouring attractive forces and lower the surface tension of the solution.

Fluid flows from areas of low to high surface tension ( $\gamma$ ). This is known as the Marangoni effect. The Marangoni effect describes the mass transfer along an interface between two fluids due to a surface tension gradient. This causes convective flows in a bulk solution as well as inside of a “vehicle”. The following sections describe systems which take advantage of this effect to achieve activation of droplets along the liquid/gas interface.

#### **2.4.1 Surfactant Saturated Systems**

A surfactant saturated system is one in which surfactants are dissolved in the solution up to their particular CMC. This ensures that the surfactant molecules are concentrated at the interface instead of forming micelles. Marangoni flow can be induced if the surface tension of a targeted area is controlled. In order to induce movement through changes of

the surface tension, the surfactant's surface activity has to be altered. To control the surface activity, stimuli-responsive surfactants are used [64]. In this fashion, if the correct stimulus is applied to a targeted area of the system, Marangoni flows can be induced on demand. Photo-responsive surfactants have been used to externally control the surface tension of aqueous solutions. Direct irradiation of a targeted area is relatively simple and wavelengths can be tuned for particular molecules. Photo-responsive surfactants possessing two isomers with different surface activities have been shown to work in this fashion. Unidirectional movement of a micro-vehicle resting on an aqueous solution that contains photo-sensitive surfactant is achieved by irradiation of a specific area around the vehicle. This breaks the surface tension symmetry around the droplet and creates the Marangoni-like flows which drive the droplet either away or towards the light source. An example of a photo-switchable azobenzene surfactant (AzoTAB) is shown in Figure 2.4.

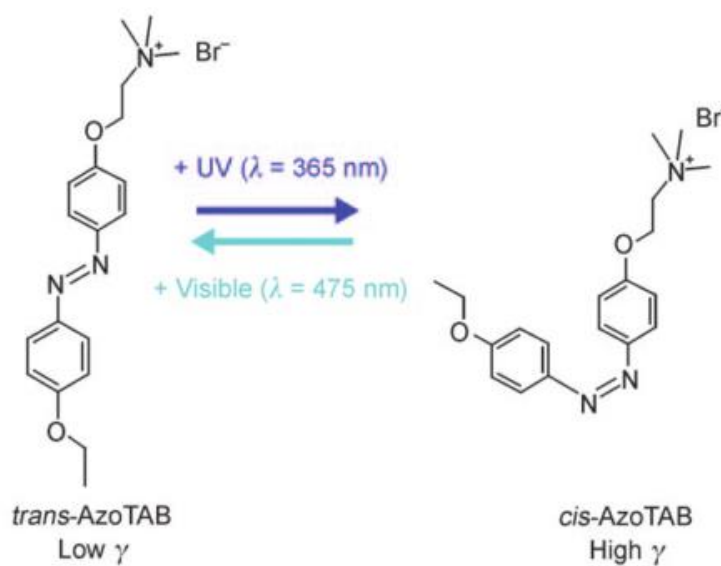


Figure 2.4 Photo-induced confirmation change of AzoTAB between its two isomers: from *trans* (high  $\gamma$ ) and to *cis* (low  $\gamma$ ). Adapted from [65] with permission from The Royal Society of Chemistry.

Diguet *et al.* [66] demonstrated photo-triggered movement using an oleic acid droplet resting on an aqueous solution containing the AzoTAB surfactant (Figure 18). The droplet of oleic acid can be moved by irradiating half of the droplet with either 365 nm or 475 nm light. When the AzoTAB surfactant is exposed to 365 nm of light, it is made to isomerise to its *cis* configuration. In this configuration the AzoTAB has a higher

surface tension ( $8 \text{ mN m}^{-1}$ ) than in the *trans* configuration ( $7 \text{ mN m}^{-1}$ ). Therefore, when half of the droplet was illuminated with 365 nm light it was made to follow the light source as the surface activity of the surfactant was higher compared with the non-irradiated section. When the droplet was irradiated with light of 475 nm, the AzoTAB isomerised to its *trans* configuration and thus lowered the surface tension of the solution, which resulted in the droplet being repelled by the light.

In order to achieve continuous droplet movement, the droplet was followed with the light source or trapped using a trap consisting of both light wavelengths (365 nm and 475 nm). Multiple droplets were also manipulated in a petri dish in this fashion.

Photo-actuation can also be used to control the flow within a microfluidic system. Recently it was demonstrated that the AzoTAB surfactant could be used to change the flow in a microfluidic system from laminar to segmented flow (droplets) [65]. Initially the system had a two-phase flow, one flow was aqueous (which contained the AzoTAB surfactant) and the second was an oil phase. When the aqueous phase was illuminated with light of 365 nm, the AzoTAB isomerised to its *cis* configuration and the interfacial energy of the aqueous solution on the substrate was increased which fragmented the solution into monodisperse droplets (Figure 2.5). When the light source was removed, the flow returned to laminar. This was a reversible process and the flow was successfully switched multiple times in the same experiment [65].

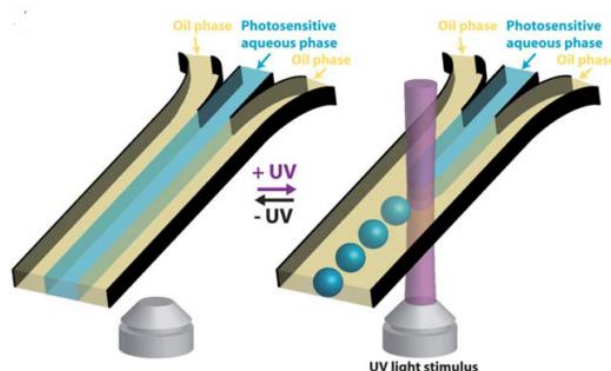


Figure 2.5 Cartoon illustrating the photoreversible fragmentation of a two phase (aqueous/oil) liquid flow from a continuous flow (no UV light applied) to a segmented flow (UV light applied). Reproduced from [65] with permission from The Royal Society of Chemistry.

A recent study by Toyota *et al.* [67] demonstrated an autonomous droplet which spontaneously moved once placed in an aqueous solution in which “fuel” surfactant had been dispersed. The surfactant used was (N-(4-[3-[trimethylammonio]ethoxy]benzylidene)-4-octylaniline bromide) while the droplets contained a catalyst which hydrolysed the surfactant. The self-propelled movement of these droplets can be described in three stages. The first stage involves the hydrolysis of the “fuel” surfactant at the surface of the oil droplets (which contained the catalyst). During the hydrolysis of the “fuel” surfactant there was a fluctuation of the rate of hydrolysis and this caused a symmetry-breakage of all the potential reactive sites on the surface of the droplet. This resulted in the hydrolysed product being accumulated at the most reactive sites. The second stage involved an imbalance of interfacial tension being created between the side of the droplet which accumulated the product and the side of the droplet which did not accumulate any product. Because of this imbalance of interfacial tension, lateral movement of the hydrolysed product was created on the surface of the droplet. The hydrolysed surfactant did not dissolve into the initial droplet since it was lipophilic and instead it aggregated to form small waste droplets. As a consequence, the waste droplets grew in size until they became too large and were subsequently released from the droplet (Figure 2.6). The interfacial energy of the leading edge of the droplet was lower than the waste covered trailing edge, creating interfacial dynamic fluctuation. This fluctuation combined with the accumulation and release of product resulted in the self-propelled motion of the droplets. In the final stage the leading edge of the droplet would pick additional fuel surfactant which was then converted into the lipophilic product as the droplet moved. This continuous collection and hydrolysis of the fuel surfactant further fed the interfacial imbalance and created internal convection inside the droplet, thus sustaining droplet movement. As long as there was “fuel” surfactant within the aqueous solution and the catalyst inside of the droplet was active, the droplet would continue to move. Although in this paper the system is not in a micro-channel nor is it controlled by external stimuli, this report opens up new avenues for stimuli-responsive actuation in a micro-channel. If a chemical reaction can be triggered by external stimulation then precise unidirectional movement can be achieved.

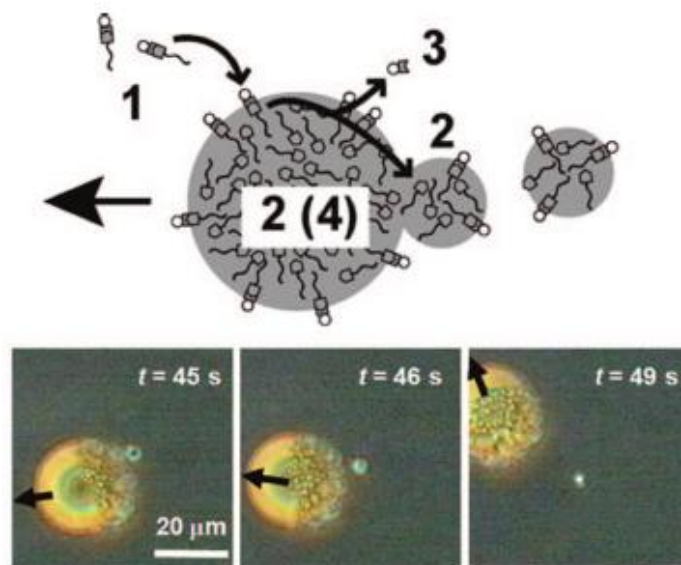


Figure 2.6 (a) Illustration of reaction happening on the exterior of the droplet and (b) fluorescent images of the droplet in motion. Reprinted with permission from [67]. Copyright (2009) American Chemical Society.

Jitka Čejkova *et al* [68] recently reported a simple decanol droplet system which is capable of mimicking a variety of biological process including reversible chemotactic movement, the ability to detect and move towards the strongest source of chemoattractant, stimuli responsive chemotactic movement and delivery of chemical cargo. In this study the decanol droplet is able to sense and move across aqueous solutions of sodium deaconate in the direction of NaCl gradients (Figure 2.7).

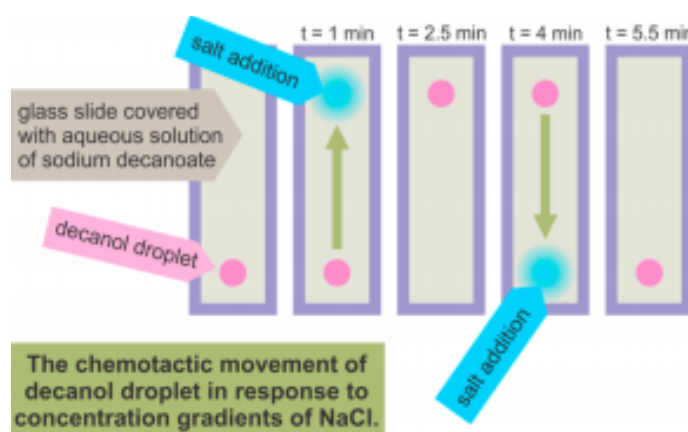


Figure 2.7 Illustration representing the reversible chemotactic movement of decanol droplets in NaCl gradients. Reprinted with permission from [68] Copyright © 2014, American Chemical Society.

The chemotactic movement is a result of Marangoni type convection forces developed as a result of interfacial tensions gradients caused by the addition of NaCl. As the NaCl diffuses into the aqueous solution, it dilutes the amount of sodium deaconate molecules thus raising the surface tension of the solution resulting in a surface tension gradient leading to the source of addition. When no NaCl source is present in the system the decanol droplets move in random motion, this is due to the dissolution of the droplet itself into the aqueous solution (decanol is a weak surfactant). To achieve reversal chemotactic movement of the decanol droplet, the group developed a system of time delayed additions of salt (Figure 2.7). This ensures that a stronger NaCl gradient was created with each new addition, which led to the droplet moving to the new site.

To test whether the droplet would travel towards a stronger source of chemoattractant, the group dissolved varying concentrations of NaCl in nitrobenzene. This had the added advantage that the gradient could be maintained for longer due to the immiscibility of the nitrobenzene with the aqueous solution. To test whether the droplet would “choose” a chemoattractant source based on strength, a simple maze channel was designed, where in one end of the channel a nitrobenzene droplet containing 10  $\mu\text{mol}$  of NaCl was placed and at the other end of the channel a droplet which contained 50  $\mu\text{mol}$  was placed (Figure 2.8). In every run the droplet always chemotactically moved towards and merged with the most concentrated NaCl source.

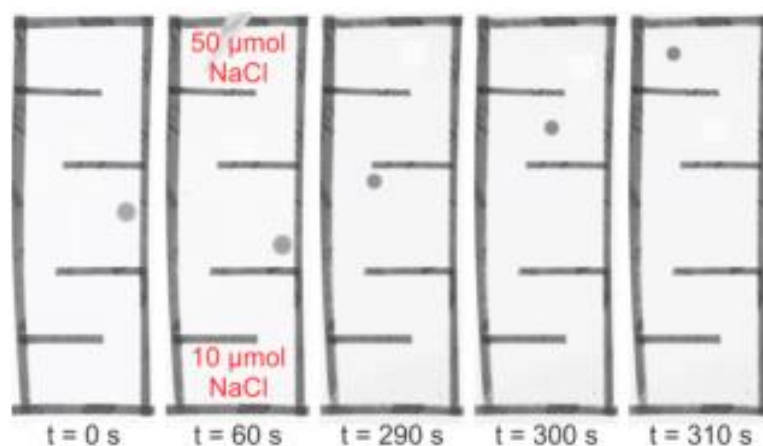


Figure 2.8 Snapshots showing that the decanol droplets were attracted by the stronger NaCl source. Reprinted with permission from [68] Copyright © 2014, American Chemical Society.

To demonstrate stimuli-responsive chemotactic movement the group encapsulated small NaCl salt crystals in paraffin particles which had a melting point of 42 °C. When the paraffin particles were placed into a solution of sodium deaconate below this temperature, no chemotactic movement was observed. However, when the area around the wax particles was locally heated to above this temperature, the wax melted and slowly released the salt crystals which dissolved into the aqueous system and resulted in the chemotactic movement of the decanol droplets.

Finally the authors tested whether it was possible to carry and delivery chemical payloads. To do this, the decanol droplets where saturated with solid iodine which produced dark orange droplets.  $\beta$ -carotene was added to the nitrobenzene droplets which produced a red colour. The nitrobenzene droplet was placed at one end of a simple maze channel and the decanol droplet was placed at the start; once the decanol droplet chemotactically found and merged with the nitrobenzene droplet a green colour change was observed which indicated the iodination reaction of the  $\beta$ -carotene.

#### **2.4.2 “Vehicle” Contained Surfactants**

Movement of “vehicles” which contain the “fuel” surfactant is achieved by only releasing the surfactant upon external stimulation, as opposed to having the surfactant dispersed in the aqueous solution. This ensures that the surface tension is only modified around the droplet upon surfactant release, resulting in self-sufficient droplets. Vehicles that use this type of propulsion mechanism will continue to move as long as both the stimulus and the surfactant are present in the system.

Grzybowski *et al.* [69] demonstrated this effect by developing smart droplets which were capable of solving complex mazes through the triggered release of a pH sensitive surfactant. The surfactant used was 2-hexyldecaonic acid (HDA). When the HDA was subjected to a basic solution it was deprotonated to a more surface active form,  $DA^-$ . The surfactant was contained within an oil or organic solvent such as dichloromethane. The droplet was able to solve the maze by following a pH gradient. This was achieved by filling the maze with a basic solution (pH 12) and placing an acidic gel at the end of the maze, creating a pH gradient. When the droplet was placed at the start of the maze (high pH) the surfactant diffused out of the droplet into the solution. Since the pH was higher behind the droplet than in front of it, more  $DA^-$  was generated behind the droplet (Figure 2.9). This created a surface tension gradient around the droplet,

which in turn generated Marangoni like flows in the solution and also within the droplet. These flows pushed the droplet towards the area of highest surface tension, which was the exit of the maze (location of the acidic gel). As the droplet approached the exit of the maze it began to slow down as the concentration of  $\text{DA}^-$  decreased due to the lower pH of the solution. However, as there was always a higher concentration of the  $\text{DA}^-$  behind the droplet, the surface tension gradient was maintained, driving the droplet towards the exit of the maze.

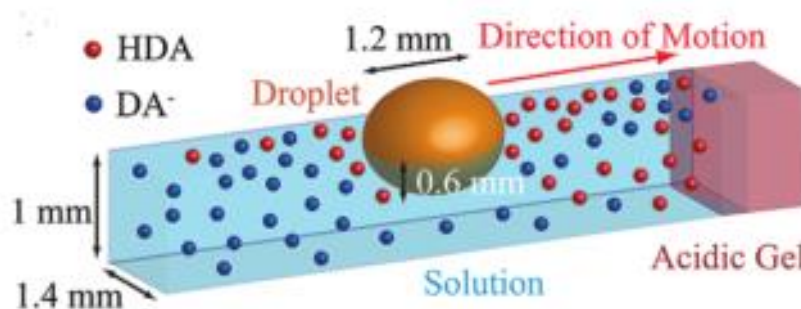


Figure 2.9 Distribution of HDA and  $\text{DA}^-$  around a droplet in a pH gradient. Reprinted with permission from ([69]). Copyright (2010) American Chemical Society.

Using the same droplet composition, self-dividing droplets were also demonstrated [70]. These self-dividing droplets were highly pH sensitive and only divided if placed on a highly basic solution. Actuation in this instance was very similar to the previous example, however, in this case the uneven distribution of the  $\text{DA}^-$  caused the droplet to spin and pull in different directions which eventually lead to droplet splitting. An interesting application for this mechanism was cargo distribution. If cargo was placed within the initial droplet, upon splitting it was observed that the cargo was distributed evenly among the newly formed daughter droplets.

Lopez *et al.* [71] demonstrated that propulsion of a micro-boat could be achieved by incorporating an ionogel which was soaked in ethanol, into the boat design (Figure 2.10). When placed in water, the boat moved spontaneously in random directions. When the ionogel touched the water, ethanol molecules were expelled from the ionogel matrix at the rear of the boat and replaced with water molecules. The large difference in surface tension between water and ethanol caused an asymmetrical surface tension gradient between the end and the front of the boat, causing the boat to move in a forward motion. Lopez and co-workers explained that speed and direction of the boat was controlled by

the size of the ionogel and stated that with larger gels speed increased while directional control decreased. Using smaller ionogels resulted in slower boat speeds with increased control over directional movement, probably due to release of less surfactant.

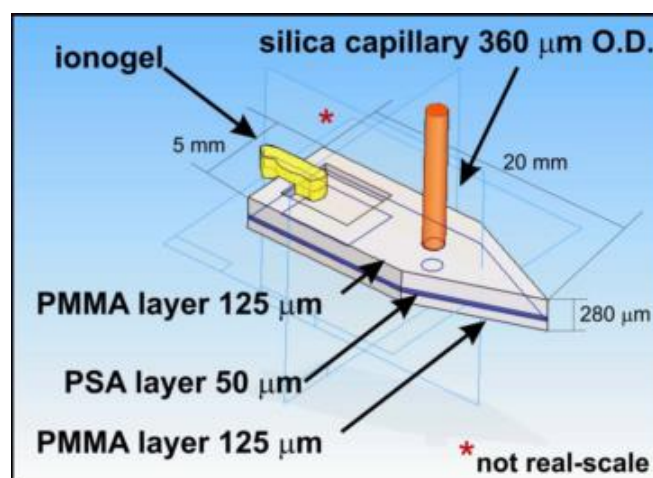


Figure 2.10 Schematic of micro-boat which contains the ethanol soaked ionogel.

Luo *et al.* [72] have demonstrated surfactant driven actuation by developing a micro-boat which contained a reservoir to hold the surfactant, namely isopropyl alcohol (IPA). When the boat was placed on water the surfactant left the boat and interacted with the water behind the boat, lowering the surface tension, and causing propulsion of the boat. The boat could travel up a 94.5 cm long channel with speeds of up to  $10 \text{ cm s}^{-1}$ . The volume of surfactant (in the boat) and the volume of water (in the channel) both determined the speed of the boat as the propulsion force of the boat was dependent on the concentration of the IPA. During the experiments, water from the channel would enter the reservoir, thus reducing the concentration of the IPA, which in turn reduced the surface tension drop and lowered the speed of the boat.

The “toy boat” mechanism by which a small cardboard boat could be propelled on water by adding a small amount of surfactant (hand soap) to the rear of the boat [73], inspired this type of surfactant driven synthetic vehicle. However, this effect is short lived as the small amount of surfactant is quickly depleted and since the surfactant will remain at the surface of the water, the surface tension will no longer be modified by supplementary surfactant addition.

Sen *et al.* [63] described a novel method for vehicle movement in which the surfactant (needed for propulsion) was produced via a chemical reaction. These vehicles contained the polymer poly(2-ethyl cyanoacrylate) (PECA) which is an FDA approved polymer. When placed in a basic solution (1M NaOH) PECA underwent a

deesterification reaction, which resulted in rapid depolymerisation of PECA producing smaller molecules (ethanol) which were surface active (Figure 2.11).

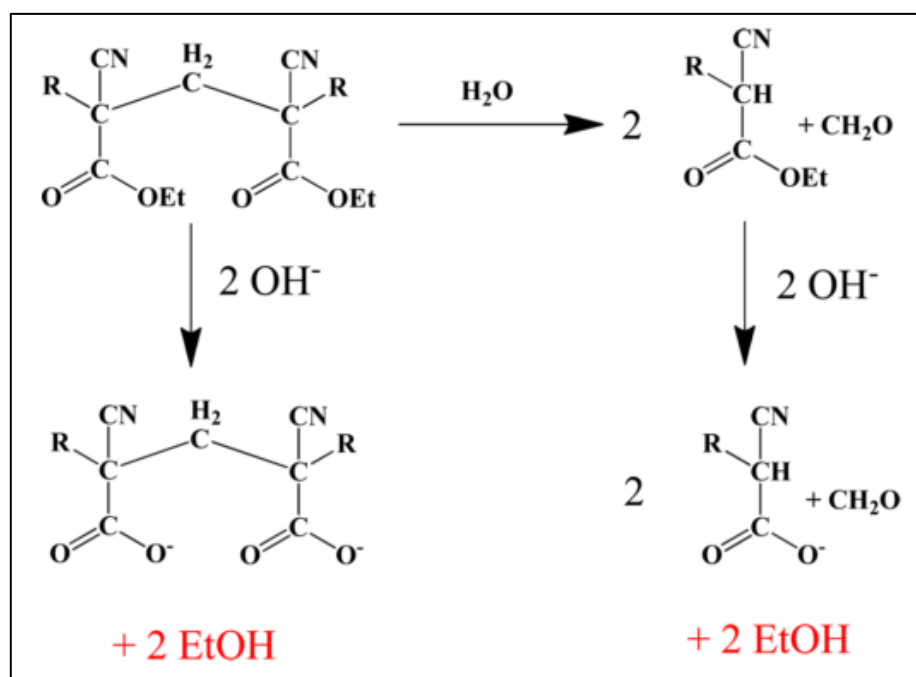
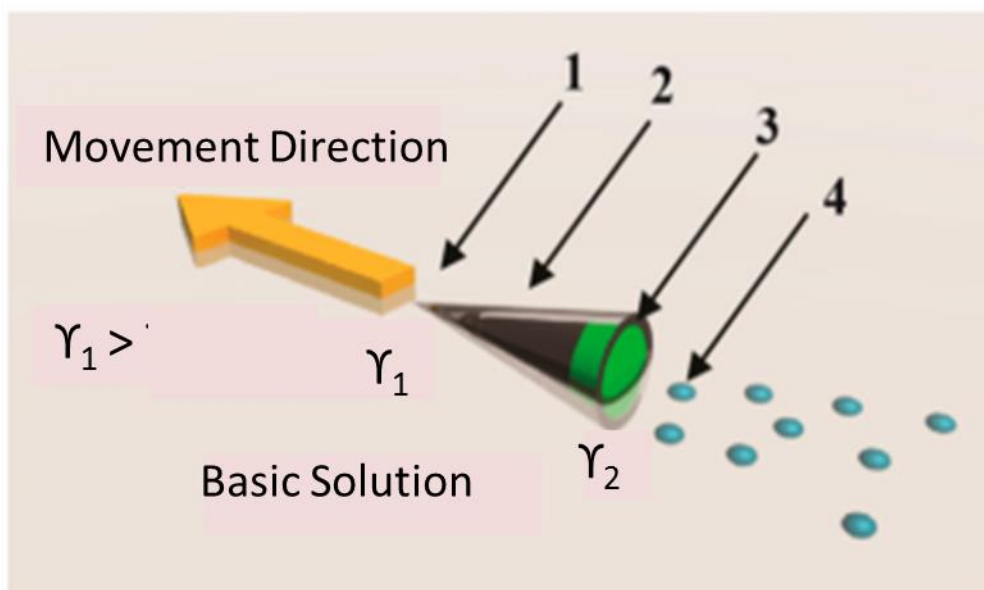


Figure 2.11 Mechanism for the depolymerisation of the polymer PECA. Reprinted with permission from ([63]). Copyright (2013) American Chemical Society.

Pipette tips were used as the vehicle in this study. One end of the tip was sealed with PDMS, which ensured that the chemical reaction could only occur at the open end of the pipette tip (Figure 26). The ethanol produced lowered the surface tension of the solution behind the pipette tip thus breaking the surface tension symmetry, which produced Marangoni like flows and propelled the vehicle forward (Figure 2.12). The vehicles in this study were capable of self-generating surface tension gradients while unidirectional movement was assured as the chemical reaction could only occur at one end of the tip. This type of “propulsion” mechanism also allowed for actuation in various media such as salt solutions and artificial serum. This was achieved by coating ion exchange beads with PECA; the ion exchange beads actively released OH<sup>-</sup> ions which triggered the depolymerisation of PECA, thus promoting vehicle “propulsion”. The asymmetrical coating of the PECA again ensured that unidirectional movement was achieved.



- |               |                              |
|---------------|------------------------------|
| 1: Sealed End | 2: Motor Body                |
| 3: PECA Fuel  | 4: Depolymerisation Products |

Figure 2.12 Schematic of actuation of PECA loaded vehicle. Reprinted with permission from ([63]). Copyright (2013) American Chemical Society.

Ban *et al.* [74] have shown the self-propelled motion of oil droplets at neutral pH. The droplet used in this study contained the surfactant di(2-ethylhexyl) phosphoric acid (DEHPA). These droplets showed autonomous random movement due to Marangoni like flows created from the release of the DEHPA surfactant. As the pH of the aqueous solution was increased, the DEHPA was deprotonated, and its release from the droplet caused a decrease in the interfacial tension between the droplet and solution. This created circulating flow within the droplet. The motion of the droplet was maintained due to the cycle of deprotonated DEHPA being released into the aqueous phase and protonated DEHPA being supplied to the interface from within the droplet (Figure 2.13). Since the movement of the droplet was dependent on the deprotonation of the DEHPA surfactant, it was switched on and off by controlling the pH of the aqueous solution. Below pH 6 the droplet did not move due to DEHPA not being deprotonated (and not being released). Above pH 6 the droplets would move spontaneously. However, the movement of the droplet was random and the direction was solely based on how the droplet was placed on top of the solution.

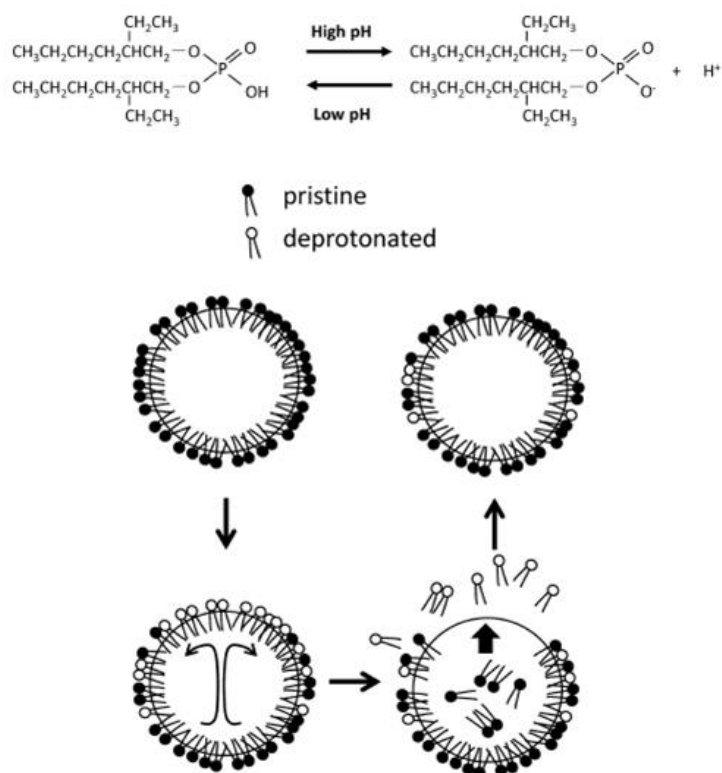


Figure 2.13 Structure of DEPHA surfactant and mechanism of movement of the oil droplet. Movement is due to the deprotonation of the DEPHA, which results in Marangoni convection within the droplet. This was maintained due to the replenishment of protonated DEPHA at the droplet/liquid interface. Reprinted with permission from ([74]). Copyright (2013) American Chemical Society.

Using the DEPHA surfactant, Ban *et al.* [75] demonstrated self-propelled droplets which moved in the direction of a higher concentration of heavy metal ions. In this study, Ban and co-workers again used an oil droplet which contained the DEPHA surfactant. However, two stimuli were used to control the movement of the droplet. Firstly, adjusting the pH to achieve droplet mobility and secondly creating metal ions gradients to move the droplets in a unidirectional fashion.

The self-propelled motion of the droplets remained the same as in the previous example. However, the movement of the droplets towards higher concentrations of metal ions can be explained as follows; when the oil droplet was placed on a solution with a pH above 6, the interface of the droplet was covered with negatively charged DEPHA molecules. These negatively charged molecules served as receptors for positively charged metal ions in the aqueous phase. When a gradient of metal ions was present in the solution, a DEPHA-metal complex was formed at the interface. When this complex was

released into the aqueous solution, it created a surface tension gradient around the droplet. This caused Marangoni like flows which drove the droplet towards the area of highest concentration of metal ions. The speed of the droplet was controlled by adjusting the pH of the solution accordingly.

In a different approach, Florea *et al.* [76] demonstrated unique “photo-chemopropulsion” mechanism for droplet movement. The lipophilic droplets in this study were composed of the pH sensitive surfactants HDA and Chromoionophore I (CI) in DCM. Within the droplet, the weak acid HDA was deprotonated to  $DA^-$  through interactions with the weak base CI, which resulted in production of  $CI-H^+$ , a very efficient cationic surfactant. This surfactant associated with the  $DA^-$  to form the salt  $[CI-H^+][DA^-]$ . The term photo-chemopropulsion was used as the release of the surfactant  $CI-H^+$  was controlled by altering the pH of the aqueous solution using a white light source. When the pH of the solution on which the droplet was resting was lowered below the  $pK_b$  of the  $DA^-$ , the  $CI-H^+$  surfactant was released from the droplet into the aqueous solution (Figure 2.14). Once released, the surfactant altered the surface tension symmetry around the droplet and created Marangoni like flows which drove the droplet away from the light source. The authors stated that the rate of the pH change can be controlled by the light intensity, producing droplet unidirectional movement with speeds up to  $4000 \mu m s^{-1}$ .

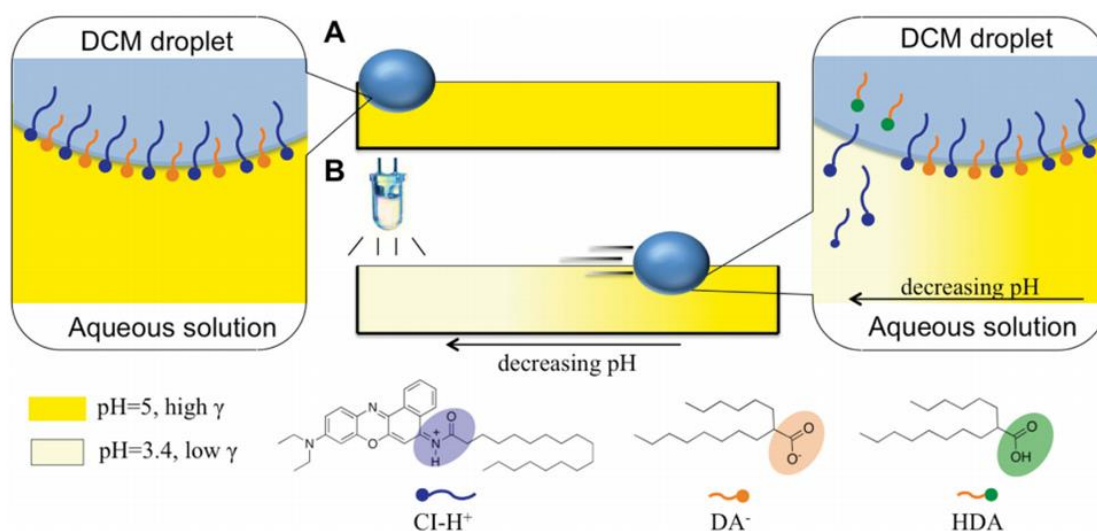


Figure 2.14 Photo-chemopropulsion of a micro droplet which is resting on an aqueous solution containing the photochromic molecule, spiropyran. A – depicts the droplet before white light irradiation and B – depicts the droplet after white light irradiation. After the introduction of the light source, the cationic surfactant  $CI-H^+$  is released, breaking the surface tension symmetry of

the solution around the droplet and creating Marangoni like flows which drive the droplet away from the white light source. Reproduced from [76].

Florea and co-workers were able to control the pH of the aqueous solution by using an acidic photochromic molecule, namely a sulfonic acid spiropyran derivative (SP-SO<sub>3</sub>H). Dissolution of SP-SO<sub>3</sub>H in the aqueous solution resulted in the dissociation of the sulfonic acid and the ring opening of the SP to form an equilibrium mixture of two merocyanine (MC) forms, protonated merocyanine (MCH<sup>+</sup>-SO<sub>3</sub><sup>-</sup>) which is the predominant form, and deprotonated merocyanine (MC-SO<sub>3</sub><sup>-</sup>). When the white light source was introduced, the MC-SO<sub>3</sub><sup>-</sup> and MCH<sup>+</sup>-SO<sub>3</sub><sup>-</sup> were converted back to the spiropyran sulfonate (SP-SO<sub>3</sub><sup>-</sup>) form, releasing a proton (H<sup>+</sup>) in the process (Figure 2.15). This in turn caused the pH of the aqueous solution to drop from about pH 5 to around pH 3.4. Therefore, the authors were able to precisely control the pH (5.0 to 3.4) of a specific area of the solution, causing on demand surfactant release from the droplet to the aqueous solution. Using this method Florea and co-workers were able to achieve contactless control of the speed and directional movement of the droplet using only a white light source.

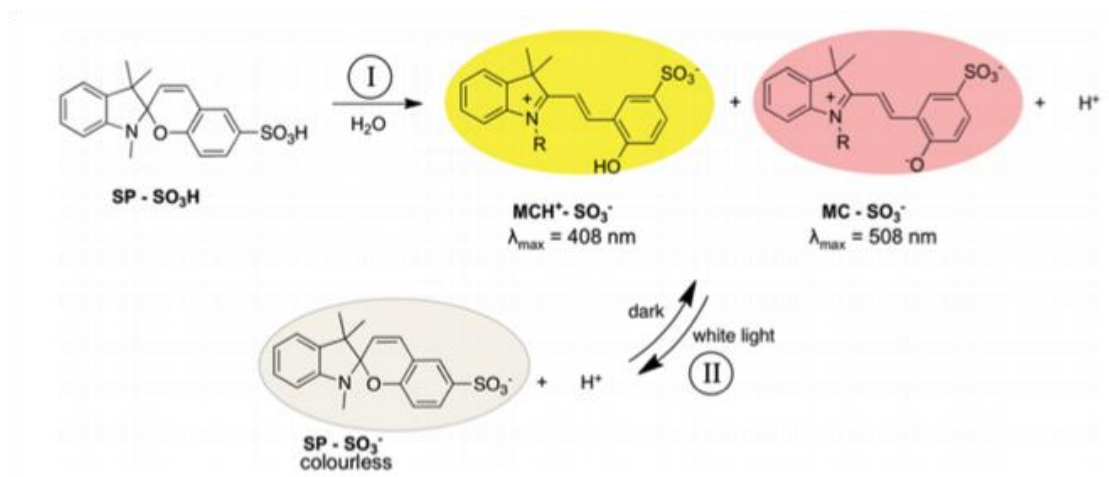


Figure 2.15 Structural change of the SP-SO<sub>3</sub>H photochromic molecule when dissolved in an aqueous solution under different illumination conditions. Reproduced from [76].

Another system in which the surfactant is contained within the “vehicle” is based on Ionic liquids. Francis *et al* [77] demonstrate the chemotactic movement of ionic liquid droplets, specifically droplets of trihexyl(tetradecyl)phosphonium chloride ([P<sub>6,6,6,14</sub>][Cl]). These ionic liquids were designed to move across the air/liquid interface and the motion was

controlled by the triggered release of the  $[P_{6,6,6,14}]^+$ , which is a very efficient cationic surfactant and a constituent of the IL droplet (Figure 2.16).

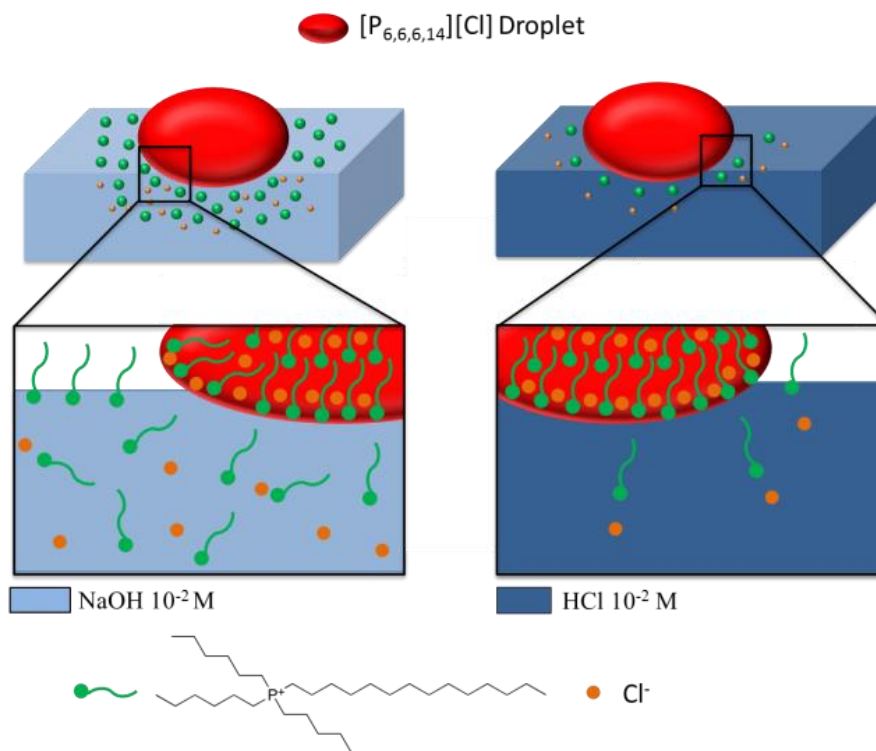


Figure 2.16 Diagram showing composition and relative solubility of  $[P_{6,6,6,14}][Cl]$  in solutions of  $10^{-2}$  M NaOH and  $10^{-2}$  M HCl. Reproduced from [77].

When the surfactant diffuses from the droplet into the aqueous phase it resulted in a drop of the local surface tension. The rate at which the surfactant was released depended on the solubility of the closely associated counter ion within the IL, in this case  $Cl^-$ . Any transfer of the  $Cl^-$  ion must be balanced by an equivalent transfer of  $[P_{6,6,6,14}]^+$  in order to maintain overall charge neutrality within the droplet. The rate of release of  $Cl^-$  was, in turn, dependent on the local aqueous  $Cl^-$  concentration at the IL/aqueous boundary. Therefore, when a droplet of  $[P_{6,6,6,14}][Cl]$  was placed onto a aqueous solution, which had an imposed  $Cl^-$  concentration gradient, there was a differential release of  $[P_{6,6,6,14}]^+$  from the droplet into the aqueous solution. This resulted in the formation of an asymmetric surface tension gradient around the droplet, generating Marangoni like flows and driving the droplet from areas of low surface tension to high surface tension (Figure 2.17).

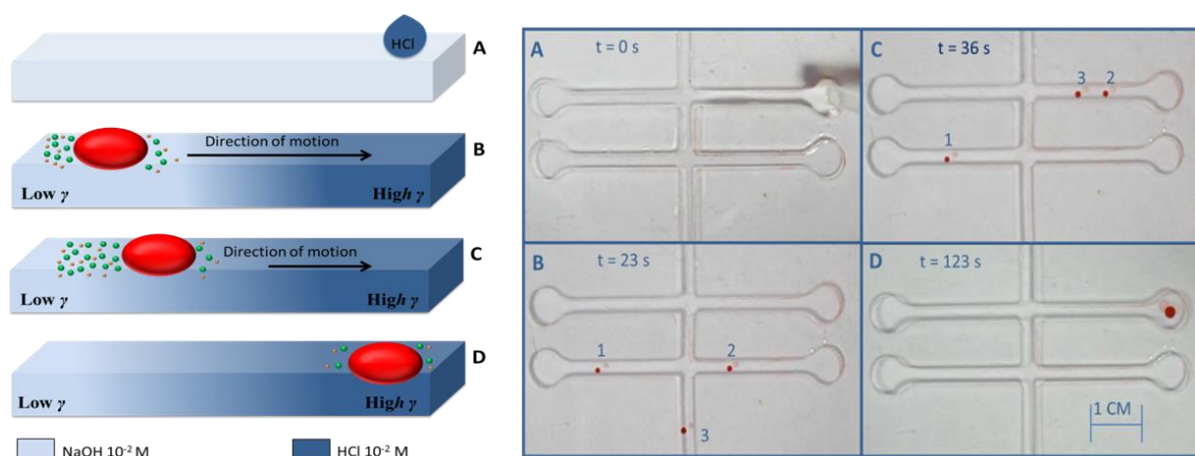


Figure 2.17 Schematic representation showing the chemotactic movement of Ionic liquid droplets in open fluidic channels (left) and sequence of video frames showing the chemotactic movement of multiple Ionic liquid droplets in an open fluidic channel (right). A– Depicts the creation of  $\text{Cl}^-$  gradient, the channels were initially filled with a solution of  $10^{-2}$  M NaOH, at the desired destination a few drops of a  $10^{-2}$  M solution of HCl was placed. B– Shows the initial placement of the Ionic liquid droplet(s). C – The droplet(s) are propelled towards the highest area of surface tension. D – The droplet arrives at the desired destination. Reproduced from [77].

In this study Francis and coworkers demonstrated multiple ways to generate the required  $\text{Cl}^-$  gradients, however, the generated gradients are short lived and quickly come to equilibrium. This means the droplets can only be moved to a single destination for a limited period of time unless a mechanism for dynamic creation of local gradients is employed.

Francis *et al.* [78] have recently reported electro-tactically moved ionic liquid droplets, in which the mechanism for movement of these droplets remains the same as the previous example, but the  $\text{Cl}^-$  gradients required for droplet movement are electrochemically generated using 3D printed electrodes embedded within the fluidic channels. In this paper, droplets of  $[\text{P}_{6,6,6,14}][\text{Cl}]$  were electro-tactically moved across the air/liquid interface of  $10^{-3}$  M NaCl electrolyte solutions. When an external electric field was applied across an electrolyte solution, the mobile ions migrated towards their respective electrodes; *i.e.* anions towards the anode and cations towards the cathode, creating a  $\text{Cl}^-$  concentration gradient along the channel. When a voltage was applied, a droplet of  $[\text{P}_{6,6,6,14}][\text{Cl}]$  placed at the cathode asymmetrically released  $[\text{P}_{6,6,6,14}]^+$  and autonomously moved towards the anode. Upon reversing the polarity of the electrodes, the gradient was also reversed and hence droplet movement could be reversed. In addition to this, the droplets could be steered into side channels at junctions, by polarizing appropriate electrode pairs (Figure

2.18). Electrotactic movement of the droplets allowed concentration gradients to be established and varied dynamically, and maintained for longer periods of time. This in turn enabled flexible control of microdroplet movement, introducing the ability to control the speed (depends on applied voltage), reversibility, and redirection into side channels.

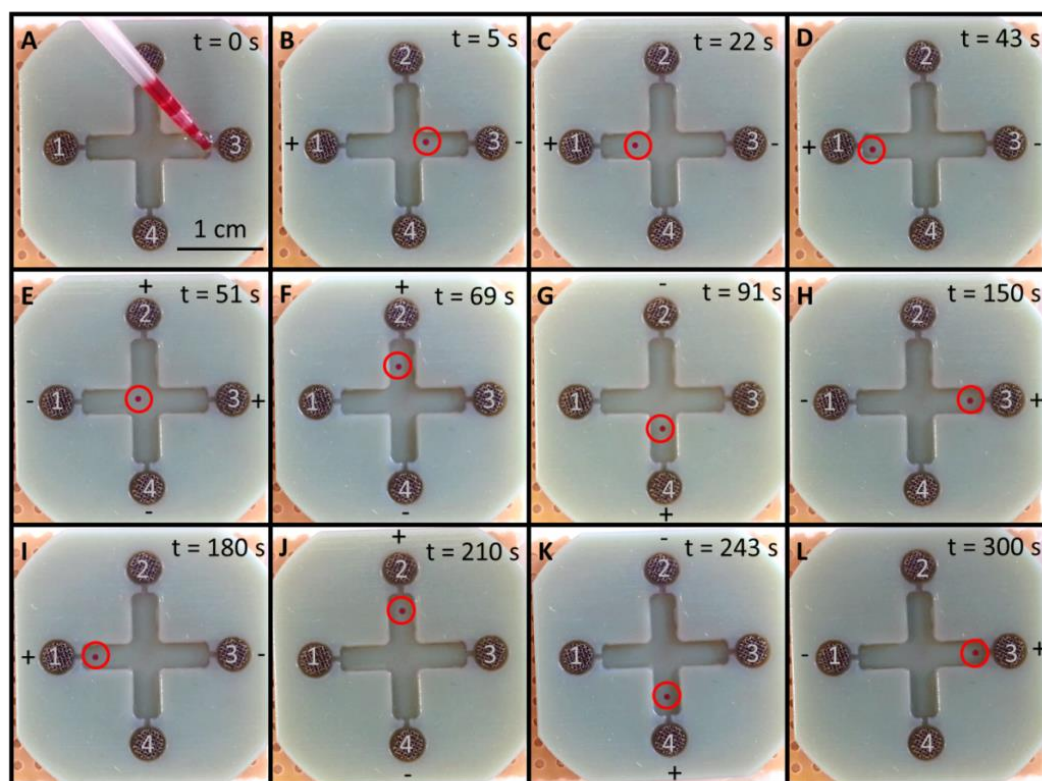
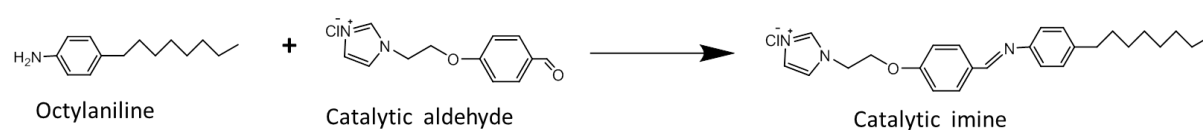


Figure 2.18 Sequence of snapshots showing the electrotactic movement of an Ionic liquid droplet. The channels are filled with a  $10^{-3}$  M solution of NaCl and a potential difference of 9 V is applied across selected electrodes A – The droplet is introduced B – D The droplet is propelled from cathode (3) to anode (1). E – The polarity of electrodes (3) and (1) is reversed and the droplet begins to move to electrode (3). F – As the droplet approaches the junction, the potential difference is applied between electrodes (2) and (4) and removed from electrodes (3) and (1). The droplet then begins to migrate toward anode (2). G – Upon arriving at anode (2) the polarity of electrode (2) and (4) is reversed and the droplet moves towards the new anode (4). H – Upon arriving at anode (4) the potential is again reversed and using a similar method to sequence F the droplet is returned to the starting position. I – L shows the process repeated in the same run. Reproduced from [78] , © 2016 Elsevier B.V. All rights reserved.

Actuation of micro “vehicles” through localized changes in surface tension offers unique unidirectional control. However, there are still many challenges to face, such as moving the “vehicle” to defined specific areas within fluidic channels. Ideally, the vehicles should be controlled in a contactless manner, they should move spontaneously and require as little energy input as possible to achieve actuation. There is currently a movement towards tactic, functional and reactive droplets. This can be achieved by looking to nature for inspiration and many groups are reporting droplets which have biomimetic qualities, such as acting as vessels for chemical reactions [79], droplets with functional lipid bilayers [80,81], droplets which can mimic DNA transcription and translation [82] and even droplets which show self-reproduction [83].

Li Sheng and Kensuke Kurihara [83], for example, report a novel vesicle-formation system. In this autocatalytic system octylaniline oil droplets act as a scaffold to produce vesicles by direct addition of a water-soluble catalytic aldehyde to form self-reproducing oil droplets. These droplets can then be transformed into giant vesicles *via* a further addition of a hydrophilic membrane precursor. In the study the catalytic aldehyde and octylaniline are combined together as an oil phase and dispersed in an aqueous solution as oil droplets. A condensation reaction between octylaniline and the catalytic aldehyde produces a catalytic imine, which further catalyzes the condensation reaction (Figure 33). Since this new catalytic imine is amphiphilic, its production resulted in more octylaniline being incorporated into the droplets from the aqueous phase, which in turn resulted in further reactions between the two precursors to produce more catalytic imine.



*Figure 2.19 Condensation reaction between octylaniline and the catalytic aldehyde which produces a catalytic imine. Reproduced from [83] with permission from The Royal Society of Chemistry.*

During the reaction the oil droplets began to increase in size until they reached a certain size threshold (5 – 25  $\mu\text{m}$ ), at this point they began to divide to produce smaller droplets (1 – 5  $\mu\text{m}$ ). This repeated growth and division indicated that in their system, the droplets maintained their composition and continued to produce the catalytic imine even after the division process (Figure 2.20).

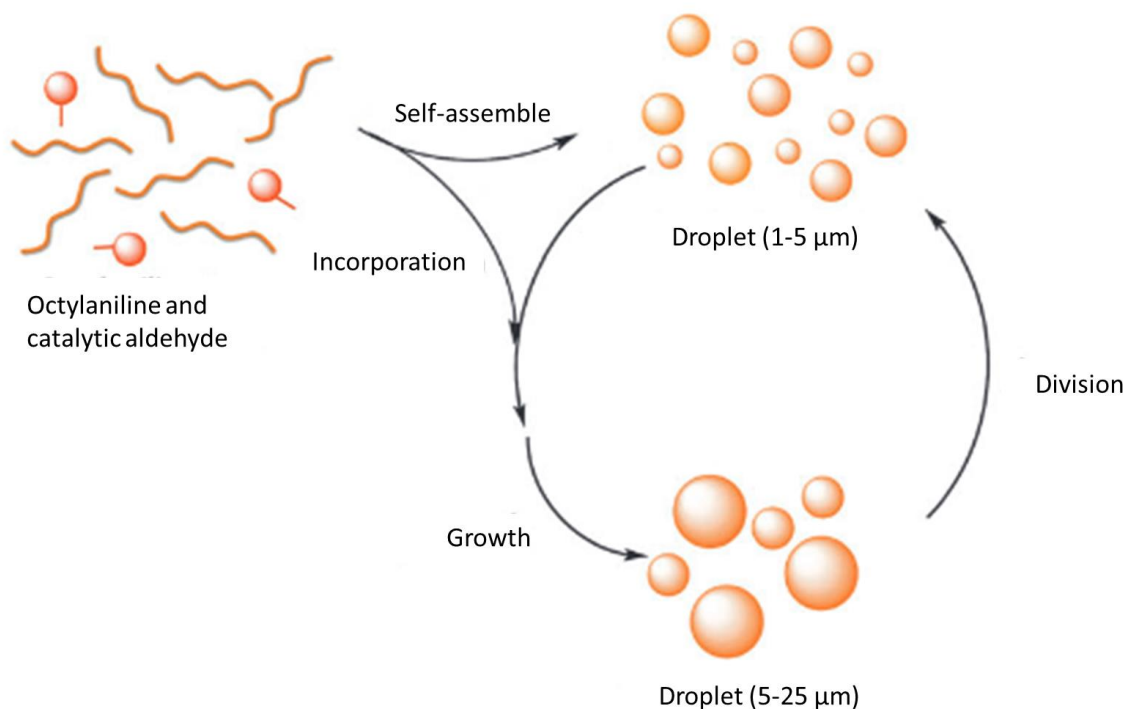


Figure 2.20 Schematic of the self-reproducing oil droplets. Reproduced from [83] with permission from The Royal Society of Chemistry.

Introduction of a hydrophilic membrane precursor into the system resulted in the formation of tubular giant vesicles (length of 50  $\mu\text{m}$ ). In the presence of the catalytic aldehyde, the octylaniline reacted with the hydrophilic membrane precursor to form vesicular membrane molecule (Figure 2.21).

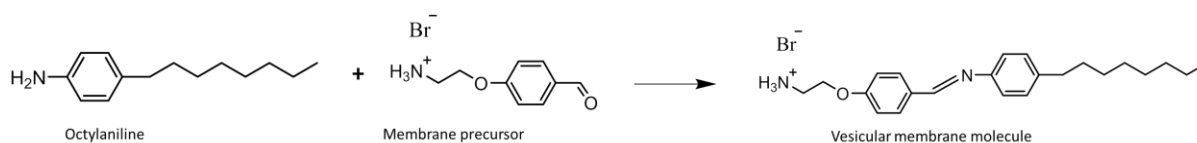


Figure 2.21 Reaction between octylaniline and the membrane precursor which produces the vesicular membrane molecule. Reproduced from [83] with permission from The Royal Society of Chemistry.

This reaction occurs initially in the aqueous phase, and according to Sheng this reaction may be also be capable of self-reproducing. The vesicular membrane molecules are then taken up by the oil droplets and slowly replace the octylaniline molecules. This replacement results in the transformation of the oil droplets into tubular and spherical giant vesicles. This study is of great interest as these droplets have begun to mimic

primitive metabolic activity and also shows signs of early evolution of the droplets into larger more robust vesicles.

## 2.5 Conclusions and Outlook

We believe that the use of stimuli-responsive materials in microfluidics forms the core of autonomous microfluidic-based analytical devices, which are of considerably lower cost compared to their etched silicon (glass) counterparts, more biomimetic in nature and offer increased adaptability. Although this chapter is focused on the use of stimuli-responsive materials for fluid movement at the microscale, it gives the reader an insight into how the incorporation of such materials into microfluidics can allow for additional tasks *beyond the transport of reagents or samples*.

In living organisms, the fluidics system (*e.g.* cardiovascular system) performs multiple complex functions (*e.g.* sensing, detection, repair, waste removal; pH and temperature stabilization) in addition to the transport of fluids. Such characteristics of biological systems could be transferred into microfluidics through the creative use of adaptive materials and chemistries, to enable fundamental breakthroughs in chem/bio-sensing device performance. However, the future of biomimetic microfluidics relies on convincing demonstrators and their application in real scenarios where advanced functions such as autonomous fluid handling, sensing, detection and repair of damage, self-management and healing, could be demonstrated.

## 2.6 References

1. Stone, H.A.; Stroock, A.D.; Ajdari, A. Engineering flows in small devices. *Annual Review of Fluid Mechanics* **2004**, *36*, 381-411.
2. Gravesen, P.; Branebjerg, J.; Sondergaard, Jensen, O. Microfluidics-a review. *J. Micromech. Microeng. J. Micromech. Microeng* **1993**, *3*, 16-82.
3. Issadore, D.; Franke, T.; Brown, K.A.; Westervelt, R.M. A microfluidic microprocessor: Controlling biomimetic containers and cells using hybrid integrated circuit/microfluidic chips. *Lab on a chip* **2010**, *10*, 2937-2943.
4. Beebe, D.J.; Mensing, G.A.; Walker, G.M. Physics and applications of microfluidics in biology. *Annu. Rev. Biomed. Eng* **2002**, *4*, 261-286.
5. He, M.; Herr, A.E. Automated microfluidic protein immunoblotting. *Nat. Protocols* **2010**, *5*, 1844-1856.
6. Plessy, C.; Desbois, L.; Fujii, T.; Carninci, P. Population transcriptomics with single-cell resolution: A new field made possible by microfluidics. *BioEssays* **2013**, *35*, 131-140.

7. Argentiére, S.; Gigli, G.; Irini Gerges, M.M.; Blasi, L. Smart microfluidics: The role of stimuli- responsive polymers in microfluidic devices. In *Advances in Microfluidics*, InTech: 2012.
8. Tang, S.K.; Whitesides, G.M. Basic microfluidic and soft lithographic techniques. *Optofluidics: Fundamentals, Devices and Applications* **2010**, 7-32.
9. Zhang, D.; Men, L.; Chen, Q. Microfabrication and applications of opto-microfluidic sensors. *Sensors* **2011**, *11*, 5360-5382.
10. Benito-Lopez, F.; Antoñana-Díez, M.; Curto, V.F.; Diamond, D. Modular microfluidic valve structures based on reversible thermoresponsive ionogel actuators. *Lab on a Chip* **2014**, *14*, 3530.
11. Ter Schiphorst, J.; Coleman, S.; Stumpel, J.E.; Ben Azouz, A.; Diamond, D.; Schenning, A.P.H.J. Molecular design of light-responsive hydrogels, for in situ generation of fast and reversible valves for microfluidic applications. *Chemistry of Materials* **2015**, *27*, 5925-5931.
12. Prettyman, J.B.; Eddington, D.T. Leveraging stimuli responsive hydrogels for on/off control of mixing. *Sensors & Actuators: B. Chemical* **2011**, *157*, 722-726.
13. Beebe, D.J.; Moore, J.S.; Bauer, J.M.; Yu, Q.; Liu, R.H.; Devadoss, C.; Jo, B.-H. Functional hydrogel structures for autonomous flow control inside microfluidic channels. *Nature* **2000**, *404*, 588-590.
14. Richter, A.; Klatt, S.; Paschew, G.; Klenke, C. Micropumps operated by swelling and shrinking of temperature-sensitive hydrogels. *Lab on a chip* **2009**, *9*, 613-618.
15. Florea, L.; Martin-Mayor, A.; Bou-Ali, M.M.; Meagher, K.; Diamond, D.; Tutar, M.; Benito-Lopez, F. Adaptive coatings based on polyaniline for direct 2d observation of diffusion processes in microfluidic systems. *Sensors and Actuators B: Chemical* **2016**, *231*, 744-751.
16. Riahi, R.; Tamayol, A.; Shaegh, S.A.M.; Ghaemmaghami, A.M.; Dokmeci, M.R.; Khademhosseini, A. Microfluidics for advanced drug delivery systems. *Current Opinion in Chemical Engineering* **2015**, *7*, 101-112.
17. Pfeiffer, S.A.; Nagl, S. Microfluidic platforms employing integrated fluorescent or luminescent chemical sensors: A review of methods, scope and applications. *Methods and Applications in Fluorescence* **2015**, *3*, 034003.
18. i Solvas, X. Droplet microfluidics: Recent developments and future applications. *Chem. Commun.* **2011**, *47*, 1936-1942.
19. Teh, S.-Y.; Lin, R.; Hung, L.-H.; Lee, A. Droplet microfluidics. *Lab on a chip* **2008**, *8*, 198-220.
20. Weibel, D.; Whitesides, G. Applications of microfluidics in chemical biology. *Curr. Opin. Chem. Biol.* **2006**, *10*, 584-591.
21. Whitesides, G.M. The origins and the future of microfluidics. *Nature* **2006**, *442*, 368-373.
22. Baigl, D. Photo-actuation of liquids for light-driven microfluidics: State of the art and perspectives. *Lab on a chip* **2012**, *12*, 3637-3653.
23. Park, S.-Y.; Kalim, S.; Callahan, C.; Teitell, M.; Chiou, E. A light-induced dielectrophoretic droplet manipulation platform. *Lab on a chip* **2009**, *9*, 3228-3235.
24. Pei Yu, C.; Hyejin, M.; Hiroshi, T.; Chang-Jin, K.; Ming, C.W. Light actuation of liquid by optoelectrowetting. *Sensors and Actuators A: Physical* **2003**, *104*, 222-228.
25. Han-Sheng, C.; Alope, K.; Steven, T.W. Open optoelectrowetting droplet actuation. *Appl. Phys. Lett.* **2008**, *93*, 9064104.

26. Pei, S.N.; Valley, J.K.; Neale, S.L.; Jamshidi, A.; Hsu, H.-Y.; Wu, M.C. In *Light-actuated digital microfluidics for large-scale, parallel manipulation of arbitrarily sized droplets*, Micro Electro Mechanical Systems (MEMS), 2010 IEEE 23rd International Conference on, 2010; IEEE: pp 252-255.
27. Wang, S.; Song, Y.; Jiang, L. Photoresponsive surfaces with controllable wettability. *Journal of Photochemistry and Photobiology C: Photochemistry Reviews* **2007**, *8*, 18-29.
28. Chaeyeon, S.; Kipom, K.; Kyuyong, L.; Hyuk Kyu, P. Thermochemical control of oil droplet motion on a solid substrate. *Appl. Phys. Lett.* **2008**, *93*, 084102.
29. Vikram, P.; Nadjoua, M.; Subramanian, R.S. Thermocapillary motion of a liquid drop on a horizontal solid surface. *Langmuir* **2008**, *24*.
30. Zhenjun, J.; Xiaoyang, H.; Nam-Trung, N.; Patrick, A. Thermocapillary actuation of droplet in a planar microchannel. *Microfluid. Nanofluid.* **2007**, *5*, 205-214.
31. Darhuber, A.; Valentino, J.; Troian, S. Planar digital nanoliter dispensing system based on thermocapillary actuation. *Lab on a chip* **2010**, *10*, 1061-1071.
32. Gomba, J.; Homsy, G. Regimes of thermocapillary migration of droplets under partial wetting conditions. *J. Fluid Mech.* **2010**, *647*, 125-142.
33. Darhuber, A.A.; Valentino, J.P.; Troian, S.M.; Wagner, S. Thermocapillary actuation of droplets on chemically patterned surfaces by programmable microheater arrays. *Journal of Microelectromechanical Systems* **2003**, *12*, 873-879.
34. Bormashenko, E.; Pogreb, R.; Bormashenko, Y.; Musin, A.; Stein, T. New investigations on ferrofluidics: Ferrofluidic marbles and magnetic-field-driven drops on superhydrophobic surfaces. *Langmuir : the ACS journal of surfaces and colloids* **2008**, *24*, 12119-12122.
35. Rida, A.; Gijs, M. Manipulation of self-assembled structures of magnetic beads for microfluidic mixing and assaying. *Anal. Chem.* **2004**, *76*, 6239-6246.
36. Zhao, Y.; Fang, J.; Wang, H.; Wang, X.; Lin, T. Magnetic liquid marbles: Manipulation of liquid droplets using highly hydrophobic fe<sub>3</sub>o<sub>4</sub> nanoparticles. *Advanced materials (Deerfield Beach, Fla.)* **2010**, *22*, 707-710.
37. Wen, C.-Y.; Yeh, C.-P.; Tsai, C.-H.; Fu, L.-M. Rapid magnetic microfluidic mixer utilizing ac electromagnetic field. *Electrophoresis* **2009**, *30*, 4179-4186.
38. Wang, Y.; Zhao, Y.; Cho, S.K. Efficient in-droplet separation of magnetic particles for digital microfluidics. *Journal of Micromechanics and Microengineering* **2007**, *17*, 2148.
39. Zhao, Y.; Fang, J.; Wang, H.; Wang, X.; Lin, T. Magnetic liquid marbles: Manipulation of liquid droplets using highly hydrophobic fe<sub>3</sub>o<sub>4</sub> nanoparticles. *Adv. Mater.* **2010**, *22*, 707-710.
40. Choi, K.; Ng, A.; Fobel, R.; Wheeler, A. Digital microfluidics. *Annu. Rev. Anal. Chem. (Palo Alto Calif.)* **2012**, *5*, 413-440.
41. Fair, R.B. Digital microfluidics: Is a true lab-on-a-chip possible? *Microfluid. Nanofluid.* **2007**, *3*, 245-281.
42. Vijay, S.; Vamsee, K.P.; Richard, B.F. An integrated digital microfluidic lab-on-a-chip for clinical diagnostics on human physiological fluids: the science and application of droplets in microfluidic devices. *Lab on a Chip* **2004**, *4*, 310-315.
43. Zhishan, H.; Jeremy, L.R.; Allen, E.E.; Vijay, S.; Vamsee, K.P.; Wiley, A.S.; Jonathan, L.B.; Thomas, G.M.; Michael, G.P. Multiplexed real-time polymerase chain reaction on a digital microfluidic platform. *Anal. Chem.* **2010**, *82*, 2310-2316.

44. Chang, Y.-H.; Lee, G.-B.; Huang, F.-C.; Chen, Y.-Y.; Lin, J.-L. Integrated polymerase chain reaction chips utilizing digital microfluidics. *Biomed. Microdevices* **2006**, *8*, 215-225.
45. Abdelgawad, M.; Watson, M.; Wheeler, A. Hybrid microfluidics: A digital-to-channel interface for in-line sample processing and chemical separations. *Lab on a chip* **2009**, *9*, 1046-1051.
46. Barbulovic-Nad, I.; Yang, H.; Park, P.; Wheeler, A. Digital microfluidics for cell-based assays. *Lab on a chip* **2008**, *8*, 519-526.
47. Luk, V.; Wheeler, A. A digital microfluidic approach to proteomic sample processing. *Anal. Chem.* **2009**, *81*, 4524-4530.
48. Paik, P.Y.; Pamula, V.K.; Chakrabarty, K. Adaptive cooling of integrated circuits using digital microfluidics. *Very Large Scale Integration (VLSI) Systems, IEEE Transactions on* **2008**, *16*, 432-443.
49. Walker, S.W.; Shapiro, B. Modeling the fluid dynamics of electrowetting on dielectric (ewod). *Journal of Microelectromechanical Systems* **2006**, *15*, 986-1000.
50. Saeki, F.; Baum, J.; Moon, H.; Yoon, J.-Y.; Kim, C.; Garrell, R. Electrowetting on dielectrics (ewod): Reducing voltage requirements for microfluidics. *Polym. Mater. Sci. Eng* **2001**, *85*, 12-13.
51. Gong, J.; Kim, C.-J.C. All-electronic droplet generation on-chip with real-time feedback control for ewod digital microfluidics. *Lab on a chip* **2008**, *8*, 898-906.
52. Malic, L.; Brassard, D.; Veres, T.; Tabrizian, M. Integration and detection of biochemical assays in digital microfluidic loc devices. *Lab on a chip* **2010**, *10*, 418-431.
53. Wang, L.; Flanagan, L.; Monuki, E.; Jeon, N.; Lee, A. Dielectrophoresis switching with vertical sidewall electrodes for microfluidic flow cytometry. *Lab on a chip* **2007**, *7*, 1114-1120.
54. Li, Y.; Dalton, C.; Crabtree, H.; Nilsson, G.; Kaler, K. Continuous dielectrophoretic cell separation microfluidic device. *Lab on a chip* **2007**, *7*, 239-248.
55. Cummings, E. Streaming dielectrophoresis for continuous-flow microfluidic devices. *IEEE engineering in medicine and biology magazine : the quarterly magazine of the Engineering in Medicine & Biology Society* **2003**, *22*, 75-84.
56. Rohit, R.; Devens, G.; Antonio, A.G.; Mark, H.; Taraci, J.L.; Clement, T.; Dailey, J.W.; Picraux, S.T. Lotus effect amplifies light-induced contact angle switching. *The Journal of Physical Chemistry B* **2004**, *108*, 12640-12642.
57. Siewierski, L.; Brittain, W.; Petrash, S.; Foster, M. Photoresponsive monolayers containing in-chain azobenzene. *Langmuir* **1996**, *12*, 5838-5844.
58. Oh, S.-K.; Nakagawa, M.; Ichimura, K. Photocontrol of liquid motion on an azobenzene monolayer. *J. Mater. Chem.* **2002**, *12*, 2262-2269.
59. Vikram, P.; Nadjoua, M.; Subramanian, R.S. Thermocapillary motion of a liquid drop on a horizontal solid surface. *Langmuir* **2008**, *24*, 5185-5193.
60. Wixforth, A.; Strobl, C.; Gauer, C.; Toegl, A.; Scriba, J.; v Guttenberg, Z. Acoustic manipulation of small droplets. *Anal. Bioanal. Chem.* **2004**, *379*, 982-991.
61. Guttenberg, Z.; Müller, H.; Habermüller, H.; Geisbauer, A.; Pipper, J.; Felbel, J.; Kielpinski, M.; Scriba, J.; Wixforth, A. Planar chip device for pcr and hybridization with surface acoustic wave pump. *Lab on a Chip* **2005**, *5*, 308-317.
62. Paul, B.; Craig, P.B.; Julian, E. Stimuli-responsive surfactants. *Soft Matter* **2013**, *9*, 2365-2374.

63. Zhang, H.; Duan, W.; Liu, L.; Sen, A. Depolymerization-powered autonomous motors using biocompatible fuel. *J. Am. Chem. Soc.* **2013**, *135*, 15734-15737.
64. Brown, P.; Butts, C.P.; Eastoe, J. Stimuli-responsive surfactants. *Soft Matter* **2013**, *9*, 2365-2374.
65. Diguët, A.; Li, H.; Queyriaux, N.; Chen, Y.; Baigl, D. Photoreversible fragmentation of a liquid interface for micro-droplet generation by light actuation. *Lab on a chip* **2011**, *11*, 2666-2669.
66. Diguët, A.; Guillermic, R.-M.; Magome, N.; Saint-Jalmes, A.; Chen, Y.; Yoshikawa, K.; Baigl, D. Photomanipulation of a droplet by the chromocapillary effect. *Angewandte Chemie (International ed. in English)* **2009**, *48*, 9281-9284.
67. Toyota, T.; Maru, N.; Hanczyc, M.; Ikegami, T.; Sugawara, T. Self-propelled oil droplets consuming "fuel" surfactant. *J. Am. Chem. Soc.* **2009**, *131*, 5012-5013.
68. Cejkova, J.; Novak, M.; Stepanek, F.; Hanczyc, M.M. Dynamics of chemotactic droplets in salt concentration gradients. *Langmuir* **2014**, *30*, 11937-11944.
69. Lagzi, I.; Soh, S.; Wesson, P.; Browne, K.; Grzybowski, B. Maze solving by chemotactic droplets. *J. Am. Chem. Soc.* **2010**, *132*, 1198-1199.
70. Browne, K.; Walker, D.; Bishop, K.; Grzybowski, B. Self-division of macroscopic droplets: Partitioning of nanosized cargo into nanoscale micelles. *Angewandte Chemie (International ed. in English)* **2010**, *49*, 6756-6759.
71. Byrne, R.; Lopez, F.; Scaramagnani, S.; Higgins, M.; Wallace, G.G.; Diamond, D. Beads, boats and switches: Making things happen with molecular photoswitches. *IEEE* **2009**, 139-143.
72. Luo, C.; Li, H.; Liu, X. Propulsion of microboats using isopropyl alcohol as a propellant. *Journal of Micromechanics and Microengineering* **2008**, *18*, 067002.
73. Charles, R.; Ashley, B.; Tiddo Jonathan, M. Easy demonstration of the marangoni effect by prolonged and directional motion: "Soap boat 2.0". *J. Chem. Educ.* **2013**, *90*, 1353-1357.
74. Ban, T.; Yamagami, T.; Nakata, H.; Okano, Y. Ph-dependent motion of self-propelled droplets due to marangoni effect at neutral ph. *Langmuir* **2013**, *29*, 2554-2561.
75. Ban, T.; Tani, K.; Nakata, H.; Okano, Y. Self-propelled droplets for extracting rare-earth metal ions. *Soft matter* **2014**, *10*, 6316-6320.
76. Florea, L.; Wagner, K.; Wagner, P.; Wallace, G.G.; Benito-Lopez, F.; Officer, D.L.; Diamond, D. Photo-chemopropulsion–light-stimulated movement of microdroplets. *Adv. Mater.* **2014**, *26*, 7339-7345.
77. Francis, W.; Fay, C.; Florea, L.; Diamond, D. Self-propelled chemotactic ionic liquid droplets. *Chem. Commun.* **2015**, *51*, 2342 - 2344.
78. Francis, W.; Wagner, K.; Beirne, S.; Officer, D.L.; Wallace, G.G.; Florea, L.; Diamond, D. Electrotactic ionic liquid droplets. *Sensors Actuators B: Chem.* **2017**, *239*, 1069-1075.
79. Bain, R.M.; Pulliam, C.J.; They, F.; Cooks, R.G. Accelerated chemical reactions and organic synthesis in leidenfrost droplets. *Angew. Chem. Int. Ed.* **2016**, *55*, 10478-10482.
80. Funakoshi, K.; Suzuki, H.; Takeuchi, S. Lipid bilayer formation by contacting monolayers in a microfluidic device for membrane protein analysis. *Anal. Chem.* **2006**, *78*, 8169-8174.
81. Holden, M.A.; Needham, D.; Bayley, H. Functional bionetworks from nanoliter water droplets. *J. Am. Chem. Soc.* **2007**, *129*, 8650-8655.
82. Torre, P.; Keating, C.D.; Mansy, S.S. Multiphase water-in-oil emulsion droplets for cell-free transcription–translation. *Langmuir* **2014**, *30*, 5695-5699.

83. Sheng, L.; Kurihara, K. Transformation of oil droplets into giant vesicles. *Chem. Commun.* **2016**, *52*, 7786-7789.

## **Chapter 3:**

### **Application of Ionic Liquid Materials in Microfluidic Devices**

#### **3.1 Abstract**

#### **3.2 Introduction**

#### **3.3 Ionic liquids for Actuators**

#### **3.4 Ionic Liquids for Sensing**

#### **3.5 Ionic Liquids for Reagent Storage**

#### **3.6 Ionic liquids in Segmented Flow Microfluidics**

##### **3.6.1 Electrowetting on Dielectric (EWOD) Based Microfluidics**

##### **3.6.2 Chemotactic Ionic Liquids**

##### **3.6.3 Ionic Liquids as Microreactors**

#### **3.7 Conclusions**

#### **3.8 Acknowledgements**

#### **3.9 References**

## Chapter 3

---

# Application of Ionic Liquid Materials in Microfluidic Devices\*

---

**\*Application of Ionic Liquid Materials in Microfluidic Devices**, T Akyazi, J Saez, A Tudor, C Delaney, **W Francis**, D Diamond, L Basabe-Desmonts, L Florea\* and F Benito-Lopez\*. *Ionic Liquid Devices*. 978-1-78801-181-5, 2017

### **3.1 Abstract**

“Lab-on-a-Chip” (LOC) and microfluidics enable the manipulation of fluids at small length scales (from micrometers to millimeters). These systems often have well-defined fabrication processes and are capable of integrating multiple functional elements, to provide complete sample-in/answer-out systems. Nevertheless, the development of fully integrated microfluidic devices still faces some considerable obstacles, including fluidic control, miniaturisation and high costs.

Due to their unique properties, ionic liquids have arisen as smart solutions to circumvent some of the hurdles facing current LOC technologies. They can directly benefit microfluidic devices by aiding miniaturised fabrication and passive microfluidic elements for fluid control, sensing and sample storage. Improved chemical reactions and separation, in addition to power generation, temperature control, and electrowetting show potential for reducing manufacturing costs and widening market possibilities.

In this chapter we will look over and discuss the fundamental applications of ionic liquids within microfluidic systems.

### **3.2 Introduction**

Ionic liquids are drawing an increasing interest both in academia and in industry as confirmed by the growing number of publications and patents in the area [1,2]. Ionic liquids (ILs) are salts, completely constituted of ions with melting temperatures below 100 °C, which is a result of their low-charge density and low symmetry ions [1,3-5]. ILs are categorised as “green” solvents since they are, potentially, green alternatives to volatile organic compounds due to mainly their two outstanding properties: negligible volatility and conventional non-flammability [4-7]. Their unique properties are not limited to non-volatility and non-flammability; they have an excellent solvation ability for organic, inorganic and organometallic compounds with improved selectivity, high thermal stability (decomposition temperatures around 300–500 °C), high chemical stabilities (extremely redox robust), and lastly, high ionic conductivity all of which highly extends the variety of their applications [1-3,8-15]. Nevertheless, other properties, such as biodegradability and toxicity are not yet successfully overtaken, and they should be considered in ILs applications [7].

One of the main advantages concerning the applicability of ILs is the ability to tailor their physical and chemical properties (such as their polarities and affinities, their thermo-physical properties, biodegradation ability or toxicological features, as well as their hydrophobicity and solution behaviour) by a proper manipulation of the cation/anion chemical structure [16-21]. This feature gives them the name of ‘designer solvent’ and favours their use, particularly in the extraction, separation and analysis of value-added compounds from biomass [1-3,21,22]. Moreover, these tuneable properties are enabling rapid advances in devices and processes for the production, storage and efficient use of energy [1,23].

In many applications, the immobilisation of ILs in a solid or semisolid substrate, while keeping their specific properties, is a main requirement in order to generate useful devices. This is possible by the introduction of a new class of hybrid materials, ionogels. Ionogels preserve the important properties of the ILs (liquid-like dynamics and ion mobility) in a solid or a gel like structure, enabling easy shaping, manipulation and integration, increasing remarkably the potential application of ILs in fundamental areas such as energy, environment and analysis [24,25].

In recent years, researchers started to make use of the exceptional features of ILs and ionogels in the microfluidics area and many papers which include the incorporation of ILs materials in microfluidic systems have been published. “Lab-on-a-Chip” (LOC) / “micro-Total Analysis Systems”(μTAS) or microfluidic (continuous flow, microarray and droplet-based) analysis systems empower the manipulation of fluids at small scales (from a few micrometers up to a millimetre) and small volumes (nL to μL). Microfluidic devices run a series of fluidic unit operations on a platform which is designed with a well-defined fabrication technology and provide a consistent approach for miniaturisation, integration, automation and parallelisation of bio-chemical processes [26,27]. They have the greatest capability of integration of multiple functional elements into a small structure to produce absolute sample-in/answer-out systems [26]. The incorporation of functionalities such liquid handling, temperature control and detection components for sensing allows fast analysis and improves selectivity compared to conventional devices [26,27]. Nevertheless, the development of fully integrated microfluidic devices is still facing some compelling obstacles, including fluidic control, miniaturisation and high costs [26,28]. Considering the critical requirement of fluid control and fluid transport processes and high detection performance within these platforms, microfluidic devices have adopted a wide range of passively or actively controlled, high performance

components, such as microfluidic separators, actuators (valves and pumps), reactors, sample/biomolecule storage, sensing elements which are although sophisticated and achieve their tasks efficiently, are as well costly, highly increasing the price and so decreasing the final market possibilities of microfluidic devices.

Ionic liquids have excellent properties that could be used to improve microfluidic devices, since they are low-cost, easily obtainable materials. Their features make them very good and multifunctional candidates for improving the capabilities of microfluidic devices by building miniaturised / passive microfluidic elements for fluid control, sensing, sample storage, microfluidic separation, microreactors (nanoparticle synthesis), power generators, temperature controllers, electrowetting of surface, etc. whereas decreasing the manufacturing costs compared with conventional devices and widens the market possibilities. In this chapter we will look over the fundamental applications of ionic liquids within microfluidic devices. We will summarise ILs integration in microfluidic devices, **Table 3.1**, as well as their reported applications in Lab-on-a Chip devices and systems.

*Table 3.1 Ionic liquid names and abbreviations.*

| <b>Ionic liquid name</b>   | <b>Abbreviation</b>                         |
|--|---|
| triisobutyl(methyl) phosphonium tosylate                           | [P <sub>1,4,4,4</sub> ][Tos]                |
| tetrabutylphosphonium dicyanamide                                  | [P <sub>4,4,4,4</sub> ][DCA]                |
| trihexyltetradecyl phosphonium dicyanamide                         | [P <sub>6,6,6,14</sub> ][DCA]               |
| trihexyltetradecyl phosphonium bis(trifluoromethanesulfonyl) imide | [P <sub>6,6,6,14</sub> ][Ntf <sub>2</sub> ] |
| trihexyltetradecyl phosphonium dodecylbenzenesulfonate             | [P <sub>6,6,6,14</sub> ][DBSA]              |
| trihexyltetradecyl phosphonium chloride                            | [P <sub>6,6,6,14</sub> ][Cl]                |
| 1-Methyl-3-octylimidazolium tetrafluoroborate                      | [OMIM][BF <sub>4</sub> ]                    |
| 1-ethyl-3-methylimidazolium methyl sulphate                        | [EMIM][MeSO <sub>4</sub> ]                  |
| 1-ethyl-3-methyl imidazolium ethyl sulfate                         | [EMIM][EtSO <sub>4</sub> ]                  |
| 1-butyl-3-methylimidazolium hydrogen sulphate                      | [BMIM][HSO <sub>4</sub> ]                   |
| 1-ethyl-3-methyl imidazolium tetrafluoroborate                     | [EMIM][BF <sub>4</sub> ]                    |
| 1-ethyl-3-methylimidazolium dicyanamide                            | [EMIM][DCA]                                 |
| 1-Butyl-3-methylimidazolium tetrafluoroborate                      | [BMIM][BF <sub>4</sub> ]                    |
| 1-Butyl-3-methylimidazolium hexafluorophosphate                    | [BMIM][PF <sub>6</sub> ]                    |
| 1-Butyl-3-methylimidazolium dodecanesulfonate                      | [BMIM][DoS]                                 |
| 1-Butyl-3-methylimidazolium bis(trifluoromethanesulfonyl)imide     | [BMIM][NTf <sub>2</sub> ]                   |
| 1-Hexyl-3-methylimidazolium bis(trifluoromethanesulfonyl)imide     | [HMIM][NTf <sub>2</sub> ]                   |
| 1-Butyl-1-butyl-4-methylpyridinium tetrafluoroborate               | [BMPy][BF <sub>4</sub> ]                    |

### 3.3 Ionic Liquids for Actuators

In 2007 Sugiura *et. al* [29] proposed photo-responsive microfluidic hydrogel valves by copolymerising *N*-isopropylacrylamide (NiPAAm) with a photochromic acrylic benzospiropyran ester (BSP) moiety. Prior to photo-polymerisation, the cocktail mixture of the monomer and the photochromic unit was dissolved in 1-butanol, together with a UV initiator and crosslinker. The photoresponse mechanism of these hydrogels comes as a result of the benzospiropyran moiety present in the copolymer matrix. When the copolymer had been kept in the dark and exposed to an aqueous solution of HCl, the benzospiropyran moiety protonates, changing its conformation to the protonated merocyanine form. When in this conformation, the presence of charges on its backbone contributes to it being more hydrophilic than the closed benzospiropyran conformation. Thus, it absorbs more water and, by irradiating it with white light, it can be reversed to the more hydrophobic benzospiropyran form, together with the release of water. The authors have shown that valves obtained from this material can perform, if preconditioned overnight in acidic conditions, to open and stop the flow inside a poly(dimethyl siloxane) (PDMS) microfluidic device.

Building on this work, Benito-Lopez *et. al.* [30] synthesised photo-responsive ionogel valves in microfluidic channels by copolymerising NiPAAm and BSP using a mixture of 1-butanol and phosphonium ionic liquids as the solvent. Four different ILs were used, namely triisobutyl(methyl) phosphonium tosylate ([P<sub>1,4,4,4</sub>][Tos]), trihexyltetradecyl phosphonium dicyanamide ([P<sub>6,6,6,14</sub>][DCA]), trihexyltetradecyl phosphonium bis(trifluoromethanesulfonyl) imide ([P<sub>6,6,6,14</sub>][Ntf<sub>2</sub>]), and trihexyltetradecyl phosphonium dodecylbenzenesulfonate ([P<sub>6,6,6,14</sub>][DBSA]), respectively. The resulting crosslinked polymers were left to swell in 1 mM HCl solution for 2 h to reach their maximum swelling capabilities. Following this, they were irradiated with a white light LED until they shrank to their minimum size. In all cases, the time needed for this operation was 100 s. The hydrogel which exhibited maximum shrinking was the control hydrogel, followed by the [P<sub>6,6,6,14</sub>][DCA], [P<sub>1,4,4,4</sub>][Tos], [P<sub>6,6,6,14</sub>][DBSA], and [P<sub>6,6,6,14</sub>][Ntf<sub>2</sub>], respectively. Following this, the monomer mixtures were polymerised in microfluidic devices that featured inlet ports connected to five micro-channels which converged into a single microchannel with an outlet port. In each of the five micro-channels there was a circular reservoir with a diameter of 500 µm and a height of 175 µm where the monomer mixtures were photopolymerised. The micro-channels were 500 µm in width and 50 µm in height. After photopolymerisation, the microfluidic device was flushed with 1 mM HCl to swell the hydrogels. After the hydrogels were swollen and

were blocking the channels, a vacuum was applied to the outlet to facilitate the flow and water containing different coloured dyes was placed at each of the inlets. The valves were actuated using a white light LED with a power output of  $1 \text{ mW} \cdot \text{cm}^{-2}$ . Actuation times were 2 s for the control hydrogel, 4 s for the  $[\text{P}_{6,6,6,14}][\text{DCA}]$ , 18s for the  $[\text{P}_{1,4,4,4}][\text{Tos}]$ , 44 s for the  $[\text{P}_{6,6,6,14}][\text{DBSA}]$ , and 49 s for the  $[\text{P}_{6,6,6,14}][\text{Ntf}_2]$  ionogel, respectively (**Figure 3.1**). This example shows that through the incorporation of different ionic liquids of varying hydrophilic/hydrophobic character, inside ionogel matrices, actuation times can be modulated on demand. The time for the hydrogels to revert back to their original size is approximately 30 min, which lead the researchers to conclude that this type of valve would be best suited for single-use devices.

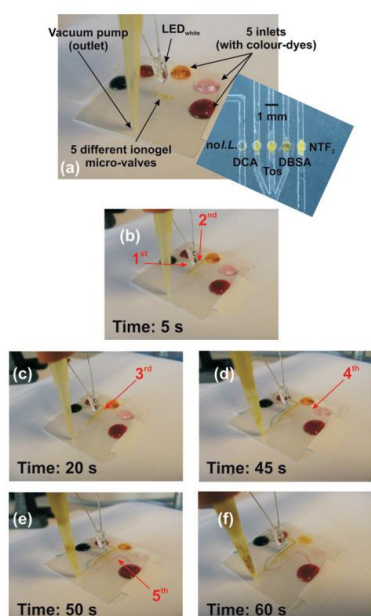


*Figure 3.1 Image of the microfluidic manifold showing the performance of the ionogel microfluidic valves: (a) all microvalves are closed under the applied vacuum. White light is applied for the time specified in each picture (b) Hydrogel (no IL present) valve is first to actuate followed by ionogels incorporating [DCA]- (c), [Tos]- (d), [DBSA]- (e), [NTf<sub>2</sub>]- (f). Numbers and arrows indicate when the channel is filled with the dye due to microvalve actuation. Reproduced from Benito-Lopez et al. [30] with permission from The Royal Society of Chemistry.*

A more comprehensive study of such photo-responsive ionogel materials was later performed by Czugala *et. al* [31] who studied the photo-responsive behaviour of pNiPAAm-co-BSP ionogels made using phosphonium ILs as solvents. Three different phosphonium ILs were chosen for this study: trihexyltetradecyl phosphonium chloride  $[\text{P}_{6,6,6,14}][\text{Cl}]$ ,  $[\text{P}_{6,6,6,14}][\text{DCA}]$  and  $[\text{P}_{6,6,6,14}][\text{Ntf}_2]$ , respectively, and ionogel actuators were photo-polymerised in four different shapes of varying surface area to volume ratios

(SA/V): rings, 250  $\mu\text{m}$  discs, 500  $\mu\text{m}$  discs, and lines, respectively. Their change in size was determined by the change in height, as measured using digital microscopy. By measuring the amount of hydration for each ionogel shape, it was determined that the  $[\text{P}_{6,6,6,14}][\text{Ntf}_2]$  swelled the most, at a value of 109-180 % of the initial gel height (right after photo-polymerisation), followed by  $[\text{P}_{6,6,6,14}][\text{DCA}]$  ionogels (40-58 %), and lastly the  $[\text{P}_{6,6,6,14}]\text{Cl}$  ionogels (20-27 %). Following this, the shrinking behaviour of the ionogels was analysed and it was determined that after 30 min of white light irradiation, the  $[\text{P}_{6,6,6,14}][\text{Ntf}_2]$  ionogels shrunk by 108 %, 15% of their initial height, followed by the  $[\text{P}_{6,6,6,14}][\text{DCA}]$  ionogels shrunk by 42 %, reaching also 15 % of their initial height, while the  $[\text{P}_{6,6,6,14}]\text{Cl}$  ionogels shrunk only by 16 %, reaching 4 % of their initial height (**Figure 3.2**). The kinetics of the swelling and shrinking behaviours were also determined and in each case the  $[\text{P}_{6,6,6,14}][\text{Ntf}_2]$  ionogels exhibited the highest rates of swelling and shrinking at  $(5.3 \pm 0.1) \cdot 10^{-2}$  s and  $(29 \pm 4) \cdot 10^{-2}$  s, followed by  $[\text{P}_{6,6,6,14}][\text{DCA}]$  at  $(4.5 \pm 0.3) \cdot 10^{-2}$  s and  $(8.3 \pm 0.9) \cdot 10^{-2}$  s, and  $[\text{P}_{6,6,6,14}]\text{Cl}$  at  $(3.9 \pm 0.2) \cdot 10^{-2}$  s and  $(9 \pm 2) \cdot 10^{-2}$  s, respectively. The high swelling and shrinking values attributed to the  $[\text{P}_{6,6,6,14}][\text{Ntf}_2]$  are believed to stem from the fact that this ionic liquid possesses a highly delocalised charge on the S-N-S backbone of the  $\text{Ntf}_2^-$  anion, which makes it interact less with the charged moieties of the polymer. This leads to more freedom for the polymer backbone to interact with the hydration medium. In the case of the  $[\text{P}_{6,6,6,14}][\text{Cl}]$ , this effect is inhibited by the localised charge on the chloride ion, thus associating more strongly to the polymer backbone. The  $[\text{P}_{6,6,6,14}][\text{DCA}]$  ionogels would have an intermediate behaviour between these two states. Based on these results, the  $[\text{P}_{6,6,6,14}][\text{Ntf}_2]$  ionogels were incorporated in a glass-poly(dimethyl siloxane) microfluidic device as light actuated valves. Using a fiber optic to irradiate with white light, the ionogel valve opened after 180 s, allowing liquid to pass through the microfluidic channel [31].

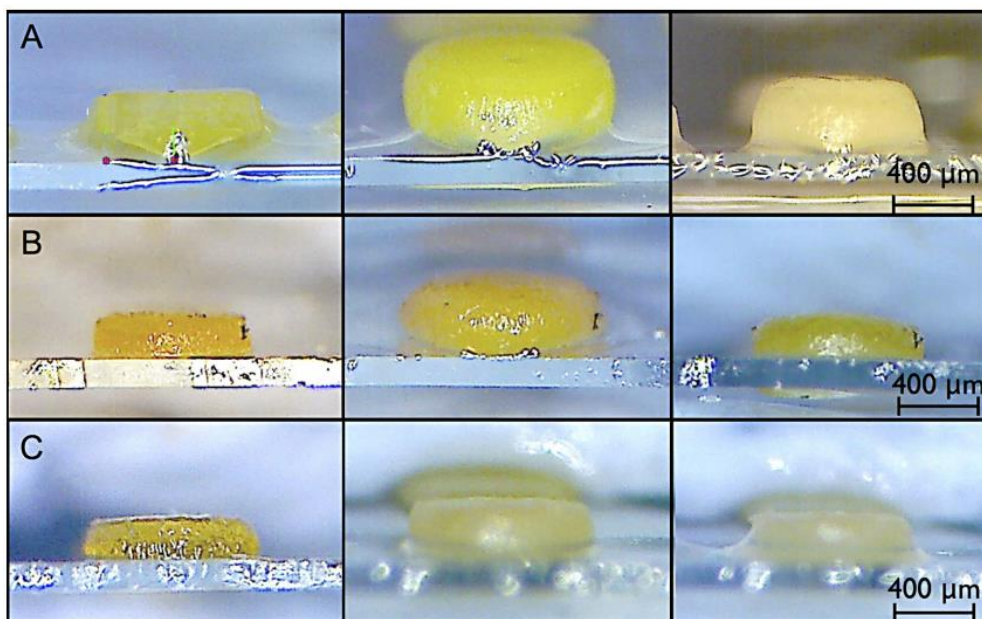


Figure 3.2 Microscope images of ionogel discs made of: (a)  $[P_{6,6,6,14}][NTf_2]$ , (b)  $[P_{6,6,6,14}][DCA]$  and (c)  $[P_{6,6,6,14}][Cl]$  after photopolymerisation (left); swelling in 1mM HCl solution for 2h (middle) and shrinking upon white light irradiation (right). Reproduced from Czugała *et. al* [31]. Copyright © 2014 Elsevier B.V. All rights reserved.

An application of these materials was demonstrated by Czugała *et. al* [32] by using the  $[P_{6,6,6,14}][DCA]$  ionogels as photo-responsive valves in a microfluidic analysis platform for the detection of nitrite anions in water. The nitrite assay was done using the Griess reagent and the change in colour was determined using a Paired Emitter Detector Diode (PEDD) arrangement integrated in the microfluidic holder. The emitter diode has a wavelength of 540 nm, while the detector diode has its maximum absorption at 660 nm. Part of the light produced by the emitter diode is absorbed by the Griess-nitrite complex, which has its maximum absorption at 547 nm, while the rest reaches the detector diode and is transformed into a photo current. The amount of photo current generated is proportional to the concentration of nitrite within the sample. By connecting the PEDD setup to a microcontroller fitted with a wireless radio antenna, the data was sent to a PC, where it was stored and analysed. The monomer mixture was photopolymerised using UV light in a circular reservoir with a radius of 500  $\mu\text{m}$  and a height of 225  $\mu\text{m}$ . The reservoir sat at the junction of a Y-shaped microchannel that separated the sample from the Griess reagent (**Figure 3.3a**). To operate the valve, the microchannel was filled with 1 mM HCl and left to swell for 2h in the dark. The opening of the valve was performed with irradiation from a white light LED that was also mounted on the microfluidic device

holder. By irradiating with a power of  $1 \text{ mW}\cdot\text{cm}^{-2}$ , the ionogel valve opened after  $30 \pm 5 \text{ s}$  ( $n=3$ ) (**Figure 3.3b**) and was operated at a pressure of 25 mbar; pressures higher than  $31 \pm 4 \text{ mbar}$  ( $n=3$ ) deformed the materials and the valves failed. After the ionogel shrunk, the reagent mixture was pumped through the microchannel where it mixed and moved to the detection area for analysis. The calibration curve was made using concentrations of nitrite from  $0.2 \text{ mg}\cdot\text{L}^{-1}$  to  $1.2 \text{ mg}\cdot\text{L}^{-1}$ , in  $0.2 \text{ mg}\cdot\text{L}^{-1}$  steps and performed in triplicate. This yielded a  $R^2$  value of 0.98, a level of detection (LOD) of  $34.0 \pm 0.1 \text{ }\mu\text{g}\cdot\text{L}^{-1}$  and a level of quantification (LOQ) of  $115 \pm 3 \text{ }\mu\text{g}\cdot\text{L}^{-1}$ , compared to a  $R^2$  value of 0.99, LOD value of  $1.50 \pm 0.02 \text{ }\mu\text{g}\cdot\text{L}^{-1}$ , and a LOQ of  $14.8 \pm 0.2 \text{ }\mu\text{g}\cdot\text{L}^{-1}$  for a UV-Vis spectrophotometer. The results obtained for the microfluidic platform are lower than the detection limits set by the World Health Organisation. Following this, freshwater samples from the Tolka River in Dublin, Ireland were analysed with both the portable platform and the UV-Vis spectrophotometer. The close nature of both sets of results proved the suitability of such a microfluidic device and detector for the accurate monitoring of nitrates in real-life samples.

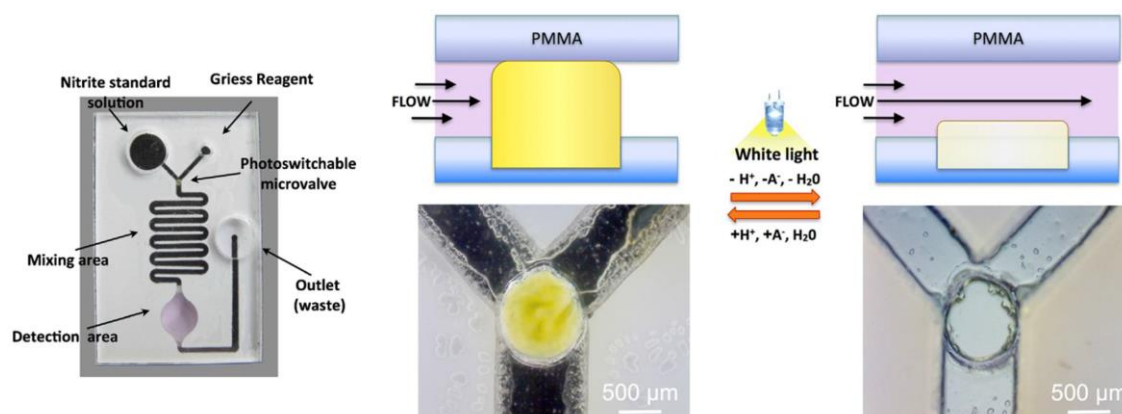


Figure 3.3 Picture of the microfluidic device fabricated in PMMA: PSA polymer by  $\text{CO}_2$  laser ablation (left). Schematic (top) and images (bottom) of the photoresponsive microvalve in closed (middle) and opened (right) state. Reproduced from Czugała *et. al* [32]. Copyright © 2013 Elsevier B.V. All rights reserved.

Thermo-responsive actuation was also proposed for micro-valves fabricated using poly(*N*-isopropylacrylamide) polymer (pNiPAAm) gels [33]. To synthesise these materials, all the components for the monomer mixture were dissolved in 1-ethyl-3-methyl imidazolium ethyl sulfate [EMIM][EtSO<sub>4</sub>]. The addition of this IL, as demonstrated prior by Gallagher *et. al*, [34] improves the swelling and shrinking

capabilities of the pNiPAAm materials, together with lowering the LCST. The microfluidic devices in this study were fabricated using a cutting plotter to cut 100  $\mu\text{m}$  thick layers of cyclic olefin polymer (COP) and thermally bonded, to obtain a microfluidic device with a total area of 1  $\text{mm}^2$  and a total maximum thickness of 1 mm. The resulting microfluidic devices possessed a circular reservoir, which was filled with the monomeric mixture and photopolymerised using UV light. Following this, the resulting microfluidic devices were mounted in a microfluidic holder with an incorporated heating element which could thermally actuate the ionogel valve. The characterisation of the ionogel valves was performed by connecting the inlet of the microfluidic device to a syringe pump with a set flow rate of 1000  $\text{nL}\cdot\text{min}^{-1}$ , while the outlet was connected to a flow micro-sensor. Using this experimental setup, the failure pressure of the valves was determined to be  $1100 \pm 100$  mbar ( $n = 5$ ) and they successfully operated at 200 mbar after being exposed to pressures higher than 1100 mbar. Setting the heating element of the microfluidic holder at a temperature higher than 50  $^{\circ}\text{C}$ , the valves opened  $4 \pm 1$  s ( $n = 5$ ), after the temperature of the ionogel passed its LCST. Recovery was achieved in  $32 \pm 2$  s ( $n = 5$ ), after the temperature dropped below the LCST of the ionogel valves (**Figure 3.4**). Furthermore, after 10 repetitions, there was no discernable drop in valve performance, showing the potential of these materials as cost-effective reversible valves.

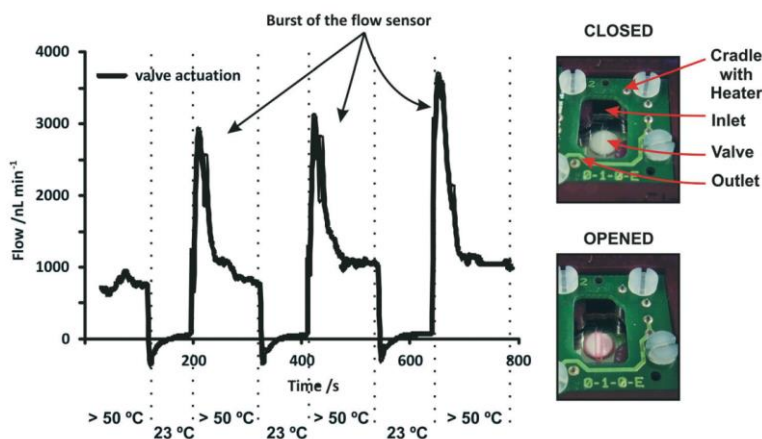


Figure 3.4 Flow profile during three full actuation cycles (left) and photo of the microfluidic device containing the thermo-actuated valve and the microfluidic holder with integrated heaters at the bottom. High flow spikes are due to the stabilisation of the microflow sensor after opening of the valve. Reproduced from Benito-Lopez, et. al [33] with permission from The Royal Society of Chemistry.

Electro-actuation of IL based micro-valves has also been studied. Ghamsari *et. al* [35] demonstrated the use of bulky gels based on the 1-ethyl-3-methyl imidazolium tetrafluoroborate ionic liquid ([EMIM][BF<sub>4</sub>]), poly(vinylidene fluoride) (PVDF), and single-walled carbon nanotubes (SWCNT), respectively, as low-voltage micro-valve actuators. Bucky gels are gel-like mixtures of carbon nanotubes and ILs which benefit from both the high electrical conductivity associated with carbon nanotubes and the properties of ILs, such as high temperature and electrochemical stability. Bucky gel actuators (BGA) are composite materials which feature a polymer electrolyte core, in this case an ionogel of [EMIM][BF<sub>4</sub>] and PVDF, inserted between two layers of electrodes made out of bulky gels. Applying voltage to this composite will make it bend in the direction of the applied voltage (**Figure 3.5a and b**). The electrode components composite was made by mixing all the aforementioned constituents with dimethylacetamide (DMAC) in a ball mill until a black gel mass was obtained. The resulting gel was cast in PDMS moulds and dried until all the DMAC had evaporated. The ionogel layer was fabricated in the same way, without the addition of SWCNT to the constituent mixture. The resulting layers were then hot-pressed together and covered in a layer of PDMS to increase the adhesion of the resulting BGA to the walls of the microfluidic device, which would ensure better sealing during operation. The actuation properties of the BGA are dependent on the total thickness of the device and on the ratio between the electrolyte layers. Three devices were tested to determine which generates the maximum amount of force by application of a voltage sweep between 4 and 10 V. The devices had thicknesses of 281.9 (BGA1), 322.6 (BGA2), and 393.7 (BGA3), and thickness ratios of 0.73, 1.20, and 0.87, respectively. The results indicated that BGA3 generated a force of 80 mN, which was the highest generated force of the three BGAs. BGA1 and BGA2 generated forces of 38 and 41 mN, respectively. By enclosing the BGAs in a PDMS layer, the forces generated when a voltage is applied are increased between 14 to 23 %. Taking into account that the BGAs will be used in an aqueous medium, a voltage sweep between 2 and 10 V confirmed that there are no bubbles formed due to the hydrolysis. All three BGAs were fitted to microfluidic devices to cover an inlet channel that was fabricated from a tube (**Figure 3.5c and d**). The tests consisted of using three different operating voltages, namely 5, 8 and 10 V and six different frequencies: 250, 125, 100, 50, 25, and 0 mHz respectively. For all the BGAs, the results indicated that the higher the voltages and the lower the frequency, the better they are suited for use as microfluidic valves. The best results were obtained at 10 V and 0 mHz, at which the flow

rate was reduced by 93 %. In all experiments, a leakage flow was present, which led the researchers to determine that the design of the device can be improved to minimise the reoccurrence of this phenomenon.

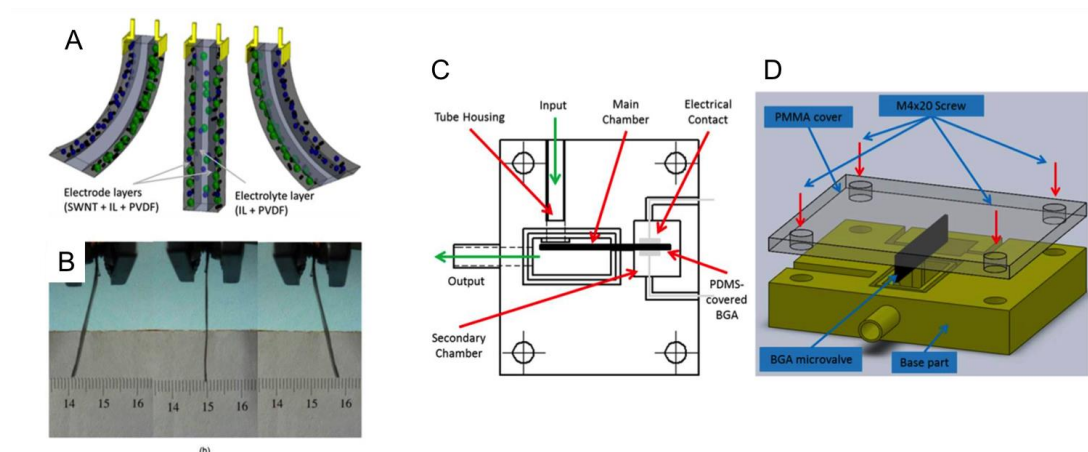


Figure 3.5 (a) BGA bending motion as a result of ion transfer between layers; direction of bending can be reversed by changing the polarity of the applied potential; (b) BGA strip bended (10 V, 0.1 Hcolor); (c) Base part and (d) 3D view of the flow regulator assembly. Reprinted with permission from Ghamsari *et al.* [35]. Copyright 2013 American Chemical Society.

### 3.4 Ionic Liquids for Sensing

The use of ionic liquids (ILs) for sensing in microfluidic devices continues to gain traction, owed primarily to the ability of these materials to offer a matrix which is capable of responding to chemical and physical stimuli. The wide electrochemical windows, high conductivity, propensity to stabilise enzymes and liquid state at room temperature have carved a particular niche for these exciting new materials in the field of sensing chemical and physical changes [37]. Their ability to immobilise molecules for use in pH analysis, catalysis and electrochemistry have also brought additional application as biomolecular sensors [38].

The serendipitous growth of point-of-care (POC) technologies, in particular through organic electronics, has buttressed the development of these compounds with a tangible need for efficient protein solubilisation in specific pH and temperature ranges. One such example, by Yang *et al.* [39] shows recent inroads being made in the field of Organic Electrochemical transistors (OECTs), which have found application in the sensing of ions and antibodies. These simple transistors operate through migration of ions

from an electrolyte into a semiconductor, which is often fabricated from a doped polymer, such as poly(3,4-ethylenedioxythiophene) doped with poly(styrene sulfonate) (PEDOT : PSS). By using redox enzymes, such as glucose oxidase in Phosphate Buffer Solution (PBS), it has been possible to achieve micromolar limits of detection [39]. Recent endeavours to use RTILs as a suitable replacement for aqueous electrolytes has brought Yang *et al.* to an IL, namely triisobutyl-(methyl)-phosphonium tosylate [ $P_{1,4,4,4}$ ][Tos], for the fabrication of a new generation of OECTs (**Figure 3.6**). The hydrophilic nature of the IL, attributed to the tosylate anion, ensures that when patterned over the active area of the OECT, the material subsequently acts as a reservoir for the enzyme and mediator. Upon mixing, the mediator (ferrocene in this case) dissolves, while the enzyme remains dispersed. The presence of this dispersion can have a positive impact on the lifetime of the device by inhibiting a change in the secondary enzyme structure [40]. **Figure 3.6c** shows that the analyte, in this case a glucose solution forms directly over the area pre-defined by tridecafluoro-1,1,2,2-tetra-hydrooctyl trichlorosilane (FOTS) template. The device, which operates in the  $10^{-7}$ - $10^{-2}$  M range, well within within clinical ranges found in the blood (2–30 mM) and saliva (0.008–0.21 mM) [41] shows great potential for use as a low cost, disposable, POC device.

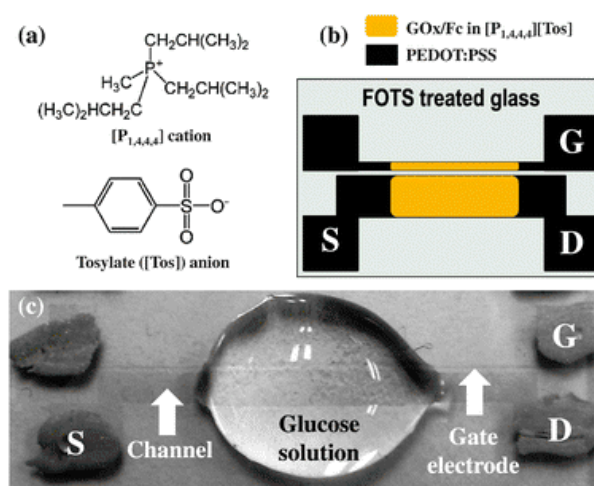


Figure 3.6 (a) Chemical structure of [ $P_{1,4,4,4}$ ][Tos]. (b) Schematic of the OECT. (c) Image of the OECT with a drop of glucose solution added. Reproduced from Yang *et al.* [39] with permission from The Royal Society of Chemistry.

This work has also been developed to sense for other clinically relevant analytes, such as lactate, through incorporation of lactate oxidase (LOx) into an OECT device [42]. In this instance a flexible ionogel based NIPAAm, N,N-methylene-bis(acrylamide)

(MBAAm) and [EMIM][EtSO<sub>4</sub>] incorporating the LOx enzyme was polymerised on the OECT device. As in the case for the glucose sensor, introduction of the specific analyte (in this case lactate), results in an increase in the drain current, which can be directly correlated to lactate concentration, as seen in **Figure 3.7a** and **b** shows a prototype fabricated from parylene worn on the forearm. [43] Such a flexible prototype, coupled with detection levels suitable for use in the clinical range, prove extremely exciting potential in the fields of sport science and patient care. The conformability of an ionogel incorporated into the OECT device, offers a flexibility not previously possible with more rigid conjugated polymers.

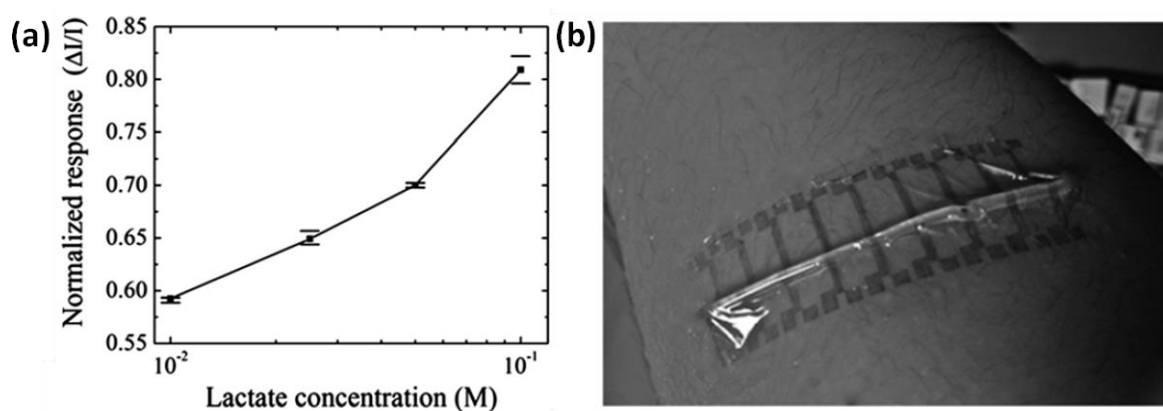


Figure 3.7 a) Normalised response vs. lactate concentration for the OECT and b) Flexible OECT on the forearm. Adapted from Khodagholy *et al.* [43] with permission from The Royal Society of Chemistry.

A true understanding of the effect that ILs have on enzymes, has recently been developed by Curto *et al.* [44], in particular for choline-based ILs containing LOx enzyme. They conclude that hydrated ILs can provide the necessary hydrogen bonding for necessary stabilisation of proteins, in addition to controlling the proton buffering within the medium. Interestingly, when stored in choline chloride, over a 140 day period at 5 °C, 80 % of the initial activity of LOx.

In a similar fashion to the immobilisation of enzymes, ionic liquids can also be used to stabilise other sensing molecules such as dyes. Through ion-pair interactions, a charged dye molecule can be held in the IL or ionogel matrix without leaching. Czugała *et al.* have developed a direct application of such a system, through the use of a centrifugal disc with functionalised ionogel sensing areas [45]. The ionogel, based on poly(N-isopropyl-acrylamide) and N,N'-methylene-bis(acrylamide) and shown **Figure**

**3.8a** is used to entrap the ionic liquid, tetrabutylphosphonium dicyanamide [ $P_{4,4,4,4}$ ][DCA], and the dye molecule, bromocresol purple (BCP), shown in **Figure 3.8(b)** and **(c)**, respectively. Photopolymerisation yielded an ionogel, which responds to a variation in pH with the colour change shown in **Figure 3.8**.

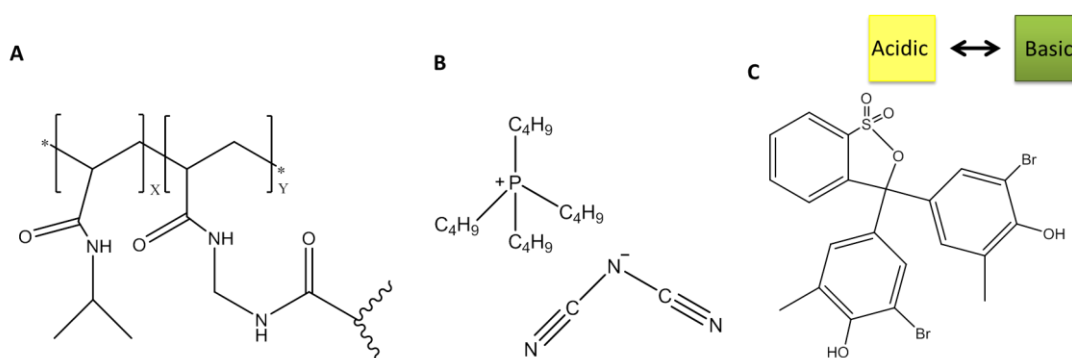


Figure 3.8 Chemical structures of A) *N*-Isopropyl-acrylamide and *N,N*-methylene-bis(acrylamide) crosslinked polymer; B) ionic liquid tetrabutylphosphonium dicyanamide [ $P_{4,4,4,4}$ ][DCA] and C) Bromocresol Purple, showing colour changes in acidic and basic environments. Reproduced from Czugala et al. [45] with permission from The Royal Society of Chemistry.

By development of a light emitting diode (LED) based detector it is possible to generate a colorimetric assay. Optimisation of the concentration of BCP concluded with a  $6 \times 10^{-3}$  M concentration which was used to generate calibration curves across a range of pH values, as shown in **Figure 3.9**. Moreover, through incorporation of these ionogel materials into a centrifugal disc device, it was possible to include a full colorimetric assay in a CD platform.

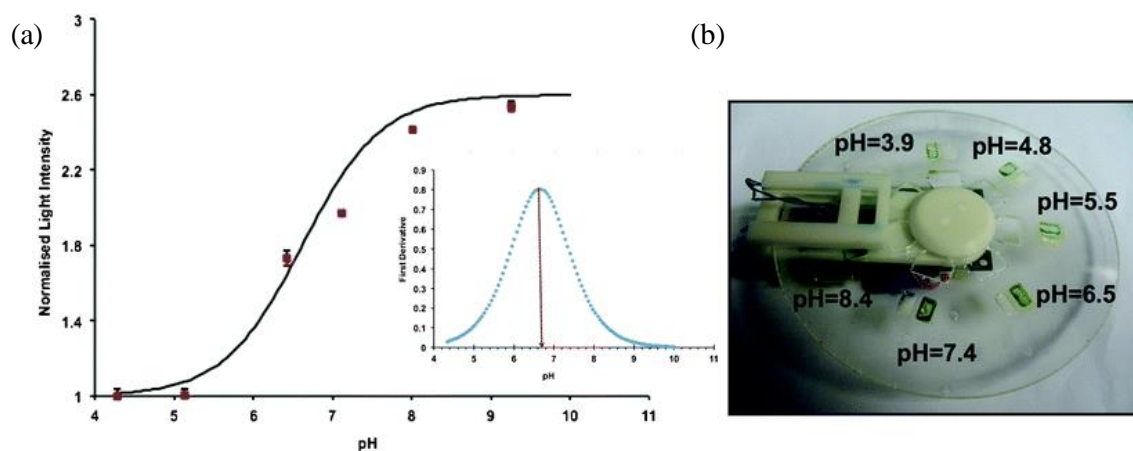


Figure 3.9 (a) Calibration curve of the sensing area of the microfluidic device using pH buffer solutions; (b) Image of the CD platform with the sensing area. Reproduced from Czugala *et al.* [45] with permission from The Royal Society of Chemistry.

In a similar fashion, Curto *et al.* [46] have extended the use of IL encapsulated pH responsive dyes to yield a simple barcode device which is capable of measuring sweat pH in real time, using colorimetric imaging through a mobile phone application (**Figure 3.10**). In a bid to further extend the lifetime of the microfluidic device, immobilisation of the ionogel on a polymethyl methacrylate (PMMA) substrate was achieved through the use of water plasma treatment, followed by silanisation. The ionogel containing the various dye molecules could then be directly bonded to the functionalised surface, through covalent attachment. By applying an algorithm which mapped to the hue saturation value (HSV) colour space it was then possible to use the mobile phone application to generate calibration curves with  $R^2$  value greater than 0.995.

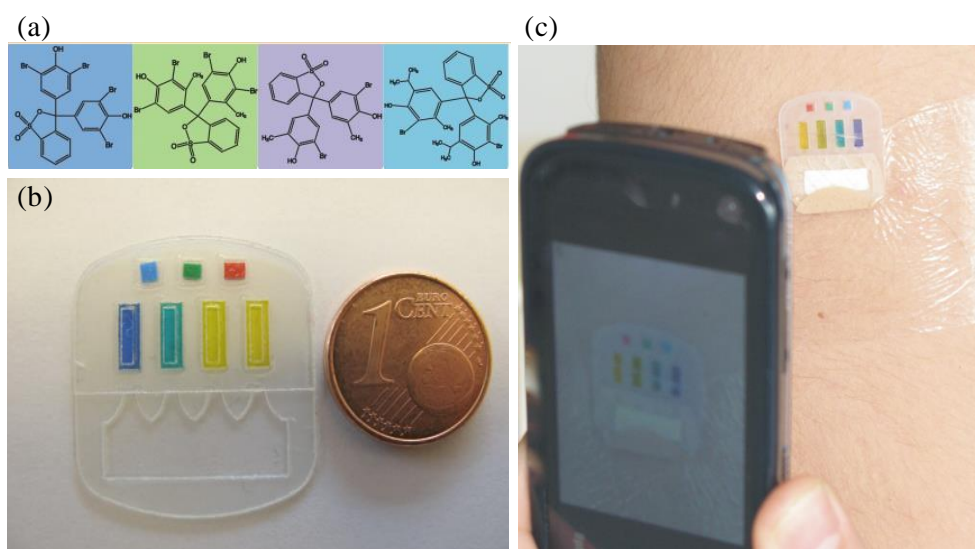


Figure 3.10 (a) Chemical structures of the pH sensitive dyes: Bromophenyl Blue (BPB), Bromocresol Green (BCG), Bromocresol Purple (BCP) and Bromothymol Blue (BTB); (b) Fabricated micro-fluidic device; (c) Smartphone application imaging on-body device. Reproduced from Curto *et al.* [46] with permission from the authors.

Not only can ionic liquids be used as vehicles for entrapping, immobilising and stabilising sensing materials, such as enzymes, dyes and stimuli responsive materials, they too can be used for their direct interactions with target molecules, most notably in the fields of capillary and microfluidic device electrophoresis. Using ILs as the

supporting electrolyte or as additives to the running buffer can dramatically increasing the speed and efficiency of operation, in addition to broadening the range of compounds which can be separated using electrophoresis. When used as background electrolytes, in a similar fashion to alkylammonium salts, ILs based on the 1-alkyl-3-methylimidazolium cation were seen to behave as electroosmotic flow modifiers through interaction of the cation either by coating the capillary wall or by migrating into the bulk solution [47]. For the separation of polyphenol compounds in grape extracts the method proved reliable and reproducible. Similarly, for microfluidic device electrophoresis, the use of dynamic coating can prove to be a viable solution to counteract the adsorption of compounds on the hydrophobic polymer materials commonly used for microfluidic fabrication. In the analysis of proteins, for example, surface modification of PDMS channels with ILs, such as 1-butyl-3-methylimidazolium dodecanesulfonate ([BMIM][DoS]) and [EMIM][BF<sub>4</sub>], can serve to inhibit adsorption of analytes [48].

### 3.5 Ionic Liquids for Reagent Storage

Due to their versatility, promising solvation properties and interactions with solute species, ionic liquids have been long proposed as alternative solvents [52-54]. Building up on this and adding their high thermal stability, negligible vapour pressure and enzymatic stability, ionic liquids and ionic liquid gels have been recently proposed as storage media in microfluidic devices. Weidmann *et al.* [55] proposed in 2012, a microfluidic deposition device using ionic liquid matrices which displayed the capability of ionic liquids as matrices for the analysis of biomolecules by MALDI-MS. The microfluidic spotting device addressed several issues of standard protocols employed for MALDI-MS sample preparation such as the co-crystallisation of sample and matrix, clogging and heterogeneity of sample spots. Since the ionic liquids did not solidify during the measurement, the sample spots remained homogeneous.

Using an ink-jet printing approach, UV-cured ionogel-based microarrays were fabricated and used them for long-term reagent storage of biotin-647 in a LOC device [56]. The ionogel cocktail was based on crosslinked *N*-isopropylacrylamide (NIPAM) and [EMIM][EtSO<sub>4</sub>] ionic liquid. Biotin-647 was added to this cocktail and the mixture was printed on 6 x 6 array of 300 µm circles (**Figure 3.11a**) on a variety of untreated substrates such as cyclic olefin copolymer (COC), cyclic olefin polymer (COP), and polypropylene (PP). Following this, the samples were exposed to UV light at 365 nm for

15s to photo-polymerise the printed cocktail and create the final ionogel matrix (**Figure 3.11b**).

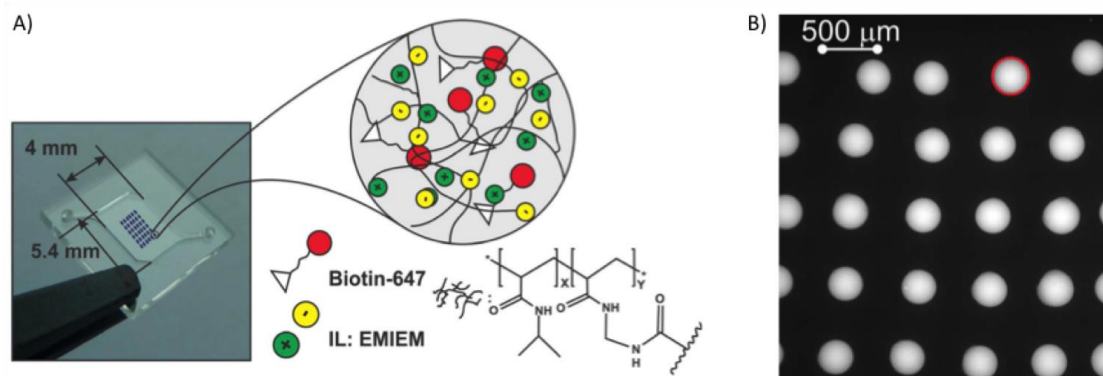


*Figure 3.11 A) Ink-jet printed ionogel microarray in the microfluidic device and representation of the composition of the ionogel spots; B) Fluorescence images of biotin-647 inside an ionogel-based microarray. Reproduced from Tijero et al. [56] with permission from Springer.*

The viability of this ionogel microarray was demonstrated for biotin-647 storage for over 1 month at room temperature while also proving to effectively keep the activity of biotin-647 in these conditions.

### 3.6 Ionic Liquids in Segmented Flow Microfluidics

Segmented flow systems offer many exciting and advantageous opportunities in the microfluidic field. Unlike continuous flow microfluidics (which use one single continuous flow), segmented flow devices typically rely on two distinct methods in order to move reagents throughout the microfluidic devices. In the first method, two immiscible flows are forced together at a T-junction, which results in one of the flows becoming the carrier while the second forms droplets [57]. The second method involves the direct manipulation of discrete individual droplets across different types of interfaces (solid-liquid, liquid-air) [58], [59]. All segmented flow systems are characterised by a high surface area to volume ratio which results in high heat and mass transfer rates; however, the biggest advantage of these types of flows is the compartmentalisation of reagents into droplets, which allows for control over both the internal and external environment which the reagents are exposed to. Dissociation of reagents from the external environment allows for numerous applications which are not otherwise able to be performed using a continuous flow system, such as having droplets acting as micro-reactors [60], cargo

transporters [61], dynamic sensors [62] or drug delivery units [63]. Due to the highly customisable nature of ionic liquids, as well as their high thermal stability and non-combustibility, ionic liquids are ideal candidates for droplet / segmented flow regimes.

### 3.6.1 Electrowetting on Dielectric (EWOD) Based Microfluidics

Electrowetting on dielectric is the phenomenon by which a discrete droplet can be electrically actuated across a series of electrodes. EWOD is one of the main forms of actuation associated with digital microfluidics and the process involves altering the wettability of a surface via an externally applied electrical field. When the electric field is applied to the device, charges accumulate at the interface between the droplet and solid surface, decreasing the interfacial tension and thus lowering the contact angle between the droplet and the surface [64]. By addressing sequential electrode pairs in the system, an interfacial tension gradient can be created between neighbouring electrodes, which the droplet will follow to a pre-determined destination. Traditionally, aqueous based droplets have been used in EWOD systems, however, due to their high thermal stability, low combustibility and minimal tendencies to corrode the metal parts of the devices, many groups have looked to ILs to replace them [65-67].

Li *et al.* [68] used high speed video microscopy to investigate the dynamic electrowetting and dewetting capabilities of ILs. In this study they employed five popular imidazolium-based ILs as probe liquids, namely 1-butyl-3-methylimidazolium tetrafluoroborate ([BMIM][BF<sub>4</sub>]), 1-butyl-3-methylimidazolium hexafluorophosphate ([BMIM][PF<sub>6</sub>]), [BMIM][NTf<sub>2</sub>], 1-hexyl-3-methylimidazolium bis(trifluoromethanesulfonyl)imide ([HMIM][NTf<sub>2</sub>]) and 1-methyl-3-octylimidazolium tetrafluoroborate ([OMIM][BF<sub>4</sub>]). The focus of this study was to observe the electrowetting at a fixed potential, followed by the dewetting once the potential had been removed. The electrowetting experiments were performed on a fluoropolymer surface (low wettability) under a fixed DC potential of 120 V. Once the electric field was introduced, the base area of the ILs increased exponentially until a maximum area was reached; once the electric field was removed the base area decreased exponentially until they assumed their initial position (**Figure 3.12**).

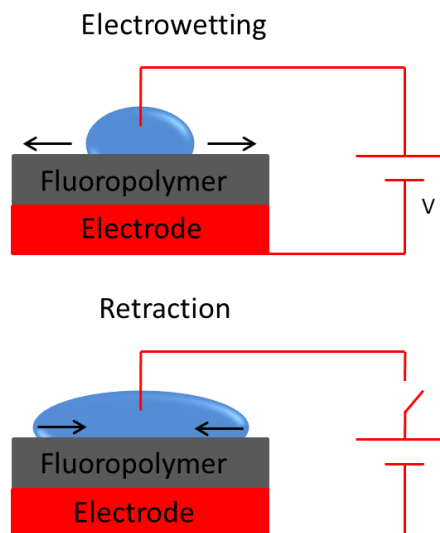


Figure 3.12 Illustration of ILs electrowetting and retraction behaviour in the presence (top) and absence (bottom) of a DC potential of 120V. Reproduced from Li *et. al* [68]. Copyright © 2013 Langmuir. All rights reserved.

The IL droplets electrowetting occurred roughly twice as fast as the subsequent retraction, due to the bulky ions within the ILs, which makes it easier to arrange the ions than to destroy their arrangement. The results showed good reversibility which was related to the low contact angle hysteresis of the ionic liquids used. This study showed that ILs can undergo reversible electrowetting behaviour, which added to the fact that ILs show good chemical stability, a large viscosity range and have varying surface tensions, making them ideal for use as electrowetting agents in a variety of applications such as variable focus lenses [69], RC filters [70] and microreactors [60].

Amin *et al.* [71] reported an interesting application for ILs which use their electrowetting capabilities. In this study the group employs ILs as soft micro-grippers in conditions of high temperatures and high vacuum, via electrowetting actuation. The group proposed the use of ILs instead of aqueous droplets as water based systems have a limited functional temperature and vacuum levels while also showing a tendency to erode electrowetting devices. ILs on the other hand, have negligible vapour pressure, high chemical and thermal stability which make them suitable candidates for use in high temperature and vacuum environments. Micro-grippers are typically used in micro-assembly tasks, where a micro-gripper should be able to pick up, hold and release an item. Classically, capillary forces are used; this is achieved by creating a liquid bridge between the object and the gripper; the capillary forces generated have enough force to

lift objects weighing a few milligrams. However, because the capillary force remains constant once the bridge is formed it is difficult to then release the item. The capillary force has to be strong enough to pick up and hold the object for it to be positioned correctly, then the force has to be reduced sufficiently to where it can be released. Amin *et al.* [72] demonstrated that electrowetting could be used to achieve this process, in a procedure similar to the example by Li *et al.* [68] described above. Once the voltage was applied, the surface became hydrophilic, lowering the contact angle of the liquid, which resulted in the formation of a bridge with the object (**Figure 3.13**). The capillary forces generated allowed for the object to be picked up and held. When the voltage was turned OFF, the surface became hydrophobic and the contact angle of the liquid was lowered, thus releasing the object. The group showed that by using [BMIM][PF<sub>6</sub>], this process could work in temperatures of up to 110 °C and vacuums up to 24 inch Hg.

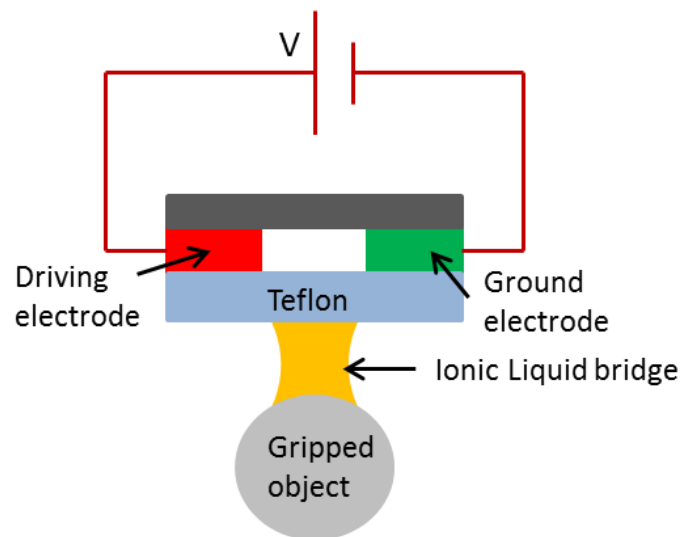


Figure 3.13 Cartoon illustration of the ionic liquid micro-gripper. Reproduced from Al Amin *et al.* [71]. Copyright © 2011 *Journal of Micromechanics and Microengineering*. All rights reserved.

The device functions as follows; firstly the gripper is moved towards the object and a high voltage is applied across the Teflon surface. This makes the surface hydrophilic, allowing the IL to form a bridge, thus creating the maximum force and picking up the object. When the voltage is reduced, the surface becomes hydrophobic, increasing the contact angle of the IL with the surface, reducing the applied capillary forces and releasing the object. The experiments indicated that ILs were ideal for use as micro-grippers in high temperature and high vacuum environments.

### 3.6.2 Chemotactic Ionic Liquids

Another segmented flow regime involves the actuation of individual droplets across the liquid-air interface through changes in the local surface tension, which is brought upon by the triggered release of a surfactant from the droplet itself. Surfactants are long chained amphiphiles which have hydrophilic “heads” and hydrophobic “tails”. When a surfactant is released into an aqueous solution (below the critical micelle concentration) it will interact with polar molecules present at the surface of the solution and will interrupt the attractive forces felt by surface molecules, distributing the local surface tension and creating flows within the bulk solution. Fluid flows from areas of low surface tension to high surface; this is known as the Marangoni effect. By designing systems in which surfactants are asymmetrically released from the droplet into the aqueous phase via external stimulation, droplets have been produced which can solve complex maze designs [73] or can be actuated through white light irradiation [74]. To date, surface tension driven segmented flow systems have mostly focused on aqueous or organic solvent based droplets, which are subject to evaporation and combustion. ILs have a broad range of surface tensions and many have showed surfactant properties [75], while also being highly customisable and overcoming the evaporation due to their negligible vapour pressure, making them promising alternatives for aqueous/organic based droplets.

Francis *et al.* [76] were the first to report on the chemotactic movement of ionic liquid droplets composed of  $[P_{6,6,6,14}]Cl$ . The IL droplets used in this study moved across the liquid-air interface via the triggered release of  $[P_{6,6,6,14}]^+$ , a very effective cationic surfactant and cationic constituent of the IL (**Figure 3.14**).

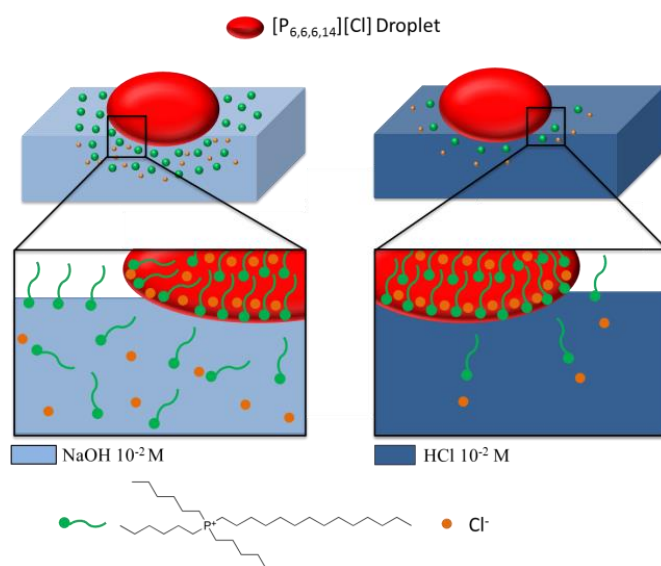


Figure 3.14 Cartoon illustrating the composition and relative solubility of  $[P_{6,6,6,14}][Cl]$  in solutions of  $10^{-2}$  M NaOH and  $10^{-2}$  M HCl. Reproduced from [76] with permission from The Royal Society of Chemistry.

When the  $[P_{6,6,6,14}]^+$  ion diffuses from the droplet into the aqueous solution it interacts with the molecules at the surface, resulting in a drop of the local surface tension. The rate of release of the surfactant is depended on the solubility of the  $Cl^-$  counter ion, as any loss of  $Cl^-$  ion must also result in an equivalent transfer of  $[P_{6,6,6,14}]^+$  in order to maintain overall charge neutrality within the droplet. Therefore, the rate of release of the counter ion was dependent on the local aqueous  $Cl^-$  concentration. Once a droplet of the IL was placed onto a aqueous solution with an imposed  $Cl^-$  concentration gradient, there was an asymmetrical release of  $[P_{6,6,6,14}]^+$  into the aqueous solution, which resulted in the formation of a surface tension gradient around the droplet. This created Marangoni like flows which caused the droplet to move towards areas of highest surface tension (**Figure 3.15**).

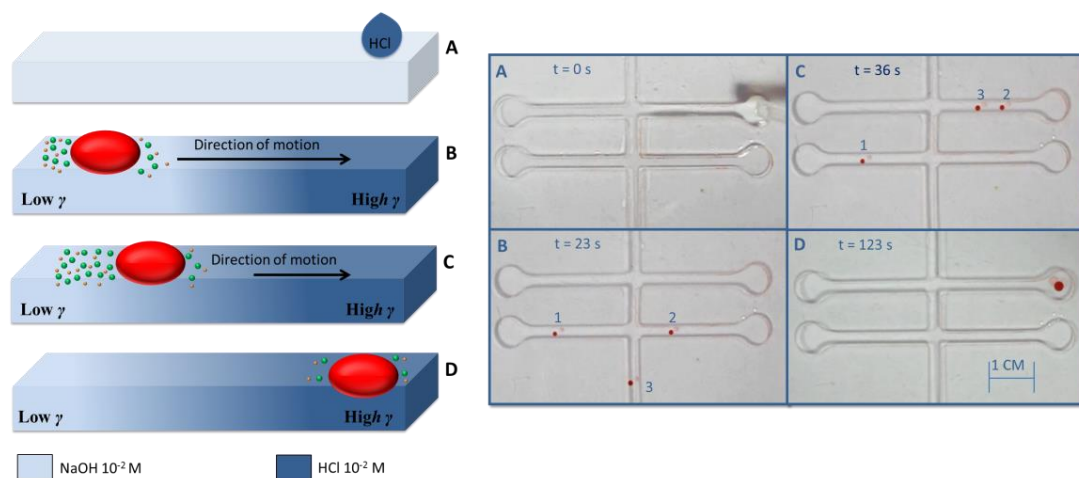


Figure 3.15 Illustration showing the chemotactic movement of ionic liquid droplets across the liquid-air interface (left) and sequence of snapshots showing the chemotactic movement of multiple Ionic liquid droplets in an open fluidic channel (right). A – Depicts the creation of  $Cl^-$  gradient; the channels were initially filled with a solution of  $10^{-2}$  M NaOH and at the desired destination a few drops of a  $10^{-2}$  M solution of HCl were placed. B– Shows the initial placement of the Ionic liquid droplet(s). C – The droplet(s) are propelled towards the highest area of surface tension. D – The droplet arrives at the desired destination. Reproduced from [76] with permission from The Royal Society of Chemistry.

Francis *et al.* [77] have also demonstrated that ionic liquids can respond to electrical stimuli and show electrotactic movement. Droplet composition and movement remains the same as for the chemotactic ionic liquid droplets described above. In this case, 3D printed electrodes, which were embedded within 3D fluidic channels, were used to generate the required ionic gradients. Francis *et al.* electrotactically actuated droplets of  $[P_{6,6,6,14}][Cl]$  across the liquid-air interface of  $10^{-3}$  M NaCl electrolyte solutions. This was achieved by imposing an external electric field across the NaCl solution which resulted in the migration of the mobile ions towards their respective counter electrodes. This phenomenon resulted in the formation of a  $Cl^-$  gradient across the channel, between opposite electrodes. Once the potential was switched ON, an IL droplet placed at the cathode would asymmetrically release surfactant and move towards the anode. By simply reversing the polarity of the electrodes, the gradient and ultimately the droplet movement could be reversed. Moreover, by selectively polarising appropriate electrode pairs the direction of the droplets could be changed and they could be steered into side channels at junctions (**Figure 3.16**). The major advantages of electrotactic movement over chemotactic movement of droplets is the ability for concentration gradients to be established and varied dynamically, and maintained for longer periods of time. This resulted in flexible control over the speed and direction of IL droplet movement.

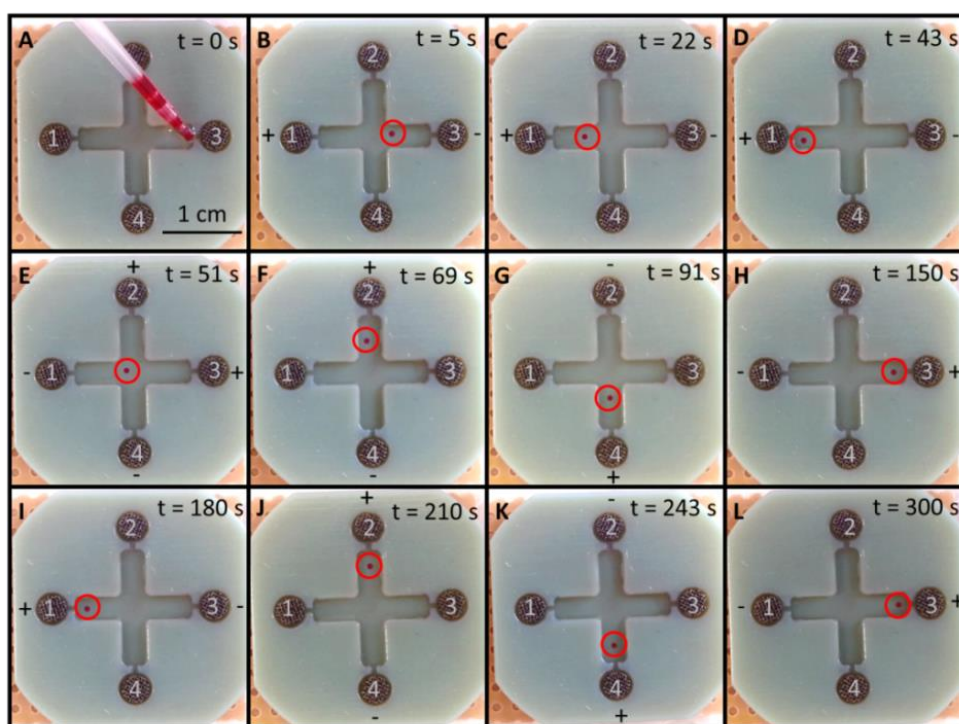


Figure 3.16 Series of snapshots which demonstrate the electrotactic movement of IL droplets. Initially the open fluidic channels are filled with a  $10^{-3}$  M solution of NaCl and a potential

*difference of 9 V is applied across selected electrodes A –introduction of the IL droplet B – D droplet moves away from cathode (3) to anode (1). E – The polarity of electrodes (3) and (1) is reversed and the droplet begins to move to electrode (3). F – As the droplet approaches the junction, the potential difference is applied between electrodes (2) and (4) and removed from electrodes (3) and (1). The droplet then begins to migrate toward anode (2). G – Upon arriving at anode (2) the polarity of electrode (2) and (4) is reversed and the droplet moves towards the new anode (4). H – Upon arriving at anode (4) the potential is again reversed and using a similar method to sequence F the droplet is returned to the starting position. I – L shows the process repeated in the same run. Reproduced from [77] , © 2016 Elsevier B.V. All rights reserved.*

The use of ILs allows for the droplets to remain stable on the surface of the aqueous solutions for much longer than traditional droplets (based on organic solvents) due to their negligible vapour pressure. When coupled with the large (and ever growing) library of ILs available and the fact that many show surfactant properties, it makes them particularly promising for applications involving autonomous droplet systems such as cargo transporters, sensing units, self-repair agents and drug delivery mechanisms.

### **3.6.3 Ionic Liquids as Microreactors**

As mentioned previously, one of the main advantages of segmented flows is the compartmentalisation of the reagents into individual discrete droplets. This has a number of unique properties. Firstly, it separates the reagents from the outside environment, and secondly it allows for the reagents to exist independently of each other within the same device, allowing the user to decide which reagents to mix, when and where. ILs particularly suit this type of application as they have been shown to be excellent solvents [78] and can be tailor made to meet the requirements for many reactions.

Dubois *et al.* [79] reported on the use of IL droplets as microreactors. The ILs were actuated in EWOD devices, in a process similar to the examples described above in which a large number of IL droplets can be efficiently moved and mixed on a Teflon based EWOD device. They also tested the viability of performing complex multi-step reactions using ILs (trimethyl-N-butylammonium bis(trifluoromethylsulfonyl)amide ([tmba][NTf<sub>2</sub>])) by the synthesis of tetrahydroquinoline, which is a three step synthetic process, **Figure 3.17**.

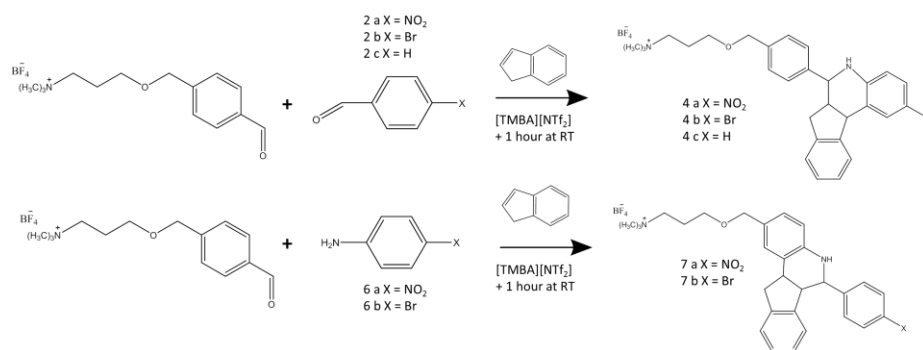


Figure 3.17 Reaction scheme for the synthesis of tetrahydroquinoline. Reprinted with permission from [79]. Copyright (2006) American Chemical Society.

As the reaction had two possible reaction routes, both were tested using the IL droplets. To perform the reaction on the EWOD device, a 0.2  $\mu\text{L}$  IL droplet of [tmba][NTf<sub>2</sub>] which contained 0.2 M of either of the task-specific onium salts (**1** or **2**, **Figure 3.18**) and 10 equivalents of trifluoroacetic acid (TFA) were placed onto the device. It was then actuated towards a second IL droplet (which contained 2.5 equivalents of either the benzaldehyde derivate (**2**) or the aniline derivate (**6**) by applying 55 V to the corresponding electrodes. Upon merging, the combined droplet was moved to, and merged with a final IL droplet which contained an excess of indene. The droplet was then allowed to incubate for one hour at room temperature. It was then removed and tested via HPLC. The results indicated a near 100 % conversion, comparable with that achieved via conventional methods. Moreover, the group was able to perform the analysis on device by actuating the final reaction droplet to an analytical area where an electrochemical analysis was performed using two gold wires. The signal reflected the concentration of the final product. This paper describes a powerful and flexible tool which takes advantage of the chemical stability, customisation and non-combustible properties of ILs to perform complex, small scale organic synthesis on a EWOD device.

Marchand *et al.* [78] demonstrated the use of ILs as soft wall-free micro-reactors for organic synthesis via a click reaction. This paper describes the synthesis of fluorescent 1,2,3-triazole by copper-catalysed 1,3 dipolar cycloaddition reaction of azides with terminal acetyls. This reaction (**Figure 3.18**) is a well-known Click chemistry reaction and results in no by-products and excellent yields.

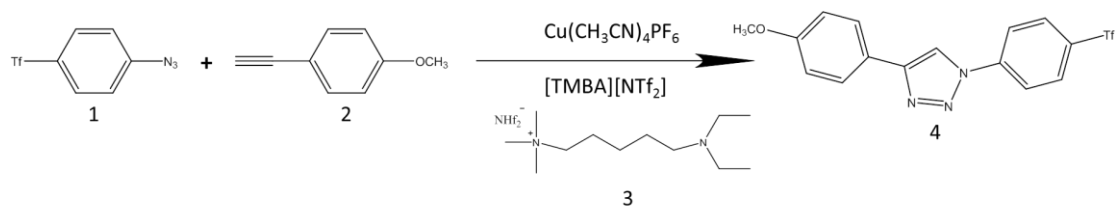


Figure 3.18 Reaction scheme for the synthesis of fluorescent 1,2,3-triazole. Reprinted with permission from [78]. Copyright (2008) American Chemical Society.

Actuation of the ILs was performed using an EWOD device and various mixing methods. To perform the reaction (without mixing) on the device, a 0.2  $\mu\text{L}$  of the IL ([tmba][NTf<sub>2</sub>]) which contained 0.2  $\text{mol L}^{-1}$  of the azide (1) and 0.01  $\text{mol L}^{-1}$  of the catalyst ( $\text{Cu}(\text{CH}_3\text{CN})_4\text{PF}_6$ ) was actuated via electrowetting (55 V) towards, and mixed with a second droplet of the same IL which contained 1  $\text{mol L}^{-1}$  of the alkyne (2) and 0.03  $\text{mol L}^{-1}$  of the support amine (3). The reaction was monitored via fluorescence spectroscopy and a 100 % conversion rate was noted after 40 min, which was confirmed via HPLC. This reaction had a long reaction time compared to standard magnetic stirring methods, due to the viscosity of the ILs. In order to overcome this problem, the group tested a number of mixing methods; firstly, the stationary droplet was heated to 40 °C via a thermoresistor placed under the device. This created Marangoni flows within the droplet, due to the substrate being at a higher temperature than the air, causing the droplet to experience a temperature gradient, which in turn generates a flow circulation within the droplet. This was proven by monitoring added fluorescent markers to the droplet. The second method involved repeatedly moving the droplet backwards and forwards between a series of electrodes. The final mixing procedure involved positioning the droplet on a module which generated surface acoustic waves (SAW); these waves generate a random and chaotic flow within the droplet which accelerates the mixing of reagents. In all cases the required reaction time was reduced, with the shortest time of 21 min being achieved when mixing via the SAW module was employed. Increasing the temperature decreased the reaction time even further to the point where it was comparable with the orthodox stirring method. This study is important as not only does it show that ILs can be used for small scale organic synthesis (via electrowetting) but it also describes methods to overcome issues with viscosity which can limit the use of ILs in synthesis.

### 3.7 Conclusions

Lab-on-a-Chip and micro-Total Analysis Systems show great potential for the integration of multiple functional elements, to produce absolute sample-in/answer-out systems. However, due to the critical need for fluid control, fluid transport, separation, sensing, the need for high performance microfluidic components can provide significant obstacles for the development of low-cost, miniaturised microfluidic devices. Ionic liquid materials offer a solution for the fabrication of low cost and high performance microfluidic elements which can improve the potential of microfluidic devices. Moreover, the promising results obtained from the use of ILs and microfluidics in separation science and chemical synthesis (nanoparticle generations) provide endless opportunity for this emerging area of research.

### 3.8 Acknowledgements

A.T., L.F., and D.D. are grateful for financial support from the Marie Curie Initial Training Network funded by the European Community's FP7 People Programme OrgBIO (Marie Curie ITN, GA607896) and Science Foundation Ireland (SFI) under the Insight Centre for Data Analytics initiative, Grant Number SFI/12/RC/2289. F.B.L. and J.S. acknowledge the Ramón y Cajal Programme (Ministerio de Economía y Competitividad) and to Marian M. De Pancorbo for letting him to use her laboratory facilities at UPV/EHU. J.S., C.D., F.B.L and D.D. also acknowledge the European Union's Seventh Framework Programme for research, technological development, and demonstration; through the NAPES project grant agreement no. 604241.

### 3.9 References

1. Petkovic, M.; Seddon, K. R.; Rebelo, L. P. N.; Pereira, C. S. Ionic liquids: a pathway to environmental acceptability. *Chemical Society Reviews*, **2011**, 40(3), 1383-1403.
2. Zhang, S; Wang, J.; Lu, X.; Zhou, Q. Structures and Interactions of Ionic Liquids 115, in: D. M. P. Mingos (Series Ed.) Structures and Bonding, Springer-Verlag, Berlin-Heidelberg, **2014**, pp.1-197.
3. Passos, H.; Freire, M. G.; Coutinho, J. A. Ionic liquid solutions as extractive solvents for value-added compounds from biomass. *Green Chemistry*, **2014**, 16(12), 4786-4815.
4. Stark, A.; Seddon, K.R. Ionic liquids, in: A. Seidel (Ed.), Kirk-Othmer Encyclopaedia of Chemical Technology 26, John Wiley & Sons, Inc., Hoboken, New Jersey, **2007**, pp. 836-920.
5. Seddon, K. R. Ionic liquids for clean technology. *Journal of Chemical Technology and Biotechnology*, **1997**, 68(4), 351-356.
6. J. Dupont, P. A. Suarez and A. P. Umpierre, *Catal. Lett.*, 2000, **73**, 11-213.

7. Soares, B.; Passos, H.; Freire, C. S.; Coutinho, J. A.; Silvestre, A. J.; Freire, M. G. Ionic liquids in chromatographic and electrophoretic techniques: toward additional improvements in the separation of natural compounds. *Green Chemistry*, **2016** 18(17), 4582-4604.
8. Painter, P.; Pulati, N.; Cetiner, R.; Sobkowiak, M.; Mitchell, G.; Mathews, J. Dissolution and dispersion of coal in ionic liquids. *Energy & Fuels*, **2010**, 24(3), 1848-1853.
9. C. C. Weber, A. F. Masters and T. Maschmeyer, *Green Chem.*, 2013, **15**, 655-2679.
10. Earle, J.; Esperança, M.; Gilea, A.; Lopes, N.; Rebelo, P.; Magee, W.; Seddon R.; Widegren, A. The distillation and volatility of ionic liquids. *Nature*. **2006**, 439(7078), 831-834.
11. Wilkes, J. S. A short history of ionic liquids—from molten salts to neoteric solvents. *Green Chemistry*, **2002**, 4(2), 73-80.
12. MSS Esperança, J.; Canongia Lopes, J. N.; Tariq, M.; Santos, L. M.; Magee, J. W.; Rebelo, L. P. N. Volatility of Aprotic Ionic Liquids □ A Review. *Journal of Chemical & Engineering Data*, **2009**. 55(1), 3-12.
13. Rogers Robin, D.; Seddon K, R.. Chemistry. Ionic Liquids--Solvents of the Future. *Science*, **2003**, 302(5646), 792-3.
14. Guo, F.; Zhang, S.; Wang, J.; Teng, B.; Zhang, T.; Fan, M. Synthesis and applications of ionic liquids in clean energy and environment: a review. *Current Organic Chemistry*, **2015**, 19(5), 455-468.
15. Zhang, J.; Bond, A. M. Practical considerations associated with voltammetric studies in room temperature ionic liquids. *Analyst*, **2005**, 130(8), 1132-1147.
16. Rebelo, L. P. N.; Lopes, J. N. C.; Esperanca, J. M.; Guedes, H. J.; Łachwa, J.; Najdanovic-Visak, V.; Visak, Z. P. Accounting for the unique, doubly dual nature of ionic liquids from a molecular thermodynamic and modeling standpoint. *Accounts of chemical research*, **2007**, 40(11), 1114-1121.
17. Welton, T. Ionic liquids in catalysis. *Coordination Chemistry Reviews*, **2004**, 248(21), 2459-2477.
18. Rogers, R. D.; Seddon, K. R.; Ionic liquids 11 IB: Fundamentals, Progress, Challenges, and Opportunities, American Chemical Society Symposium Series, Washington D.C, 2005.
19. Ranke, J.; Stolte, S.; Störmann, R.; Arning, J.; Jastorff, B. Design of sustainable chemical products the example of ionic liquids. *Chemical Reviews*, **2007**, 107(6), 2183-2206.
20. Earle, M. J.; Seddon, K. R. (2000). Ionic liquids. Green solvents for the future. *Pure and applied chemistry*, **2000**, 72(7), 1391-1398.
21. Freire, M. G.; Claudio, A. F. M.; Araujo, J. M.; Coutinho, J. A.; Marrucho, I. M.; Lopes, J. N. C.; Rebelo, L. P. N. Aqueous biphasic systems: a boost brought about by using ionic liquids. *Chemical Society Reviews*, **2012**, 41(14), 4966-4995.
22. Freire, M, G.; Ana R, R.; Teles, M A R.; Bernd S.; Catarina N.; Pedro J. Carvalho; Dmitry V; Evtuguin, L.; and Joao A C;. Thermophysical characterization of ionic liquids able to dissolve biomass, *Journal of Chemical & Engineering Data* 56, no. 12 **2011**, 4813-4822.

23. Wishart, J. F. Energy applications of ionic liquids. *Energy & Environmental Science*, **2009**, 2(9), 956-961.
24. Le Bideau, J.; Viau, L.; Vioux, A. Ionogels, ionic liquid based hybrid materials. *Chemical Society Reviews*, **2011**, 40(2), 907-925.
25. Marr, P. C.; Marr, A. C. Ionic liquid gel materials: applications in green and sustainable chemistry. *Green Chemistry*, **2016**, 18(1), 105-128.
26. Culbertson, C. T.; Mickleburgh, T. G.; Stewart-James, S. A.; Sellens, K. A.; Pressnall, M. Micro total analysis systems: fundamental advances and biological applications. *Analytical chemistry*, **2013**, 86(1), 95-118.
27. Livak-Dahl, E.; Sinn, I.; Burns, M. Microfluidic chemical analysis systems. *Annual review of chemical and biomolecular engineering*, **2011**, 2, 325-353.
28. Byrne, R.; Benito-Lopez, F.; Diamond, D. Materials science and the sensor revolution. *Materials Today*, **2010**, 13(7), 16-23.
29. Sugiura, S.; Sumaru, K.; Ohi, K.; Hiroki, K.; Takagi, T.; Kanamori, T. Photoresponsive polymer gel microvalves controlled by local light irradiation. *Sensors and Actuators A: Physical* **2007**, 140, 176-184.
30. Benito-Lopez, F.; Byrne, R.; Răduță, A.; Vrana, N.; McGuinness, G.; Diamond, D. Ionogel-based light-actuated valves for controlling liquid flow in micro-fluidic manifolds. *Lab on a Chip* **2009**, 10, 195-201.
31. Czugala, M.; O'Connell, C.; McKeon, A.; Sanchez, F.C.; Munoz-Berbel, X.; Llobera, A.; Diamond, D.; Benito-Lopez, F. Photo-patterning of ionogel microstructures for on-chip microvalve applications controlled by fiber optics. *IEEE* **2013**, 1695-1698.
32. Czugala, M.; Fay, C.; O'Connor, N.E.; Corcoran, B.; Benito-Lopez, F.; Diamond, D. Portable integrated microfluidic analytical platform for the monitoring and detection of nitrite. *Talanta* **2013**, 116, 997-1004.
33. Benito-Lopez, F.; Antoñana-Díez, M.; Curto, V.F.; Diamond, D.; Castro-López, V. Modular microfluidic valve structures based on reversible thermoresponsive ionogel actuators. *Lab on a Chip* **2014**, 14, 3530-3538.
34. Gallagher, S.; Kavanagh, A.; Ziołkowski, B.; Florea, L.; MacFarlane, D.R.; Fraser, K.; Diamond, D. Ionic liquid modulation of swelling and lcst behavior of n-isopropylacrylamide polymer gels. *Physical chemistry chemical physics : PCCP* **2014**, 16, 3610-3616.
35. Ghamsari, A.K.; Zegeye, E.; Jin, Y.; Woldesenbet, E. Application of bucky gel in fabrication of a low-voltage rapid microvalve for flow regulation. *ACS Applied Materials & Interfaces* **2013**, 5, 5408-5412.
36. Akyazi, T.; Saez, J.; Elizalde, J.; Benito-Lopez, F. Fluidic flow delay by ionogel passive pumps in microfluidic paper-based analytical devices. *Sensors and Actuators B: Chemical* **2016**, 233, 402-408.
37. Kavanagh, A.; Byrne, R.; Diamond, D.; Fraser, K.J. Stimuli responsive ionogels for sensing applications—an overview. *Membranes* **2012**, 2, 16.
38. Behera, K.; Pandey, S.; Kadyan, A.; Pandey, S. Ionic liquid-based optical and electrochemical carbon dioxide sensors. *Sensors* **2015**, 15, 29813.
39. Yang, S.Y.; Cicoira, F.; Byrne, R.; Benito-Lopez, F.; Diamond, D.; Owens, R.M.; Malliaras, G.G. Electrochemical transistors with ionic liquids for enzymatic sensing. *Chemical Communications* **2010**, 46, 7972-7974.

40. Madeira Lau, R.; Sorgeddrager, M.J.; Carrea, G.; van Rantwijk, F.; Secundo, F.; Sheldon, R.A. Dissolution of candida antarctica lipase b in ionic liquids: Effects on structure and activity. *Green Chemistry* **2004**, *6*, 483-487.
41. Yamaguchi, M.; Mitsumori, M.; Kano, Y. Noninvasively measuring blood glucose using saliva. *IEEE Engineering in Medicine and Biology Magazine* **1998**, *17*, 59-63.
42. Khodagholy, D.; Curto, V.F.; Fraser, K.J.; Gurfinkel, M.; Byrne, R.; Diamond, D.; Malliaras, G.G.; Benito-Lopez, F.; Owens, R.M. Organic electrochemical transistor incorporating an ionogel as a solid state electrolyte for lactate sensing. *Journal of Materials Chemistry* **2012**, *22*, 4440-4443.
43. Khodagholy, D.; Curto, V.F.; Fraser, K.J.; Gurfinkel, M.; Byrne, R.; Diamond, D.; Malliaras, G.G.; Benito-Lopez, F.; Owens, R.M. Organic electrochemical transistor incorporating an ionogel as a solid state electrolyte for lactate sensing. *Journal of Materials Chemistry* **2012**, *22*, 4440.
44. Curto, V.F.; Scheuermann, S.; Owens, R.M.; Ranganathan, V.; MacFarlane, D.R.; Benito-Lopez, F.; Diamond, D. Probing the specific ion effects of biocompatible hydrated choline ionic liquids on lactate oxidase biofunctionality in sensor applications. *Physical Chemistry Chemical Physics* **2014**, *16*, 1841-1849.
45. Czugala, M.; Gorkin Iii, R.; Phelan, T.; Gaughran, J.; Curto, V.F.; Ducree, J.; Diamond, D.; Benito-Lopez, F. Optical sensing system based on wireless paired emitter detector diode device and ionogels for lab-on-a-disc water quality analysis. *Lab on a Chip* **2012**, *12*, 5069-5078.
46. Curto, V.F.; Fay, C.; Coyle, S.; Byrne, R.; Diamond, D.; Benito-Lopez, F. In *Wearable micro-fluidic ph sweat sensing device based on colorimetric imaging techniques*, microTAS, Seattle Washington, 2011; Seattle Washington.
47. Yanes, E.G.; Gratz, S.R.; Baldwin, M.J.; Robison, S.E.; Stalcup, A.M. Capillary electrophoretic application of 1-alkyl-3-methylimidazolium-based ionic liquids. *Analytical Chemistry* **2001**, *73*, 3838-3844.
48. Xu, Y.; Wang, E. Ionic liquids used in and analyzed by capillary and microchip electrophoresis. *Journal of Chromatography A* **2009**, *1216*, 4817-4823.
49. Choi, D.Y.; Kim, M.H.; Oh, Y.S.; Jung, S.-H.; Jung, J.H.; Sung, H.J.; Lee, H.W.; Lee, H.M. Highly stretchable, hysteresis-free ionic liquid-based strain sensor for precise human motion monitoring. *ACS Applied Materials & Interfaces* **2016**.
50. Wu, C.-Y.; Liao, W.-H.; Tung, Y.-C. Integrated ionic liquid-based electrofluidic circuits for pressure sensing within polydimethylsiloxane microfluidic systems. *Lab on a Chip* **2011**, *11*, 1740-1746.
51. Liu, M.-C.; Shih, H.-C.; Wu, J.-G.; Weng, T.-W.; Wu, C.-Y.; Lu, J.-C.; Tung, Y.-C. Electrofluidic pressure sensor embedded microfluidic device: A study of endothelial cells under hydrostatic pressure and shear stress combinations. *Lab on a Chip* **2013**, *13*, 1743-1753.
52. Welton, T. Room-temperature ionic liquids. Solvents for synthesis and catalysis. *Chemical reviews* **1999**, *99*, 2071-2084.
53. Rogers, R.D.; Seddon, K.R. Ionic liquids--solvents of the future? *Science* **2003**, *302*, 792-793.
54. Kunz, W.; Häckl, K. The hype with ionic liquids as solvents. *Chemical Physics Letters* **2016**, *661*, 6-12.
55. Weidmann, S.; Kemmerling, S.; Mdlar, S.; Stahlberg, H.; Zenobi, R. Ionic liquids as matrices in microfluidic sample deposition for high-mass matrix-assisted laser desorption/ionization mass spectrometry. *European Journal of Mass Spectrometry* **2012**, *18*, 279.

56. Tijero, M.; Díez-Ahedo, R.; Benito-Lopez, F.; Basabe-Desmouts, L.; Castro-López, V.; Valero, A. Biomolecule storage on non-modified thermoplastic microfluidic chip by ink-jet printing of ionogels. *Biomicrofluidics* **2015**, *9*, 044124.
57. van Steijn, V.; Kreutzer, M.T.; Kleijn, C.R. M-piv study of the formation of segmented flow in microfluidic t-junctions. *Chem. Eng. Sci.* **2007**, *62*, 7505-7514.
58. Gong, J. All-electronic droplet generation on-chip with real-time feedback control for ewod digital microfluidics. *Lab on a Chip* **2008**, *8*, 898-906.
59. Baigl, D. Photo-actuation of liquids for light-driven microfluidics: State of the art and perspectives. *Lab on a chip* **2012**, *12*, 3637-3653.
60. Dubois, P.; Marchand, G.; Fouillet, Y.; Berthier, J.; Douki, T.; Hassine, F.; Gmouh, S.; Vaultier, M. Ionic liquid droplet as e-microreactor. *Anal. Chem.* **2006**, *78*, 4909-4917.
61. Moon, I.; Kim, J. Using ewod (electrowetting-on-dielectric) actuation in a micro conveyor system. *Sensors and Actuators A: physical* **2006**, *130*, 537-544.
62. Srinivasan, V.; Pamula, V.; Pollack, M.; Fair, R. In *A digital microfluidic biosensor for multianalyte detection*, Micro Electro Mechanical Systems, 2003. MEMS-03 Kyoto. IEEE The Sixteenth Annual International Conference on, 2003; IEEE: pp 327-330.
63. Xu, Q.; Hashimoto, M.; Dang, T.T.; Hoare, T.; Kohane, D.S.; Whitesides, G.M.; Langer, R.; Anderson, D.G. Preparation of monodisperse biodegradable polymer microparticles using a microfluidic flow-focusing device for controlled drug delivery. *Small* **2009**, *5*, 1575-1581.
64. Choi, K.; Ng, A.; Fobel, R.; Wheeler, A. Digital microfluidics. *Annu. Rev. Anal. Chem. (Palo Alto Calif.)* **2012**, *5*, 413-440.
65. Nanayakkara, Y.S.; Moon, H.; Payagala, T.; Wijeratne, A.B.; Crank, J.A.; Sharma, P.S.; Armstrong, D.W. A fundamental study on electrowetting by traditional and multifunctional ionic liquids: Possible use in electrowetting on dielectric-based microfluidic applications. *Anal. Chem.* **2008**, *80*, 7690-7698.
66. Paneru, M.; Priest, C.; Sedev, R.; Ralston, J. Static and dynamic electrowetting of an ionic liquid in a solid/liquid/liquid system. *J. Am. Chem. Soc.* **2010**, *132*, 8301-8308.
67. Millefiorini, S.; Tkaczyk, A.H.; Sedev, R.; Efthimiadis, J.; Ralston, J. Electrowetting of ionic liquids. *J. Am. Chem. Soc.* **2006**, *128*, 3098-3101.
68. Li, H.; Paneru, M.; Sedev, R.; Ralston, J. Dynamic electrowetting and dewetting of ionic liquids at a hydrophobic solid-liquid interface. *Langmuir* **2013**, *29*, 2631-2639.
69. Hu, X.; Zhang, S.; Qu, C.; Zhang, Q.; Lu, L.; Ma, X.; Zhang, X.; Deng, Y. Ionic liquid based variable focus lenses. *Soft Matter* **2011**, *7*, 5941-5943.
70. Nanayakkara, Y.S.; Moon, H.; Armstrong, D.W. A tunable ionic liquid based rc filter using electrowetting: A new concept. *ACS Applied Materials & Interfaces* **2010**, *2*, 1785-1787.
71. Al Amin, A.; Jagtiani, A.; Vasudev, A.; Hu, J.; Zhe, J. Soft microgripping using ionic liquids for high temperature and vacuum applications. *Journal of Micromechanics and Microengineering* **2011**, *21*, 125025.
72. Vasudev, A.; Zhe, J. In *A capillary microgripper using electrowetting*, 2008 17th Biennial University/Government/Industry Micro/Nano Symposium, 2008; IEEE: pp 6-10.
73. Lagzi, I.; Soh, S.; Wesson, P.; Browne, K.; Grzybowski, B. Maze solving by chemotactic droplets. *J. Am. Chem. Soc.* **2010**, *132*, 1198-1199.

74. Florea, L.; Wagner, K.; Wagner, P.; Wallace, G.G.; Benito-Lopez, F.; Officer, D.L.; Diamond, D. Photo-chemopropulsion–light-stimulated movement of microdroplets. *Adv. Mater.* **2014**, *26*, 7339-7345.
75. Anderson, J.L.; Pino, V.; Hagberg, E.C.; Sheares, V.V.; Armstrong, D.W. Surfactant solvation effects and micelle formation in ionic liquids. *Chem. Commun.* **2003**, 2444-2445.
76. Francis, W.; Fay, C.; Florea, L.; Diamond, D. Self-propelled chemotactic ionic liquid droplets. *Chem. Commun.* **2015**, *51*, 2342 - 2344.
77. Francis, W.; Wagner, K.; Beirne, S.; Officer, D.L.; Wallace, G.G.; Florea, L.; Diamond, D. Electrotactic ionic liquid droplets. *Sensors Actuators B: Chem.* **2017**, *239*, 1069-1075.
78. Marchand, G.; Dubois, P.; Delattre, C.; Vinet, F.; Blanchard-Desce, M.; Vaultier, M. Organic synthesis in soft wall-free microreactors: Real-time monitoring of fluorogenic reactions. *Anal. Chem.* **2008**, *80*, 6051-6055.

## **Chapter 4:**

### **Self-Propelled Chemotactic Ionic Liquid Droplets**

#### **4.1 Abstract**

#### **4.2 Introduction**

#### **4.3 Experimental**

##### **4.3.1 Materials and Methods**

##### **4.3.2 Micro-Channel Fabrication**

##### **4.3.3 Surface Tension Measurements**

##### **4.3.4 Video Processing Analysis**

#### **4.4 Results and Discussion**

##### **4.4.1 $^{31}\text{P}$ and $^1\text{H}$ NMR Spectroscopy**

##### **4.4.2 Propulsion Mechanism**

##### **4.4.3 Droplet Tracking and Gradient Analysis**

#### **4.5 Conclusions**

#### **4.6 References**

## Chapter 4

---

# Self-Propelled Chemotactic Ionic Liquid Droplets<sup>\*</sup>

---

**\*Self-propelled chemotactic ionic liquid droplets, W. Francis, C. Fay, L. Florea, D. Diamond, *Chemical communications*, **51**, 2342 – 2344, 2015.**

## 4.1 Abstract

Herein, we report for the first time, the spontaneous chemotactic movement of an ionic liquid (IL) droplet at an aqueous-air interface. These single component droplets are self-propelling and can be guided to specific destinations in open fluidic channels through the use of chemoattractants such as sodium chloride (NaCl) or hydrochloric acid (HCl). The droplets consist of the IL Trihexyl(tetradecyl)phosphonium chloride ( $[P_{6,6,6,14}][Cl]$ ) and a small amount of red dye for better visualization. They are designed to move in an open fluidic channel. The movement of the droplets is controlled by the triggered release of the  $[P_{6,6,6,14}]^+$ , a very efficient cationic surfactant, which is a constituent of the IL droplet.

In the presence of a  $Cl^-$  gradient in the aqueous phase, an asymmetrical surface tension gradient is created, leading to a Marangoni like flow, which causes the droplet to move from areas of low surface tension towards areas of high surface tension. The surface tension gradient is created by the asymmetric release of  $[P_{6,6,6,14}]^+$  from the IL droplet into the aqueous phase. The rate of  $[P_{6,6,6,14}]^+$  release depends on the concentration of the chloride in the aqueous solution, as the formation of free  $[P_{6,6,6,14}]^+$  (the active surfactant at the air-aqueous interface) through dissociation of the relatively closely associated  $[P_{6,6,6,14}][Cl]$  ions in the IL depends on the local  $Cl^-$  concentration at the IL-aqueous boundary. Using these methods videos of the IL droplets moving to pre-determined locations were captured. Multiple droplets were also moved to the same location where upon arrival merging occurred. The speed of the droplets was analysed using a custom written program.

This type of triggered surfactant release through external stimulation aims to achieve new means for controlling droplet movement within microfluidic devices, as well as developing biomimetic synthetic vehicles with integrated functionalities such as detection of chemoattractant gradients, signaling, sensing and repair.

## 4.2 Introduction

The ability to move in response to an external stimulus is essential for many life forms. Certain cells such as bacteria, somatic cells, and other single cell or multicellular organisms move in response to chemical stimuli present within their surrounding environment [1, 2]. This phenomenon is known as chemotaxis and it is crucial for many biological processes such as feeding or fleeing toxins, migration and action of somatic cells such as those involved in the immune system [3, 4], reproductive cells [5] and enzymes [6]. Notably there are only few

equivalents of similar chemotactic-driven “micro-vehicles” in the synthetic world. Inspired by chemotactic organisms we developed synthetic biomimetic droplets which are self-propelled and capable of navigating a microfluidic network by introducing chemoattractants at the target destination within the fluidic channel.

Various mechanisms to initiate and direct the movement of micro-droplets have been reported, including switchable wettability of a substrate surface via chemical [7, 8] or electro-chemical stimuli [9, 10], or using temperature gradients [11, 12], magnetic [13] or acoustic forces [14] and even photo-stimulation to actuate droplets [15]. However, all of these methods involve relatively complex experimental arrangements and/or multi-component droplets, and require applied external energy to create droplet movement.

Surfactant release has been employed to control the surface tension of aqueous systems in order to generate spontaneous movement of droplets at the aqueous-air interface in a contactless manner. When placed into an aqueous system the surfactant will interact with the water molecules and lower the surface tension of the solution. When the surface tension of a liquid is altered, liquid flows from areas of low surface tension to areas of high surface tension; a phenomenon known as the Marangoni effect [16]. Control over the droplet direction can be achieved by creating conditions under which asymmetric release of pre-loaded surfactant from the droplet occurs. Using stimuli-responsive surfactants, smart droplets have been designed which can solve complex mazes [17], or move towards/away from a light source [18, 19]. We have investigated a number of strategies for generating spontaneous movement in droplet microvehicles based on the generation of concentration gradients of chemoattractants diffusing from a target destination within a fluidic system. Chemoattractants are chemical agents which induce positive chemotaxis in living organisms, in the same manner that chemorepellents induce negative chemotaxis. In contrast to previous studies, in which the degree of protonation of surfactant molecules underpins droplet mobility, we demonstrate spontaneous droplet movement arising from modulation of  $\text{Cl}^-$  solubility, for example, through the creation of  $\text{Cl}^-$  gradients in the aqueous phase generated from concentrated NaCl and HCl sources.

Furthermore, to our knowledge, this is the first example of the spontaneous chemotactic movement of droplets composed solely of an ionic liquid (IL) at the aqueous-air interface. The chemotactic droplets presented here consist of the IL ( $[\text{P}_{6,6,6,14}][\text{Cl}]$ ) and a small amount of red dye (1-(methylamino)anthraquinone), which is added solely for better visualization, see Figure 4.1.

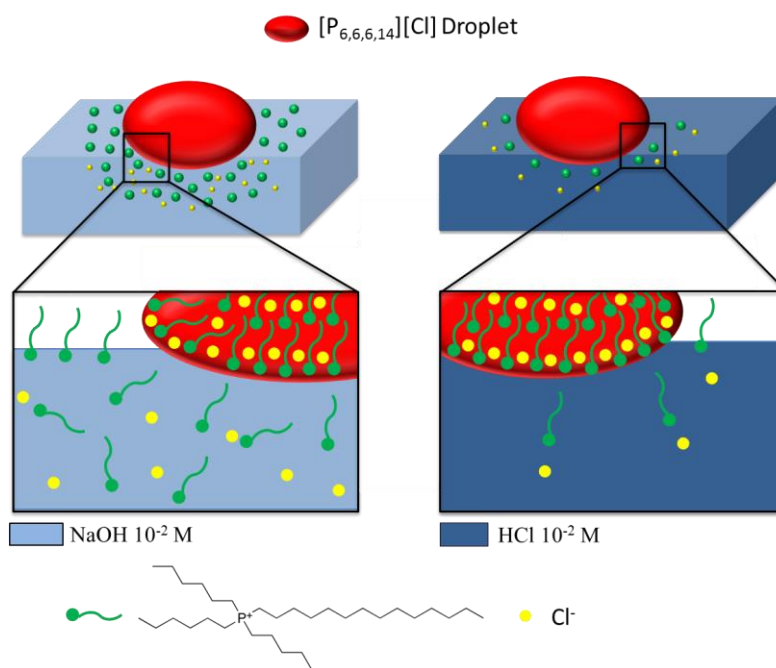


Figure 4.1 Diagram showing the relative solubility of [P<sub>6,6,6,14</sub>][Cl] droplet in solutions of 10<sup>-2</sup> M NaOH (left) and solutions of 10<sup>-2</sup> M HCl (right).

### 4.3 Experimental

#### 4.3.1 Materials and Methods

Hydrochloric acid (HCl) (Sigma-Aldrich® Ireland Ltd), Sodium hydroxide (NaOH) (Sigma-Aldrich® Ireland Ltd), Sodium chloride (NaCl) (Sigma-Aldrich® Ireland Ltd), Dichloromethane (DCM) (Sigma-Aldrich® Ireland Ltd) and 1-(methylamino)anthraquinone red dye (Sigma-Aldrich® Ireland Ltd) were all used as purchased.

The polyacrylamide hydrogel was synthesized by mixing 2.8 mmol of acrylamide (Sigma-Aldrich® Ireland Ltd) with 3 mol % N,N-Methylenebisacrylamide (mBIS) (Sigma-Aldrich® Ireland Ltd) and 1 mol % phenylbis(2,4,6-trimethylbenzoyl)phosphine oxide (PBPO) (Sigma-Aldrich® Ireland Ltd), using 500 µl of 4:1 (V:V) dimethyl sulfoxide (DMSO) (Sigma-Aldrich® Ireland Ltd) : deionised water as the solvent. The hydrogel was polymerized for 2 minutes under white light.

The Ionic liquid (IL) trihexyl(tetradecyl)phosphonium chloride ([P<sub>6,6,6,14</sub>][Cl]) (Sigma-Aldrich® Ireland Ltd) was purified by dissolving 5 ml of the IL in 10 ml of

dichloromethane. The solution was then treated with activated charcoal and left to reflux at 40°C for 12 hours. The carbon was removed by vacuum filtration, after which it was passed through aluminium oxide (activated, basic, Brockmann, Sigma-Aldrich® Ireland Ltd). Finally the solvent was removed under vacuum for 48 hrs.

**Nuclear magnetic resonance (NMR)** was performed to determine if the IL was undergoing any chemical reaction with NaOH. <sup>1</sup>H-NMR and <sup>31</sup>P-NMR spectroscopy was performed using a Bruker Avance® spectrometer (400 MHz). Approximately 10 mg of sample per 1 ml of deuterated chloroform (CDCl<sub>3</sub>) (Sigma-Aldrich® Ireland Ltd) was used in the experiments.

#### **4.3.2 Micro-Channel Fabrication**

Fabrication of the channels used in this study was carried out using the program AutoCAD 2014 for the channel design. A CO<sub>2</sub> laser ablation system (Optec Laser Micro-machining Systems, Belgium) was then used to cut the structures from a 1.1 mm poly(methyl methacrylate) (PMMA) sheet which had a 50 µm double sided pressure sensitive adhesive (PSA) (AR8890, Adhesives Research, Ireland) layer attached. Once cut, the protective layer from the PSA was removed and then the PMMA/PSA layer was laminated with another 1.1 mm PMMA sheet. The final channels were 2 mm wide and 1.1 mm high.

#### **4.3.3 Surface Tension Measurements**

Surface tension measurements were performed with a FTA200 Dynamic Contact Angle Analyser using the pendant drop method.

Various compositions of the solutions used in the study were tested. In order to measure the surface tension effect that the IL surfactant had on each solution, the surface tension of each solution was tested with (*c* = 1mg/ml) and without the IL surfactant, see Table 4.1. To prepare the solutions for the surface tension measurements, 1 mg of the IL was added to 1 ml of the aqueous solution. This proportion was chosen as it was similar to the quantity of the IL (droplet) per aqueous solution in the fluidic channel.

Table 4.1 Surface tension measurements of solutions used in the study, with and without the IL surfactant added.

| Solution                                       | $\gamma_1$<br>(mN/m) | $\gamma_2$<br>(mN/m) | $\gamma_3$<br>(mN/m) | AVG $\gamma$<br>(mN/m) |
|--|----------------------|----------------------|----------------------|------------------------|
| HCl $10^{-2}$ M                                | 74.13                | 74.39                | 73.82                | 74.11                  |
| HCl $10^{-2}$ M/[P <sub>6,6,6,14</sub> ][Cl]   | 72.1                 | 72.08                | 73.51                | 72.56                  |
| HCl $10^{-2}$ M/[P <sub>6,6,6,14</sub> ][DCA]  | 72.92                | 72.95                | 73.6                 | 73.16                  |
| NaOH $10^{-2}$ M                               | 72.39                | 73.32                | 73.66                | 73.12                  |
| NaOH $10^{-2}$ M/[P <sub>6,6,6,14</sub> ][Cl]  | 33.29                | 33.5                 | 33.4                 | 33.40                  |
| NaOH $10^{-2}$ M/[P <sub>6,6,6,14</sub> ][DCA] | 73.48                | 73.2                 | 72.84                | 73.17                  |
| NaCl $10^{-2}$ M                               | 72.45                | 74.59                | 74.68                | 73.91                  |
| NaCl $10^{-2}$ M/[P <sub>6,6,6,14</sub> ][Cl]  | 72.62                | 73.44                | 73.51                | 73.19                  |
| NaCl $10^{-5}$ M                               | 73.96                | 74.08                | 74.67                | 74.24                  |
| NaCl $10^{-5}$ M/[P <sub>6,6,6,14</sub> ][Cl]  | 38.24                | 38.52                | 38.52                | 38.43                  |
| KBr $10^{-2}$ M                                | 71.75                | 72.67                | 73.6                 | 72.67                  |
| KBr $10^{-2}$ M/[P <sub>6,6,6,14</sub> ][Cl]   | 40.92                | 39.74                | 40.75                | 40.47                  |
| KBr $10^{-5}$ M                                | 71.85                | 72.85                | 72.53                | 72.41                  |
| KBr $10^{-5}$ M/[P <sub>6,6,6,14</sub> ][Cl]   | 34.64                | 35.12                | 34.37                | 34.71                  |
| KCl $10^{-2}$ M                                | 72.37                | 71.02                | 72.86                | 72.08                  |
| KCl $10^{-2}$ M/[P <sub>6,6,6,14</sub> ][Cl]   | 66.31                | 64.32                | 66.04                | 65.56                  |
| KCl $10^{-5}$ M                                | 69.05                | 71.88                | 71.96                | 70.96                  |
| KCl $10^{-5}$ M/[P <sub>6,6,6,14</sub> ][Cl]   | 34.88                | 34.64                | 34.68                | 34.73                  |
| NaI $10^{-2}$ M                                | 73.94                | 74.77                | 73.72                | 74.14                  |
| NaI $10^{-2}$ M/[P <sub>6,6,6,14</sub> ][Cl]   | 59.28                | 61.58                | 62.35                | 61.07                  |
| NaI $10^{-5}$ M                                | 73.05                | 73.57                | 72.81                | 73.14                  |
| NaI $10^{-5}$ M/[P <sub>6,6,6,14</sub> ][Cl]   | 34.46                | 34.48                | 34.58                | 34.51                  |

#### 4.3.4 Video Processing Analysis

In order to calculate droplet speed, videos were captured, that were then analysed by tracking the droplet through means of a custom-written vision system program. This was achieved by firstly controlling the visual environment by separating the background (channels: white/grey – weak in colour intensity) to that of the droplets of interest (droplet: red – strong in colour intensity), see Figure 4.2 - left. Classification of pixel groups corresponding to the droplet was therefore possible.

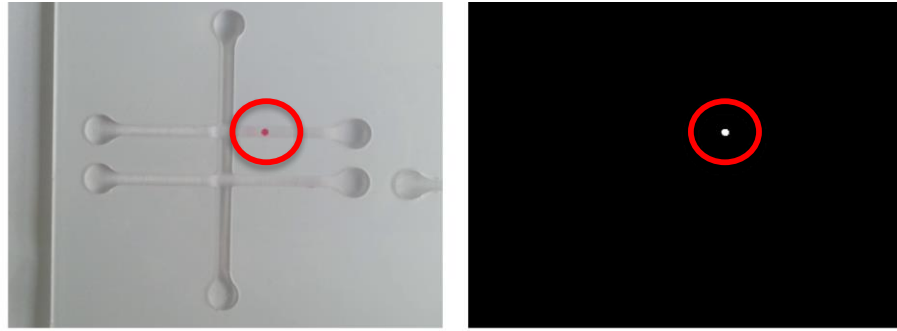


Figure 4.2 Example of a captured image from Video 4.1 (left) with processed mask image (right). The droplet position is ringed in both images.

Transformation from the captured sRGB colour space to the HSV colour space allowed for a separation of colour (Hue), colour intensity (Saturation), and light intensity (Value) into their constituent components (3 channels). A threshold applied to the channel resulted in a mask image as shown in Figure 4.2 (right). Areas of white-connected pixels were grouped together using a connected component analysis algorithm. Information describing each connected region was extracted (*e.g.* size, shape), which allowed the program to discount noise and/or other artefacts through a series of filters. This formed the basis of a similarity-matching algorithm, which when applied to matching regions in each successive frame allowed tracking of the droplet throughout the video. Data such as the frame in which the droplet appeared and its location (region's centre x, y coordinates) were recorded for later analysis.

During video capturing, the camera was fixed orthogonal to the chip. A conversion of units (from pixels to mm) was therefore, possible through the known distance of a straight channel's distal end-points (60 mm) and measurement of corresponding points in captured frames. The distance which each droplet travelled from frame-to-frame was calculated (using the standard Euclidian algorithm) and the total distance travelled of each droplet was subsequently determined. Finally, using the frame number the time was calculated using the constant captured frame rate of 25 fps set on the capturing device.

## 4.4 Results and Discussion

### 4.4.1 $^{31}\text{P}$ and $^1\text{H}$ NMR spectroscopy

Although it was previously confirmed that tetraalkylphosphonium halides can be mixed with concentrated sodium hydroxide or ammonia without any degradation [20, 21], several reports state that tetraalkylphosphonium IL salts are not always stable in the presence of hydroxides or other bases, and may undergo Hoffmann or  $\beta$ -elimination in the presence of a strong base, which results in the formation of a tertiary phosphine oxide and alkane [20]. In order to confirm that the propulsion mechanism of the droplets is due to the triggered release of the surfactant and not due to chemical reaction, the stability of trihexyl(tetradecyl)phosphonium chloride ionic liquid was investigated by analysis of the products formed after mixing the ionic liquid phase with aqueous NaOH. For this, a small amount of the IL ( $\approx 10$  mg) was added to an excess of NaOH  $10^{-2}$  M ( $\approx 1$  ml). The solution was stirred overnight and the product was then extracted with DCM. The DCM was removed by evaporation and a  $^{31}\text{P}$ -NMR spectrum of the extraction was recorded.

No increase in the amount of phosphine oxide (resonance signal of phosphine oxide is situated at 49.6 ppm [21]) was found on treatment with NaOH, and only the resonance signal of the trihexyl(tetradecyl)phosphonium cation at 32.7 ppm was observed (Figure 4.3). This indicates that there was no chemical reaction between the NaOH and the droplet.

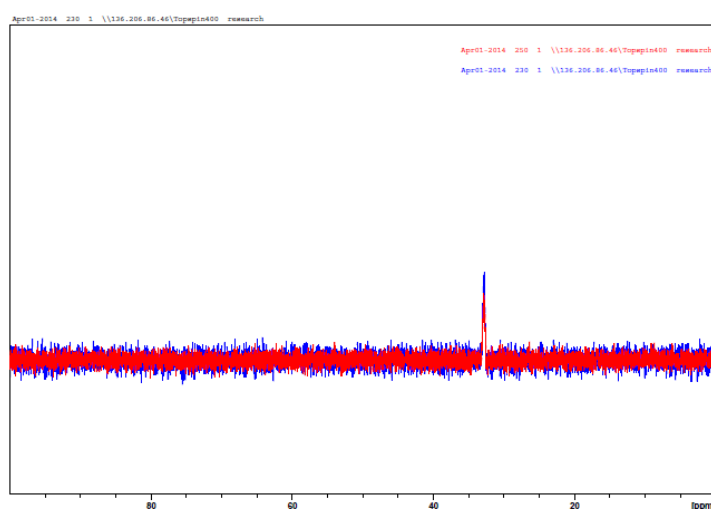


Figure 4.3  $^{31}\text{P}$  spectra of the cleaned  $[\text{P}_{6,6,6,14}][\text{Cl}]$  before (blue) and after extraction (red).

The  $^1\text{H}$  NMR spectrum also showed that only the IL was present after the extraction.

$[\text{P}_{6,6,6,14}][\text{Cl}]$   $^1\text{H}$  NMR (400 MHz,  $\text{CDCl}_3$ ): 0.86 – 0.88 (m, 12H,  $\text{CH}_3$ ), 1.2 – 1.3 (d, 32H,  $\text{CH}_2$ ), 1.49 (s, 16H,  $\text{CH}_2$ ), 2.4 (m, 8H,  $\text{CH}_2$ ). (Figure 4.4)

This is also an indication that no other compound is formed during the propulsion process.

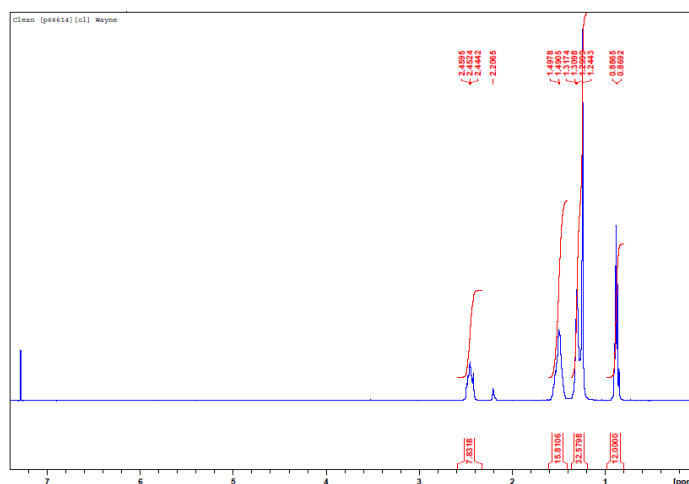


Figure 4.4  $^1\text{H}$  NMR spectrum of a sample of cleaned  $[\text{P}_{6,6,6,14}][\text{Cl}]$ , after extraction study.

#### 4.4.2 Propulsion Mechanism

Droplet movement arises due to the asymmetric release of  $[\text{P}_{6,6,6,14}]^+$ , a very efficient cationic surfactant, which is a constituent of the IL droplet. When  $[\text{P}_{6,6,6,14}]^+$  diffuses from the droplet into the aqueous solution, it causes a sudden drop of the surface tension of the solution (see Table S1). The rate of  $[\text{P}_{6,6,6,14}]^+$  release depends on the solubility of the closely associated  $\text{Cl}^-$  anion (Table S1), as the formation of free  $[\text{P}_{6,6,6,14}]^+$  (the active surfactant at the air-water boundary) in the aqueous phase depends on the local  $\text{Cl}^-$  concentration at the IL-aqueous boundary [22]. In  $[\text{P}_{6,6,6,14}][\text{Cl}]$ , the  $\text{Cl}^-$  anion is strongly associated with the  $[\text{P}_{6,6,6,14}]^+$  cation, rendering the IL strongly lipophilic, which enables droplets to be formed on the water-air interface. The  $[\text{P}_{6,6,6,14}]^+$  cation is only sparingly soluble in water, and its partition into the aqueous phase from the IL droplet phase is strongly modulated by the local  $\text{Cl}^-$  solubility. Hence, in the presence of an aqueous phase  $\text{Cl}^-$  gradient, differential release of  $[\text{P}_{6,6,6,14}]^+$  occurs and an asymmetric surface tension gradient is created, leading to a Marangoni like flow, which causes the droplet to move from areas of low surface tension towards areas of high surface tension (Figure 4.5).

To demonstrate this effect, three different techniques for generating the gradients underpinning

chemotactic propulsion were employed. In the first method the channels were initially filled with a solution of  $10^{-2}$  M NaOH followed by the addition of 100  $\mu$ l – 200  $\mu$ l of  $10^{-2}$  M HCl at the desired destination. For the second method the channels were again initially filled with a solution of  $10^{-2}$  M NaOH but this time a polyacrylamide hydrogel previously soaked in  $10^{-2}$  M HCl was placed at the desired destination. In the third approach the channels were initially filled with a solution of  $10^{-5}$  M NaCl followed by the addition of NaCl crystals ( $\sim$  10 mg) at the desired destination. In each case, 10 – 30 s after the addition of the chemoattractant, small droplets ( $\sim$  10  $\mu$ l) of  $[P_{6,6,6,14}][Cl]$  were placed at specific locations and these spontaneously moved to the desired destination (Figure 4.5). As soon as a droplet was placed in the channel it began moving along the channel towards the source of the chemoattractant traversing corners on its way. (See Video 4.1, 4.2, 4.3 and 4.4, Appendix A).

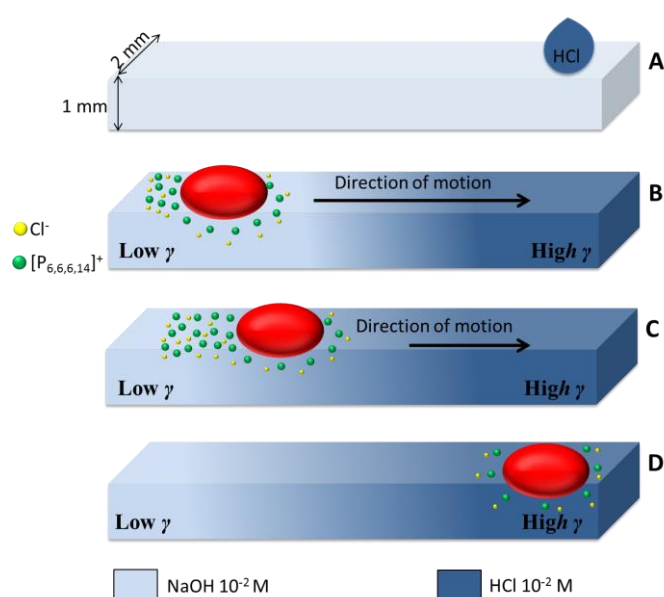


*Figure 4.5 Schematic representation showing the movement of the  $[P_{6,6,6,14}][Cl]$  droplet in open fluidic channels. A – Depicts the creation of the  $Cl^-$  gradient. The channel was initially filled with NaOH  $10^{-2}$  M solution. Then at the desired destination two or three drops of HCl  $10^{-2}$  M solution were added (right); B – The IL droplet was placed at the NaOH end of the channel causing surfactant to diffuse into the solution, thus breaking the surface tension symmetry around the droplet; C – Droplet is propelled towards areas of highest surface tension; D – Droplet arrives at the desired destination.*

The droplet can be placed in any position within the fluidic network and in every case it spontaneously finds the chemoattractant source. In control experiments in which the chemoattractant was not added, the droplets either did not move or moved randomly due to uncontrolled release of the surfactant. Due to the dynamics of the formation of the ion gradient along the channel(s), the time when a droplet was placed relative to the

introduction of the chemoattractant, affected its speed towards the source. This was investigated by releasing a number of droplets (6 in total) at different times and at various locations along the fluidic network (Figure 4.6). The droplet movement was tracked using a custom-written vision system program. The gradients required for droplet propulsion were analysed using a low-cost and readily available technology [23]. Typical droplet speeds estimated using this program was found to be in the range  $0.5 - 4 \text{ mm s}^{-1}$  over the first 30 seconds.

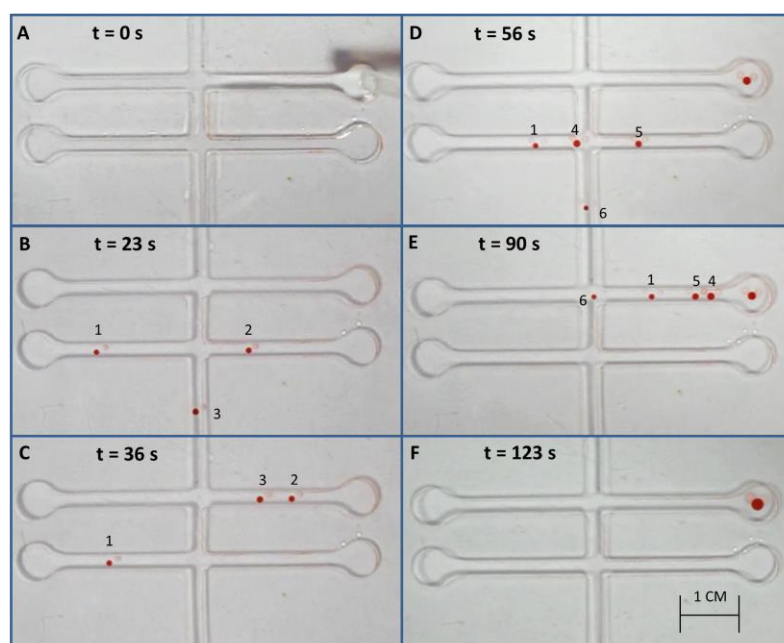


*Figure 4.6 Sequence of video frames showing multiple droplets travelling towards the source of chemoattractant ( $100\text{-}200 \mu\text{l}$  of  $10^{-2} \text{ M HCl}$ ). **A** – The channels were filled with a solution of  $10^{-2} \text{ M NaOH}$  and the chemoattractant ( $100\text{-}200 \mu\text{l}$  of  $10^{-2} \text{ M HCl}$ ) was added at the desired destination; **B** – Placement of first three droplets. **C** – First two droplets moving towards the chemoattractant source; **D** – Placement of final three droplets; **E** – Movement of all droplets toward chemoattractant source; **F** – All droplets arrive at destination and merge.*

In control experiments, when droplets of trihexyl(tetradecyl)phosphonium dicyanamide ( $[\text{P}_{6,6,6,14}][\text{DCA}]$ ) ionic liquid were placed into the same gradients (as the  $[\text{P}_{6,6,6,14}][\text{Cl}]$ ) no movement was observed. This behaviour can be explained through inhibition of the aqueous solubility of  $[\text{P}_{6,6,6,14}]^+$  due to the  $\text{DCA}^-$  anion, which is less soluble in the aqueous phase than the  $\text{Cl}^-$  ion [20].

This interpretation is supported by the observation that no significant change in the surface tension of the aqueous solution occurs after the addition of a droplet of [P<sub>6,6,6,14</sub>][DCA] (See Table 4.1).

As the partition of the sparingly soluble cationic surfactant into the aqueous phase is modulated by the solubility of the anion component of the IL, any gradient in the aqueous phase composition that affects anion (in this case Cl<sup>-</sup>) solubility can be used to control droplet movement. Thus the chemotactic behaviour of the droplet is not limited to Cl<sup>-</sup> ion gradients but is also observed with potassium bromide (KBr) and sodium sulphate (Na<sub>2</sub>SO<sub>4</sub>) gradients (see Table 4.1). This shows that the chemotactic movement of these droplets is affected by any factor that affects Cl<sup>-</sup> partition from the droplet, such as the ionic strength of the solution (which also inhibits the cation solubility).

#### **4.4.2 Droplet Tracking and Gradient Analysis**

In order to calculate the movement speed of the droplets several videos were captured which demonstrates droplets travelling towards the source of a chemoattractant. At times 4s, 5s and 6s, 110 – 170 µl of chemoattractant were added to desired destination within the fluidic channel, upper right arm (See Video 4.1, Appendix A). The chemoattractant was then given 10 s to sufficiently propagate along the channels whereupon at time 16s a single droplet was introduced along the lower right channel (see Figure 4.7, position b). It was observed that the droplet begins to travel towards the source of chemoattractant, slowly at first, followed by an increase in its speed, until it comes to an eventual stop at the chemoattractant location source. The rate of release of the surfactant from the droplet is dependent on the Cl<sup>-</sup> concentration at the IL/aqueous boundary, and the steepness of the Cl<sup>-</sup> gradient determines the speed of the droplet.

The droplet's progress over time from its introduction to the channel, to arrival at the source is presented in Figure 4.7.

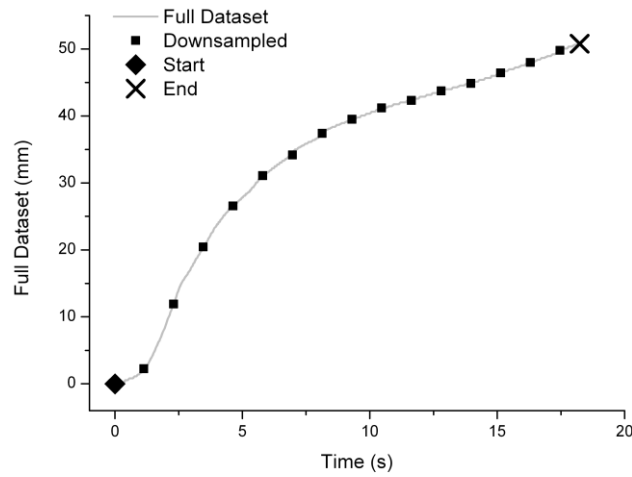


Figure 4.7 Tracking of the droplet's distance from its point of entry ( $t_0$ ) towards its end position/source of chemoattractant (X). Grey line – full dataset at every video frame. Black squares – down sampled data points from full dataset (every 35<sup>th</sup> point).

The above approach was expanded to investigate the movement of multiple droplets at different locations within the channel network, see Figure 4.6. In a similar manner to video mentioned above, a  $\text{Cl}^-$  ion gradient was created by adding several droplets of  $\text{HCl } 10^{-2} \text{ M}$  chemoattractant at the desired location within the fluidic network. Initially the channel was filled with a  $\text{NaOH } 10^{-2} \text{ M}$ , followed by addition of 6 individual droplets at different locations and times see Figure 4.8 and Table 4.2 for details.

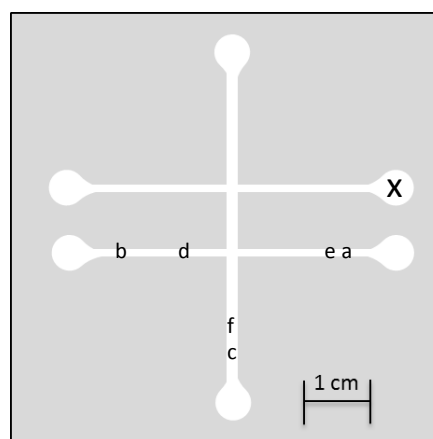


Figure 4.8 Fluidic network diagram showing the locations where each solution was introduced. (X) Chemoattractant, (a) Droplet a, (b) Droplet b, (c) Droplet c, (d) Droplet d, (e) Droplet e, (f) Droplet f.

Table 4.2 Time and location of addition of HCl solution and droplets, as in Video 4; see Figure 2.7 for location correlation.

| Time(s) | Solution Introduced | Location |
|---------|---------------------|----------|
| 0       | HCl                 | X        |
| 21      | Droplet a           | a        |
| 24      | Droplet b           | b        |
| 27      | Droplet c           | c        |
| 53      | Droplet d           | d        |
| 57      | Droplet e           | e        |
| 61      | Droplet f           | f        |

The distance travelled by each droplet from their respective entry points to the  $Cl^-$  ion source was tracked as a function of time, see Figure 4.9. In each case the plots resulted in a similar trend as before (Figure 4.7). The droplets tend to start slow but soon speed up, then slow down again upon arrival at the  $Cl^-$  source. For droplets that have a relatively smooth passage from point of entry to the chemoattractant source, the distance travelled as a function of time fits approximately to a sigmoid model. The typical average speed of the droplets over the first 30s is between 0.5-4 mm/s. Variations from this profile *e.g.* droplets b, e, f (Figure 4.9) may be due to the droplet changing direction at branches in the fluidic network.

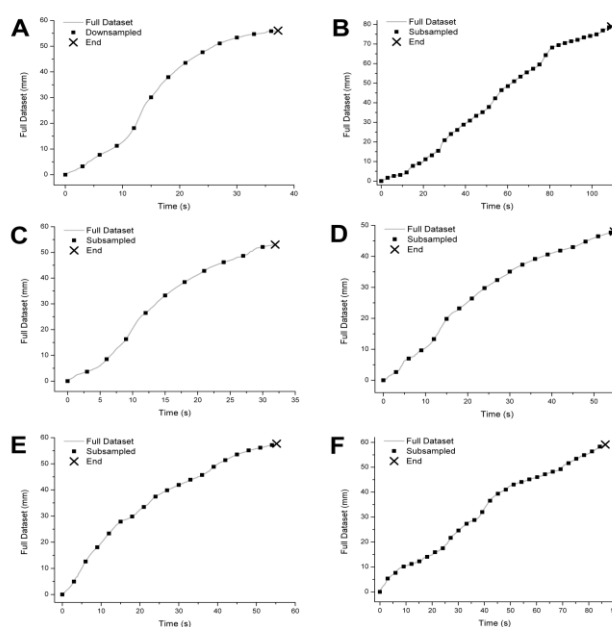


Figure 4.9 Tracking of all 6 droplets in Video 4.4 introduced in the sequence presented in table 4.2. (A) Droplet a, (B) Droplet b, (C) Droplet c, (D) Droplet d, (E) Droplet e, (F) Droplet f, (X)  $Cl^-$  source and end location of each droplet movement.

## 4.5 Conclusions

In conclusion we have demonstrated a simple single component biomimetic droplet that spontaneously moves in a direction determined by an external chemical gradient. This biomimetic-type movement enables the droplets to find the pathway to the source of the chemoattractant from different initial starting positions in a microfluidic network. Since the droplets are self-propelled and spontaneously travel along the liquid-air interface by release of surfactant-type cations, they require no external energy source. Since there is a large library of ILs available, this opens up numerous means of creating gradients for these droplets to follow. Moreover, ILs have negligible vapour pressure, low combustibility and high thermal stability. [20] These properties make them extremely useful as micro-scale “vehicles” compared to conventional organic droplets that are subject to evaporation and which can be flammable. ILs have also been shown to be good solvents for numerous chemical species and have been used in a wide range of reactions, including harsh reactions such as Grignard reactions, [24, 25] broadening the potential applications for these biomimetic chemotactic droplets. It is envisioned that these droplets could be used for dynamic sensing (*e.g.* in this case they indicate the direction of increasing Cl<sup>-</sup> concentration in the channels through their movement), energy-free molecular-cargo transport and as micro-vessels that can perform chemical reactions at pre-determined locations (*e.g.* through fusion of droplets that contain reaction precursors).

## 4.6 References

1. Van Haastert, P.J.; Devreotes, P.N. Chemotaxis: signalling the way forward. *Nature reviews Molecular cell biology* **2004**, *5*, 626-634.
2. Adler, J. Chemotaxis in bacteria. *Science* **1966**, *153*, 708-716.
3. Wu, J.Y.; Feng, L.; Park, H.-T.; Havlioglu, N.; Wen, L.; Tang, H.; Bacon, K.B.; Jiang, Z.-h.; Zhang, X.-c.; Rao, Y. The neuronal repellent Slit inhibits leukocyte chemotaxis induced by chemotactic factors. *Nature* **2001**, *410*, 948-952.
4. Jeon, N.L.; Baskaran, H.; Dertinger, S.K.; Whitesides, G.M.; Van De Water, L.; Toner, M. Neutrophil chemotaxis in linear and complex gradients of interleukin-8 formed in a microfabricated device. *Nature biotechnology* **2002**, *20*, 826-830.
5. Spehr, M.; Gisselmann, G.; Poplawski, A.; Riffell, J.A.; Wetzel, C.H.; Zimmer, R.K.; Hatt, H. Identification of a testicular odorant receptor mediating human sperm chemotaxis. *Science* **2003**, *299*, 2054-2058.
6. Funamoto, S.; Meili, R.; Lee, S.; Parry, L.; Firtel, R.A. Spatial and temporal regulation of 3-phosphoinositides by PI 3-kinase and PTEN mediates chemotaxis. *Cell* **2002**, *109*, 611-623.

7. Chaudhury, M.K.; Whitesides, G.M. How to make water run uphill. *Science* **1992**, *256*, 1539-1541.
8. Smith, J.D.; Dhiman, R.; Anand, S.; Reza-Garduno, E.; Cohen, R.E.; McKinley, G.H.; Varanasi, K.K. Droplet mobility on lubricant-impregnated surfaces. *Soft Matter* **2013**, *9*, 1772-1780.
9. Wheeler, A.R.; Moon, H.; Bird, C.A.; Ogorzalek Loo, R.R.; Kim, C.-J.C.; Loo, J.A.; Garrell, R.L. Digital microfluidics with in-line sample purification for proteomics analyses with MALDI-MS. *Analytical Chemistry* **2005**, *77*, 534-540.
10. Gong, J. All-electronic droplet generation on-chip with real-time feedback control for EWOD digital microfluidics. *Lab on a chip* **2008**, *8*, 898-906.
11. Paul, B.; Craig, P.B.; Julian, E. Stimuli-responsive surfactants. *Soft Matter* **2013**, *9*, 2365-2374.
12. Darhuber, A.A.; Valentino, J.P.; Troian, S.M.; Wagner, S. Thermocapillary actuation of droplets on chemically patterned surfaces by programmable microheater arrays. *Journal of Microelectromechanical Systems* **2003**, *12*, 873-879.
13. Zhao, Y.; Fang, J.; Wang, H.; Wang, X.; Lin, T. Magnetic liquid marbles: manipulation of liquid droplets using highly hydrophobic Fe<sub>3</sub>O<sub>4</sub> nanoparticles. *Advanced materials (Deerfield Beach, Fla.)* **2010**, *22*, 707-710.
14. Wixforth, A.; Strobl, C.; Gauer, C.; Toegl, A.; Scriba, J.; v Guttenberg, Z. Acoustic manipulation of small droplets. *Analytical and bioanalytical chemistry* **2004**, *379*, 982-991.
15. Han-Sheng, C.; Aloke, K.; Steven, T.W. Open optoelectrowetting droplet actuation. *Applied Physics Letters* **2008**, *93*, 9064104.
16. Velarde, M.G. Drops, liquid layers and the Marangoni effect. *Phil. Trans. R. Soc. A* **1998**, 829-842.
17. Lagzi, I.; Soh, S.; Wesson, P.; Browne, K.; Grzybowski, B. Maze solving by chemotactic droplets. *Journal of the American Chemical Society* **2010**, *132*, 1198-1199.
18. Diguët, A.; Guillermic, R.-M.; Magome, N.; Saint-Jalmes, A.; Chen, Y.; Yoshikawa, K.; Baigl, D. Photomanipulation of a droplet by the chromocapillary effect. *Angewandte Chemie (International ed. in English)* **2009**, *48*, 9281-9284.
19. Florea, L.; Wagner, K.; Wagner, P.; Wallace, G.G.; Benito-Lopez, F.; Officer, D.L.; Diamond, D. Photo-Chemopropulsion—Light-Stimulated Movement of Microdroplets. *Advanced materials* **2014**, *26*, 7339-7345.
20. Fraser, K.J.; MacFarlane, D.R. Phosphonium-based ionic liquids: An overview. *Australian journal of chemistry* **2009**, *62*, 309-321.
21. Wellens, S.; Vander Hoogerstraete, T.; Møller, C.; Thijs, B.; Luyten, J.; Binnemans, K. Dissolution of metal oxides in an acid-saturated ionic liquid solution and investigation of the back-extraction behaviour to the aqueous phase. *Hydrometallurgy* **2014**, *144*, 27-33.
22. Thompson, D.; Coleman, S.; Diamond, D.; Byrne, R. Electronic structure calculations and physicochemical experiments quantify the competitive liquid ion association and probe stabilisation effects for nitrobenzospiropyran in phosphonium-based ionic liquids. *Physical Chemistry Chemical Physics* **2011**, *13*, 6156-6168.
23. Florea, L.; Fay, C.; Lahiff, E.; Phelan, T.; O'Connor, N.E.; Corcoran, B.; Diamond, D.; Benito-Lopez, F. Dynamic pH mapping in microfluidic devices by integrating adaptive coatings based on polyaniline with colorimetric imaging techniques. *Lab on a chip* **2013**, *13*, 1079-1085.

24. Welton, T. Room-temperature ionic liquids. Solvents for synthesis and catalysis. *Chemical reviews* **1999**, *99*, 2071-2084.
25. Itoh, T.; Kude, K.; Hayase, S.; Kawatsura, M. Design of ionic liquids as a medium for the Grignard reaction. *Tetrahedron Letters* **2007**, *48*, 7774-7777.

## **Chapter 5:**

### **Electrotactic Ionic liquid droplets**

#### **5.1 Abstract**

#### **5.2 Introduction**

#### **5.3 Experimental**

##### **5.5.1 Materials**

##### **5.5.2 Micro-Channel and Electrodes Fabrication**

##### **5.5.3 Methods**

#### **5.4 Results and Discussion**

##### **5.4.1 Droplet Movement**

##### **5.4.2 Channel Current Study**

##### **5.4.3 Cl<sup>-</sup> Concentration Gradient Visualisation**

#### **5.5 Conclusions**

#### **5.6 Acknowledgments**

#### **5.7 References**

## Chapter 5

---

# Electrotactic Ionic Liquid Droplets\*

---

\***Electrotactic ionic liquid droplets**, W. Francis, K. Wagner, S. Beirne, D. Officer, G. Wallace, L. Florea and D. Diamond, *Sensors and Actuators B*. 239 (2017) 1069-1075.

## 5.1 Abstract

To our knowledge, this work describes the first example of electro-guided, self-propelled droplets composed solely of an ionic liquid (IL), namely trihexyl(tetradecyl)phosphonium chloride ( $[P_{6,6,6,14}][Cl]$ ). These self-propelled droplets travel along an aqueous-air boundary to desired destinations within the fluidic network. Electrotactic movement of the droplets is due to asymmetric electro-stimulated release of a constituent of the IL droplet, the  $[P_{6,6,6,14}]^+$  ion, which is a very efficient cationic surfactant, through electrochemically generated  $Cl^-$  gradients. The direction and speed of movement can be controlled by switching the impressed voltage (typically 5 - 9V) ON or OFF, and by changing the polarity of the electrodes in contact with the electrolyte solution.

The  $Cl^-$  gradients required for droplet movement are electrochemically generated using 3D printed electrodes which are embedded within the fluidic channels. On demand creation of these  $Cl^-$  gradients electrochemically allows reversible droplet movement over extended periods of time, and provides a means for precise control over the droplet trajectory.

## 5.2 Introduction

The movement of cells and other biological entities is essential to the survival of all life. This is true from single celled organisms to the largest and most complex forms of life such as mammals. Fluid and cells are transported throughout large complex bodies through active pumping, while nutrients are transported in and out of cells through the use of special biological “microvehicles” known as vesicles. Inside the cell there are motor proteins which shuttle cargo around the cytosol, such as specialised walking molecules known as kinesins [1]. Helicase is another unique biological motor whose main function is to separate two annealed nucleic acid strands (for example within DNA or RNA) [2]. This type of micro-molecular movement is triggered and controlled through chemical and electrical impulses.

Many single cell and multicellular organisms move in response to chemical stimuli present in their environment [3], a phenomenon known as chemotaxis. Prokaryotic cells such as bacteria use chemotaxis to find sources of food or flee harmful toxins, while eukaryotic and somatic cells have much more complex functions which rely on this behaviour. For example, lymphocytes use chemotaxis behaviour to follow a

chemical trail left by a pathogen and then destroy the harmful intruder [4,5]. The passage of vesicles carrying cargo in and out of the cell relies on chemical gradients to transfer their cargo [6], while other examples of chemically driven biological motors include enzymes that can follow a chemical signal to the corresponding substrate [7], and sperm cells, which use prominent flagella composed of a core of microtubules, powered by flagellar dynein, to propel themselves through the female reproductive tract [8].

The movement of biological organisms is not solely triggered through chemical stimuli; in fact, much of the movement of animal and plant cells is due to the generation of an electric current. For example, in mammals, the onset of wound healing is due to weak electric currents which are generated immediately upon receiving the wound [9]. Humans and mammals are found to have a natural electrical gradient across healthy, intact skin due to the secretion of chloride ( $\text{Cl}^-$ ) ions and the absorption of sodium ( $\text{Na}^+$ ) ions, which results in the outer layers of the skin being more negatively charged than the inner layers. Upon receiving a wound (sufficient to cause skin breakage) there is a flow of positively charged ions emitted from the wound that generates an electric current perpendicular to the skin at the site of the wound [9]. This electric current induces the migration of keratinocytes and mammalian epithelial cells to the wound and triggers the onset of healing [10]. Movement of cells in response to an electric field is termed galvanotaxis or electrotaxis [11]. Synthetically induced electrotaxis is mainly used to direct the movement of cells in both *in-vitro* and *in-vivo* experiments, as it offers better control over on-demand movement of cells compared to solely controlling movement through chemotaxis [12]. An exciting use of electrotactic-guided cells is *in-vivo* wound healing, in which cells are guided to specific destinations to encourage the growth or repair of damaged tissue [9]. Other groups have made impressive progress towards using electro-guided cells for the repair of the brain and central nervous system [13,14]. Treatment of neurological diseases with electrical stimulation has advanced significantly in recent years, for example through demonstrations that electric fields can enhance neuroplasticity processes. When electric fields within the physiological range were applied *in-vitro* the movement of several different neural cells types was induced. This ability to induce the movement of specific neural cells to specific destinations with the added benefit of enhancing neuroplasticity processes could potentially give rise to dramatic improvements in the treatment of neurological and psychiatric diseases [13].

Although the chemotactic and electrotactic response of living organisms has been extensively researched, there is a notable lack of reports into synthetic approaches that

mimic these forms of movement. Inspired by the electrotactic movement of living organisms, here we describe for the first time, simple synthetic droplets composed solely of an ionic liquid that can be guided at the liquid-air interface using electro-generated ion gradients.

In recent years, multiple approaches have been investigated for the generation of micro-droplet movement, including alteration of the wettability of the substrate through chemical [15,16] or electrochemical means [17,18]. Other forms of stimuli, including temperature [19], magnetic [20], light [21], and acoustic forces [22] have also been used for the actuation and guidance of micro-droplets. Although these approaches permit individual droplet control through external stimulation, they generally require relatively complicated experimental arrangements [17] or complex droplet compositions [23].

Surfactant release has been employed as another contactless method for controlled movement of droplets that rest at the liquid/air interface [23]. When surfactants are released into an aqueous system, they locate at the liquid/air interface with the polar heads embedded in the water phase and the non-polar tails projecting out of the solution. The release of surfactant lowers the surface tension of the system, and once this occurs, a spontaneous movement of liquid is created from areas of low surface tension, to areas of high surface tension, a phenomenon known as the Marangoni effect [24]. By creating conditions wherein asymmetrical release from the droplet of a pre-loaded surfactant occurs, directional control over the droplet movement can be achieved. Using this premise, “smart droplets” were developed which can solve complex mazes by following a pre-established pH gradient [23]. Photo-controlled droplet movement was also achieved by asymmetric release of surfactant through localised creation of a pH gradient using a photo-acid generator [25]. Another approach involved the use of photo-responsive azobenzene surfactants for droplet manipulation at the air/liquid interface [26]. Electrochemical control over the surface tension of a liquid metal was also demonstrated through the formation and removal of a surface oxide on liquid metals by applying low voltages ( $<1$  V) [27]. When the surface oxide is present on the liquid metal it acts as a surfactant and significantly lowers the interfacial tension between the liquid metal and the electrolyte solution (from  $\sim 500$  mJ/m<sup>2</sup> to near zero). Removal of the surface oxide restores the surface tension of the liquid metal. This technique allowed for shape-reconfiguration of liquid metals alloys of gallium and their guidance through a fluidic channel.

Previously we reported chemotactic droplets composed solely of an ionic liquid namely trihexyl(tetradecyl)phosphonium chloride ( $[P_{6,6,6,14}][Cl]$ ) that moved due to triggered release of the cationic surfactant  $[P_{6,6,6,14}]^+$  and were guided to specific destinations through chemically generated ion gradients [28]. Ionic liquids are ideal solvents for the development of smart vessels and “vehicles” due to their negligible vapour pressure, high thermal stability and low combustibility, making them significantly more stable when compared to conventional droplet systems based on organic solvents. [29]  $[P_{6,6,6,14}][Cl]$  in particular has a high viscosity and is relatively hydrophobic which means that it can form stable droplets on aqueous/air interfaces [29]. Ionic liquids have also been previously shown to exhibit extended electrochemical windows [30-33]. Buzzeo *et al.* [33] examined the electrochemical window of several Ionic liquids (1-ethyl-3-methylimidazolium bis(trifluoromethylsulfonyl)imide ( $[C_2mim][NTf_2]$ ), *n*-hexyltriethylammonium bis(trifluoromethylsulfonyl)-imide ( $[N_{6,2,2,2}][NTf_2]$ ), 1-hexyl-3-methylimidazolium trifluorotris-(pentafluoroethyl)phosphate ( $[C_6mim][FAP]$ ) and tris(*n*-hexyl)tetradecylphosphonium trifluorotris-(pentafluoroethyl)phosphate ( $[P_{6,6,6,14}][FAP]$ )) using cyclic voltammetry at gold and platinum microelectrodes (diameter of 10  $\mu m$ ). When the neat ILs were used as electrolytes,  $[P_{6,6,6,14}][FAP]$  showed no redox activity in the range of -5 V to 5 V at the gold electrode, and no redox activity in the range of -4 to 4 V at the platinum electrode. The electrochemical window of this IL could potentially extend over a wider range, however, these were the limits set for the experiments performed by Buzzeo *et al.*. No redox activity was observed for  $[N_{6,2,2,2}][NTf_2]$  between -4 V and 4 V for both electrodes and no activity was shown for both  $[C_2mim][NTf_2]$  and  $[C_6mim][FAP]$  between -2 V and 2V (at both electrodes). This extended electrochemical window shows that ILs are stable electrolytes for use across a broad potential range.

Herein we report reversible electrotactic movement of the same  $[P_{6,6,6,14}][Cl]$  droplets to specific destinations through electrochemically generated  $Cl^-$  gradients. To our knowledge this is the first demonstration of spontaneous electrotactic movement of droplets composed solely of an IL at the aqueous/liquid interface. The electrotactic movement presented is not only reversible and repeatable, but the droplet trajectory and speed can be controlled by electrode polarity and applied potential, respectively.

## 5.3 Experimental

### 5.3.1 Materials

Sodium chloride (NaCl) (Sigma-Aldrich® Ireland Ltd), Trihexyl(tetradecyl)phosphonium chloride ( $[P_{6,6,6,14}][Cl]$ ) (Sigma-Aldrich® Ireland Ltd), N, N-Dimethyl-9,9'-biacridinium dinitrate (lucigenin) (Sigma-Aldrich® Ireland Ltd) and 1-(methylamino)anthraquinone red dye (Sigma-Aldrich® Ireland Ltd) were all used as purchased.

### 5.3.2 Micro-Channel and Electrodes Fabrication

The titanium mesh electrodes (4 x 4 electrodes, each with a diameter of 3.5 mm and 8 mm in height) were 3D printed using a Realizer SLM-50 printer (**Figure 5.1**). 3D printing produces high surface area electrodes while also allowing facile integration of the electrodes into a single platform, as the design and shape of the individual electrodes can be tuned to match the design of the fluidic channel.

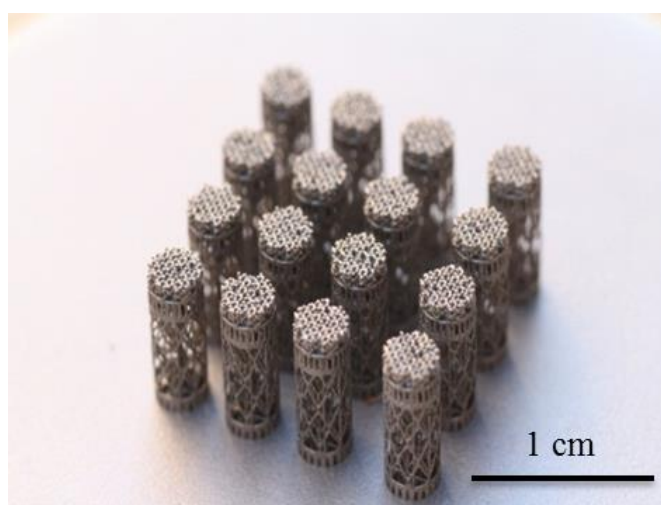


*Figure 5.1 3D printed titanium mesh electrodes.*

Following printing, the electrodes were embedded into fluidic channels. Two different types of channels were used. In the first case, the channels were designed in Solid Works CAD modelling software and fabricated in acrylate ABS-Like™ Polyjet photopolymer (Stratasys) using an Objet350 Connex 3D printer. The channels were 2.5 mm deep, 3 mm in width and the distance between opposing electrodes was 16 mm, see **Figure 5.2a**. A narrow channel which was 0.5 mm wide and 1 mm in length was placed

between the electrodes and the fluidic system in order to prevent the droplet from crushing into the electrodes.

In the second case, the channels were designed in AutoCAD 2014, and a CO<sub>2</sub> laser ablation system (Epilog Zing Laser Series) was used to cut the channels in 1 mm poly(methylmethacrylate) (PMMA) sheet that had a 50 μm double-sided pressure-sensitive adhesive (PSA) layer pre-attached. Once cut, the protective layer from the PSA was removed and the PMMA/PSA layer was laminated with another 1 mm PMMA sheet. The obtained channels were 2 mm wide, 1 mm high, with a 2 cm distance between the electrodes and a 4 mm diameter hole for electrode placement, see **Figure 5.2b**.

For both types of channels, following printing, the 3D mesh titanium electrodes were inserted into the placement holes incorporated into the channel design. The electrodes were then secured in position using UV curable glue and the channel was placed onto a breadboard to facilitate the connection of the extruding pins from electrodes to the wires connecting to the power supply. Two different channel configurations for electro-stimulation of droplets were obtained (**Figure 5.2**).

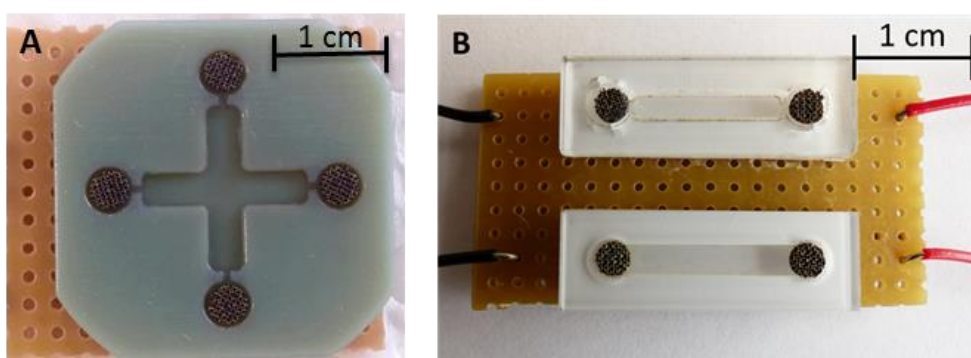


*Figure 5.2 Channels for electro-stimulation of droplets showing embedded 3D printed titanium electrodes; A) Cross-shape 3D printed channels in ABS Polyjet Photopolymer (Stratasys) based on acrylic monomers B) Laser cut PMMA channel.*

### 5.3.3 Methods

#### Droplet movement

To achieve electrotactic droplet movement, the channels were initially filled with electrolyte solution of varying concentration,  $10^{-2}$  M NaCl and  $10^{-3}$  M NaCl, respectively. The voltage was then applied to the electrodes (5 – 9 V); after 10 – 30 s the droplet was

placed at the cathode (-) and spontaneously moved towards the anode (+). When the polarity of the active electrodes was reversed, the droplets moved in the opposite direction.

### **Current Generation Study**

In order to study the current generated when applying a voltage across the NaCl solution, the channels were initially filled with electrolyte solution ( $10^{-2}$  M NaCl and  $10^{-3}$  M NaCl, respectively) and the required voltage was supplied to the electrodes (1 – 10 V). The current range was then measured using an M Digital Multimeter (N73CG).

### **Cl<sup>-</sup> Concentration Gradient Visualisation**

In order to visualise the generation of the Cl<sup>-</sup> gradient, a  $10^{-3}$  M NaCl solution containing  $10^{-4}$  M lucigenin was made and placed in the straight PMMA fluidic channel (the channels were 2 mm wide, 1 mm high, with a 2 cm distance between the electrodes) and 9V was applied across the solution. To demonstrate the reversibility of the Cl<sup>-</sup> gradient, the polarity of the electrodes was switched after the desired time. A 369 nm LED was used to excite the fluorescent lucigenin dye. Videos of the gradient generation were captured using a Panasonic DMC-FZ200 camera.

## **5.4 Results and Discussions**

### **5.4.1 Droplet Movement**

The droplets used in this study were composed solely of the ionic liquid [P<sub>6,6,6,14</sub>][Cl] and a small amount of red dye (1-(methylamino)anthraquinone) used only for better visualisation. Due to the strong association of the Cl<sup>-</sup> anion with the [P<sub>6,6,6,14</sub>]<sup>+</sup> cation, the IL is highly hydrophobic and is able to form a stable droplet at the air-water interface

[34]. The movement of the droplet is due to the controlled asymmetric release of the sparingly soluble  $[P_{6,6,6,14}]^+$ , which behaves as a cationic surfactant at the air-water boundary. Previously we have shown that when 1 mg/ml of this IL was placed into a  $10^{-2}$  M solution of NaCl only a negligible drop in surface tension was observed (from  $\sim 73.9$  to  $\sim 73.2$  mN/m). However, when the same volume of the IL was placed into a lower concentration of this electrolyte (*e.g.*  $10^{-5}$  M NaCl) there was a large drop in surface tension (from  $\sim 74.2$  to  $\sim 38.4$  mN/m) [28]. This shows that the  $[P_{6,6,6,14}]^+$  does behave as a strong cationic surfactant preferentially in low ionic strength solutions. When  $[P_{6,6,6,14}]^+$  diffuses from the droplet into the aqueous solution, its surfactant character causes a sudden drop of the surface tension of the solution [28]. The rate of release of surfactant is controlled by the solubility of the  $Cl^-$  ion, as any  $Cl^-$  transfer from the droplet to the aqueous phase must be balanced by an equivalent transfer of  $[P_{6,6,6,14}]^+$  to maintain overall charge neutrality. Release of  $Cl^-$  ions from the droplet depends on the local aqueous  $Cl^-$  concentration at the IL-aqueous phase boundary. Hence, in the presence of an aqueous phase  $Cl^-$  gradient, differential release of  $[P_{6,6,6,14}]^+$  occurs across the droplet boundary and a surface tension gradient is created which generates Marangoni-like liquid flow causing the droplet to move towards areas of higher surface tension (*i.e.* lower  $[Cl^-]$ ).

In this study, the  $Cl^-$  gradients within the electrolyte solutions were electrochemically generated. When an external electric field is applied across a NaCl solution, a  $Cl^-$  concentration gradient is created as the  $Na^+$  ions migrate towards the cathode and  $Cl^-$  ions towards the anode. When a  $[P_{6,6,6,14}][Cl]$  droplet is placed on the surface of this solution, the  $Cl^-$  concentration gradient causes an asymmetrical release of the  $[P_{6,6,6,14}]^+$  cationic surfactant which propels the droplet towards the anode. Furthermore, the applied electric field may cause a Faradic rearrangement of the charged ions within the IL droplet (**Figure 5.3**), thereby creating ion concentration gradients which may reinforce the droplet movement mechanism [35]. This ion rearrangement occurs due to the bipolar electrode (BPE) effect. The BPE effect describes the phenomena by which an electronic conductor (which is in contact with an ionically conductive phase) can be polarised, via an electric field, despite the fact it is not in contact with the external power supply [36]. We believe a similar effect is occurring within the droplet. This Faradic rearrangement of the ILs constituent ions may result in the  $Cl^-$  anions migrating toward the side of the droplet facing the anode and the  $[P_{6,6,6,14}]^+$  cations migrating toward the side of the droplet facing the cathode. However, due to the very strong coulombic ion-pairing within the IL [34], we believe that this effect is minimal and droplet movement is

mainly due to the asymmetrical release of the surfactant in response to the external ionic strength gradient.

Hence, when a voltage is applied (5-9 V), a  $[P_{6,6,6,14}][Cl]$  droplet positioned near to a cathode (-) will release the cationic surfactant  $[P_{6,6,6,14}]^+$  in an asymmetrical manner, creating Marangoni like flows which drive the droplet towards the anode (+) (**Figure 3.3**).

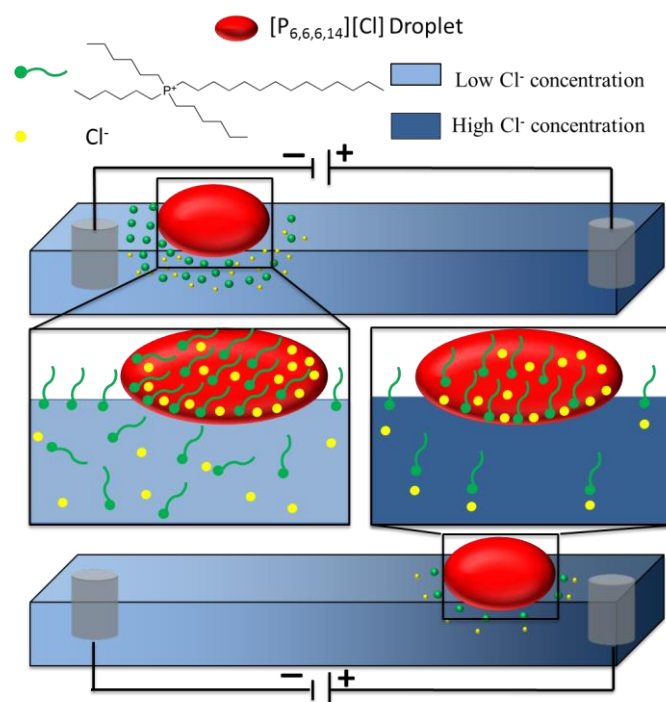


*Figure 5.3 Diagram which depicts the relative release of the  $[P_{6,6,6,14}]^+$  surfactant from the  $[P_{6,6,6,14}][Cl]$  droplet in lower  $Cl^-$  concentration (at the cathode, left) and in higher  $Cl^-$  concentration (at the anode, right) when 9 V is applied to a solution of  $10^{-3}$  M NaCl.*

Using this approach we have shown that the droplets can be very effectively guided along channels from the cathode (-) towards the anode (+). In addition to reversing direction within a channel, the droplets can be ‘steered’ into side channels at junctions, by polarizing appropriate electrode pairs. This can be seen in **Figure 5.4**, which shows a droplet being guided to each electrode twice within the fluidic network (See Video 5.1, Appendix B).

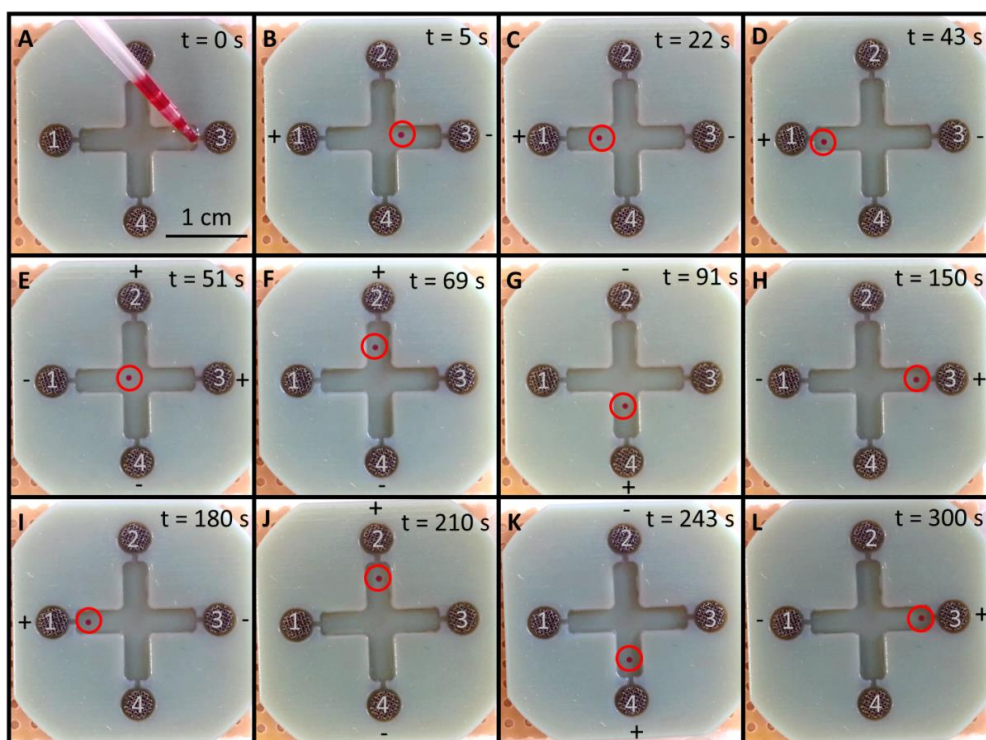
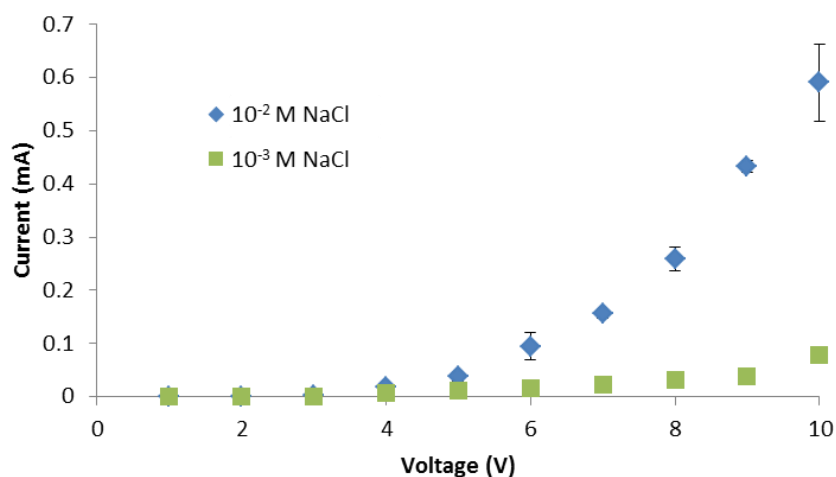


Figure 5.4 Sequence of video frames demonstrating controlled movement of the [P6, 6,6,14][Cl] droplet using potential differences applied across pairs of electrodes 1-4. The channels are filled with a solution of  $10^{-3}$  M NaCl and a 9 V potential difference is applied across selected electrode pairs. A – Introduction of the droplet onto the aqueous solution; B – C - The droplet is propelled from the initial cathode (3) towards the opposite anode (1); D – The droplet arrives at electrode (1); E – The polarity of the electrodes is then reversed and the droplet moves back towards electrode (3); F – As the droplet approaches the centre point, the potential difference is applied across electrodes (2 - cathode) and (4 - anode) and the droplet is diverted into the cross channel; G – Upon arrival at electrode (2) the polarity is reversed, and the droplet moves towards electrode (4); H – Using a similar approach, the droplet is made to return to the original starting position. I – L The process is repeated, showing that the droplet can be moved to each electrode multiple times. (For full video see Appendix B, video 5.1)

#### 5.4.2 Channel Current Study

Figure 5.5 show the current values obtained when 1 – 10 V was applied between neighbouring electrodes (distance between electrodes = 2 cm) for different concentrations of NaCl ( $10^{-2}$  M and  $10^{-3}$  M, respectively). Despite the difference in current observed for each concentration, unidirectional movement of the droplet was not achieved unless a voltage of 5 V or higher was applied. The oxidation potential for Cl to be oxidised to  $\text{Cl}_2$  is 1.36 V (at a normal hydrogen electrode) [37] while the potential for  $\text{H}_2\text{O}$  electrolysis is

1.23 V (130 mV less than  $\text{Cl}^-$  oxidation). However, due to the large over potential of oxygen and the pacification of the titanium electrodes, the oxidation of  $\text{Cl}^-$  may be more energetically favourable compared to water electrolysis. This may result in the formation of  $\text{Cl}^-$  gradients within the channel and droplet movement at 5 V despite the fact that there is no visible bubble generation (from the electrolysis of water). For  $10^{-2}$  M NaCl solution, bubbles due to electrolysis were visible at the cathode when the applied voltage was 7 V or greater. In the case of the  $10^{-3}$  M NaCl solution, this was not observed for voltages below 10 V. Bubble generation due to electrolysis disrupts droplet movement in the vicinity of the electrodes, and therefore, electrostatic droplet movement experiments were performed and analysed below these threshold values. No electrolysis of the electrolyte solution is observed under our experimental conditions because of a combination of two parameters; the first is the pacification of the titanium electrodes (with titanium oxide) which greatly reduces the efficiency of the electrode and secondly is the low current density of the electrolyte solutions which also impedes electrolysis.



*Figure 5.5 Current generated when the applied voltage was varied over the range 1 – 10 V for  $10^{-2}$  M and  $10^{-3}$  M NaCl solutions, respectively. Error bars are standard deviations for  $n = 3$  replicate measurements. Unidirectional movement was first observed at 5 V for all of the solutions. Visible gas generation was first observed at the electrodes at 7 V for  $10^{-2}$  M solutions and at 10 V for the  $10^{-3}$  M solutions.*

As expected, the current increased as the voltage was raised above *ca.* 5V, and the current obtained increased significantly with electrolyte concentration. The speed of the droplet movement was also dependent on a number of parameters, which include the time at which the droplet was placed (in relation to the moment the potential was applied), the volume of the droplet and the interfacial contact area between the droplet and the aqueous solution. However, when these parameters were held relatively constant, an increase in droplet speed was observed with increasing applied voltage (below visible gas generation values). For example, droplet speeds of 1 - 2 mm s<sup>-1</sup> were obtained when a potential of 9 V was applied to a 10<sup>-3</sup> M NaCl solution. No controlled movement of the droplet was observed at any of the NaCl electrolyte concentrations studied until voltages of at least 5 V were applied. These results indicate that unless an ion gradient is generated across the length of the channel (by means of the applied voltage), no asymmetrical release of surfactant from the droplet into the aqueous solutions occurs, and no droplet movement happens. Rather, in the absence of the ion gradient, either no movement or random motion of the droplet is observed.

### 5.4.3 Cl<sup>-</sup> Concentration Gradient Visualisation

In order to confirm the presence of a Cl<sup>-</sup> gradient within the channel, a study was performed using the fluorescent dye lucigenin. The fluorescence of lucigenin is highly quenched by Cl<sup>-</sup>, and therefore, if a Cl<sup>-</sup> gradient is created in the channel via the applied voltage, a gradient in the fluorescence of the solution should also be observed. The PMMA channels were filled with a solution of 10<sup>-3</sup> M NaCl containing 10<sup>-4</sup> M lucigenin and a 369 nm led light source was used to excite the dye. The experiment was recorded in a dark room. As can be seen in **Figure 5.6** and video 5.2 (Appendix B), approximately 10 minutes after application of 9 V across the electrodes, a fluorescent gradient becomes visible in the channel. This continues to develop, and is fully formed and stable after approximately 30 minutes. Video 5.3 (Appendix B) shows that the formation of the fluorescent gradient is reversible. In this case, after allowing Cl<sup>-</sup> gradient formation for 10 min at an applied voltage of 9 V, the polarity of the electrodes was reversed. It was observed that after additional 10 minutes the fluorescent gradient also had reversed. Video 5.4 (Appendix B) shows the same experiment performed with a solution of 10<sup>-4</sup> M lucigenin in deionised water. The video shows that despite the 9V applied voltage across

the solution, there was no visible difference in the fluorescence across the channel due to the absence of  $\text{Cl}^-$  ions in solution. The visualisation of a fluorescent gradient in the NaCl solutions and the absence of one in water is further proof for the formation of an extended  $\text{Cl}^-$  gradient in the fluidic channel. This extended gradient has also been shown previously when NaCl was used as the electrolyte for electro-controlled actuation of polyelectrolyte-doped gels that were submerged in an ionic solution. Application of an electrical potential ( $5 \text{ V cm}^{-1}$ ) between two graphite electrodes placed 6 cm apart created an asymmetrical redistribution of the mobile ions causing osmotic pressure differences inside the gel and therefore, asymmetric swelling inducing unidirectional movement of the hydrogel “walker” [38].

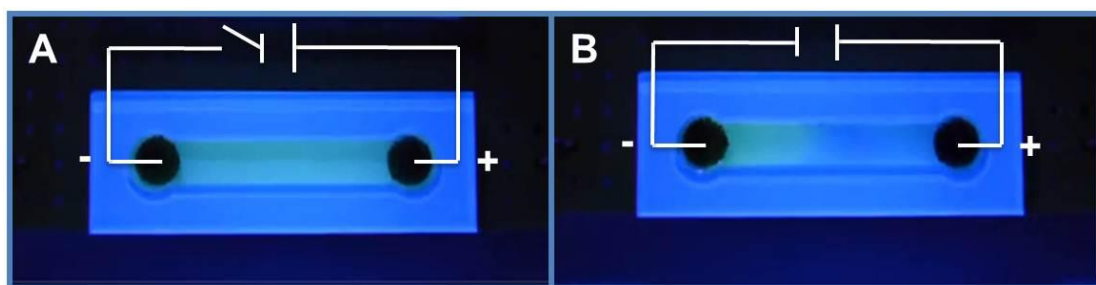


Figure 5.6 Snapshots showing the fluorescent gradient due to quenching of the lucigenin dye by  $\text{Cl}^-$  anions in the case when a solution of  $10^{-3} \text{ M NaCl}$  containing  $10^{-4} \text{ M lucigenin}$  was used. A) The fluorescence of the solution when no voltage is applied. B) The fluorescence of the solution when 9 V was applied for 30 minutes.

This visualisation study supports the contention that the movement of the droplets is due to asymmetrical release of  $[\text{P}_{6,6,6,14}]^+$  cationic surfactant, which is due to the presence of an electrochemically generated  $\text{Cl}^-$  gradient. Control studies were also performed in which a similar IL, trihexyl(tetradecyl)phosphonium dicyanamide ( $[\text{P}_{6,6,6,14}][\text{DCA}]$ ), was investigated under the same conditions as the  $[\text{P}_{6,6,6,14}][\text{Cl}]$  droplet. No significant movement of the  $[\text{P}_{6,6,6,14}][\text{DCA}]$  was observed as the  $\text{DCA}^-$  anion is much less soluble in the aqueous solution compared to the  $\text{Cl}^-$  anion [29], and release of the surfactant  $[\text{P}_{6,6,6,14}]^+$  from the droplet is correspondingly suppressed.

ILs have been shown to be excellent solvents [39,40] and are able to solubilise and therefore, transport many organic [41] and inorganic materials, and biomaterials such as enzymes, proteins, amino acids, peptides. This further broadens the potential for these

electrotactic droplets to perform advanced functions such as being used as micro-vessels for chemical reactions at pre-determined locations, dynamic sensing units, cargo carriers and possible drug-delivery systems. These properties make them better suited as micro-scale “vehicles” compared to conventional organic solvent droplets, which have a limited life-time due to evaporation. Traditional organic droplets also require further addition of surfactant to achieve movement, while the movement of the IL droplets is determined entirely by the inherent surfactant behaviour of the IL itself.

## 5.5 Conclusions

In conclusion, we have demonstrated that simple single component IL droplets can move spontaneously and be guided to multiple destinations within a fluidic chip in the presence of electrochemically generated  $\text{Cl}^-$  gradients. Electrotactic droplets allow for reversible movement and permit the user to change the course of the droplet by simply changing which electrodes are being addressed within the chip. Movement of electrotactic droplets require relatively simple means of achieving actuation *i.e* by simply inserting a small number of electrodes within a fluidic chip (2 – 4) and by applying relatively low voltages (5 – 9 V). Since there is already a large and ever growing library of ILs available, this opens up the possibility of creating electrotactic droplets with “designer” properties [29]. Some ILs offer attractive possibilities for electrochemical experiments, via extended electrochemical windows in aqueous media [30-33] and stability across a broad voltage range. Furthermore, numerous droplet functions can be realised based on IL abilities to carry a wide range of solutes (reaction precursors, drug components, *etc.*), including spatial and temporal control of reactions within fluidics systems by merging droplets at pre-determined locations or through triggered release of cargo at specific locations.

## 5.6 Acknowledgements

This work has been supported by Science Foundation Ireland under Insight initiative, grant SFI/12/RC/2289 and European Union Marie Curie People Programme Mask: PIRSES-GA-2010-269302, and the Australian Research Council Centre of Excellence

Scheme (Project Number CE 140100012). The authors also wish to acknowledge the Australian National Fabrication Facility (ANFF) for access to design and additive fabrication capabilities. The authors would like to acknowledge the helpful input from Prof. Robert Forster to the manuscript.

## 5.7 References

1. Goldstein, L.S.; Yang, Z. Microtubule-based transport systems in neurons: The roles of kinesins and dyneins. *Annu. Rev. Neurosci.* **2000**, *23*, 39-71.
2. Yoneyama, M.; Kikuchi, M.; Natsukawa, T.; Shinobu, N.; Imaizumi, T.; Miyagishi, M.; Taira, K.; Akira, S.; Fujita, T. The rna helicase rig-i has an essential function in double-stranded rna-induced innate antiviral responses. *Nat. Immunol.* **2004**, *5*, 730-737.
3. Van Haastert, P.J.; Devreotes, P.N. Chemotaxis: Signalling the way forward. *Nature reviews Molecular cell biology* **2004**, *5*, 626-634.
4. Larsen, C.G.; Anderson, A.O.; Appella, E.; Oppenheim, J.J.; Matsushima, K. The neutrophil-activating protein (nap-1) is also chemotactic for t lymphocytes. *Science* **1989**, *243*, 1464-1466.
5. Wu, J.Y.; Feng, L.; Park, H.-T.; Havlioglu, N.; Wen, L.; Tang, H.; Bacon, K.B.; Jiang, Z.-h.; Zhang, X.-c.; Rao, Y. The neuronal repellent slit inhibits leukocyte chemotaxis induced by chemotactic factors. *Nature* **2001**, *410*, 948-952.
6. Naccache, P.; Showell, H.; Becker, E.; Sha'afi, R. Transport of sodium, potassium, and calcium across rabbit polymorphonuclear leukocyte membranes. Effect of chemotactic factor. *The Journal of cell biology* **1977**, *73*, 428-444.
7. Funamoto, S.; Meili, R.; Lee, S.; Parry, L.; Firtel, R.A. Spatial and temporal regulation of 3-phosphoinositides by pi 3-kinase and pten mediates chemotaxis. *Cell* **2002**, *109*, 611-623.
8. Spehr, M.; Gisselmann, G.; Poplawski, A.; Riffell, J.A.; Wetzel, C.H.; Zimmer, R.K.; Hatt, H. Identification of a testicular odorant receptor mediating human sperm chemotaxis. *Science* **2003**, *299*, 2054-2058.
9. Zhao, M.; Song, B.; Pu, J.; Wada, T.; Reid, B.; Tai, G.; Wang, F.; Guo, A.; Walczysko, P.; Gu, Y. Electrical signals control wound healing through phosphatidylinositol-3-oh kinase- $\gamma$  and pten. *Nature* **2006**, *442*, 457-460.
10. Nuccitelli, R. A role for endogenous electric fields in wound healing. *Curr. Top. Dev. Biol.* **2003**, *58*, 1-26.
11. Lin, F.; Baldessari, F.; Gyenge, C.C.; Sato, T.; Chambers, R.D.; Santiago, J.G.; Butcher, E.C. Lymphocyte electrotaxis in vitro and in vivo. *The Journal of Immunology* **2008**, *181*, 2465-2471.
12. Ahirwar, D.K.; Nasser, M.W.; Jones, T.H.; Sequin, E.K.; West, J.D.; Henthorne, T.L.; Javor, J.; Kaushik, A.M.; Ganju, R.K.; Subramaniam, V.V. Non-contact method for directing electrotaxis. *Sci. Rep.* **2015**, *5*.
13. Jahanshahi, A.; Schönfeld, L.-M.; Lemmens, E.; Hendrix, S.; Temel, Y. In vitro and in vivo neuronal electrotaxis: A potential mechanism for restoration? *Mol. Neurobiol.* **2014**, *49*, 1005-1016.
14. Meng, X.; Arocena, M.; Penninger, J.; Gage, F.H.; Zhao, M.; Song, B. Pi3k mediated electrotaxis of embryonic and adult neural progenitor cells in the presence of growth factors. *Exp. Neurol.* **2011**, *227*, 210-217.

15. Chaudhury, M.K.; Whitesides, G.M. How to make water run uphill. *Science* **1992**, *256*, 1539-1541.
16. Smith, J.D.; Dhiman, R.; Anand, S.; Reza-Garduno, E.; Cohen, R.E.; McKinley, G.H.; Varanasi, K.K. Droplet mobility on lubricant-impregnated surfaces. *Soft Matter* **2013**, *9*, 1772-1780.
17. Gong, J.; Kim, C.-J.C. All-electronic droplet generation on-chip with real-time feedback control for ewod digital microfluidics. *Lab on a chip* **2008**, *8*, 898-906.
18. Pollack, M.G.; Fair, R.B.; Shenderov, A.D. Electrowetting-based actuation of liquid droplets for microfluidic applications. *Appl. Phys. Lett.* **2000**, *77*, 1725-1726.
19. Darhuber, A.A.; Valentino, J.P.; Troian, S.M.; Wagner, S. Thermocapillary actuation of droplets on chemically patterned surfaces by programmable microheater arrays. *Journal of Microelectromechanical Systems* **2003**, *12*, 873-879.
20. Lombardi, D.; Dittrich, P.S. Droplet microfluidics with magnetic beads: A new tool to investigate drug-protein interactions. *Anal. Bioanal. Chem.* **2011**, *399*, 347-352.
21. Chiou, P.-Y.; Chang, Z.; Wu, M.C. Droplet manipulation with light on optoelectrowetting device. *Microelectromechanical Systems, Journal of* **2008**, *17*, 133-138.
22. Wixforth, A.; Strobl, C.; Gauer, C.; Toegl, A.; Scriba, J.; v Guttenberg, Z. Acoustic manipulation of small droplets. *Anal. Bioanal. Chem.* **2004**, *379*, 982-991.
23. Lagzi, I.; Soh, S.; Wesson, P.; Browne, K.; Grzybowski, B. Maze solving by chemotactic droplets. *J. Am. Chem. Soc.* **2010**, *132*, 1198-1199.
24. Velarde, M.G. Drops, liquid layers and the marangoni effect. *Phil. Trans. R. Soc. A* **1998**, 829-842.
25. Florea, L.; Wagner, K.; Wagner, P.; Wallace, G.G.; Benito - Lopez, F.; Officer, D.L.; Diamond, D. Photo - chemopropulsion - light - stimulated movement of microdroplets. *Adv. Mater.* **2014**, *26*, 7339-7345.
26. Diguët, A.; Guillermic, R.-M.; Magome, N.; Saint-Jalmes, A.; Chen, Y.; Yoshikawa, K.; Baigl, D. Photomanipulation of a droplet by the chromocapillary effect. *Angewandte Chemie (International ed. in English)* **2009**, *48*, 9281-9284.
27. Khan, M.R.; Eaker, C.B.; Bowden, E.F.; Dickey, M.D. Giant and switchable surface activity of liquid metal via surface oxidation. *Proceedings of the National Academy of Sciences* **2014**, *111*, 14047-14051.
28. Francis, W.; Fay, C.; Florea, L.; Diamond, D. Self-propelled chemotactic ionic liquid droplets. *Chem. Commun.* **2015**, *51*, 2342 - 2344.
29. Fraser, K.J.; MacFarlane, D.R. Phosphonium-based ionic liquids: An overview. *Aust. J. Chem.* **2009**, *62*, 309-321.
30. Ong, S.P.; Andreussi, O.; Wu, Y.; Marzari, N.; Ceder, G. Electrochemical windows of room-temperature ionic liquids from molecular dynamics and density functional theory calculations. *Chem. Mater.* **2011**, *23*, 2979-2986.
31. Vaughan, J.; Dreisinger, D. Electrodeposition of aluminum from aluminum chloride-trihexyl (tetradecyl) phosphonium chloride. *J. Electrochem. Soc.* **2008**, *155*, D68-D72.
32. Zhang, S.; Sun, N.; He, X.; Lu, X.; Zhang, X. Physical properties of ionic liquids: Database and evaluation. *J. Phys. Chem. Ref. Data* **2006**, *35*, 1475-1517.

33. Buzzeo, M.C.; Hardacre, C.; Compton, R.G. Extended electrochemical windows made accessible by room temperature ionic liquid/organic solvent electrolyte systems. *Chemphyschem* **2006**, *7*, 176-180.
34. Thompson, D.; Coleman, S.; Diamond, D.; Byrne, R. Electronic structure calculations and physicochemical experiments quantify the competitive liquid ion association and probe stabilisation effects for nitrobenzospiropyran in phosphonium-based ionic liquids. *PCCP* **2011**, *13*, 6156-6168.
35. Mavré, F.o.; Anand, R.K.; Laws, D.R.; Chow, K.-F.; Chang, B.-Y.; Crooks, J.A.; Crooks, R.M. Bipolar electrodes: A useful tool for concentration, separation, and detection of analytes in microelectrochemical systems. *Anal. Chem.* **2010**, *82*, 8766-8774.
36. Mavré, F.o.; Anand, R.K.; Laws, D.R.; Chow, K.-F.; Chang, B.-Y.; Crooks, J.A.; Crooks, R.M. Bipolar electrodes: A useful tool for concentration, separation, and detection of analytes in microelectrochemical systems. ACS Publications: 2010.
37. Du, J.; Chen, Z.; Chen, C.; Meyer, T.J. A half-reaction alternative to water oxidation: Chloride oxidation to chlorine catalyzed by silver ion. *J. Am. Chem. Soc.* **2015**, *137*, 3193-3196.
38. Morales, D.; Palleau, E.; Dickey, M.D.; Velev, O.D. Electro-actuated hydrogel walkers with dual responsive legs. *Soft Matter* **2014**, *10*, 1337-1348.
39. Welton, T. Room-temperature ionic liquids. Solvents for synthesis and catalysis. *Chem. Rev.* **1999**, *99*, 2071-2084.
40. Itoh, T.; Kude, K.; Hayase, S.; Kawatsura, M. Design of ionic liquids as a medium for the grignard reaction. *Tetrahedron Lett.* **2007**, *48*, 7774-7777.
41. Gallagher, S.; Kavanagh, A.; Florea, L.; MacFarlane, D.R.; Fraser, K.J.; Diamond, D. Temperature and pH triggered release characteristics of water/fluorescein from 1-ethyl-3-methylimidazolium ethylsulfate based ionogels. *Chem. Commun.* **2013**, *49*, 4613-4615.

## **Chapter 6:**

### **Multi-Functional Chemotactic Droplets**

#### **6.1 Abstract**

#### **6.2 Introduction**

#### **6.3 Experimental**

##### **6.3.1 Materials**

##### **6.3.2 Actuation through Localised Changes in Wettability**

###### 6.3.2.1 Micro-Channel Fabrication

###### 6.3.2.2 Absorbance Measurements

###### 6.3.2.3 Experimental Setups

#### **6.4 Results and Discussion**

##### **6.4.1 Droplet Movement**

##### **6.4.2 Signal and Seeker Droplets**

##### **6.4.3 Droplets Making Decisions**

##### **6.4.5 Sensing and Reporting**

##### **6.4.5 Detection and Repair of Damage**

#### **6.5 Conclusions**

#### **6.6 Acknowledgments**

#### **6.7 References**

## Chapter 6

---

### Multi-Functional Chemotactic Droplets

---

## 6.1 Abstract

Herein, we have developed signalling and seeking IL droplets, which chemotactically find each other in open fluidic networks by harnessing the chemical potential of their constituents and their environment. Each entity within the complex system is in direct control of its autonomous motion, predefined by the chemistry of the IL components. For example, the signal droplet, which is stationary, creates a chemical gradient inside the fluidic channel through release of the IL surfactant. In response to this signal, the seeker droplet is enabled to chemotactically find the signaller droplet and merge with it, in a manner similar to the triggered cell migration seen in chemokine proteins. Additionally, we present chemotactic IL droplets which interact intimately with their fluidic system, offering the ability to make decisions, perform chemical reactions, carry out dynamic sensing-reporting and implement damage detection-repair. Such self-directed, multi-purpose movement of micro “vehicles” offers many intriguing opportunities in the microfluidics field. This could potentially stimulate novel research in open droplet microfluidic devices, where the driving force for movement is dictated by the chemistry of the fluidic system itself, rather than through external control by the user. The realization of multifunctional biomimetic fluidic systems with advanced functionality, such as detection and repair of damage, self-management and healing could affect areas far beyond the frontiers of this research field.

## 6.2 Introduction

The development of protocells has been of great interest to both material scientists, who endeavour to realise synthetic analogues with biomimetic functions, and life scientists, who wish to understand evolution from the primordial soup of the primitive oceans of Earth [1,2]. Life itself somehow emerged from organic clutter, through the compartmentalisation of biomolecules and DNA polymers, into self-organised membrane-bound cells. These cells evolved over the millennia to become the basis for life as we know it today. Although infinitely more complex, living cells are thought to evolve from droplets of chemicals, which have been proposed as feasible models for protocells [2]. It has been theorised that droplets could have served to encapsulate certain functional molecules into lipid bound vesicles which could elongate and divide under specific conditions to create

primitive models of self-replication [2]. The desire to synthetically imitate the movement exhibited by living organisms has been treated with a similar intrigue. Movement of cells in response to a change in environment is known as taxis, wherein responding to chemical changes is known as chemotaxis. Usually chemotaxis is followed by a biological action or response; the release of signalling proteins (known as Chemokines) for example, from infected or damaged cells, act as a chemoattractant to trigger immune responses [3]. A family of cytotoxic T cells, known as killer T cells, can respond to these immune triggers to track, attack and neutralise cancer cells, infected or damaged cells [4]. Neutrophils, a type of white blood cells with chemotactic capabilities, are also attracted by cytokines (another family of signalling proteins) following a trauma [5]. Once recruited to the source of injury they induce acute inflammation and further signal other white blood cells to the site. Scientists have attempted to develop synthetic models, which can mimic either the movement or functionality of these biological organisms. In this context, droplets offer a promising route for the evolution of protocellular design, owed to the two distinctive regions, at the core and interface, which can be highly customized to offer the possibility for individual functions. The interfacial region, for example, could provide locomotion (via interfacial interactions) while the inner region can release molecular cargo to perform pre-programmed functions under specific conditions. Several droplet systems equipped with biomimetic functionalities have been developed in recent years including primitive locomotion[6,7], primitive metabolism[8], translation/transcription processes[9] and self-replication[10,11], among others[12-17]. Although these examples show exciting biomimetic capabilities, they are all highly specialized systems with limited functionality.

Previously, we reported self-propelled chemotactic ionic liquid droplets[18] composed solely of the IL trihexyl(tetradecyl)phosphonium chloride ( $[P_{6,6,6,14}][Cl]$ ) that moved spontaneously along an ionic concentration gradient (e.g.  $Cl^-$ ) on a liquid-air interface to a pre-determined destination. In this paper, we demonstrate the versatile functionality of these IL droplets. Not only do they exhibit biomimetic locomotion, but through the inclusion of functional molecules, they can also be used to perform a variety of tasks, including reversible movement, signalling and seeking behaviour, molecular cargo transport, decision making, sensing and reporting, elongation and division, and system damage detection and repair (Figure

6.1). These functions are inherent to the development of self-propelled multi-functional droplet-type protocell models, and will contribute to the emergence of a new sub-field in droplet-based microfluidics, in which autonomous functional behaviour arises spontaneously from the chemistry of the fluidic system itself, rather than through external control.

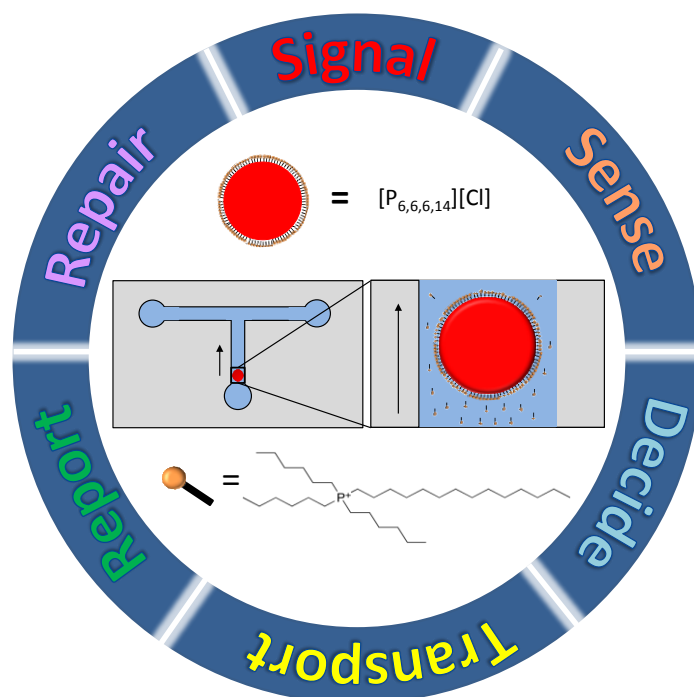


Figure 6.1 Diagram showing the different functionalities of the IL droplets demonstrated in this study. Inset depicts the movement of the  $[P6,6,6,14][Cl]$  IL droplet due to the asymmetric release of  $[P6,6,6,14]^+$  from the droplet in the aqueous solution.

## 6.3 Experimental

### 6.3.1 Materials

Hydrochloric acid (HCl), Sodium hydroxide (NaOH), Sodium chloride (NaCl), Potassium fluoride (KF), Potassium chloride (KCl), Potassium bromide (KBr), Cobalt (II) nitrate hexahydrate ( $Co(NO_3)_2 \cdot 6H_2O$ ), Copper (II) Nitrate tetrahydrate ( $Cu(NO_3)_2 \cdot 4H_2O$ ), Phenol red sodium salt, Bromothymol Blue, Bromocresol Purple, Sodium alginate, 2-(5-Bromo-2-pyridylazo)-5-(diethylamino)phenol

(PADAP), trihexyl(tetradecyl) phosphonium chloride ( $[P_{6,6,6,14}][Cl]$ ) and trihexyl(tetradecyl)phosphonium dicyanamide ( $[P_{6,6,6,14}][DCA]$ ) were purchased from Sigma-Aldrich® Ireland Ltd. Potassium iodide (KI) and Calcium Chloride Dihydrate ( $CaCl_2 \cdot 2H_2O$ ) were purchased from Honeywell Riedel-de-Haën™ and AnalaR NORMAPUR®, respectively. All chemicals were used as received.

### 6.3.2 Methods

#### 6.3.2.1 Micro-Channel Fabrication

The fluidic channels were designed using AutoCAD 2016. A CO<sub>2</sub> laser ablation system (Epilog Zing Laser Series) was used to cut the design into 2 mm thick PMMA sheets (which had a 50 μm double-sided pressure-sensitive adhesive (PSA) layer pre-attached). After cutting, the PSA protective layer was removed and the PMMA/PSA was attached to a PMMA backing. The channel used for *signalling and seeking* functionality had a T shape, with each arm having a length of 19 mm and a width of 3 mm (See Figure C.1). The channels used for *decision making* and *sensing* functionalities were designed in a T shape (See Video 6.2), where each arm had a length of 21.5 mm, a width of 4 mm and a depth of 2.1 mm. For *detection and repair of damage* the channels were also designed in a T shape with each arm having a length of 21.5 mm, a width of 2.5 mm and a depth of 2.1 mm. Narrow channels were also placed into the sidewalls of each arm to simulate damage to the channel. These narrow channels had a width of 0.25 mm and a thickness of 0.5 mm (Figure C.9).

#### 6.3.2.2 Absorbance Measurements

UV-Vis Spectroscopy was used to measure the absorbance/transmittance of the IL droplets containing various components ( $Cu(NO_3)_2$ ,  $Co(NO_3)_2$ ,  $Cu^{2+}$ -PADAP complex,  $Co^{2+}$ -PADAP complex, Bromothymol Blue, Bromocresol Purple,  $CaCl_2$  and Ca-alginate polymer, respectively). The absorbance spectra were recorded in reflectance mode using 2 fiber-optic light guides connected to a Miniature Fiber Optic Spectrometer (USB4000 - Ocean Optics). The light source used was a DH 2000 FHS Deuterium – Halogen light source (Top Sensor Systems). For out of channel measurements the droplet was placed into a custom

fabricated holder, which also contained a slot for the optical fiber (Figure S2). The in-house-designed holder was fabricated using a 3D printer (Dimension SST 768) in black acrylonitrile butadiene styrene co-polymer (ABS) plastic in order to minimise interference from ambient light. For in-channel measurements, the optical fiber was held 5 mm above the channel using a clamp. Crosslinking of alginate polymers in the presence of  $\text{Ca}^{2+}$  was tracked using time-dependent transmittance by measuring the absorbance increase at 700 nm for 20 min. At this wavelength there is no interference from any other absorbance bands meaning that the increase in absorbance is solely caused by crosslinking of the alginate polymer due to the presence of  $\text{Ca}^{2+}$  ions. Data from the spectrometer was processed using Spectrasuite software provided by Ocean Optics Inc.

### **6.3.2.3 Experimental setups**

The experimental designs used for the demonstration of different functionalities of the chemotactic droplets are detailed in the Appendix C (C.1-C.4).

## **6.4 Results and Discussion**

### **6.4.1 Droplet Movement**

Droplet movement at the aqueous solution/air interface was generated by simply placing the droplet in an ionic strength gradient. We previously showed that for ionic liquid droplets composed of  $[\text{P}_{6,6,6,14}][\text{Cl}]$  this behaviour arises from the asymmetric release of the  $[\text{P}_{6,6,6,14}]^+$  anion from the droplet into the aqueous phase.  $[\text{P}_{6,6,6,14}]^+$  is a very effective anionic surfactant and once introduced into the solution it generates Marangoni like flows [18]. The rate of release of the surfactant is controlled by the solubility of counter ion; in this case  $\text{Cl}^-$ . Therefore, in the presence of an ionic strength gradient in the aqueous phase, an asymmetrical surface tension gradient is generated, leading to Marangoni like flows, which drive the droplet from areas of low surface tension towards areas of high surface tension. The droplet will continue to move once the gradient is maintained.

### **6.4.2 Signalling and Seeking Chemotactic Droplets**

Signaller and seeker [droplets containing  $P_{6,6,6,14}^+$ ] were developed to chemotactically find each other in open fluidic networks. A signaller droplet ( $10^{-2}$  M  $Cu(NO_3)_2$  or  $10^{-2}$  M  $Co(NO_3)_2$  in  $[P_{6,6,6,14}][DCA]$ ) releases an ionic chemoattractant ( $Cu(NO_3)_2$  or  $Co(NO_3)_2$ ) and due to the low solubility of the DCA anion, it remains stationary [19]. Release of the chemoattractant enables the seeker droplet ( $10^{-2}$  M PADAP in  $[P_{6,6,6,14}][Cl]$ ) to chemotactically find the signalling droplet and merge with it at its stationary location. This system is somewhat reminiscent of neutrophil cells that have the capability to chemotactically seek out and merge with invading pathogens inside the body. This pre-programmed locomotion can also be coupled with a number of different functionalities. For example if appropriate precursors are added to both droplets, a reaction can take place upon merging. This allows spatial-temporal control of chemical reactions in fluidic networks in the absence of any external stimulation. To demonstrate this effect, PADAP was added to the seeker droplet. PADAP has a high affinity for a variety of heavy metal ions, including  $Co^{2+}$  and  $Cu^{2+}$ , with whom it forms a complex with the metal-ion at  $pH > 8$ . PADAP has previously been shown to be a good spectrophotometric reagent for use in sensors for optical detection of heavy metal ions [20,21]. In order to test if the seeker and signaller droplets could be used for metal ion sensing,  $10^{-2}$  M  $Cu(NO_3)_2$  or  $Co(NO_3)_2$  was added to the  $[P_{6,6,6,14}][DCA]$  signaller droplet, and  $10^{-2}$  M PADAP added to the  $[P_{6,6,6,14}][Cl]$  seeker droplet. Following this, the channels were filled with a solution of  $10^{-2}$  M NaOH and the signaller droplet was placed at the desired destination. After 10 – 30s the seeker droplet containing the PADAP was introduced to the channel. The seeker droplet then migrated towards the signaller (See Figure 6.2, Figure C.1 and Video 6.1). Once at the destination, the droplets merged and their contents mixed and reacted to form the metal ion-PADAP complex. The absorbance spectra of the droplets were recorded before and after merging. The  $[P_{6,6,6,14}][DCA]$  signalling droplet which contained the  $Cu^{2+}$  salt ( $10^{-2}M$ ) had a yellow colour with an absorbance peak centred at  $\sim 425$  nm (Figure 6.3 A). The  $[P_{6,6,6,14}][DCA]$  signalling droplet which contained  $Co^{2+}$  salt ( $10^{-2}M$ ) had a blue colour with an absorbance peak centred at 620 nm (Figure 6.3 B). The PADAP containing droplet had an orange colour with an absorbance peak centred at  $\sim 520$  nm which corresponds to the 3-bromopyridinium ion and a shoulder peak at 580 nm which could be due to

the presence of a tautomeric imine [22] (Figure 6.3 A and B). The absorbance of each of the IL droplets was measured and recorded in reflectance mode using two fiber-optic light guides which were connected to a miniature fiber optic spectrometer (USB4000- Ocean Optics) and aligned using a custom fabricated holder (Figure C.2). After merging of the signalling and seeking droplet, the colour of the droplet slowly began to change due to complexation of the metal ions. In the case of the  $\text{Cu}^{2+}$  ion the binding ratio is 1:1 and results in a square planar or tetrahedral complex, forming a purple colour with an absorbance centred at  $\lambda_{\text{max}} \sim 550$  [23].  $\text{Co}^{2+}$  forms a 1:2 ratio complex ( $\text{Co}^{2+} : 5\text{-Br-PADAP}$ ) resulting in an octahedral complex, with an absorption also centred at  $\lambda_{\text{max}} \sim 550$  (Figure 6.3) [22].

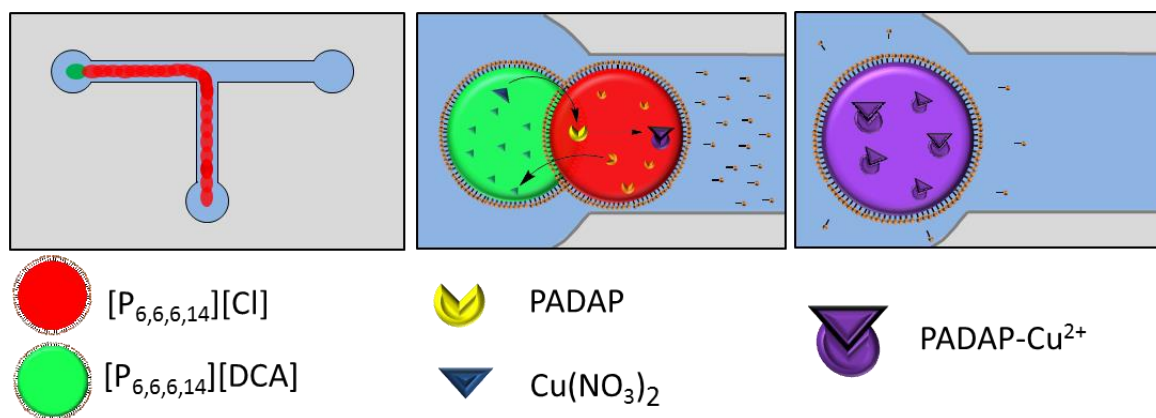


Figure 6.2 Diagram showing the movement behaviour of the signaller ( $10^{-2}\text{M Cu}(\text{NO}_3)_2$  or  $10^{-2}\text{M Co}(\text{NO}_3)_2$  in  $[\text{P}_{6,6,6,14}][\text{DCA}]$ ) and seeker ( $10^{-2}\text{M PADAP}$  in  $[\text{P}_{6,6,6,14}][\text{Cl}]$ ) droplets. Once the signaller (green) droplet was placed,  $\text{Cu}(\text{NO}_3)_2$  or  $\text{Co}(\text{NO}_3)_2$  diffused from the droplet into the aqueous phase, generating an ionic strength gradient. This gradient enabled the seeker droplet (red) to chemotactically find and merge with the signaller droplet.

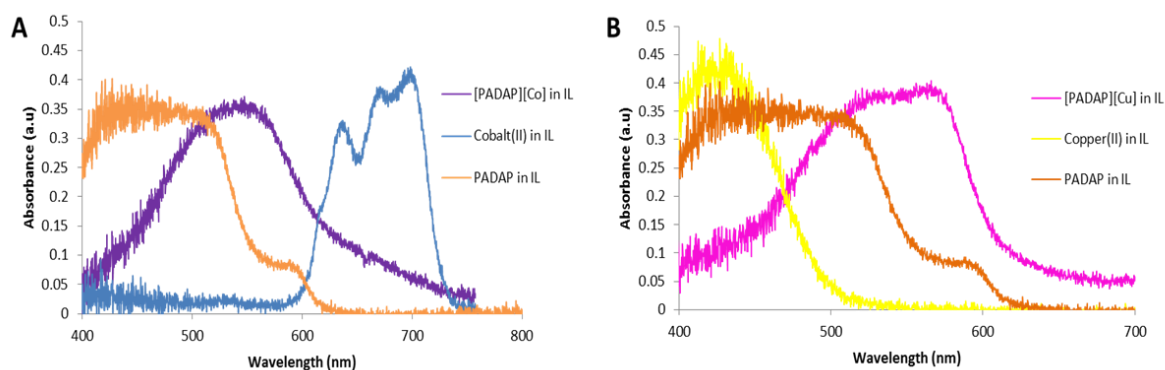


Figure 6.3 A) Absorbance spectra of three IL droplets ( $[PADAP][Co]$  in IL, PADAP in  $[P_{6,6,6,14}][Cl]$  and  $Co^{2+}$  in  $[P_{6,6,6,14}][DCA]$ ) showing  $Co^{2+}$  detection; B) Absorbance spectra of three IL droplets ( $[PADAP][Cu]$  in IL, PADAP in  $[P_{6,6,6,14}][Cl]$  and  $Cu^{2+}$  in  $[P_{6,6,6,14}][DCA]$ ) showing  $Cu^{2+}$  detection.

### 6.4.3 Droplets Making Decisions

To demonstrate decision making, a droplet of  $[P_{6,6,6,14}][Cl]$  (and a small amount of 1-(methylamino)anthraquinone red dye for visualisation) was simultaneously subjected to two different gradients. In the first instance, a T-shaped channel was used and a different concentration of the same chemoattractant (HCl) was added simultaneously into the opposite arms of the T-junction (Figure C.3, Table C.1). For a detailed explanation of the experimental arrangement, see Appendix C section C.2. As expected, in every case the droplet always moved towards the stronger gradient and found the chemoattractant source of highest concentration. As mentioned before, the rate of release is controlled by the solubility of the  $Cl^-$  ion. Therefore, more  $Cl^-$  and associated  $[P_{6,6,6,14}]^+$  surfactant will be released from the side of the droplet exposed to lower concentration of chemoattractant (e.g.  $Cl^-$ ) in the external solution and the droplet will spontaneously move towards the site of highest aqueous  $Cl^-$  concentration. Following this, the chemotactic droplets were investigated for their capability to choose between different halides as chemoattractants. As before, a T-shaped channel was used and equal concentrations of different halide salts (e.g. KF, KCl, KBr and KI) were introduced simultaneously in the opposite arms of the T-junction (Table 6.1). A detailed explanation of the experimental procedure is outlined in Appendix C, section C.2.

In every case, the droplets migrated preferentially to the source of the larger halide ion (Table 6.1, Video 6.3). This selectivity can again be explained by the relative solubility of the  $\text{Cl}^-$  counterion in halide salt solutions. The solubility of  $\text{Cl}^-$  counterions from the IL increases in solutions of potassium halide salts in the following order:  $\text{I}^- > \text{Br}^- > \text{Cl}^- > \text{F}^-$ . We have previously demonstrated that this increased anion solubility causes enhanced  $[\text{P}_{6,6,6,14}]^+$  surfactant release in  $\text{Br}^-$  solutions vs  $\text{Cl}^-$ , or  $\text{I}^-$  solutions vs.  $\text{Br}^-$  and  $\text{Cl}^-$  solutions of the same concentration (Table 4.1, Francis et al.[18]). This results in a greater asymmetric release of  $[\text{P}_{6,6,6,14}]^+$  from the droplet in the order of  $\text{I}^- > \text{Br}^- > \text{Cl}^- > \text{F}^-$  gradients, and therefore, the droplet will always follow the trajectory where the surface tension difference between the back and the front of the droplet is the greatest. This means the  $[\text{P}_{6,6,6,14}][\text{Cl}]$  droplet will choose the chemoattractant as predicted by the Hofmeister series ( $\text{SO}_4^{2-} < \text{HPO}_4^{2-} < \text{OH}^- < \text{F}^- < \text{CH}_3\text{COO}^- < \text{Cl}^- < \text{Br}^- < \text{NO}_3^- < \text{I}^- < \text{ClO}_4^- < \text{SCN}^-$ ). [24,25]. This droplet movement mimics the ability of single celled organisms to respond to varying signals found in their environment. They can seek the greatest concentration of food source or flee from toxins by choosing between chemical gradients within their locality

Table 6.1 Halide pairs included in each test and the destination the droplet chose in each case.

| Conc (mol L <sup>-1</sup> ) | KF | KCl | KBr | KI |
|-----------------------------|----|-----|-----|----|
| 0.1                         |    | X   |     |    |
| 0.01                        |    |     | X   |    |
| 0.01                        |    |     | X   |    |
| 0.05                        |    |     | X   |    |
| 0.1                         |    |     | X   |    |
| 0.001                       |    |     |     | X  |
| 0.01                        |    |     |     | X  |
| 0.001                       |    |     |     | X  |
| 0.01                        |    |     |     | X  |
| 0.1                         |    |     |     | X  |
| 0.001                       |    |     |     | X  |
| 0.01                        |    |     |     | X  |

\*Coloured cells indicate the chemoattractant pair used; X indicates the final destination of the droplet. For example (row 1) when 0.1M KF and KCl solutions were used as chemoattractants, the droplet's destination was the source of KCl (marked with X).

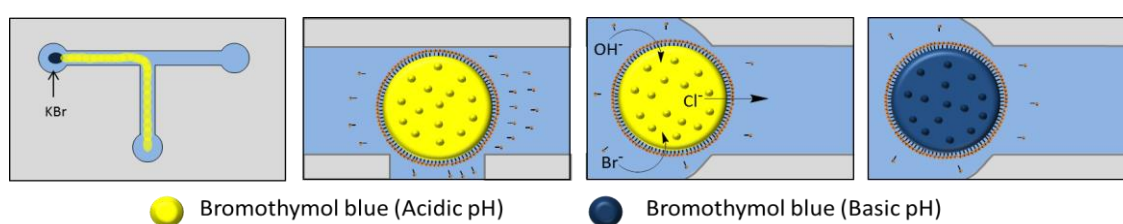
#### 6.4.4 Sensing and Reporting

It was observed that when the [P<sub>6,6,6,14</sub>][Cl] chemotactic droplets were subjected to Br<sup>-</sup> or I<sup>-</sup> chemical gradients, the droplets often dispersed into smaller ‘daughter’ droplets as they got closer to the plume source, possibly due to enhanced uptake of the external aqueous solution. In order to investigate this behavior, pH indicator dyes (Phenol red or Bromothymol blue) were added to the droplet (4% w/v) and the chemical gradients were created as before (Figure 6.4), using 0.001M, 0.01M or 0.1M KBr or KI solutions (Appendix C, C.3). It was observed that as the IL droplet moved spontaneously towards the KBr (or KI) source, it could sense and report the pH of the solution through which it was traversing (Video 6.4-6.6). In order to investigate this colour change, a miniature spectrometer (USB4000 - Ocean Optics) and fiber optic probe with a custom fabricated holder was used to measure the absorbance of droplet before and after its introduction to the system (Figure 6.4). The bromothymol blue droplet was initially a yellow colour indicating the presence of the dye in its protonated form, with an absorbance  $\lambda_{\text{max}} \sim 450$  nm. Upon nearing or reaching the destination the droplet changed to a blue colour with a characteristic absorbance at  $\lambda_{\text{max}} \sim 650$  nm (deprotonated dye). Similar behaviour was observed in the case of phenol red, which changed from an orange colour ( $\lambda_{\text{max}} = 525$  nm, protonated form) to a purple colour ( $\lambda_{\text{max}} = 575$  nm, deprotonated form) in the proximity of the chemoattractant source. This sensing and reporting of the aqueous solution pH is due to ion exchange between the Cl<sup>-</sup> of the [P<sub>6,6,6,14</sub>][Cl] IL and the Br<sup>-</sup> (or I<sup>-</sup>) present in the aqueous solution. This ion exchange between the anions of the IL and the anions present in the aqueous solution is dependent on the affinity of the anion for the aqueous phase compared to the IL. It has been previously demonstrated that anion exchange in Phosphonium-based ILs increases in the order SO<sub>4</sub><sup>2-</sup> < F<sup>-</sup> < Cl<sup>-</sup> < Br<sup>-</sup> < NO<sub>3</sub><sup>-</sup> < I<sup>-</sup> < ClO<sub>4</sub><sup>-</sup> < SCN<sup>-</sup> < Tf<sub>2</sub>N<sup>-</sup>, as again predicted by the Hofmeister series [26]. This occurs as hydrophobic anions (with low charge density) such as Tf<sub>2</sub>N<sup>-</sup>, SCN<sup>-</sup>, ClO<sub>4</sub><sup>-</sup> and I<sup>-</sup> are preferentially dissolved in the IL phase, while more hydrophilic anions such as Cl<sup>-</sup>, F<sup>-</sup> and SO<sub>4</sub><sup>2-</sup> are preferentially dissolved in aqueous phase. As the charge density decreases from (SO<sub>4</sub><sup>2-</sup> to Tf<sub>2</sub>N<sup>-</sup>), anions with a lower charge density are less hydrated and have a higher affinity for the IL phase [26]. This ion exchange within the IL droplet resulted in a more permeable droplet/water interface. As the Br<sup>-</sup> ions entered the droplet, it is likely that OH<sup>-</sup> ions were also

taken up, resulting in the colour change of the droplet. As expected, both of the colour changes indicate sensing of a solution with a pH above the  $pK_a$  of the respective dyes ( $\sim 7.0$  for Bromothymol blue and  $\sim 8.0$  for Phenol red). This is in agreement with the experimental conditions, where the measured pH of the aqueous solution ( $10^{-2}M$  NaOH) was 12.

*Figure 6.4 Diagram showing the sensing ability of the IL droplets. The sensing droplets were composed of bromothymol blue (4% w/v) in  $[P_{6,6,6,14}][Cl]$ . The channels were filled with a solution of  $10^{-2} M$  NaOH and a solution of  $0.001M$  KBr was used as a chemoattractant. It was observed that as the IL droplet moved spontaneously towards the KBr source, it could sense and report the pH of the solution through which it was traversing (Video 6.4-6.6). As the droplet neared the chemoattractant source an ion exchange within the IL droplet resulted in a more permeable droplet/water interface. As the  $Br^-$  ions entered the droplet, it is likely that  $OH^-$  ions were also taken up, resulting in the colour change of the droplet containing Bromothymol blue from yellow ( $pH < 7$ ) to blue ( $pH > 7$ ).*

To better visualise the flux within the droplet during the ion exchange, an aigoDigital Microscope-GE5 with a detachable objective (lens of X60) was used to record the droplet as it travel towards the destination changing colour (Figure 6.5, Figure C.5 and Video 6.7). An identical experiment was also run which measured the spectra of the droplet every minute for 6 minutes (Figure 6.5). The results



clearly show convective, Marangoni-type flows generated within the droplet as ion exchange occurs. Such Marangoni flows are not observable in the absence of the ion exchange process (Figure C.6-C.7). These droplets are capable of mimicking the ability of living cells to sense and exchange cargo with their external environment. Moreover, as ion exchange is governed by the composition of the ionic liquid with respect to the chemoattractant, it can therefore, be accurately predicted and controlled. The endless permutations of IL and chemoattractant means that these IL droplets can not only choose between a multitude of chemical

gradients but are also capable of sustaining and sensing selective ion transfer across the droplet/aqueous interface.

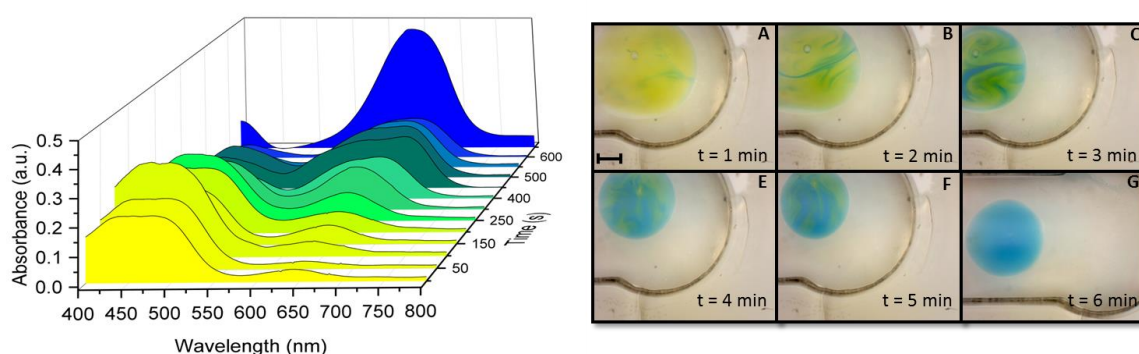


*Figure 6.5 Absorbance spectra of the  $[P_{6,6,6,14}][Cl]$  droplet containing bromothymol blue vs. time, reflecting the change in maximum absorbance as the droplet migrated across the NaOH solution ( $10^{-2}$  M) when  $70\mu\text{l}$  of  $0.005\text{M}$  KBr solution was used as chemoattractant (left). Microscope images showing the Marangoni-like flows and the influx of  $\text{OH}^-$  ions into the droplet upon reaching the destination. Scale bar represents 1 mm (right).*

### 6.3.5 Detection and Repair of Damage

In this section we demonstrate that  $[P_{6,6,6,14}][Cl]$  IL droplets containing 4% w/v  $\text{CaCl}_2$  which were able to chemotactically find and seal a leak in a fluidic system. For a detailed description of the experimental conditions, see Appendix C, C.4. The chemoattractant used in this study was a  $60\mu\text{l}$  aliquot composed of 1:1 (V:V)  $10^{-2}$  M HCl:  $0.05\text{M}$  KBr solution containing 0.5% w/v sodium alginate. Upon arriving to the destination by following the KBr gradient, the ion exchange between the  $\text{Cl}^-$  of the IL and the  $\text{Br}^-$  from the aqueous solution, resulted in the uptake of alginate chains into the droplet. Within the droplet, the  $\text{Ca}^+$  ions act as an ionic crosslinker for the alginate chains resulting in the generation of a crosslinked hydrogel [27] which seals the damage (Figure 6, Figure C.9-C.10, Video 6.8). In order to track this gelation, the absorbance of the droplet was recorded at 700 nm over 20 minutes (Figure C.11) using a miniature fiber optic spectrometer (USB4000 - Ocean Optics). The graph clearly shows an exponential growth, indicating that the alginate polymers that were taken up by the droplet, from the aqueous phase, have been completely crosslinked and the droplet has solidified. These droplets could constitute a primitive model for platelets, which are found in

mammalian blood. When a mammal receives a wound severe enough to break the skin, platelets aggregate together at the wound to seal it and stop the bleeding [28].

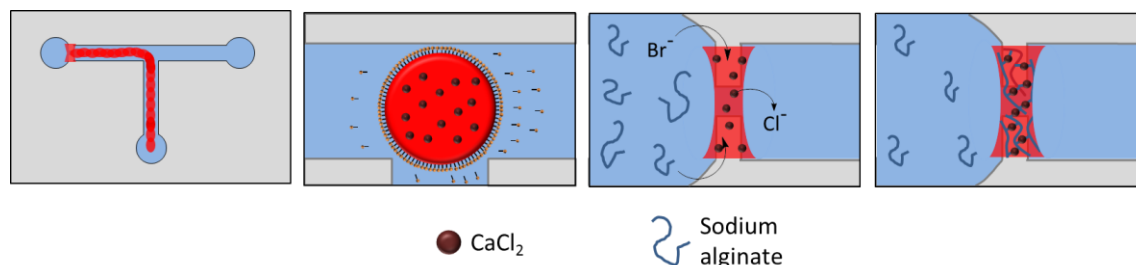


*Figure 6.6 Diagram showing the  $\text{CaCl}_2$  containing droplet migrating across the liquid/air interface of a solution of  $10^{-2}$  M NaOH towards the source of “damage”, upon the addition of the chemoattractant solution (60  $\mu\text{l}$  aliquot composed of 1:1 (V:V)  $10^{-2}$  M HCl: 0.05M KBr solution containing 0.5% w/v sodium alginate). Upon reaching the damage area, the repair functionality starts by creating a crosslinked gel composed of calcium alginate, that seals the damage.*

## 6.5 Conclusion

In conclusion, we have developed multi-functional IL droplets which are capable of cargo transport, seeking and signalling, decision making, detection and repair of damage. We have further developed our understanding of the mechanisms of unidirectional motion in such systems and presented the utility of performing a broad range of practical tasks in the absence of further external stimuli. The examples shown in this study represent only a fraction of the potentially broad scope of these droplets. As the droplets are composed of ILs, which have negligible vapour pressure, low combustibility and high thermal stability, they are aligned perfectly for use as micro-scale vehicles. Additionally, because the ‘fuel’ is a component of the IL itself, the further addition of functional components appears not to inhibit movement. The large library of ILs available, allows for countless combinations of gradients and fine tuning of the anion-cation pairing. This paves the way for the creation of more complex droplet systems whose movement, selectivity and chemical reactivity can be controlled by 1) their innate constituents, 2) the nature of the fluid they traverse, 3) the chemistry of the other droplets they encounter and 4) their intimate response to external substrates. The potential of combinatorial movement and reactivity, with additional dimensionality achieved through liquid and surface contributions, may now offer a field of untapped possibility.

## 6.6 Acknowledgements

This project has been funded by Science Foundation Ireland under the Insight initiative, grant SFI/12/RC/2289. CD and DD also acknowledge the European Union's Seventh Framework Programme for research and technological development, through the NAPES project grant agreement no. 604241.

## 6.7 References

1. Golestanian, R. Origin of life: Division for multiplication. *Nature Physics* **2016**.
2. Zwicker, D.; Seyboldt, R.; Weber, C.A.; Hyman, A.A.; Jülicher, F. Growth and division of active droplets provides a model for protocells. *Nature Physics* **2016**.
3. Baggiolini, M. Chemokines and leukocyte traffic. *Nature* **1998**, *392*, 565.
4. Matsuda, J.L.; Naidenko, O.V.; Gapin, L.; Nakayama, T.; Taniguchi, M.; Wang, C.-R.; Koezuka, Y.; Kronenberg, M. Tracking the response of natural killer t cells to a glycolipid antigen using cd1d tetramers. *J. Exp. Med.* **2000**, *192*, 741-754.
5. Baggiolini, M.; Walz, A.; Kunkel, S. Neutrophil-activating peptide-1/interleukin 8, a novel cytokine that activates neutrophils. *J. Clin. Invest.* **1989**, *84*, 1045.
6. Cejkova, J.; Novak, M.; Stepanek, F.; Hanczyc, M.M. Dynamics of chemotactic droplets in salt concentration gradients. *Langmuir* **2014**, *30*, 11937-11944.
7. Banno, T.; Asami, A.; Ueno, N.; Kitahata, H.; Koyano, Y.; Asakura, K.; Toyota, T. Deformable self-propelled micro-object comprising underwater oil droplets. *Sci. Rep.* **2016**, *6*.
8. Hanczyc, M.M. Metabolism and motility in prebiotic structures. *Philosophical Transactions of the Royal Society of London B: Biological Sciences* **2011**, *366*, 2885-2893.
9. Shimizu, Y.; Inoue, A.; Tomari, Y.; Suzuki, T.; Yokogawa, T.; Nishikawa, K.; Ueda, T. Cell-free translation reconstituted with purified components. *Nat. Biotechnol.* **2001**, *19*, 751-755.
10. Luisi, P.L. Autopoietic self-reproduction of fatty acid vesicles. *Biochemistry* **1988**, *27*, 1881-1888.
11. Sheng, L.; Kurihara, K. Transformation of oil droplets into giant vesicles. *Chem. Commun.* **2016**.
12. Hanczyc, M.M. Droplets: Unconventional protocell model with life-like dynamics and room to grow. *Life* **2014**, *4*, 1038-1049.
13. Holden, M.A.; Needham, D.; Bayley, H. Functional bionetworks from nanoliter water droplets. *J. Am. Chem. Soc.* **2007**, *129*, 8650-8655.
14. Dubois, P.; Marchand, G.; Fouillet, Y.; Berthier, J.; Douki, T.; Hassine, F.; Gmouh, S.; Vaultier, M. Ionic liquid droplet as e-microreactor. *Anal. Chem.* **2006**, *78*, 4909-4917.
15. Marchand, G.; Dubois, P.; Delattre, C.; Vinet, F.; Blanchard-Desce, M.; Vaultier, M. Organic synthesis in soft wall-free microreactors: Real-time monitoring of fluorogenic reactions. *Anal. Chem.* **2008**, *80*, 6051-6055.

16. Bain, R.M.; Pulliam, C.J.; They, F.; Cooks, R.G. Accelerated chemical reactions and organic synthesis in leidenfrost droplets. *Angew. Chem.* **2016**.
17. Hadorn, M.; Boenzli, E.; Sørensen, K.T.; Fellermann, H.; Hotz, P.E.; Hanczyc, M.M. Specific and reversible DNA-directed self-assembly of oil-in-water emulsion droplets. *Proceedings of the National Academy of Sciences* **2012**, *109*, 20320-20325.
18. Francis, W.; Fay, C.; Florea, L.; Diamond, D. Self-propelled chemotactic ionic liquid droplets. *Chem. Commun.* **2015**, *51*, 2342 - 2344.
19. Fraser, K.J.; MacFarlane, D.R. Phosphonium-based ionic liquids: An overview. *Aust. J. Chem.* **2009**, *62*, 309-321.
20. Vaughan, A.A.; Narayanaswamy, R. Optical fibre reflectance sensors for the detection of heavy metal ions based on immobilised br-padap. *Sensors Actuators B: Chem.* **1998**, *51*, 368-376.
21. Ferreira, S.L.; Costa, A.S.; de Jesus, D.S. Derivative spectrophotometric determination of nickel using br-padap. *Talanta* **1996**, *43*, 1649-1656.
22. Oxspring, D.; Maxwell, T.; Smyth, W. Uv-visible spectrophotometric, adsorptive stripping voltammetric and capillary electrophoretic study of 2-(5'-bromo-2'-pyridylazo)-5-diethylaminophenol and its chelates with selected metal ions: Application to the determination of co (iii) in vitamin b12. *Anal. Chim. Acta* **1996**, *323*, 97-105.
23. Topçu, S.; Menek, N.; Eren, E. Thermodynamic studies of 2-(5-bromo-2-pyridylazo)-5-diethylamino) phenol cu (ii), co (ii), ni (ii) and zn (ii) complexes. *Dyes and pigments* **2001**, *50*, 29-33.
24. Hofmeister, F. Zur lehre von der wirkung der salze. *Naunyn-Schmiedeberg's Archives of Pharmacology* **1888**, *25*, 1-30.
25. Salis, A.; Ninham, B.W. Models and mechanisms of hofmeister effects in electrolyte solutions, and colloid and protein systems revisited. *Chemical Society Reviews* **2014**, *43*, 7358-7377.
26. Dupont, D.; Depuydt, D.; Binnemans, K. Overview of the effect of salts on biphasic ionic liquid/water solvent extraction systems: Anion exchange, mutual solubility, and thermomorphic properties. *The Journal of Physical Chemistry B* **2015**, *119*, 6747-6757.
27. Blandino, A.; Macias, M.; Cantero, D. Formation of calcium alginate gel capsules: Influence of sodium alginate and cacl 2 concentration on gelation kinetics. *J. Biosci. Bioeng.* **1999**, *88*, 686-689.
28. Born, G.; Cross, M. The aggregation of blood platelets. *The Journal of physiology* **1963**, *168*, 178.

## **Chapter 7: Spiropyran Based Hydrogels Actuators - Walking in the Light**

### **7.1 Abstract**

### **7.2 Introduction**

### **7.3 Experimental**

#### **7.3.1 Materials**

#### **7.3.2 Gel Preparation**

#### **7.3.3 Photo-Mask Fabrication**

#### **7.3.4 Ratcheted Channel Fabrication**

#### **7.3.5 Hydrogel Walker Relative Area and Relative Leg Distance Analysis**

#### **7.3.6 Rheology**

#### **7.3.7 Hydrogel Walker Actuation**

### **7.4 Results and Discussion**

#### **7.4.1 Hydrogel Walker**

#### **7.4.2 Mechanical Properties**

#### **7.4.3 Relative Area and Relative Leg Distance Analysis**

### **7.5 Conclusion**

### **7.6 Acknowledgements**

### **7.7 References**

## Chapter 7

---

# Spiropyran Based Hydrogels Actuators - Walking in the Light\*

---

\***Spiropyran Based Hydrogels Actuators - Walking in the Light**, W. Francis, A. Dunne, C. Delaney L. Florea, D. Diamond, *Sensors & Actuators: B. Chemical*, 2017, 250, 608–616

## 7.1 Abstract

Herein we report on the synthesis of a bipedal hydrogel walker, based on *N*-isopropylacrylamide-*co*-acrylated spiropyran-*co*-acrylic acid p(NIPAAm-*co*-SP-*co*-AA). Due to the presence of the photochromic spiropyran molecule in the polymer structure, these hydrogels reversibly shrink and swell in aqueous environments when exposed to different light conditions. When placed onto a ratcheted surface, the actuation of the bipedal gel produces a walking motion by taking a series of steps in a given direction, as determined by the optimised design of the ratchet scaffold. We anticipate that such biomimetic hydrogel walkers could form the basis of light-actuated soft robots capable of more advanced functions such as autonomous migration to specific locations accompanied by triggered release of molecular cargo.

## 7.2 Introduction

The motile behaviour of life forms, from the most primitive to the more complex, has long fascinated scientists who remain captivated by their ability to navigate through challenging environments in response to external stimuli. The simple earthworm, for example, has been the focus of attention for scientific groups who attempt to achieve synthetic mimicry of its means of movement [1-3]. The earthworm's body is composed of cylinder-shaped segments which are filled with a fixed volume of incompressible fluid and its movement is attributed to the contraction of the circular and longitudinal muscle layers which run through the body of the worm. When the longitudinal muscles contract, the worm is made shorter and the liquid is forced into the sides of the cavity, causing the body to widen. Conversely, contraction of the circular muscles serves to elongate the worm's body. Sequential fine control over the length of individual segments allows the worm to move in one direction [4]. More advanced means of locomotion, as exhibited by humans and other large mammals, is controlled through interaction of both soft and hard materials. Many groups, studying soft and hard robotics, have looked to the human body for inspiration [5-7]. To date however, the hard robotics field has failed to produce devices that can match the functionalities offered by biology, such as flexibility, adaptability and self-repair observed in even the simplest living organisms (*e.g.* cells, bacteria, jellyfish and

worms). These types of functionality cannot be offered by present robotics technologies, mainly because of the lack of mechanical compliance between the conventional robotics and the biological systems. For implantable devices this hard-soft material mismatch can lead to tissue damage and foreign body response, resulting in hypoxia, acidosis, thrombosis and implant rejection [8]. Great recent progress has been made at the macro-scale towards soft-fluidics by using soft elastomers with embedded pneumatic networks [9,10]. These actuators contain inflatable channels fabricated in elastomeric materials which are configured to create specific movement when pressure is applied. Dielectric elastomers have also been proposed for the realisation of soft electro-actuators, however, their main disadvantage remains the typically large actuation voltage needed [11,12]. Currently, soft-robotics may offer actuators of modest complexity, which exhibit increased compliance with biological matrices. Biological inspiration has also led to the realisation of stimuli-responsive soft actuators through the use of hydrogels as a primitive mimic of biological tissue. Hydrogels comprise a broad range of polymeric materials which are capable of holding large volumes of water, due to their hydrophilic nature. Incorporation of stimuli-responsive compounds into the gel structure can be used to control the gel's overall hydrophilic character. This offers a means to modulate the volume and shape of the hydrogel structure through the expulsion or absorption of water from the surrounding environment. A large number of stimuli-responsive mechanisms for these gels have been reported, including thermal [13,14], pH [15], magnetic [16], glucose [17], antigen [18], electro [19], photo [20], and even multi-responsive hydrogels [21,22]. Of particular interest is the development of hydrogels with biomimetic properties [23,24], such as the ability to walk [25]. Yang *et al* [26] developed an arc shaped hydrogel based on poly(2-acrylamido-2-methylpropanesulfonic acid-*co*-acrylamide) (poly(AMPS-*co*-AAm)), which was able to walk across a ratcheted surface upon electrical stimulation. The hydrogel contained cross-linked networks bearing bound negatively-charged sulfonic groups. In sodium chloride (NaCl) solutions, upon the application of an electric potential, the free ions of the NaCl electrolyte move towards their respective counter electrodes. Inside the hydrogel however, only the cations of the bound negatively-charged sulfonic groups are mobile and can move towards the cathode. This ion motion creates an ionic concentration gradient within the hydrogel and in turn an osmotic pressure difference within the hydrogel walker. This translates into a bending motion towards the cathode upon

application of an electric field. Depending on the position of the electrodes, one side of the gel experiences a greater osmotic pressure difference, resulting in bending/deformation of the hydrogel. The bending behaviour is reversible and repeatable through successive "on/off " application of an electric field. When placed on a ratcheted surface and by repeatedly applying an electric field, a hydrogel arc can be made to “walk”. When the electric field is switched “on” the gel will shrink, resulting in the legs of the gel to come closer. Because of the shape of the ratchet, only one leg can move and the trailing leg will be “dragged” across the ratchet steps. When the electric field is removed the gel will expand, but as the trailing leg cannot expand back against the ratchet, the leading leg will be pushed forward.

Development of other forms of hydrogel stimulation offer more promising means of fine-tuning actuation. The use of photo-responsive hydrogels offers the possibility of accurately controlling irradiance, time, distance, position and wavelength of the light while offering non-contact stimulus that can be applied in a non-invasive manner. The incorporation of photo-responsive compounds in the modulation of hydrogels has been widely documented, most notably through the use of spiropyrans (SP), which also offer added sensitivity to pH, solvent polarity and metal ions [27-29]. Our group has been one of the pioneers in demonstrating that incorporation of spiropyran into gel structures (hydrogels [30] and ionogels [31,32]) can be used for the fabrication of photo-controlled liquid flow micro-fluidic manifolds [33], reversible microfluidic valves [34] and photo-programmable surface topographies [35]. The photo-responsive hydrogels used in these studies were typically composed of copolymers of *N*-isopropylacrylamide-*co*-acrylated spiropyran-*co*-acrylic acid (p(NIPAAm-*co*-SP-*co*-AA), in a molar ratio of 100:1:5. In an acidic environment SP is protonated, generating the more hydrophilic (MC-H<sup>+</sup>) form. Absorption of water from the external environment thereby results in expansion of the hydrogel. Upon irradiation with white light ( $\lambda_{\text{max}} = 422 \text{ nm}$ ) MC-H<sup>+</sup> releases a proton causing it to isomerize back to the more hydrophobic SP form. This increase in hydrophobicity results in the expulsion of water and the contraction of the gel. The addition of acrylic acid into the hydrogel backbone provides an internal source of protons for reversible switching [20] removing the need for an external acidic environment and enabling the switching of SP to MC-H<sup>+</sup> to occur in neutral conditions. This allows for reversible photo-actuation to be performed in deionised water.

Expanding on this work, herein we present photo-responsive hydrogel walkers based on p(NIPAAm-co-SP-co-AA). These walkers can reversibly shrink and expand via on/off white light irradiation. When submerged in water and placed onto a ratcheted surface the walkers can achieve a unidirectional walking motion when exposed to different light conditions. These hydrogels offer a promising route for the development of directed locomotion in soft light robotics.

## 7.3 Experimental

### 7.3.1 Materials

N-isopropylacrylamide 98% (NIPAAm), N,N'-methylenebisacrylamide 99% (MBIS), Phenylbis(2,4,6 trimethyl benzoyl) phosphine oxide 97% (PBPO), acrylic acid (180-200ppm MEHQ as inhibitor) 99% (AA), tetrahydrofuran 99% (THF), anhydrous dichloromethane (50-150 ppm amylene as stabilizer) 99% (DCM), ethyl acetate 99%, n-hexane 95%, were acquired from Sigma Aldrich, Ireland and used as received. 1',3',3'-Trimethyl-6-acryloylspro(2H-1-benzopyran-2,2-indoline) (SP-A) was synthesised as described elsewhere [20].

### 7.3.2 Gel Preparation

The hydrogel walkers were synthesised using a monomeric cocktail which consisted of 200 mg NIPAAm, 8 mg MBIS (3 mol% relative to NIPAAm), 6 mg SP-A (1 mol% relative to NIPAAm), 7 mg PBPO (1 mol% relative to NIPAAm) and 6  $\mu$ L AA (5 mol% relative to NIPAAm) dissolved in 500  $\mu$ L of the polymerisation solvent (4:1 vol: vol, THF: DI water). This gel composition was previously optimised by Ziółkowski *et al.* [20], who developed self-protonating p(NIPAAm-co-spiropyran-co-acrylic acid) hydrogel photoactuators, and Dunne *et al.* [30], who optimised the polymerisation solvent ratios, in order to achieve ideal pore sizes and ultimately improved upon the swelling and shrinking times obtained by Ziółkowski [20]. The arc-shaped hydrogel walkers were prepared by using a home-made cell consisting of a PMMA mask (**Figure 7.1**), a glass slide and a glass cover slide separated by a 500  $\mu$ m high spacer made out of poly(methyl methacrylate)/pressure sensitive adhesive (PMMA/PSA). The cell was filled by capillary action with the monomer solution and subsequently exposed to white light through the mask (Figure 8). The polymerisation time was

varied from 40 to 50 s, in order to compare polymerisation times with walker functionality. The white light source used was a Dolan-Jenner-Industries Fiber-Lite LMI LED lamp with two gooseneck waveguides placed at a distance range of 1 to 2 cm from the platform. The light intensity measured with a Multicomp LX-1309 light meter was 310 - 320 kLux. After polymerisation, the hydrogel walkers were washed gently with ethanol and DI water to remove any unpolymerised material and allowed to swell in deionised water for 4-6 hours to ensure full hydration.

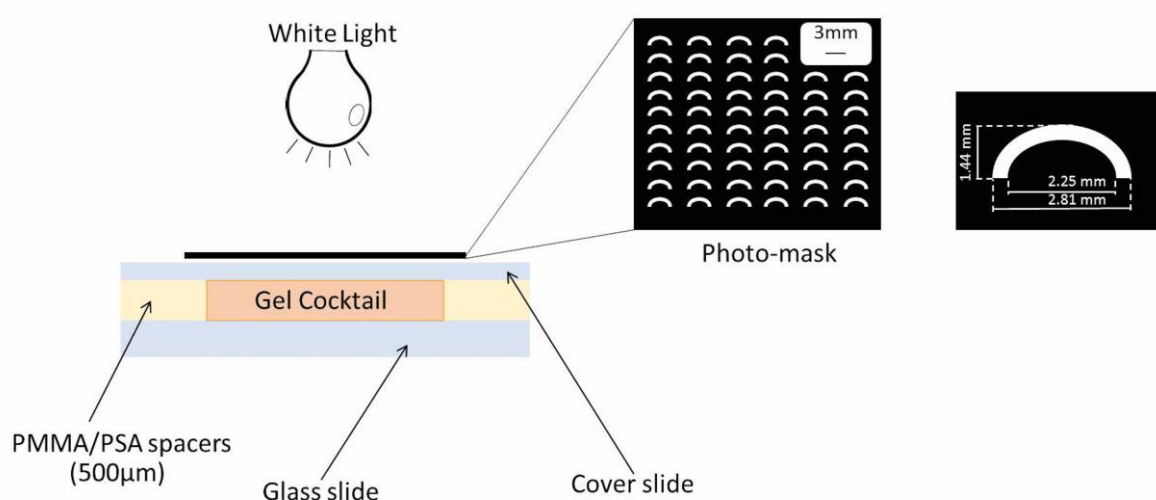


*Figure 7.1 Side view of in-house made cell for gel polymerisation; insets show the photomask including specific measurements of a single arc-shaped walker.*

### 7.3.3 Photo-Mask Fabrication

The photo-mask used for gel polymerisation was firstly designed using AutoCAD 2014 and cut from a 1 mm thick sheet of black PMMA using a CO<sub>2</sub> laser ablation system (Epilog Zing Laser Series). The mask contained a 7 x 5 array of walkers of 1.44 mm height, 2.81 mm (outer) distance between the legs, and a width of 0.56 mm.

### 7.3.4 Ratcheted Channel Fabrication

The ratcheted systems in this study were first designed using AutoCAD 2014 and a CO<sub>2</sub> laser ablation system (Epilog Zing Laser Series) was used to cut the required pieces out of black PMMA sheets. To assemble the ratcheted channel, a back PMMA layer, the ratchet layer and a glass slide were attached (**Figure 7.2**). The back layer and the main ratchet section were cut from 1 mm black PMMA. To avoid melting of the

ratchet during laser cutting, 50  $\mu\text{m}$  PSA was hand cut and applied to both sides after cutting. The back layer was joined with the main section first, then the glass slide was attached. Using clamps, the three sections were placed under pressure overnight. The ratcheted channel had a length of 45 mm, a 1 mm width and a height of 12 mm, while the ratchets had a height of 0.5 mm and a 7 mm distance between two consecutive ratchets.

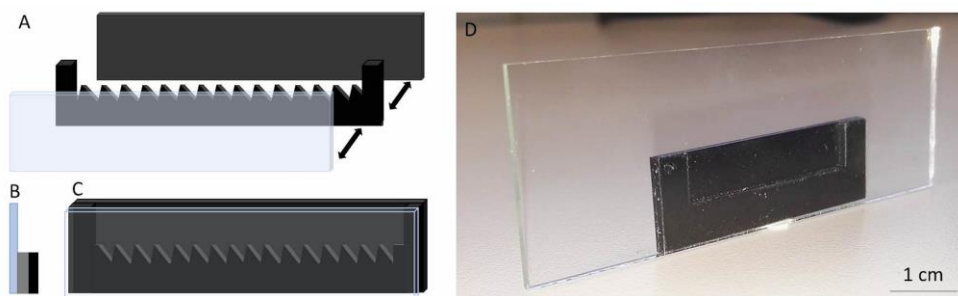


Figure 7.2 A) Schematic diagram showing the individual components of the ratcheted channel: glass slide, ratcheted channel bottom with side walls in black PMMA and PMMA back layer; Cartoon showing side (B) and front (C) views of the channel after assembly and D) Photo of the real ratcheted channel.

### 7.3.5 Hydrogel walker relative area and relative leg distance analysis

The distance between the walker's legs and the area measurements of the freestanding hydrogel walkers were performed using Image J (1.47v) software. For each polymerisation time, three hydrogel samples were measured. The relative area % (Eq. 7.1) and relative Legs distance% (Eq. 7.2) were calculated using the following equations (n=3):

$$\text{Relative area (\%)} = \frac{A_t}{A_o} \times 100 \quad (\text{Eq. 7.1})$$

Where  $A_t$  = Measured area at time t and  $A_o$  = Area of a fully hydrated gel.

$$\text{Relative leg distance (\%)} = \frac{L_t}{L_0} \times 100 \quad (\text{Eq. 7.2})$$

Where  $L_t$  = Measured inner leg distance at time t and  $L_0$  = Initial inner leg distance of the fully hydrated walker.

### 7.3.6 Rheology

Rheology curing measurements were performed on the unpolymerised cocktail. The measurements were carried out using an Anton-Paar MCR301 rheometer with a CP50-2 measuring tool with a diameter of 49.97 mm and a cone angle of  $1.996^\circ$  to measure the mechanical properties during polymerisation. The rheometer had a glass plate to which 900  $\mu\text{l}$  of monomer mixture was placed and pressed with the CP50-2 tool with a space of 208  $\mu\text{m}$ . A Dolan-Jenner-Industrie Fiber-Lite LMI white light was placed under the glass plate having a light intensity of 320 kLux, measured on top of the glass plate using a LX-1309: light meter. The curing and mechanical properties of the p(NIPAAm-*co*-SPA-*co*-AA) cocktail were measured over 15 minutes with data collected every second. White light curing was initiated after 60s and after the allotted time (40s, 45s and 50s, respectively) the light was turned off. The loss and storage moduli were analysed at 0.1% strain and 1Hz oscillation frequency against time.

Polymer films of 500  $\mu\text{m}$  thickness were polymerised for the specific times (40s, 45s and 50s) in the same manner as the walkers in the absence of the photomask with a light intensity of 318 kLux. After the polymer films were hydrated, circular disks of 15 mm diameter were cut using a manual puncher and used for further rheology analysis. The polymer discs from the various polymerisation times were placed under the PP15 rheometer tool (15 mm diameter) of the Anton Paar MCR 301 rheometer. Amplitude sweeps were carried out at  $100 \text{ rad s}^{-1}$  angular frequency, a normal force of 1 N with a gradual strain from 0.01 – 100%. The storage modulus was monitored with data being collected every 20 seconds.

### 7.3.7 Hydrogel walker actuation

To achieve the “walking” behaviour of the hydrogels, a single walker was placed on to one of the ratcheted channels. The channel was then carefully filled with deionised water. An Aigo GE-5 microscope (using a 60x objective lens and accompanying software) was placed facing the glass side of the ratcheted channels. Finally, the white light source was adjusted so both goosenecks were pointed at the walker and had an intensity of  $\sim 305 \text{ kLux}$ . Once recording began the white light source was switched on. The walker was then monitored in real time and once the trailing leg had moved across at least one of the ratchet steps the light was removed. The gel was

then monitored in the dark and once the leading leg had been pushed at least one ratchet step, the white light source was turned back on. This was continued until the hydrogel had walked a number of steps.

## **7.4 Results and Discussion**

### **7.4.1 Hydrogel walker**

The (p(NIPAAm-*co*-SP-*co*AA)) hydrogels in this study were able to achieve reversible swelling and contraction through repeatable white light irradiation. In the absence of white light, the SP component of the gels underwent protonation to the more hydrophilic MC-H<sup>+</sup> form, due to protonation from the AA substituent (pKa ~ 4.5). Under these conditions, the gels expanded to the maximum capacity and had a yellow colour. When the hydrogels were illuminated with white light, the MC-H<sup>+</sup> was deprotonated back to the SP form (**Figure 7.3**). This resulted in a rapid colour change towards white/colourless as the gel began to contract. This is due to the hydrophobic nature of SP which causes the polymer chains within the gel to collapse and water from the gel to be expelled to the external environment (Figure 7.3).

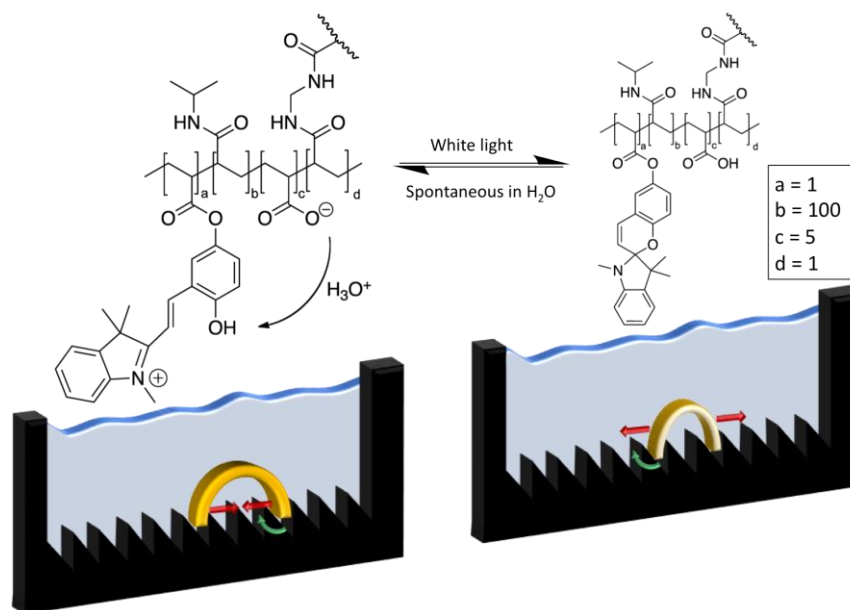
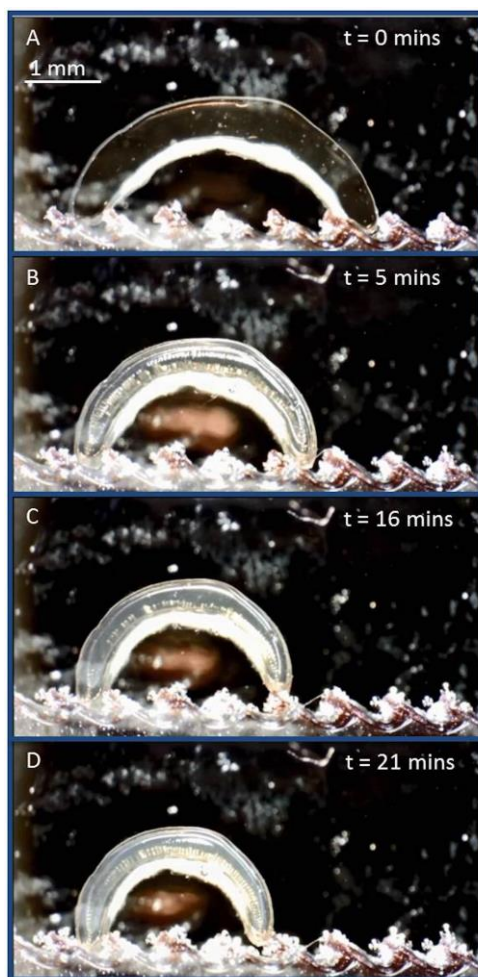


Figure 7.3 Chemical structure of the  $p(\text{NIPAAm-co-SP-co-AA})$  hydrogel walkers under different illumination conditions and the physical effect it has on the gel morphology. The AA co-polymer acted as an internal acidic source for the protonation of SP to the more hydrophilic  $\text{MC-H}^+$  form, this switch induced hydrophobicity changes resulting in the absorption of water from the external environment into the gel. When irradiated with white light ( $\lambda_{\text{max}} = 422 \text{ nm}$ )  $\text{MC-H}^+$  was deprotonated, resulting in the isomerisation back to the more hydrophobic SP form. Inside the  $p(\text{NIPAAm-co-SP-co-AA})$  hydrogel, this isomerization resulted in an expulsion of water and reduction of the gel's volume. Therefore when left in the dark the gel expanded, because of the design of the ratchet only one leg can move and thus the gel was pushed forward. When white light is introduced the gel shrank, again due to the design of the ratchet this resulted in the gel being pulled forward by the trapped leg.

To achieve the walking motion this process was performed on a ratcheted polymethyl methacrylate (PMMA) surface, from right to left, as depicted in **Figure 7.4**. After a period of white light irradiation (5 min at  $\sim 305 \text{ kLux}$  intensity), the gel began to contract, thereby causing deformation of the gel's structure. When the leading leg comes in contact with the vertical section of the ratchet step (Figure 7.4A), a gradual photo-induced reduction of the distance between the legs causes the trailing leg to be “dragged” over the bevel of the ratchet step (Figure 7.4 (B-D)).



*Figure 7.4 Series of snapshots showing the effect of light irradiation on the hydrogel walker. A) Light irradiation is initiated; B-D) Gradual reduction of inter-leg distance results in the trailing leg (right) being “dragged” over the bevel of the ratchet step.*

When the light was removed the gel would gradually begin to re-swell and regain its original colour. Swelling continued until the trailing leg became lodged on a vertical section of a ratchet step, thus causing the leading leg to be pushed over the bevel of the corresponding ratchet step. By repeating this process, the p(NIPAAm-*co*-SP-*co*-AA) walkers could be made walk in a single direction, determined by the direction of the ratchet (see **Figure 7.5**, **Figure D.2**, **Video 7.1** and **Video 7.2**).

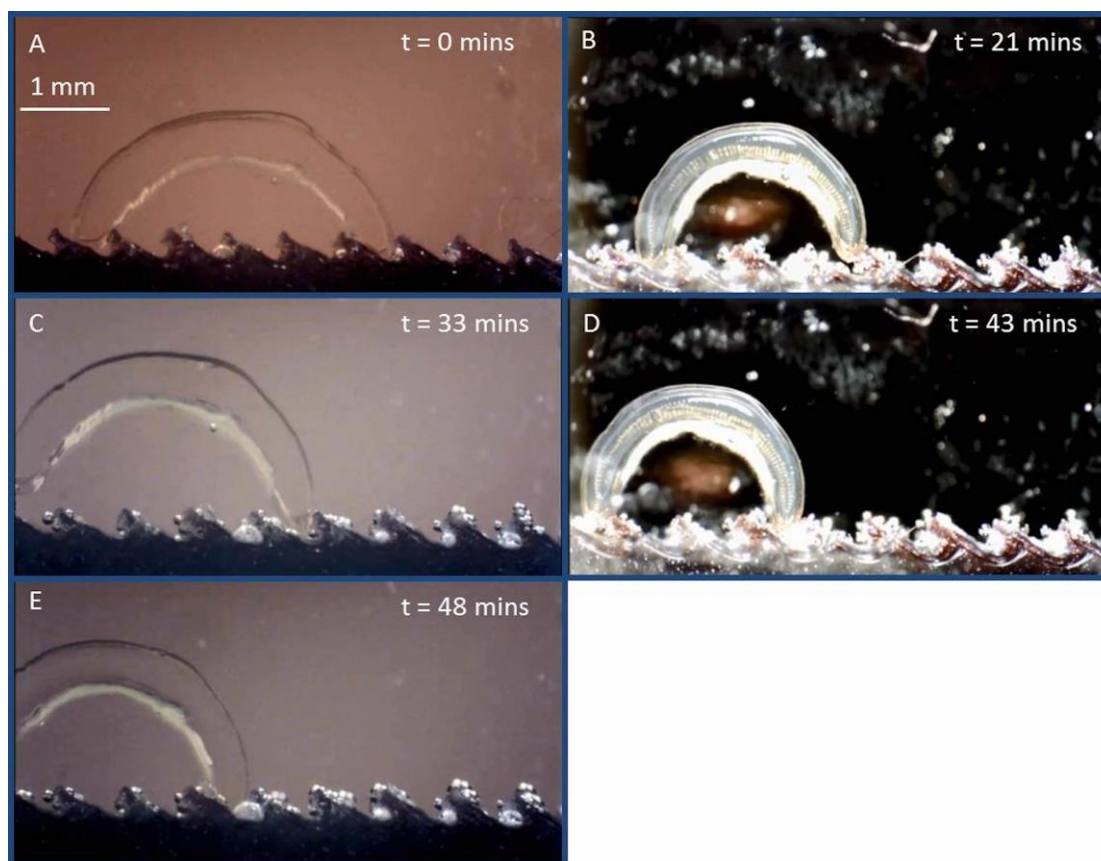


*Figure 7.5 Series of snapshots showing the walking behaviour of the hydrogel (Video 7.1). A – B shows contraction of the trailing leg. C – Swelling in the dark results in the forward leg being pushed over the ratchet. D – E The sequence is repeated which results in the gel achieving a unidirectional walking motion (right to left).*

#### **7.4.2. Mechanical properties**

To design a hydrogel walker which can actuate over a series of predefined distances, it is necessary to have a comprehensive knowledge of the mechanical properties of the hydrogel walker. The elastic nature of a hydrogel can have a dramatic influence on its ability to actuate under a given stimulus. To best understand the effect of varied degrees of cross-linking, a rheology study was used to ascertain the most appropriate curing time. Three different polymerisation times were chosen (40s, 45s and 50s, respectively), during which the monomeric cocktail was exposed to white light irradiation and the storage modulus recorded (**Figure 7.6**). The storage modulus increases abruptly when the light is turned on (time = 60s) owing to significant growth of elastic structures due to the crosslinking. When the light is turned off (after

40s, 45s and 50s, respectively) no new radicals are formed by initiation, and therefore, the increase in storage modulus is significantly slowed, as only the free radicals that are present when the light is turned off continue to propagate and terminate [36]. The hydrogels polymerised under 50s of light irradiation showed the highest storage modulus plateau at around 3700 Pa, and therefore, exhibit the greatest elastic properties of the hydrogels studied (Figure 7.6). Polymerisation times longer than 60s were not suitable as polymerisation-induced diffusion, beyond the exposed areas of the photo mask, resulted in peripheral polymerisation.

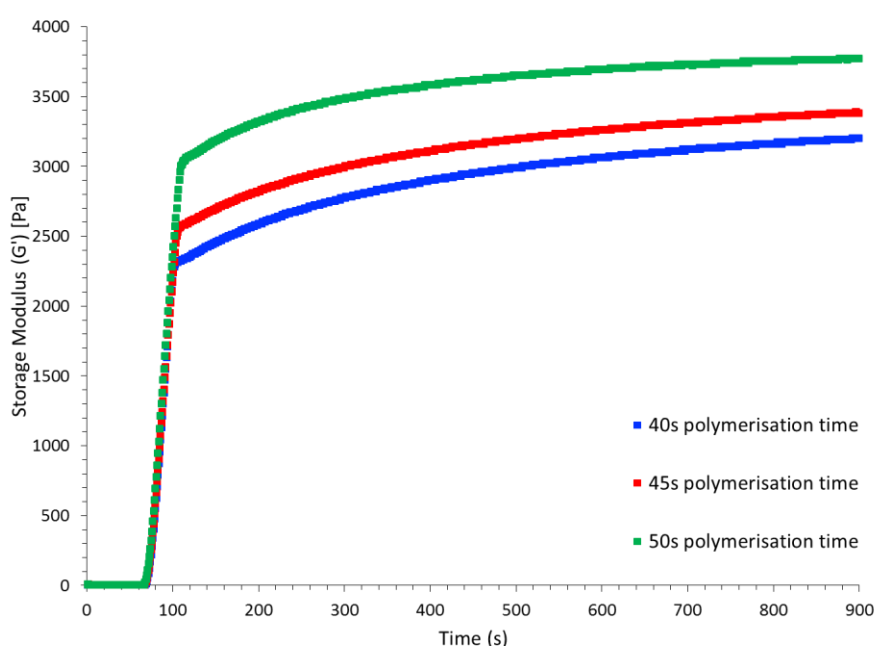


Figure 7.6 Photo-curing of hydrogels produced under different light irradiation times (40s, 45s and 50 s, respectively). White light polymerisation was initiated at  $t=60$  s.

Mechanical studies of the hydrogels were also performed after hydration, as detailed in the experimental section. It was revealed that upon hydration, the storage modulus of the hydrogels polymerised under different polymerisation times (40s, 45s, and 50s, respectively), although increasing with the polymerisation time, does not vary significantly (Figure D.1). However, amplitude sweeps reveal that the linear viscoelastic range (LVE) is significantly different and decreases with increased polymerisation time. This could be due to the fact that crosslinking density is

increasing with the polymerisation time, also causing an increase in chain entanglement. Therefore, when an increase shear stress is applied, physical interactions and entanglements will be destroyed prior to covalent bonds. As a result, the sudden decrease in  $G'$  (indicating the end of the LVE) occurs at lower shear stress for the hydrogels polymerised under a longer polymerisation time, which implies that there are more physical crosslinks and chain entanglements in these sample networks [37].

### 7.4.3. Relative area and relative leg distance analysis

Extending our knowledge of these materials to fabricate a simple hydrogel walker required not only an insight into the mechanical properties but also greater understanding of the volume change of the material during actuation cycles. On a stepped surface, it is important to fully understand both the swelling of the respective legs and maximum bipedal distance, during actuation. To determine the actuation properties of the hydrogel walkers polymerised under different polymerisation times, a study was performed to examine the effect on both the relative area of the entire gel and the distance between the legs upon irradiation with white light. Polymerisation time is an important parameter when synthesising hydrogels as it affects the crosslinking density of the hydrogel, thus its mechanical properties (Figure 7.6) and its ability to absorb and expel water and the material's shape memory [38-41].

**Figure 7.7** shows the relative area of each of the gels when exposed to three cycles of white light irradiation. It confirms, as expected, that polymerisation times plays only a minor role in the extent of swelling or contraction exhibited by the resulted hydrogel, in these particular conditions (polymerisation times of 40s, 45s and 50s, respectively). The 50 second polymerised gels showed the greatest repeatability and were better able to swell close to their original size when compared to the shorter polymerization times. Relative area change is  $A_{\text{rel. change}} = 24.14 \pm 7.43\%$  ( $n=3$ ) for the hydrogels polymerised under 40s of light irradiation,  $A_{\text{rel. change}} = 23.11 \pm 9.24\%$  ( $n=3$ ) for 45s polymerisation time and  $A_{\text{rel. change}} = 25.87 \pm 2.35\%$  ( $n=3$ ) for 50s polymerisation time, respectively. For the hydrogel polymerised under 40s of white light irradiation, there is a clear gradual decrease in the size of the hydrogel both under light and dark conditions (**40s: 2<sup>nd</sup> cycle**  $62.28 \pm 5.41\%$  (contracted);  $78.98 \pm 6.04\%$  (expanded) and **3<sup>rd</sup> cycle**  $56.94 \pm 6.41\%$  (contracted)  $75.17 \pm 7.75\%$  (expanded)). This is most

likely due to the decreased crosslinking density and physical entanglements present in these hydrogels, which may impede the hydrogels from returning to their original size.

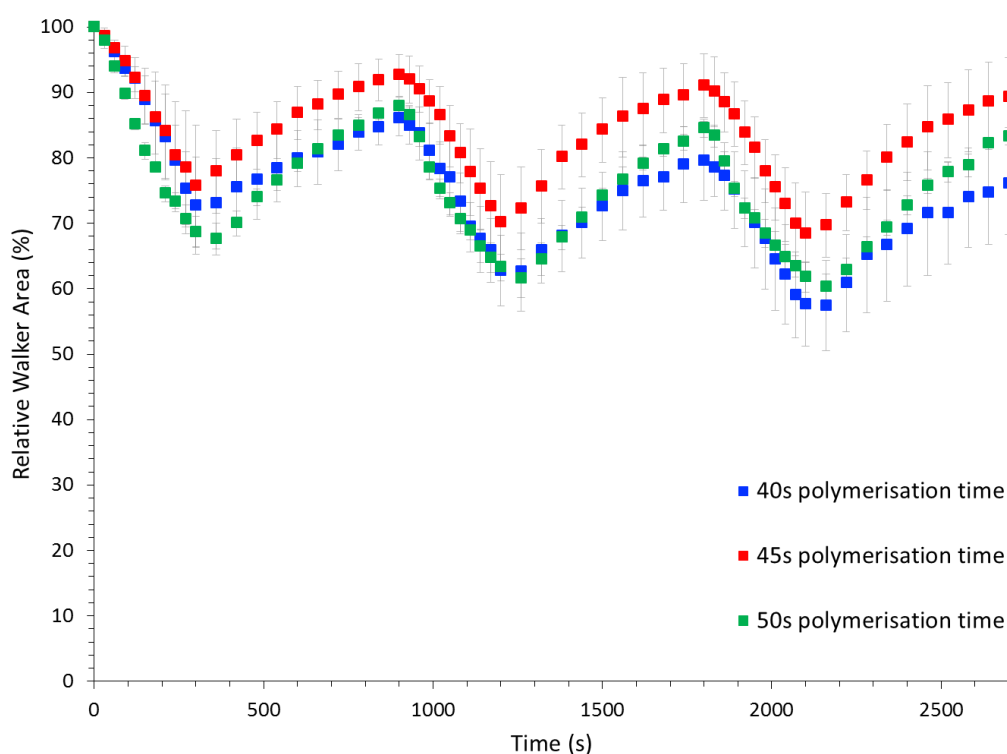


*Figure 7.7 Three photo-actuation cycles of hydrogel walkers produced after 40s, 45s and 50s of light irradiation, respectively, showing the relative changes in walker area when exposed to different illumination conditions. The measurements have been done in triplicate and the error bars represent standard deviations.*

An analysis of the relative inter-leg distance for a set of walkers of varied polymerisation time was also performed. Figure 7.6 shows the effect polymerisation times had on the actuation of the hydrogel structures, and in particular the relative changes in leg distance when the gels were exposed to different illumination conditions. As seen from Figure 7.6, polymerization times of 40s and 45s, respectively, resulted in gels with a lower storage modulus. Upon actuation, this failed to show an appreciable change on the centre angle of the arc-shaped walker. When exposed to white light all of the hydrogel walkers were able to expand and contract (Figure 7.7 and Figure 7.8), however the ones polymerised for 40s and 45s, respectively, couldn't maintain their shape and became flat when irradiated on a ratcheted surface.

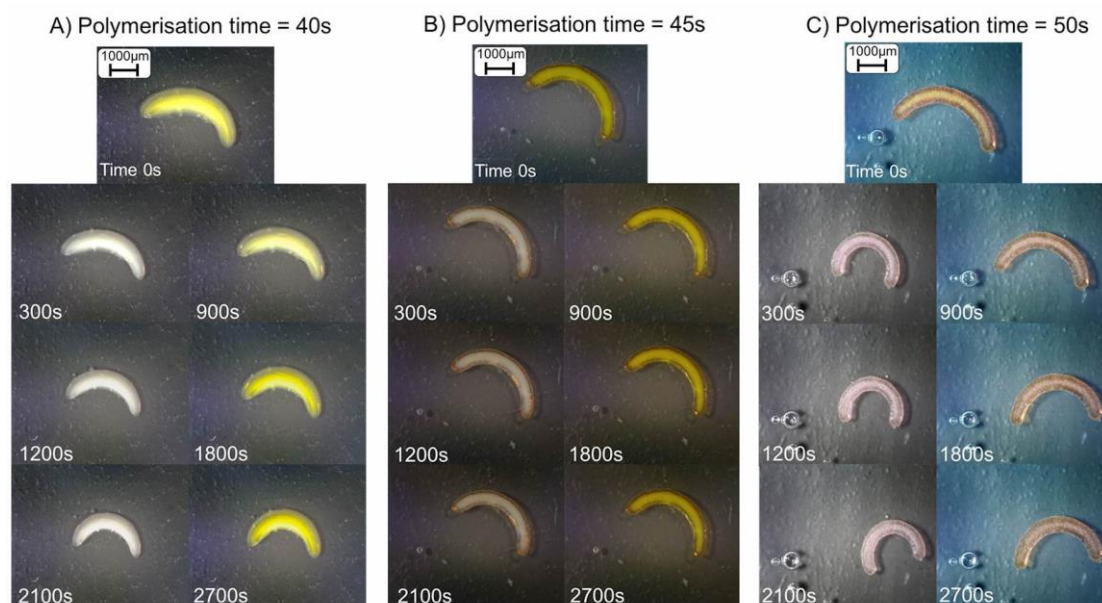


*Figure 7.8 Three photo-actuation cycles of hydrogel walkers produced after 40s, 45s and 50s of light irradiation, respectively, showing the relative changes in legs distance when exposed to different illumination conditions.*

The results of this assessment of actuation behaviour, in particular inter-leg distance, are summarised in the plots shown in **Figure 7.9**. This clearly demonstrates that the gels synthesised using a 50 second polymerisation time had the greatest reduction in distance between the legs when exposed to white light. The 40 and 45 second gels showed minor and irreproducible inter-leg distance changes and therefore, limited movement. Knowledge of the extent of change in the centre angle of the arc-shaped walker/ inter-leg distance is integral to the design of the ratcheted surface on which the walker moves. By assessing the distance between the legs before and after actuation it is possible to design ratchets of optimal dimensions to maximise the potential for unidirectional movement. These results had a direct influence on the width of ratchets used for further studies, as outlined in the experimental section.

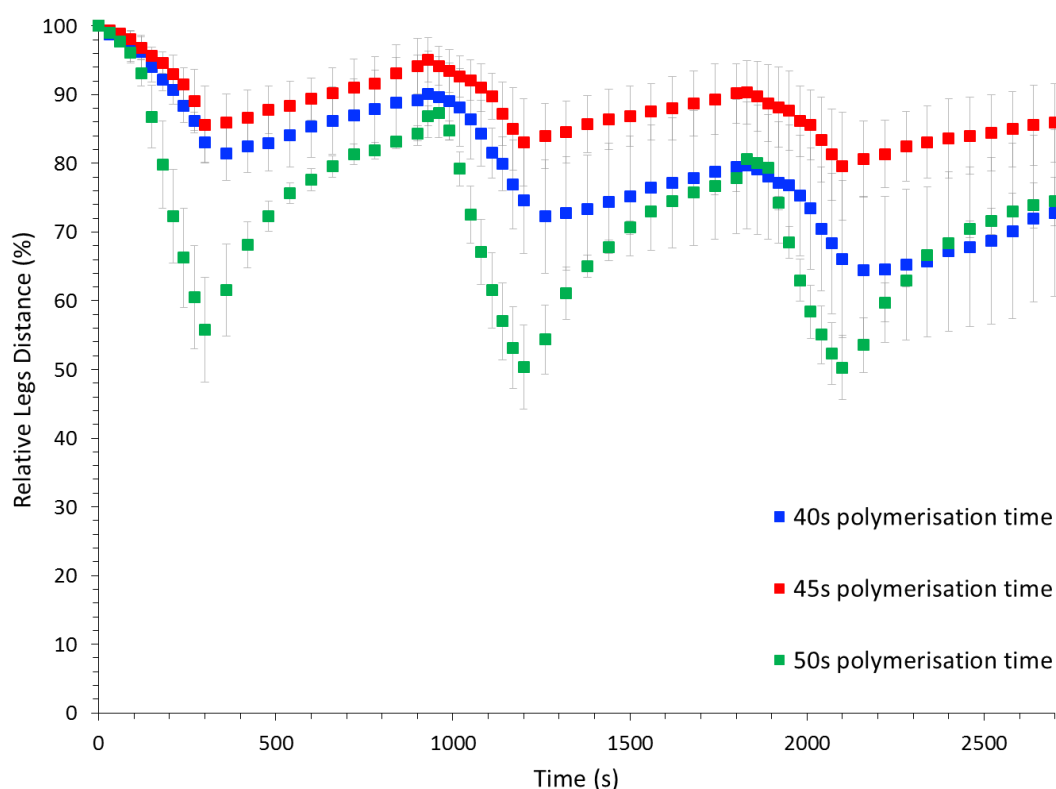


Figure 7.9 Three photo-actuation cycles of hydrogel walkers produced after 40s, 45s and 50s of light irradiation, respectively, showing the relative changes in legs distance when exposed to different illumination conditions.

As the actuation behaviour (swelling, contraction) in hydrogels is essentially diffusion controlled, the reduction of the scale of these structures can dramatically increase the rate at which these effects occur [42]. Improved kinetics of the actuation could also be realised by increasing the pore density of the hydrogel structure [43] as this can substantially reduce the overall diffusion pathlength for water uptake and release. Furthermore, modification of substituents on the photoswitch molecule produces dramatic improvements in the switching kinetics, which also contributes to the overall effectiveness of the gel actuation effect [44,45]. This in turn will allow for the realisation of soft micro-robots, capable of various forms of locomotion on a significantly reduced timescale. In addition, photo-switchable dynamic ratchet structures that emerge /disappear can be created, and linking this behaviour with the ‘walkers’ offers the intriguing possibility of externally switching between ‘on’ (ratchet features present, directed movement turned on) and ‘off’ (smooth surface restored, directed movement turned off)[35].

## 7.5 Conclusion

In conclusion, we have synthesised a hydrogel walker based on p(NIPAAm-co-SP-co-AA) which can reversibly swell and contract when submerged in water and subjected to cycles of white light irradiation. The hydrogel is able to achieve unidirectional walking when placed onto a ratcheted surface. These results show that photo-responsive hydrogels make promising candidates for the development of biomimetic soft robots which could exploit their reversible and repeatable actuation. This study opens the possibility for development of more advanced biomimetic walking soft robots which can perform tasks such as cargo transport, sensing and targeted drug delivery. The ability to control on-demand uptake and release, with porous materials of this nature, offers the possibility of localised triggered reactions upon secondary stimulation at desired destinations [46,47]. The combination of these processes could be used to achieve targeted transport, delivery and release within fluidic systems.

## 7.6 Acknowledgements

This project has been funded by Science Foundation Ireland under the Insight initiative, grant SFI/12/RC/2289. CD and DD also acknowledge the European Union's Seventh Framework Programme for research, technological development, and demonstration; through the NAPES project grant agreement no. 604241.

## 7.7 References

1. Quillin, K. Ontogenetic scaling of hydrostatic skeletons: Geometric, static stress and dynamic stress scaling of the earthworm *lumbricus terrestris*. *J. Exp. Biol.* **1998**, *201*, 1871-1883.
2. Menciassi, A.; Gorini, S.; Pernorio, G.; Dario, P. In *A sma actuated artificial earthworm*, Robotics and Automation, 2004. Proceedings. ICRA'04. 2004 IEEE International Conference on, 2004; IEEE: pp 3282-3287.
3. Murakami, Y.; Uchiyama, H.; Kurata, J.; Maeda, M. In *Dynamical locomotion analysis and a model for the peristaltic motion of earthworms*, 2006 SICE-ICASE International Joint Conference, 2006; IEEE: pp 4224-4229.
4. Quillin, K.J. Kinematic scaling of locomotion by hydrostatic animals: Ontogeny of peristaltic crawling by the earthworm *lumbricus terrestris*. *J. Exp. Biol.* **1999**, *202*, 661-674.

5. Kim, S.; Laschi, C.; Trimmer, B. Soft robotics: A bioinspired evolution in robotics. *Trends Biotechnol.* **2013**, *31*, 287-294.
6. Hirose, S.; Umetani, Y. The development of soft gripper for the versatile robot hand. *Mechanism and machine theory* **1978**, *13*, 351-359.
7. Godage, I.S.; Branson, D.T.; Guglielmino, E.; Medrano-Cerda, G.A.; Caldwell, D.G. In *Shape function-based kinematics and dynamics for variable length continuum robotic arms*, Robotics and Automation (ICRA), 2011 IEEE International Conference on, 2011; IEEE: pp 452-457.
8. Scholten, K.; Meng, E. Materials for microfabricated implantable devices: A review. *Lab on a Chip* **2015**, *15*, 4256-4272.
9. Shen, H. Meet the soft, cuddly robots of the future. *Nature* **2016**, *530*, 24-26.
10. Mosadegh, B.; Polygerinos, P.; Keplinger, C.; Wennstedt, S.; Shepherd, R.F.; Gupta, U.; Shim, J.; Bertoldi, K.; Walsh, C.J.; Whitesides, G.M. Pneumatic networks for soft robotics that actuate rapidly. *Advanced Functional Materials* **2014**, *24*, 2163-2170.
11. Yuan, X.; Changgeng, S.; Yan, G.; Zhenghong, Z. In *Application review of dielectric electroactive polymers (deaps) and piezoelectric materials for vibration energy harvesting*, Journal of Physics: Conference Series, 2016; IOP Publishing: p 012077.
12. Rossiter, J.; Walters, P.; Stoimenov, B. In *Printing 3d dielectric elastomer actuators for soft robotics*, SPIE Smart Structures and Materials+ Nondestructive Evaluation and Health Monitoring, 2009; International Society for Optics and Photonics: pp 72870H-72870H-72810.
13. Kim, J.H.; Randall Lee, T. Discrete thermally responsive hydrogel-coated gold nanoparticles for use as drug-delivery vehicles. *Drug Dev. Res.* **2006**, *67*, 61-69.
14. Weng, H.; Zhou, J.; Tang, L.; Hu, Z. Tissue responses to thermally-responsive hydrogel nanoparticles. *J. Biomater. Sci. Polym. Ed.* **2004**, *15*, 1167-1180.
15. Kim, J.-H.; Lee, T.R. Thermo-and ph-responsive hydrogel-coated gold nanoparticles. *Chem. Mater.* **2004**, *16*, 3647-3651.
16. Ozay, O.; Ekici, S.; Baran, Y.; Aktas, N.; Sahiner, N. Removal of toxic metal ions with magnetic hydrogels. *Water Res.* **2009**, *43*, 4403-4411.
17. Peppas, N.A.; Bures, C.D. Glucose-responsive hydrogels. *Encyclopedia of Biomaterials and Biomedical Engineering*, DOI **2006**, *10*.
18. Miyata, T.; Asami, N.; Uragami, T. A reversibly antigen-responsive hydrogel. *Nature* **1999**, *399*, 766-769.
19. Murdan, S. Electro-responsive drug delivery from hydrogels. *J. Controlled Release* **2003**, *92*, 1-17.
20. Ziółkowski, B.; Florea, L.; Theobald, J.; Benito-Lopez, F.; Diamond, D. Self-protonating spiropyran-co-nipam-co-acrylic acid hydrogel photoactuators. *Soft Matter* **2013**, *9*, 8754-8760.
21. Dumitriu, R.P.; Mitchell, G.R.; Vasile, C. Multi-responsive hydrogels based on n-isopropylacrylamide and sodium alginate. *Polym. Int.* **2011**, *60*, 222-233.
22. Tudor, A.; Florea, L.; Gallagher, S.; Burns, J.; Diamond, D. Poly (ionic liquid) semi-interpenetrating network multi-responsive hydrogels. *Sensors* **2016**, *16*, 219.
23. Moon, J.J.; Saik, J.E.; Poche, R.A.; Leslie-Barbick, J.E.; Lee, S.-H.; Smith, A.A.; Dickinson, M.E.; West, J.L. Biomimetic hydrogels with pro-angiogenic properties. *Biomaterials* **2010**, *31*, 3840-3847.

24. Venkatesh, S.; Sizemore, S.P.; Byrne, M.E. Biomimetic hydrogels for enhanced loading and extended release of ocular therapeutics. *Biomaterials* **2007**, *28*, 717-724.
25. Morales, D.; Palleau, E.; Dickey, M.D.; Velev, O.D. Electro-actuated hydrogel walkers with dual responsive legs. *Soft Matter* **2014**, *10*, 1337-1348.
26. Yang, C.; Wang, W.; Yao, C.; Xie, R.; Ju, X.-J.; Liu, Z.; Chu, L.-Y. Hydrogel walkers with electro-driven motility for cargo transport. *Sci. Rep.* **2015**, *5*.
27. Florea, L.; Diamond, D.; Benito-Lopez, F. Photo-responsive polymeric structures based on spiropyran. *Macromolecular Materials and Engineering* **2012**, *297*, 1148-1159.
28. Rosario, R.; Gust, D.; Hayes, M.; Jahnke, F.; Springer, J.; Garcia, A.A. Photon-modulated wettability changes on spiropyran-coated surfaces. *Langmuir* **2002**, *18*, 8062-8069.
29. Shao, N.; Jin, J.; Wang, H.; Zheng, J.; Yang, R.; Chan, W.; Abliz, Z. Design of bis-spiropyran ligands as dipolar molecule receptors and application to in vivo glutathione fluorescent probes. *J. Am. Chem. Soc.* **2009**, *132*, 725-736.
30. Dunne, A.; Delaney, C.; Florea, L.; Diamond, D. Solvato-morphologically controlled, reversible nipaam hydrogel photoactuators. *RSC Advances* **2016**, *6*, 83296-83302.
31. Benito-Lopez, F.; Antoñana-Díez, M.; Curto, V.F.; Diamond, D.; Castro-López, V. Modular microfluidic valve structures based on reversible thermoresponsive ionogel actuators. *Lab on a Chip* **2014**, *14*, 3530-3538.
32. Czugala, M.; O'Connell, C.; Blin, C.; Fischer, P.; Fraser, K.J.; Benito-Lopez, F.; Diamond, D. Swelling and shrinking behaviour of photoresponsive phosphonium-based ionogel microstructures. *Sensors Actuators B: Chem.* **2014**, *194*, 105-113.
33. Benito-Lopez, F.; Byrne, R.; Răduță, A.M.; Vrana, N.E.; McGuinness, G.; Diamond, D. Ionogel-based light-actuated valves for controlling liquid flow in micro-fluidic manifolds. *Lab on a Chip* **2010**, *10*, 195-201.
34. ter Schiphorst, J.; Coleman, S.; Stumpel, J.E.; Ben Azouz, A.; Diamond, D.; Schenning, A.P. Molecular design of light-responsive hydrogels, for in situ generation of fast and reversible valves for microfluidic applications. *Chem. Mater.* **2015**, *27*, 5925-5931.
35. Stumpel, J.E.; Ziółkowski, B.; Florea, L.; Diamond, D.; Broer, D.J.; Schenning, A.P. Photoswitchable ratchet surface topographies based on self-protonating spiropyran-nipaam hydrogels. *ACS applied materials & interfaces* **2014**, *6*, 7268-7274.
36. Ye, Q.; Spencer, P.; Wang, Y.; Misra, A. Relationship of solvent to the photopolymerization process, properties, and structure in model dentin adhesives. *Journal of Biomedical Materials Research Part A* **2007**, *80*, 342-350.
37. Shangguan, Y.; Yang, J.; Zheng, Q. Rheology of nitrile rubber with hybrid crosslinked network composed of covalent bonding and hydrogen bonding. *RSC Advances* **2017**, *7*, 15978-15985.
38. Stumpel, J.E.; Liu, D.; Broer, D.J.; Schenning, A.P. Photoswitchable hydrogel surface topographies by polymerisation-induced diffusion. *Chemistry—European Journal* **2013**, *19*, 10922-10927.
39. Huang, C.; Lv, J.-a.; Tian, X.; Wang, Y.; Yu, Y.; Liu, J. Miniaturized swimming soft robot with complex movement actuated and controlled by remote light signals. *Sci. Rep.* **2015**, *5*.

40. Maeda, S.; Hara, Y.; Sakai, T.; Yoshida, R.; Hashimoto, S. Self-walking gel. *Adv. Mater.* **2007**, *19*, 3480-3484.
41. Wang, L.; Liu, Y.; Cheng, Y.; Cui, X.; Lian, H.; Liang, Y.; Chen, F.; Wang, H.; Guo, W.; Li, H. A bioinspired swimming and walking hydrogel driven by light-controlled local density. *Advanced Science* **2015**, *2*.
42. Shibayama, M.; Tanaka, T. Volume phase transition and related phenomena of polymer gels. In *Responsive gels: Volume transitions i*, Springer: 1993; pp 1-62.
43. Ziółkowski, B.; Florea, L.; Theobald, J.; Benito-Lopez, F.; Diamond, D. Porous self-protonating spiropyran-based nipaam gels with improved reswelling kinetics. *Journal of materials science* **2016**, *51*, 1392-1399.
44. Satoh, T.; Sumaru, K.; Takagi, T.; Takai, K.; Kanamori, T. Isomerization of spirobenzopyrans bearing electron-donating and electron-withdrawing groups in acidic aqueous solutions. *PCCP* **2011**, *13*, 7322-7329.
45. Coleman, S.; ter Schiphorst, J.; Stumpel, J.E.; Ben Azouz, A.; Diamond, D.; Schenning, A.P. Molecular design of light-responsive hydrogels, for in-situ generation of fast and reversible valves for microfluidic applications. *Chem. Mater.* **2015**, *27*, 5925-5931.
46. Jiang, H.; Kobayashi, T. Ultrasound stimulated release of gallic acid from chitin hydrogel matrix. *Materials Science and Engineering: C* **2017**, *75*, 478-486.
47. Huynh, C.T.; Nguyen, M.K.; Tonga, G.Y.; Longé, L.; Rotello, V.M.; Alsberg, E. Photocleavable hydrogels for light-triggered sirna release. *Advanced healthcare materials* **2016**, *5*, 305-310.

## **Chapter 8: Future Work**

### **Introducing Functionality into Chemotactic Ionic Liquid Droplets**

#### **8.1 Micro-sized ionic liquid droplets as micro-vessels for chemical reactions at pre-determined locations.**

##### **8.1.1 Introduction**

##### **8.1.2 Polymerisation at pre-determined locations**

#### **8.2 Chemotactic droplets in non-geometrically confined environments**

##### **8.2.1 Introduction**

##### **8.2.2 Autonomous leak detection and repair**

##### **8.2.3 Controlling the chemotactic signal in open systems**

##### **8.2.4 Micro-vessels for chemical synthesis in open systems**

#### **8.3 Future prospects**

#### **8.4 References**

## Chapter 8

---

### Future Work

---

#### **Introducing Functionality into Chemotactic Ionic Liquid Droplets**

## **8.1 Micro-sized ionic liquid droplets as micro-vessels for chemical reactions at pre-determined locations**

### **8.1.1 Introduction**

Having successfully demonstrated two methods for achieving spontaneous and autonomous droplet movement to desired destinations, as described in Chapter 4 and 5 of this thesis, the next step was the introduction of additional functionality in to these smart droplets. In Chapter 6 we successfully demonstrated these droplets could successfully perform at least six different functions: decision making, cargo transport, droplet to droplet communication, sensing and damage find and repair. Although Chapter 6 does demonstrate well the versatile nature of these smart droplets, we believe that these droplets are capable of performing more complex tasks (*e.g.* programmable chemical reactions at specific locations) and can be a stepping stone for the development of soft robotics, and even as biomimetic synthetic analogs of protocells.

Microfluidics (MF) significantly reduces the volumes of reactants required, reduces reaction times and increases mass and heat transfer rates [1]. Droplet based microfluidics retain the above advantages while compartmentalization of the reactants inside individual micro-vessels provides several additional benefits such as control over interfacial properties of the solution, transport of cargo around the micro-chip (inside the vessel), the ability to perform more complex reactions (combing multiple droplets allows for multiple step reactions), the possibility of performing chemical and bio-chemical reactions at desired locations within the fluidic chip [2].

There has been a wide variety of chemical and biological reactions performed using droplet microfluidics [3-5]. Many research groups have looked at developing droplet based microfluidic chips for biological assays. Droplet microfluidics encapsulates the multiple reagents (required in many assays) inside individual droplets [6], reducing reagent volumes required for the reactions, which in turn can speed up the analysis time. Barbulovic-Nad *et al.* [7] have developed a method for the DMF (mechanism described in Chapter 1) driven cytotoxicity assay in which they tested Jurkat T-Cells. The authors first tested the viability of transporting droplets containing various concentrations of cell suspensions across an array of electrodes. It was found that there was no difference in transporting droplets containing cells compared to droplets without cells. However, it was difficult to manipulate the droplets which contained the cells as the cells tended to stick to

the substrate. This challenge was overcome through the introduction of a non-ionic surfactant, namely pluronic F68, which prevented non-specific protein adsorption. The toxicology assay involved introducing various concentrations of the surfactant tween 20 (which is lethal to mammalian cells) to the cells. This was achieved by transporting three droplets that contained the cells, the required reagents, and a fluorescent dye, respectively, across the array of electrodes, and subsequently merging the droplets together (Figure 8.1).

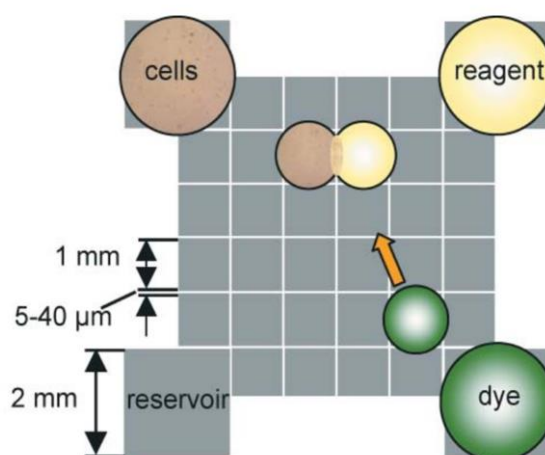


Figure 8.1 Schematic representation of the DMF chip used for the merging of the three droplets in the toxicology assay. Reproduced with permission from [7].

Using this method to move droplets across the chip had no adverse effect on cell viability or reproduction. Barbulovic-Nad *et al.* also examined the protein structures after actuation using mass spectrometry and found no adverse effects, which suggested that DMF could be used to move cells without major consequences on the biochemistry of the cells. The results showed that this novel DMF system used 30 times less reagent and its sensitivity was 20 times higher compared to the standard well plate method. There were evaporation problems in the experiments, which were overcome through controlled experimental conditions. In contrary to this approach, the chemotactic droplets we have developed in Chapter 4 and 5 are based solely on ILs, which have negligible vapour pressure and therefore, do not evaporate, showing their potential for biochemical assays. Moreover, our chemo- and electro-tactic methods use a significantly simpler method for droplet manipulation.

Brouzes *et al.* [8] have developed a droplet-based microfluidic system for high-throughput single cell screening. This work describes a method to screen a drug library

for their cytotoxic effect on U937 human monocytic cells. Similarly to the previous work described, Brouzes *et al.* tested the viability of the cells to survive and reproduce within aqueous micro-droplets over four days. The authors then developed an optically-coded droplet library for identifying droplet composition during the assay. In this work the cells were encapsulated within aqueous droplets and transported using an immiscible oil phase. The cells and reagents were introduced as separate droplets and mixed together at a specific destination within the chip which allowed for electrically controlled merging of droplet pairs. The merged droplets were then put through a mixing module which ensured a thorough mix of the cells with the dyes. This was followed by the droplets entering a delay lane which allowed the droplets to incubate for 15 minutes before going onto the detection module (Figure 8.2). Using this droplet microfluidic platform the authors successfully developed a flexible method for droplet generation and manipulation, which can be used for multiple types of cell screening. However, in order to create the flow within the chip, external pumps were required. In contrast to this approach, the chemotactic droplets described in Chapter 4 do not require any external power source to generate droplet movement. This novel method for screening of cells could possibly be improved by using chemotactic droplets.

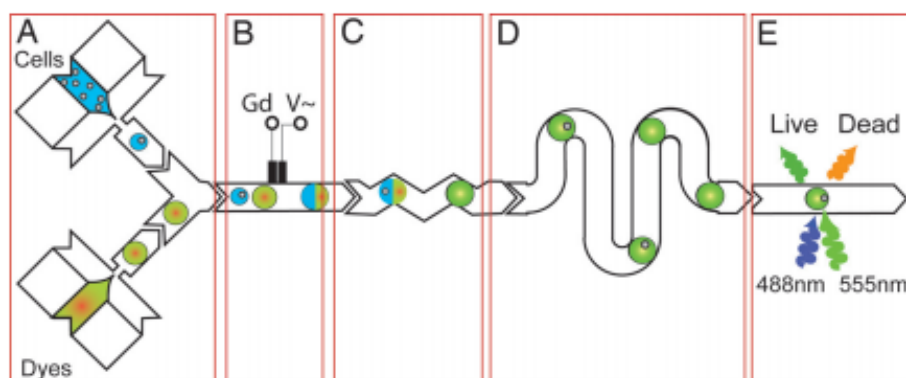


Figure 8.2 Schematic representation of the microfluidic device used for the high-throughput screening of a single cell. A – Droplets containing cells and dye are introduced to the device; B – Droplets are electronically merged; C – Contents of the two droplets are mixed together; D – Delay lane where droplets are incubated for 15 minutes; E – Detection module for detecting live and dead cells. Reproduced with permission from [8].

Another biological reaction that has been performed using droplet microfluidics is glucose detection. The development of glucose detection methods has been an area of extensive research in recent years, as there has been much interest in developing

autonomous methods for monitoring glucose levels in diabetics. Droplet microfluidics is appealing for glucose sensing because it offers several advantages over conventional systems including reduced reagent volumes and analysis time, and improved mass transfer, while offering the possibility of realising a fully automated and flexible system for glucose detection [9-11]. For example, Srinivasan *et al.* [9] have developed a DMF device for glucose detection that uses a colorimetric method based on Trinders reaction. In this system glucose was enzymatically oxidised to gluconic acid and hydrogen peroxide. Following oxidation, hydrogen peroxide was reacted with 4-aminoantipyrine and *N*-ethyl-*N*-sulfopropyl-*m*-toluidine to form a purple coloured complex ( $\lambda_{\max} = 545$  nm). The glucose sensing was performed on a DMF chip in three steps. The first step involved the introduction of the separate droplets containing the glucose sample and the sensing reagents. Using electrowetting, the droplets were merged and then mixed. The absorbance of the droplet was then recorded using a light emitting diode and a photodiode. The authors stated that the enzymatic activity was not reduced using the electrowetting technique.

In a different approach, Hadwen *et al.* [11] developed an ‘*active matrix electrowetting on dielectric device*’ (AM-EWOD) that has integrated droplet sensing capabilities including multiple bioassays. In particular it permitted colorimetric detection of glucose in human blood serum. AM-EWOD differs from standard EWOD (described in Chapter 2) in that the patterned array of electrodes was replaced by a thin film transistor array. The array also had an inbuilt impedance sensor which was used to detect the presence, location and size of the droplets. The glucose assay used was an enzymatic colorimetric assay in which glucose oxidase and horse radish peroxidase were used to produce a change in colour of the droplet with an absorbance lambda maximum centred at 514 nm. Similar to the previous example described, the droplets were loaded onto the chip where they were merged and mixed using AM-EWOD technique (Figure 8.3). The authors used a camera and a custom written program to evaluate the results, which were comparable with the standard plate method.

While the examples described above illustrate several new and exciting methods for glucose detection, both methods required relatively high voltages (20 V) and complicated chip designs (array of electrodes) to achieve droplet actuation and analyte detection. These disadvantages could potentially be addressed using the electro-tactic droplets described in Chapter 5. The fluidic channels/chips used in our studies are much

simpler (can work with only two electrodes) and a considerably smaller voltage (6 – 9 V) is required for droplet movement. These droplets are also made solely of ILs which are non-volatile and excellent solvents for a wide range of potential reactants.

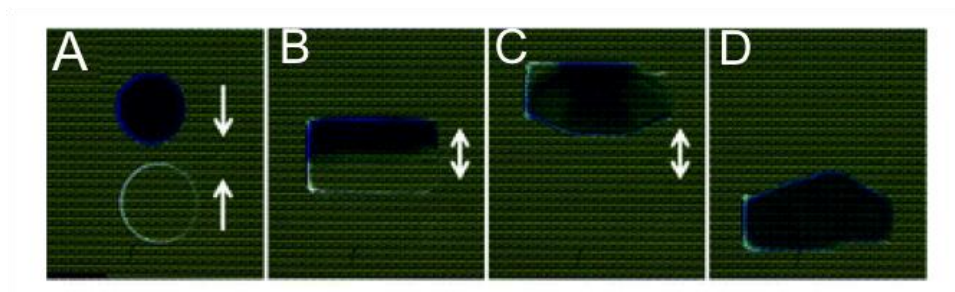


Figure 8.3 Series of snap shots showing droplet mixing using the DMF device. Firstly two heterogeneous droplets are drawn together (A); the merged droplet is then rapidly mixed by shuttling the droplet back and forth across the array of electrodes (B, C) in order to achieve full mixing (D). Reproduced with permission from [11].

Other reactions performed in droplet microfluidics include materials synthesis [2], mostly focused on the synthesis of micro- and nano- particles [12]. In these systems the reagents are generally dissolved in an aqueous solution which is then merged with an oil phase. Upon merging, the aqueous solution forms droplets, which are carried throughout the chip by the oil phase. The winding channels of the chip are used to mix the reagents within the droplets. Other reactions performed using droplet microfluidics include titrations [13] and crystal growth [14].

Generally the movement of droplets within droplet microfluidic devices is based on two types of mechanisms. In the first mechanism, droplets are formed by merging flows of immiscible liquids usually comprising an oil and aqueous phase. Upon merging of the flows, one phase forms the droplets while the second phase carries the droplets through the system. In the second mechanism, individual droplets are moved across arrays of electrodes through electrowetting. While both of these methods have several advantages over regular microfluidics, the major disadvantage is that both systems require complex set-ups, complicated chip designs or relatively large power consumption to actuate/move the droplets. We have described in Chapter 4 and 5 chemotactic and electrotactic self-propelling ionic liquid droplets. The chemotactic ionic liquids droplets provide autonomous energy-free droplet movement to desired destinations, while the electrotactic ionic liquid droplets allow for reversible movement and can be moved to

several destinations within a microfluidic chip. Both of these methods provide a means for moving droplets within microfluidic channels with either zero or very small external power. Furthermore, the experimental set-up and chip designs/fabrication for both methods are relatively simple compared to electrowetting and oil/water phase approaches.

Chapter 4 and 5 describe single component IL droplets capable of controlled movement to a pre-determined destination. These droplets have a simple composition (compared to the conventional multi-component droplets [15,16] described in Chapters 1 and 2) and relatively simple experimental set-up (compared to the various complex digital microfluidic (DMF) systems described in Chapter 2 [17,18]). These properties make IL droplets ideal candidates for micro-vessels for chemical reactions as further reagents added to the droplets should not affect their mobility.

In the following sections we will explore how these chemotactic droplets could be used to perform polymerisation reactions at pre-determined locations, how the chemotactic signal could be controlled and how autonomous leak detection and repair might be achieved.

### **8.1.2 Polymerisations at pre-determined locations**

One of the main advantages of droplet based microfluidics is that any product formed is contained within the droplet and therefore, can be transported to a collection point. This prevents any solid material from building up on the walls of the microfluidic chip. Another advantage is that the environment in which the product is contained is controlled. Many research groups have considered these advantages and employed droplet based microfluidic devices for polymerisation reactions [19,20]. An example of polymerisation reaction within droplets was shown by Li *et al.* [19], who demonstrated a multi-step microfluidic approach for polyaddition and polycondensation reactions within droplets. This process involved two successive reactions; the first reaction was the photo-initiated free radical polymerization of tri(propylene glycol) diacrylate (TPGDA) within droplets. The heat generated from this exothermic reaction initiated the second reaction which was the polycondensation of poly(propylene glycol) tolylene 2,4-diisocyanate (PU-pre) with diethanolamine (DEA). These reactions resulted in the continuous microfluidic synthesis of interpenetrating polymer network (IPN) microbeads. The reagents for the free radical polymerisation were introduced via three inlets and mixed in mixing channels. The mixed solutions were then passed into a channel which was designed to fragment the solution

from a laminar flow into droplets. These droplets were then carried into the polymerisation zone where they were irradiated with UV light to initiate polymerisation and finally onto the collection outlet (Figure 8.4).

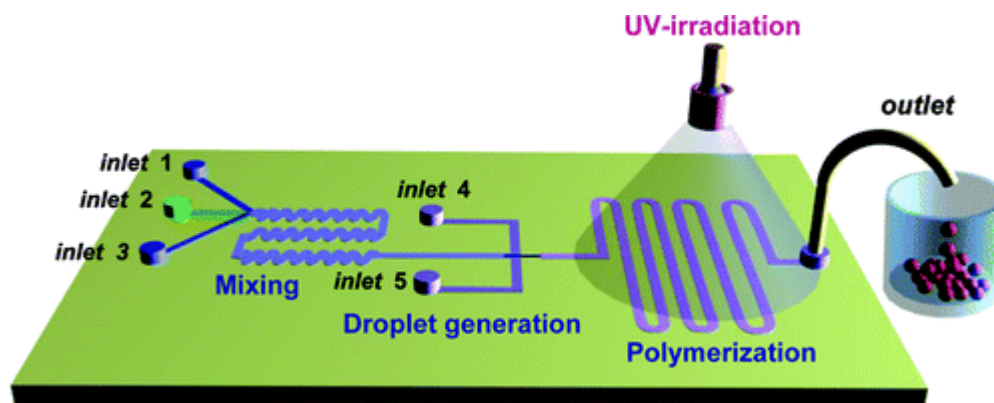


Figure 8.4 Schematic of microfluidic reactor used for the multistep polymerisation reactions within droplets. Reproduced with permission from [19].

Although this work presented a novel and exciting approach to autonomous and continuous synthesis of IPNs, it required relatively complicated experimental set-up and flow control to move both the fluid and the generated droplets. In Chapter 4 and 5 of this report we have demonstrated a much simpler method for transporting fluids around a microfluidic device; we therefore, wanted to test the possibility of moving a droplet which contained a cocktail needed for the synthesis of a polymer network to a desired destination and then perform the polymerisation at the desired location, on demand.

In order to determine if chemotactic ionic liquid droplets were suitable to be used as vessels for polymerisation reactions, a polymerisation cocktail was made by mixing 0.1936 g (400  $\mu\text{mol}$ ) of the monomer tributylhexyl phosphonium sulfopropyl acrylate [ $\text{P}_{4,4,4,6}$ ][SPA], the crosslinker polypropylene glycol diacrylate (PPO 800) (5 %), and the white light initiator phenylbis(2,4,6 trimethylbenzoyl)pospine oxide (PBPO) (2 mol%) in 0.12 mls of acetonitrile. This cocktail formulation was chosen as Tudor *et al.* had previously demonstrated that this composition was suitable for photo-polymerisation of ionogels [21][22]. 0.1 g of this cocktail was then added to 0.1 g of [ $\text{P}_{6,6,6,14}$ ][Cl]. In this mixture, the [ $\text{P}_{6,6,6,14}$ ][Cl] IL acted as the vehicle for moving the monomeric IL cocktail to the desired destination for polymerisation. For this purpose, the channels were filled with a  $10^{-2}$  M solution of NaOH followed by the addition of 100  $\mu\text{l}$  – 200  $\mu\text{l}$  of  $10^{-2}$  M HCl to

the desired destination. Once placed in the channel, the droplet began to move (movement of these chemotactic droplets is described in Chapter 4) towards the source of the chemoattractant. Although the speed of the droplet was not measured, the added cocktail did not seem to have any adverse effect on the speed of the droplet during these experiments. This was due to limited interaction between the polymerisation cocktail and the carrier IL ( $[P_{6,6,6,14}][Cl]$ ), thus the  $[P_{6,6,6,14}]$  surfactant was able to diffuse freely from the droplet into the aqueous phase. Once the droplet reached the source of chemoattractant, the droplet was exposed to white light irradiation for approximately 1 min in order to achieve the polymerisation of  $[P_{4,4,4,6}][SPA]$ . This resulted in the formation of a soft polymer gel consisting of a crosslinked poly( $[P_{4,4,4,6}][SPA]$ ) (Figure 8.5) network dispersed through the  $[P_{6,6,6,14}][Cl]$  IL droplet.

These results indicate that self-propelled ionic liquid droplets have potential to act as micro-vessels for polymerisation reactions. Future work in this area will be based on determining the ideal cocktail mixtures to create gels with desired properties at specific locations. The ratio between the “vehicle” IL and the monomeric mixture IL will also be studied in order to determine the best parameters for droplet mobility and speed.

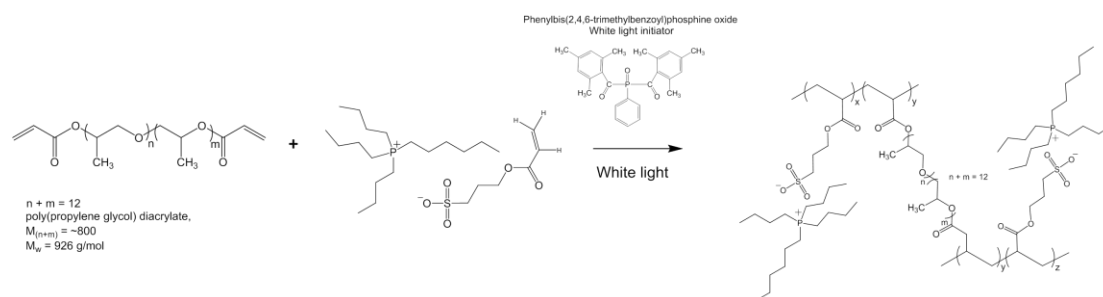


Figure 8.5 Polymerisation scheme of  $[P_{4,4,4,6}][SPA]$  for the formation of a soft polymer gel consisting of a crosslinked poly( $[P_{4,4,4,6}][SPA]$ ) network dispersed through the  $[P_{6,6,6,14}][Cl]$  IL droplet.

## 8.2 Chemotactic droplets in non-geometrically confined environments

### 8.2.1 Introduction

All of the examples of droplet movement described thus far have involved channelled environments. There have been a number of systems described in recent literature in which vehicle movement occurred across the air/liquid interface in channel free systems [16,23-25]. In these examples the “vehicles” propelled themselves in open systems (*e.g.* a petri dish) by asymmetrically altering the surface tension of the aqueous phase around the “vehicle” to induce Marangoni-like flows.

Diguet *et al.*[23] demonstrated the photo-controlled movement of an oleic acid droplet resting on an aqueous solution which contained the photo-sensitive surfactant AzoTAB. The droplet was moved by irradiating half of the droplet with 365 nm or 475 nm of light, respectively. When the AzoTAB surfactant was exposed to 365 nm of light it was made to isomerise to its *cis* configuration. In this configuration the AzoTAB had a higher surface tension ( $8 \text{ mN m}^{-1}$ ) than in the *trans* configuration ( $7 \text{ mN m}^{-1}$ ). Therefore, when half of the droplet was illuminated with 365 nm light it was made to follow the light source as the surface activity of the surfactant was higher compared with the non-irradiated section. When the droplet was irradiated with 475 nm light the AzoTAB isomerised to the *trans* configuration and thus lowered the surface tension, which resulted in the droplet being repelled by the light. In a different approach, Toyota *et al.* [25] demonstrated a unique self-propelling droplet which produced the surfactant via chemical reactions on the droplet surface. The droplets moved in a unidirectional fashion within a petri dish as the reaction that produced the surfactant required for movement only occurred at one side of the droplet.

These studies demonstrate interesting methods for moving droplets without the requirement for channels. We have already demonstrated that the droplets described in Chapter 4 and 6 could be used for various types of reactions within channelled systems. In the following section, we explore the possibility of using chemotactic droplets for 2D movement in an open system that does not contain any channels.

### 8.2.2 Autonomous leak detection and repair

The mechanism for the movement of the  $[\text{P}_{6,6,6,14}][\text{Cl}]$  chemotactic droplets is as described in Chapter 4. In this study these droplets were moved to multiple destinations inside a channel free fluidic system by sequential addition of chemoattractant. For this, a petri dish was initially filled with a solution of  $10^{-2} \text{ M}$  NaOH followed by the addition of the chemoattractant (a  $10^{-2} \text{ M}$  solution of HCl) at three different locations at different

time intervals. The HCl solution was introduced through tubes placed beneath the water level to ensure the water surface was not disturbed by the introduction of the chemoattractant. Once the chemoattractant was added, a  $\text{Cl}^-$  gradient was created leading to the source of the chemoattractant (first tube, Figure 8.6), causing the droplet to move towards the first tube. Further additions of chemoattractant resulted in stronger  $\text{Cl}^-$  gradients being produced, which resulted in the droplet migrating towards the source of fresh chemoattractant (second and third tube, respectively, Figure 8.6).

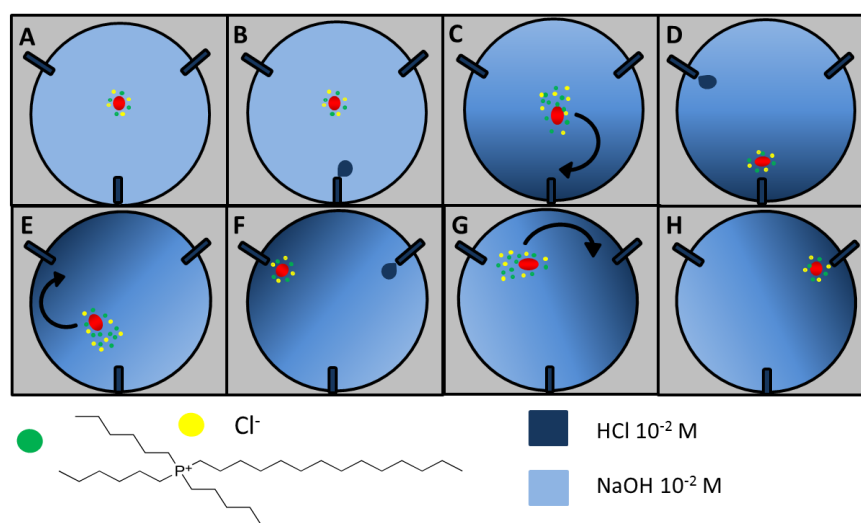


*Figure 8.6 Diagram of the two dimensional movement of a chemotactic IL droplet in a petri dish. A – Droplet is resting on the surface of the aqueous solution ( $10^{-2}$  M NaOH), no directional movement is observed; B – Introduction of chemoattractant ( $100 - 200 \mu\text{l}$  of a solution of  $10^{-2}$  M HCl) through the central tubing; C - Droplet senses the introduction of the chemoattractant and begins to move toward the source of the chemoattractant; D – Droplet arrives at the chemoattractant source and more chemoattractant is introduced through the next tubing (top left); E – The introduction of fresh chemoattractant creates a stronger gradient; F – Droplet arrives at the second chemoattractant source and fresh chemoattractant is added at a new location (third tubing, top right); G – The droplet moves towards the last source of chemoattractant; H – Droplet arrives at final destination.*

Using this method we have shown that a single droplet could be moved to three separate locations within a petri dish (Figure 8.7). Bromocresol purple was added to the HCl solution for a better visualisation of the introduction of chemoattractant. Bromocresol purple has a  $\text{pK}_a$  of 6.3. In acidic solutions below  $\text{pH}$  6.3 the dye has a yellow colour while this changes to purple at  $\text{pH}$  values greater than 6.3. As the droplet moved towards the source of the chemoattractant, it disturbed the dye present at the

surface of the solution. This was due to the release of the IL surfactant. It was observed that the disturbance was greater behind the droplet compared to the front; this further reinforced the mechanism proposed for the chemotactic droplets, which stated that the chemotaxis of the IL droplets was due to asymmetric release of surfactant from the droplet to the aqueous solution.

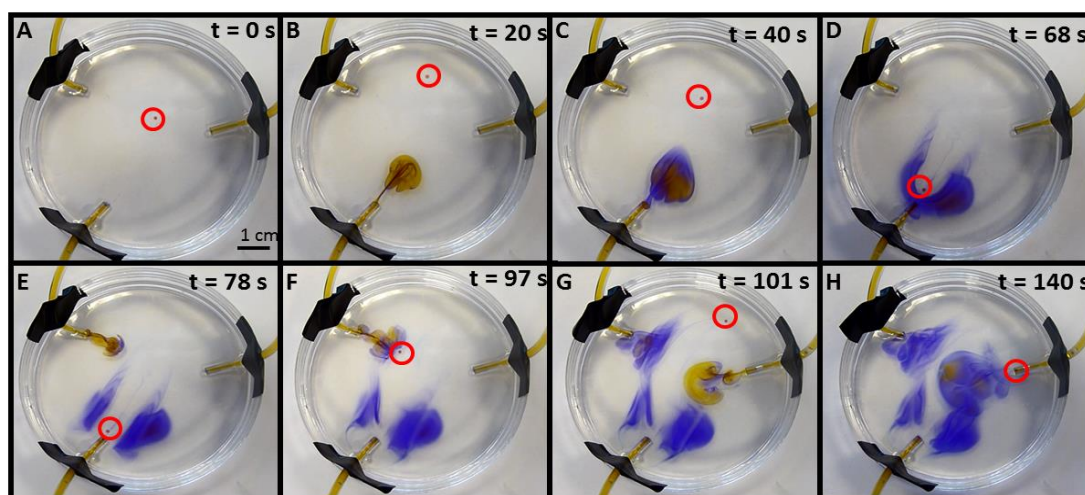


*Figure 8.7 Snapshots showing the self-propelled movement of an IL droplet to three separate locations within a petri dish upon sequential introduction of chemoattractant. A – Droplet is placed onto the  $10^{-2}$  M NaOH solution within the petri dish prior to chemoattractant addition; B – Chemoattractant ( $100 - 200 \mu\text{l } 10^{-2}$  M HCl) is introduced to the system via the first tube; C – Once the  $\text{Cl}^-$  gradient is established the droplet migrates towards the chemoattractant source; D – Droplet arrives at first chemoattractant source; E – Further chemoattractant is added via the second tube; F – Droplet migrates towards second tube; G – chemoattractant is added via the third tube; H – Droplet arrives at the third chemoattractant source. Bromocresol purple was added to the HCl solution for a better visualisation of the introduction of chemoattractant.*

If these droplets are combined with the polymerisation droplets described earlier, they could be used to detect a  $\text{Cl}^-$  leak in a fluidic device and potentially block the leak once polymerisation occurred. As these droplets are composed of ILs, the structure of the IL itself can be tailored to allow chemotactic movement in multiple chemical gradients, which means that they could be used for multiple leak detection scenarios. As much research has gone into biocompatible ILs, biocompatible surfactant ILs could be used for the production of chemotactic droplets for use in the biomedical field.

### 8.2.3 Controlling the chemotactic signal in open systems

One of the possible shortcomings of the chemotactic droplets described in Chapter 4-6 is that the signal (chemical gradient) required for droplet movement can be hard to control and maintain. In Chapter 5 this issue was addressed by introducing electrodes into the channels and applying relatively low voltages (6 – 9 V) in order to dynamically produce and maintain the chemical gradients required for droplet movement. However, in these experiments, the droplet must be constrained in channels and a power source is required to control the gradients. In a follow-up study we investigated ways in which the chemotactic signal could be turned on via chemical means in an open (non-channel) system. This enables control over where reactions will occur in 2D space and when these reactions will take place. In addition, all reagents needed for the reaction coexist separately (in different droplets) in the same environment until the chemotactic signal is turned on. Once the signal is turned on, the droplets migrate towards either the source of the chemoattractant, or towards each other, and eventually merge and react.

In order to control or “turn on” the chemotaxis signal, a three droplet system was designed. Initially, two droplets containing 2M benzoyl chloride in  $[P_{6,6,6,14}][Cl]$  were placed onto a solution of  $10^{-2}$  M NaOH in a petri dish, where they remained separate and stationary. These droplets have a low contact angle and appear relatively “flat” on the aqueous solution surface. At this stage, the surface of the droplets is saturated with benzoyl chloride. The benzoyl chloride is hydrolysed by the basic solution, resulting in the release of HCl from the droplets into the aqueous phase, creating a chemical gradient around them. However, little to no movement is observed from the droplets (any movement observed is random motion). The third “signaller” droplet contains 0.5 M of octylamine in  $[P_{6,6,6,14}][Cl]$ . When the “signaller” droplet is added to the solution, the release of the octylamine and the  $[P_{6,6,6,14}]^+$  surfactants lowers the surface tension of the aqueous phase and changes the morphology of the stationary droplets from a low contact angle to a high contact angle. This initial release of surfactant from the signaller droplets also results in the two initial droplets being pushed away from the “signaller” droplet; Due to the change of contact angle (as a result of the release of the surfactants), it is believed that at this point the  $[P_{6,6,6,14}]^+$  saturates the aqueous/droplet interface from where it can diffuse into the aqueous solution. This causes the droplets to begin attracting each other (due to the presence of the  $Cl^-$  gradient, created from the hydrolysis of benzoyl chloride) and eventually they merge at a central location. After roughly 30s the “signaller” droplet also meets and merges with the merged droplet (Figure 8.8). Similar

behaviour is obtained when the “signaller” droplet is neat  $[P_{6,6,6,14}][Cl]$ , indicating that the presence of octylamine is not essential.

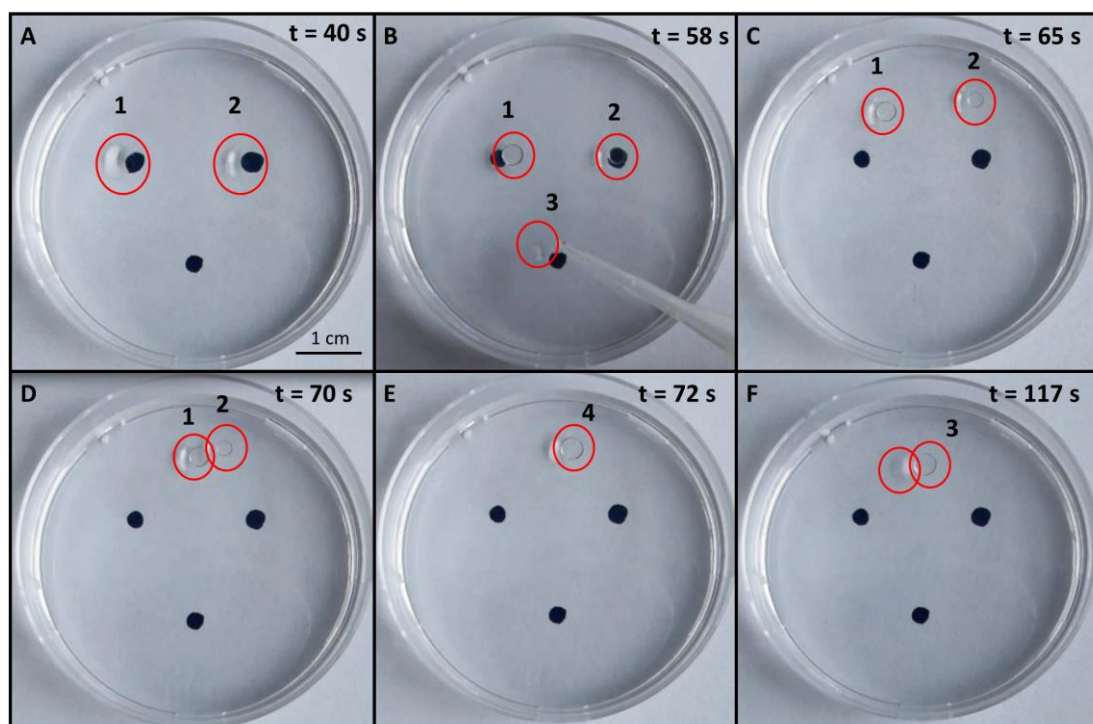


Figure 8.8 Snapshots showing control over the chemotactic signal. A – droplet 1 (2M Benzoyl chloride in  $[P_{6,6,6,14}][Cl]$ ) and droplet 2 (2M Benzoyl droplets in  $[P_{6,6,6,14}][Cl]$ ) sitting on a solution of  $10^{-2}$  M NaOH for 40s. B – droplet 3 (0.5M octylamine in  $[P_{6,6,6,14}][Cl]$ ) is added, causing a change in contact angle of droplet 1 and droplet 2. C – Droplet 1 and 2 are pushed away from droplet 3. D – Droplet 1 is attracted towards droplet 2. E – Droplet 1 and 2 merge to create droplet 4. F – droplet 3 is attracted by droplet 4.

Three control studies were performed; the first test involved three neat IL ( $[P_{6,6,6,14}][Cl]$ ) droplets which were placed onto a petri dish containing a solution of  $10^{-2}$  M NaOH. Only random motion was observed by these IL droplets with no obvious inter-droplet attraction behaviour. The second test involved placing three IL droplets (each containing 0.5 M octylamine) onto a petri dish filled with a solution of  $10^{-2}$  M NaOH; Once again no directional movement of the three droplets was observed. The third test was performed in the same manner as the second test, but with each droplet now containing 2M benzoyl chloride. Once again, no obvious attraction of the droplets was observed. It was noted that if a neat  $[P_{6,6,6,14}][Cl]$  IL was used as the signaler droplet (i.e. not containing octylamine), this could still turn on movement and attract the two 2M benzoyl chloride IL ( $[P_{6,6,6,14}][Cl]$ ) droplets. However, the speed of this process was

slower than when octylamine was included. These results are exciting as it demonstrates for the first time a system in which droplets can coexist separately, and their controlled movement and merging turned on via a separate signaler droplet. Introduction of reaction precursors into the droplets obviously offers many exciting possibilities, including localised chemical synthesis.

#### 8.2.4 Micro-vessels for chemical synthesis in open systems

In order to determine if we could use this system for chemical synthesis, a similar three droplet system was used. However, this time the two initial droplets contained precursors for the synthesis of *n*-(4-nitrophenyl)benzamide. The initial stationary droplets were (1) 2M benzoyl chloride in [P<sub>6,6,6,14</sub>][Cl] and (2) 2M 4-nitroaniline in [P<sub>6,6,6,14</sub>][DCA]. [P<sub>6,6,6,14</sub>][DCA] was used as the solvent for 4-nitroaniline because of the low solubility of the DCA<sup>-</sup> ion in the aqueous solution. This ensured that there was no obvious leaching of 4-nitroaniline into the aqueous phase while the chemotactic signal was “turned off”. The signaler droplet was 0.5M octylamine in [P<sub>6,6,6,14</sub>][Cl]. Initially the two reactive droplets were placed on the surface of the 10<sup>-2</sup> M NaOH solution. Little to no movement of these droplets was observed. Once the signaler droplet was added, the two reactive droplets underwent morphology changes (a low contact angle to a high contact angle) and moved away from the signaler droplet. In this instance only droplet (1) contains benzoyl chloride which creates a Cl<sup>-</sup> gradient attracting droplet (2) [P<sub>6,6,6,14</sub>][DCA] towards it (Figure 8.8). Once the droplets merged the precursors come in contact and the reaction is initiated (Figure 8.9). As the viscosity of the ILs is relatively high (1824 mPas[26]), and the mixing of the precursors inside the droplets is solely due to diffusion, this process is relatively slow (several hours).

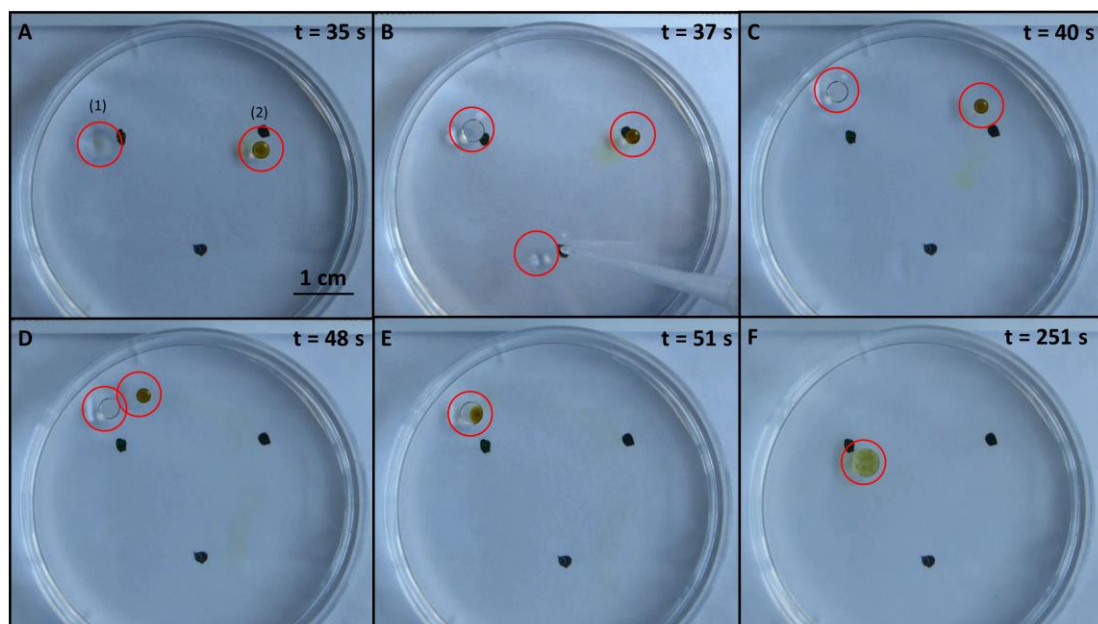


Figure 8.9 Snapshots showing chemical synthesis using chemotactic droplets in a petri dish. A – The two reactive droplets (1) 2M Benzoyl chloride in  $[P_{6,6,6,14}][Cl]$  and (2) 2M 4-Nitroaniline in  $[P_{6,6,6,14}][DCA]$  sitting on a solution of  $10^{-2}$  M NaOH. B – “signaler” droplet is added, followed by a change in morphology of the original droplets. C – Droplets are pushed away from signaler droplet. D –  $[P_{6,6,6,14}][DCA]$  droplet is attracted recruited to the  $[P_{6,6,6,14}][Cl]$  droplet. E – Droplets merge. F – Reaction occurring inside the merged droplet.

4-nitroaniline reacts with benzoyl chloride to form *n*-(4-nitrophenyl)benzamide and HCl as per the reaction scheme below (Figure 8.10).

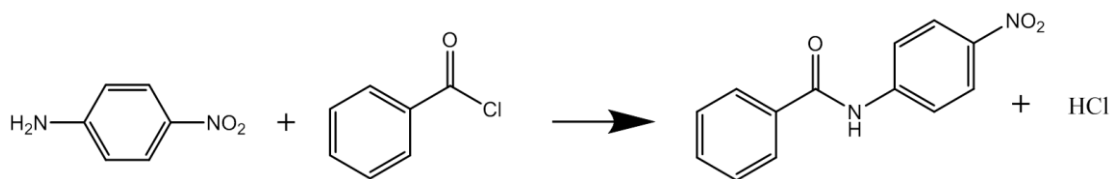


Figure 8.10 Reaction scheme between 4-nitroaniline and benzoyl chloride resulting in the formation of *n*-(4-nitrophenyl)benzamide.

In order to test whether a reaction was indeed happening within the merged droplet  $^1H$  NMR studies were performed using a 400 MHz on a Bruker Advance Ultrashield NMR spectrometer (Coventry, UK). In order to produce enough product for  $^1H$  NMR analysis, six reactions were run simultaneously. Each reaction involved placing a 10  $\mu$ l droplet of 2M benzoyl chloride in  $[P_{6,6,6,14}][Cl]$  and a 10  $\mu$ l droplet of 2M 4-nitroaniline in  $[P_{6,6,6,14}][DCA]$  onto a petri dish filled with  $10^{-2}$  M NaOH. A signaler

droplet (neat  $[P_{6,6,6,14}][Cl]$  IL) was then introduced into a separate surface location. This immediately turned on chemotactic behaviour leading to merging of the 4-nitroaniline droplets with the benzoyl chloride droplets. After 20 minutes, the reaction droplets were removed and combined into a single vial. Any remaining aqueous solution was removed via pipetting and the reaction droplet dissolved in deuterated chloroform and analysed by  $^1H$  NMR. A duplicate set of control reactions was run with the droplets left to react for a total of two hours. As previously, each of the reaction droplets were removed and combined into a single vial, dissolved in deuterated chloroform and analysed by  $^1H$  NMR. For comparison, reference  $^1H$  NMR spectra were obtained for benzoyl chloride in  $[P_{6,6,6,14}][Cl]$ , 4-nitroaniline in  $[P_{6,6,6,14}][DCA]$  and purified n-(4-nitrophenyl)benzamide (synthesised separately). All  $^1H$  NMR spectra were compared and assigned (Figure 8.10).

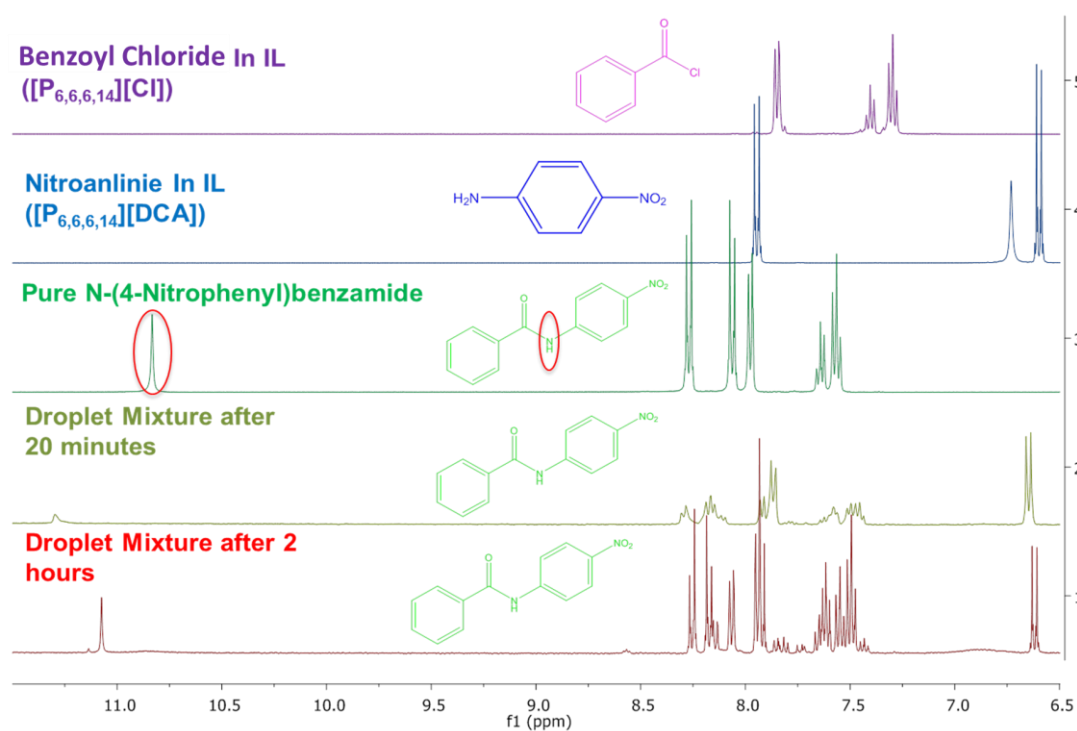


Figure 8.11.  $^1H$  NMR spectra of the (1) two hour reaction droplet, (2) the twenty minute reaction droplet, (3) pure n-(4-nitrophenyl)benzamide, (4) 4-nitroaniline in  $[P_{6,6,6,14}][DCA]$  and (5) benzoyl chloride in  $[P_{6,6,6,14}][Cl]$ .

The  $^1H$  NMR spectra for the pure n-(4-nitrophenyl)benzamide, benzoyl chloride and 4-nitroaniline all agreed with previous literature.

Benzoyl chloride  $^1H$  NMR (400 MHz,  $CDCl_3$ ): 7.4 (m, 1H, CH), 7.5 (m, 2H, CH), 7.9 (d, 2H, CH) [27].

4-nitroaniline  $^1\text{H}$  NMR (400 MHz,  $\text{CDCl}_3$ ): 6.7 (d, 2H, CH), 6.8 (s, 2H,  $\text{H}_2\text{N}$ ), 7.9 (d, 2H, CH) [28].

n-(4-nitrophenyl)benzamide  $^1\text{H}$  NMR (400 MHz,  $\text{CDCl}_3$ ): 7.5 – 7.6 (m, 3H, CH), 7.9 (d, 2 H, CH), 8.03 (d, 2 H, CH), 8.3 (d, 2 H, CH), 10.6 (s, 1H, NH) [29].

Both the droplet mixtures, after 20 minutes (spectrum 2, Figure 8.10) and after two hours (spectrum 1, Figure 8.10), contained signals arising from the starting materials benzoyl chloride (spectrum 5, Figure 8.10) and 4-nitroaniline (spectrum 4, Figure 8.10). In order to determine if a reaction was indeed occurring, the signal corresponding to the NH proton (10.6 ppm, Figure 8.10, spectrum 3) from n-(4-nitrophenyl)benzamide was monitored (highlighted in Figure 8.10, spectrum 3). As can be seen in spectrum 2 (Figure 8.10), this signal is present but very weak after 20 minutes. However, after two hours (spectrum 1, Figure 8.10) this signal is much stronger, indicating that the reaction is indeed taking place and formation of n-(4-nitrophenyl)benzamide is occurring inside the reaction droplet.

### 8.3 Future prospects

Further work in this area will involve optimising and investigating the parameters for achieving 2D movement of the droplets in channel-free systems. The role of the “signaler” droplet in controlling the chemotactic signal needs to be thoroughly investigated and the physical parameters (*i.e.* surface tension, droplet position, droplet volume) need to be optimised. A scoping exercise would be useful to determine the potential role these self-propelled droplets might play in various chemical synthesis processes.

One of the drawbacks of these droplets is that they have only been demonstrated at the liquid/air interface. Developing a system where the droplets can evolve from 2D to 3D movement will offer many exciting opportunities, for example it will allow for the location of droplets in 3D space where they can perform the same type of tasks. Submerged chemotactic droplets could work in sealed chips, making them portable and opening further avenues for potential applications. We believe that these autonomous biomimetic droplets are a stepping-stone in the development of synthetic protocell models, and they offer a truly unique way of controlling flow within microfluidic devices.

## 8.4 References

1. Haeberle, S.; Zengerle, R. Microfluidic platforms for lab-on-a-chip applications. *Lab on a Chip* **2007**, *7*, 1094-1110.
2. Song, H.; Chen, D.L.; Ismagilov, R.F. Reactions in droplets in microfluidic channels. *Angew. Chem. Int. Ed.* **2006**, *45*, 7336-7356.
3. Jebrail, M.J.; Ng, A.H.; Rai, V.; Hili, R.; Yudin, A.K.; Wheeler, A.R. Synchronized synthesis of peptide-based macrocycles by digital microfluidics. *Angew. Chem. Int. Ed.* **2010**, *49*, 8625-8629.
4. Chang, Y.-H.; Lee, G.-B.; Huang, F.-C.; Chen, Y.-Y.; Lin, J.-L. Integrated polymerase chain reaction chips utilizing digital microfluidics. *Biomed. Microdevices* **2006**, *8*, 215-225.
5. Wang, Y.; Zhao, Y.; Cho, S.K. Efficient in-droplet separation of magnetic particles for digital microfluidics. *Journal of Micromechanics and Microengineering* **2007**, *17*, 2148.
6. Guo, M.T.; Rotem, A.; Heyman, J.A.; Weitz, D.A. Droplet microfluidics for high-throughput biological assays. *Lab on a Chip* **2012**, *12*, 2146-2155.
7. Barbulovic-Nad, I.; Yang, H.; Park, P.S.; Wheeler, A.R. Digital microfluidics for cell-based assays. *Lab on a Chip* **2008**, *8*, 519-526.
8. Brouzes, E.; Medkova, M.; Savenelli, N.; Marran, D.; Twardowski, M.; Hutchison, J.B.; Rothberg, J.M.; Link, D.R.; Perrimon, N.; Samuels, M.L. Droplet microfluidic technology for single-cell high-throughput screening. *Proceedings of the National Academy of Sciences* **2009**, *106*, 14195-14200.
9. Srinivasan, V.; Pamula, V.K.; Fair, R.B. Droplet-based microfluidic lab-on-a-chip for glucose detection. *Anal. Chim. Acta* **2004**, *507*, 145-150.
10. Srinivasan, V.; Pamula, V.; Pollack, M.; Fair, R. In *A digital microfluidic biosensor for multianalyte detection*, Micro Electro Mechanical Systems, 2003. MEMS-03 Kyoto. IEEE The Sixteenth Annual International Conference on, 2003; IEEE: pp 327-330.
11. Hadwen, B.; Broder, G.; Morganti, D.; Jacobs, A.; Brown, C.; Hector, J.; Kubota, Y.; Morgan, H. Programmable large area digital microfluidic array with integrated droplet sensing for bioassays. *Lab on a Chip* **2012**, *12*, 3305-3313.
12. Hung, L.-H.; Choi, K.M.; Tseng, W.-Y.; Tan, Y.-C.; Shea, K.J.; Lee, A.P. Alternating droplet generation and controlled dynamic droplet fusion in microfluidic device for cds nanoparticle synthesis. *Lab on a Chip* **2006**, *6*, 174-178.
13. Song, H.; Li, H.-W.; Munson, M.S.; Van Ha, T.G.; Ismagilov, R.F. On-chip titration of an anticoagulant argatroban and determination of the clotting time within whole blood or plasma using a plug-based microfluidic system. *Anal. Chem.* **2006**, *78*, 4839-4849.
14. Zheng, B.; Gerds, C.J.; Ismagilov, R.F. Using nanoliter plugs in microfluidics to facilitate and understand protein crystallization. *Curr. Opin. Struct. Biol.* **2005**, *15*, 548-555.
15. Lagzi, I.; Soh, S.; Wesson, P.; Browne, K.; Grzybowski, B. Maze solving by chemotactic droplets. *J. Am. Chem. Soc.* **2010**, *132*, 1198-1199.
16. Zhang, H.; Duan, W.; Liu, L.; Sen, A. Depolymerization-powered autonomous motors using biocompatible fuel. *J. Am. Chem. Soc.* **2013**, *135*, 15734-15737.

17. Saeki, F.; Baum, J.; Moon, H.; Yoon, J.-Y.; Kim, C.; Garrell, R. Electrowetting on dielectrics (ewod): Reducing voltage requirements for microfluidics. *Polym. Mater. Sci. Eng* **2001**, *85*, 12-13.
18. Malic, L.; Brassard, D.; Veres, T.; Tabrizian, M. Integration and detection of biochemical assays in digital microfluidic loc devices. *Lab on a chip* **2010**, *10*, 418-431.
19. Li, W.; Pham, H.H.; Nie, Z.; MacDonald, B.; Güenther, A.; Kumacheva, E. Multi-step microfluidic polymerization reactions conducted in droplets: The internal trigger approach. *J. Am. Chem. Soc.* **2008**, *130*, 9935-9941.
20. Barnes, S.E.; Cygan, Z.T.; Yates, J.K.; Beers, K.L.; Amis, E.J. Raman spectroscopic monitoring of droplet polymerization in a microfluidic device. *Analyst* **2006**, *131*, 1027-1033.
21. Tudor, A.; Saez, J.; Florea, L.; Benito-Lopez, F.; Diamond, D. Poly (ionic liquid) thermo-responsive hydrogel microfluidic actuators. *Sensors Actuators B: Chem.* **2017**, *247*, 749-755.
22. Tudor, A.; Florea, L.; Gallagher, S.; Burns, J.; Diamond, D. Poly (ionic liquid) semi-interpenetrating network multi-responsive hydrogels. *Sensors* **2016**, *16*, 219.
23. Diguët, A.; Guillermic, R.-M.; Magome, N.; Saint-Jalmes, A.; Chen, Y.; Yoshikawa, K.; Baigl, D. Photomanipulation of a droplet by the chromocapillary effect. *Angewandte Chemie (International ed. in English)* **2009**, *48*, 9281-9284.
24. Byrne, R.; Lopez, F.; Scaramagnani, S.; Higgins, M.; Wallace, G.G.; Diamond, D. Beads, boats and switches: Making things happen with molecular photoswitches. *IEEE* **2009**, 139-143.
25. Toyota, T.; Maru, N.; Hanczyc, M.; Ikegami, T.; Sugawara, T. Self-propelled oil droplets consuming "fuel" surfactant. *J. Am. Chem. Soc.* **2009**, *131*, 5012-5013.
26. Fraser, K.J.; MacFarlane, D.R. Phosphonium-based ionic liquids: An overview. *Aust. J. Chem.* **2009**, *62*, 309-321.
27. Lide, D.R.; Milne, G.W. *Handbook of data on common organic compounds*. CRC press: 1995.
28. Sana, S.; Rajanna, K.C.; Reddy, K.R.; Bhooshan, M.; Venkateswarlu, M.; Kumar, M.S.; Uppalaiah, K. Ultrasonically assisted regioselective nitration of aromatic compounds in presence of certain group v and vi metal salts. *Green and Sustainable Chemistry* **2012**, *2*, 97.
29. Saeed, A.; Hussain, S.; Floerke, U. The crystal structure of 2-nitro-n-(4-nitrophenyl) benzamide. *Turkish Journal of Chemistry* **2008**, *32*, 481-486.

# Appendix A

---

## A.1 Example of droplet chemotaxis

During this project four videos were captured to demonstrate different methods of performing droplet chemotaxis.

[Video 4.1](#) demonstrates the chemotactic movement of a single ( $\sim 10 \mu\text{l}$ )  $[\text{P}_{6,6,6,14}][\text{Cl}]$  droplet. The chemoattractant in this video is a  $10^{-2} \text{ M}$  solution of hydrochloric acid (HCl). The  $\text{Cl}^-$  gradient was formed by initially filling the channel array with a  $10^{-2} \text{ M}$  solution of NaOH. At the desired destination  $100 - 200 \mu\text{l}$  of the  $10^{-2} \text{ M}$  HCl was placed. After approximately 20 s, the droplet was placed at the starting position and spontaneous movement towards the source was observed.

[Video 4.2](#) shows the chemotactic behavior of a ( $\sim 10 \mu\text{l}$ )  $[\text{P}_{6,6,6,14}][\text{Cl}]$  droplet. The chemoattractant in this video is an acrylamide gel which has been previously soaked in a  $10^{-2} \text{ M}$  solution of HCl. The  $\text{Cl}^-$  gradient was formed by initially filling the channel array with a  $10^{-2} \text{ M}$  solution of NaOH. The gel was then placed at the desired destination. After approximately 30 s, the droplet was placed at the starting position and movement towards the gel was observed.

[Video 4.3](#) presents the chemotactic movement of a ( $\sim 10 \mu\text{l}$ )  $[\text{P}_{6,6,6,14}]\text{Cl}$  droplet towards a NaCl source. The chemoattractant in this video is constituted of sodium chloride (NaCl) crystals. The  $\text{Cl}^-$  gradient was formed by initially filling the channel array with a  $10^{-5} \text{ M}$  solution of NaCl. At the desired destination crystals of NaCl ( $\sim 10 \text{ mg}$ ) were placed. After 15 s, the droplet was placed at the starting position and spontaneous movement towards the NaCl crystals was observed.

[Video 4.4](#) shows the chemotactic behavior of 6 ( $\sim 10 \mu\text{l}$ )  $[\text{P}_{6,6,6,14}]\text{Cl}$  droplets. The  $\text{Cl}^-$  gradient generation is obtained similarly as in the first video. After approximately 15 s, three droplets were placed in different starting positions. After these droplets arrive at the destination, three new droplets were placed at different locations inside the fluidic channel. Upon reaching the destination, all droplets merge to form a single larger droplet (Figure 4.6).

# Appendix B

---

## B.1 Electrotactic Ionic Liquid Droplet Video

[Video 5.1](#) presents the electrotactic behaviour of a ( $\sim 10 \mu\text{l}$ )  $[\text{P}_{6,6,6,14}][\text{Cl}]$  droplet. The channel in this video was filled with a solution  $10^{-3} \text{ M}$  NaCl and 9 V was supplied to the electrodes. To reverse the movement of the droplet the polarity of the active electrodes was reversed. To change the trajectory of the droplet, the droplet was moved to the centre of the channel and power was supplied to the electrodes at the desired destination. For convenience the speed of the video was increased by factor of 5.

## B.2 Gradient Analysis Videos

During this study several videos were captured monitoring the dynamic formation of the chloride gradient inside fluidic channels upon applying a potential, by monitoring the evolution of the fluorescence of lucigenin dye. In video 5.2 and 5.3 a solution of  $10^{-3} \text{ M}$  NaCl which contained  $10^{-4} \text{ M}$  lucigenin was used as the electrolyte and a 369 nm led light source was used to excite the dye. In video 5.4 a  $10^{-4} \text{ M}$  lucigenin solution in deionised water was used inside the channel. In all cases, 9 V was applied across the solutions.

[Video 5.2](#) demonstrates the formation of the fluorescent gradient within the electrolyte solution. The formation of a clear fluorescent gradient, was visible after  $\sim 10$  minutes. After 30 minutes the gradient was fully formed and stable. For convenience the speed of the video was increased by factor of 64.

[Video 5.3](#) shows that the formation of the fluorescent gradient was reversible. As previously (video 3.2) the gradient had begun to form after  $\sim 10$  minutes. At this point in the video the polarity of the electrodes was reversed and 9 V was applied for a further 10 minutes. After another 10 minutes it becomes clear that the fluorescent gradient has clearly reversed. For convenience the speed of the video was increased by factor of 64.

[Video 5.4](#) shows that NaCl was required to produce a fluorescent gradient. In this video deionised water was used instead of  $10^{-3} \text{ M}$  NaCl. As it can be seen, no difference across the fluorescence of the solution was noticeable after 12 minutes. For convenience the speed of the video was increased by factor of 32.

# Appendix C

---

## C.1 Signalling and seeking droplets

In this section the required gradients for droplet movement were created by initially filling the channel with a solution of  $10^{-2}$  M NaOH. A signaller droplet ( $10^{-2}$  M  $\text{Cu}(\text{NO}_3)_2$  or  $10^{-2}$  M  $\text{Co}(\text{NO}_3)_2$  in  $[\text{P}_{6,6,6,14}][\text{DCA}]$ ), which acted as the chemoattractant source) was then placed at the destination. Once introduced into the system, the seeker droplet ( $10^{-2}$  M PADAP in  $[\text{P}_{6,6,6,14}][\text{Cl}]$ ) would autonomously seek out the signaller droplet and merge with it at its location. Upon merging the cargo of both droplets would react and a colour change was observed (**Figure 6.2**, **Figure 6.3** and **Figure C.1** and **Video 6.1**). This colour change was due to the formation of the Cu-PADAP complex or Co-PADAP complex, respectively. The absorbance spectra of the signalling and seeking droplets (**Figure 6.2B, C**) were recorded as detailed in the experimental section using a bespoke holder fabricated in-house (**Figure C.2**).

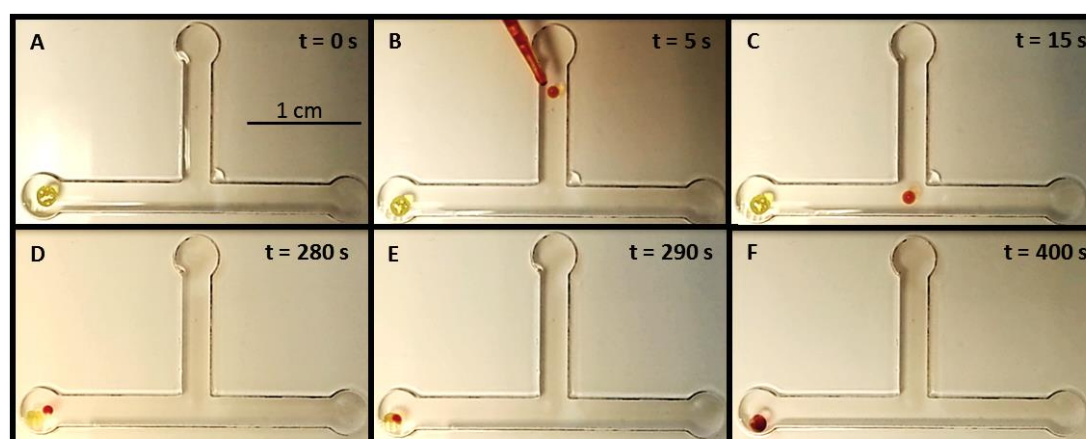


*Figure C.1 Sequence of snaps shots from video S1, which show an example of signalling and seeking droplets. A – depicts the preparation of the gradient, with the signalling droplet placed at the destination; B – The seeker droplet is introduced into the system; C – The seeker droplet migrates toward the signaller droplet; D – Seeker droplet arrived at the destination; E – Seeker droplet merged with signaller droplet; F – Colour change indicating the formation of  $\text{Cu}^{2+}$  – PADAP complex begins to occur.*

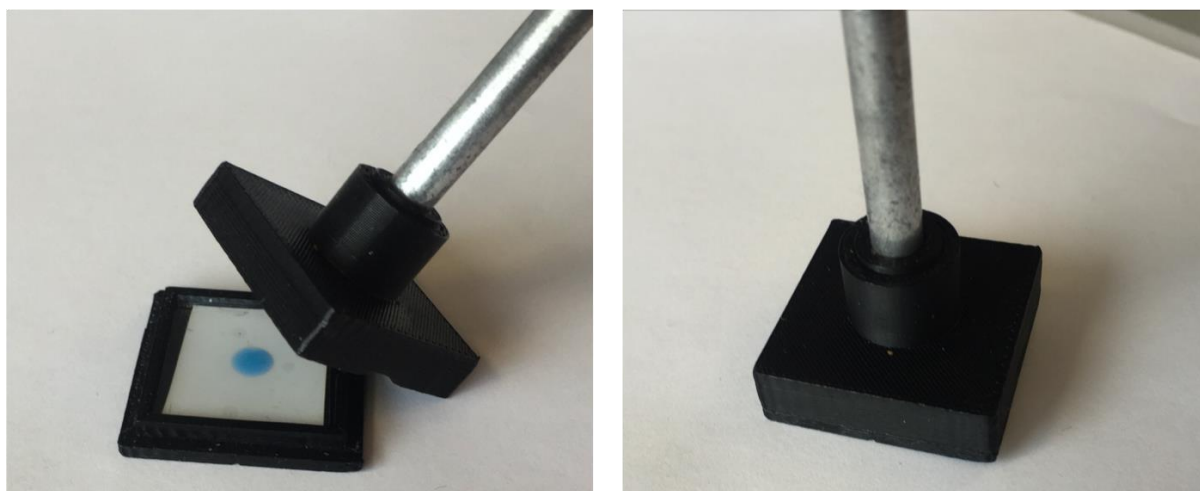


Figure C.2 Custom-made holder (left: open; right: closed) used for absorbance measurements of the droplets in this study.

## C.2 Decisions making droplets

### C.2.1 Finding the highest concentration of chemoattractant

For the demonstration of decision making, IL droplets made of  $[P_{6,6,6,14}][Cl]$  containing a small amount of 1-(methylamino)anthraquinone red dye added for visualisation were placed at the entrance of a T-shaped channel and were subjected simultaneously to two chemical gradients of different concentrations.

For this, the channel was initially filled with a solution of  $10^{-2}$  M NaOH and 50  $\mu$ l of HCl solutions (1 M,  $10^{-1}$  M or  $10^{-2}$  M, respectively) were added simultaneously at the two destinations (left and right arms of the T-shaped channel, Figure C.3). Following this, the droplet was placed into the channel (middle arm of the T shaped channel, Figure C.3). Upon reaching the T-junction, the IL droplet always travelled to the highest concentration of chemoattractant (**Figure C.3, Table C.1 and Video C.2**).

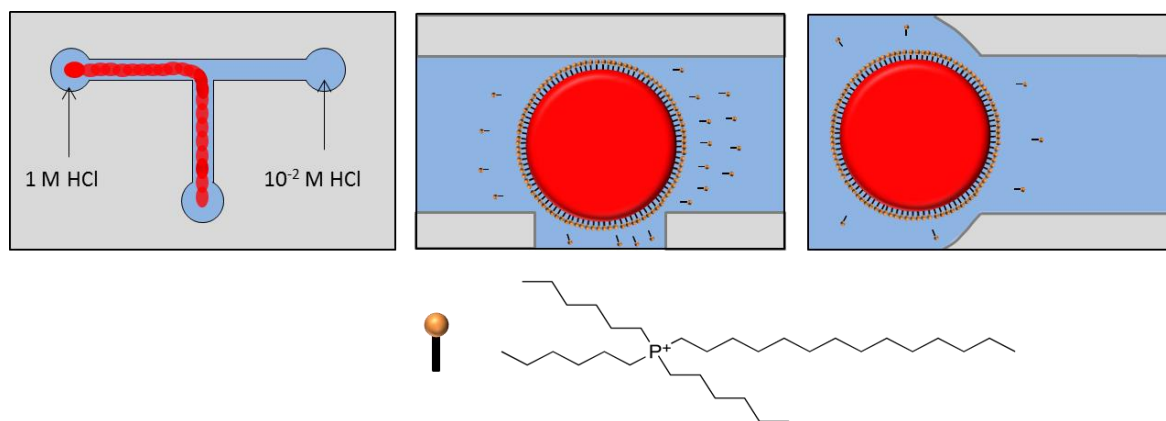


Figure C.3 Diagram showing a  $[P_{6,6,6,14}][Cl]$  droplet finding the highest concentration of HCl chemoattractant when subject simultaneously to two chemical gradients of different concentrations.

Table C.1 Table indicating HCl concentrations included in each test and final destination of the droplet in each case.

| Test No. /<br>Conc of HCl (mol L <sup>-1</sup> ) | 10 <sup>-2</sup> M | 10 <sup>-1</sup> M | 1 M |
|--|--------------------|--------------------|-----|
| 1  |                    | X                  |     |
| 2  |                    |                    | X   |
| 3  |                    |                    | X   |

\*Coloured cells indicate the concentrations used, X indicates the final destination of the droplet.

## C.2.2 Choosing between different halide salts

In order to determine the droplet's ability to choose between halide salts, the droplet was subjected simultaneously to two different chemoattractant gradients of equal concentration. The chemoattractants used were KF, KCl, KBr and KI solutions of different concentrations (1 M – 10<sup>-3</sup> M), see Table 1. For this test, a T-shaped channel was initially filled with a solution of 10<sup>-2</sup> M NaOH. At the opposite ends of the T-shaped channel, identical volumes (30 - 60 μl) of the chemoattractant solutions of identical concentration were added simultaneously. The  $[P_{6,6,6,14}][Cl]$  droplet was then placed into the central arm of the T-shaped channel from where it would migrate to the source of the preferred chemoattractant. (Table 6.1, Video 6.3).

### C.3 Cargo-Transport, Sensing and Reporting

In order to monitor the mass transfer of aqueous solution across the droplet/aqueous interface, a pH indicator dye was added to the  $[P_{6,6,6,14}][Cl]$  droplet (4% (w/v) phenol red or 4% (w/v) bromothymol blue, respectively). Initially the T-shaped channel was filled with a solution of  $10^{-2}$  M NaOH followed by the addition of 30 - 80  $\mu$ l (depending on the test) of either KI ( $1\text{ M} - 10^{-3}\text{ M}$ ) or KBr ( $1\text{ M} - 10^{-3}\text{ M}$ ) at the destination. The  $[P_{6,6,6,14}][Cl]$  droplet containing the pH indicator was added and would actively move towards the source of chemoattractant. Upon nearing or reaching the destination (depending on the halide used and its concentration) the droplet would begin to change color, indicating mass transfer of the aqueous solution (containing  $OH^-$  ions) across the droplet/aqueous interface, see **Figure C.4** and **Video 6.4**, **Video 6.5**, **Video 6.6** and **Video 6.7**.

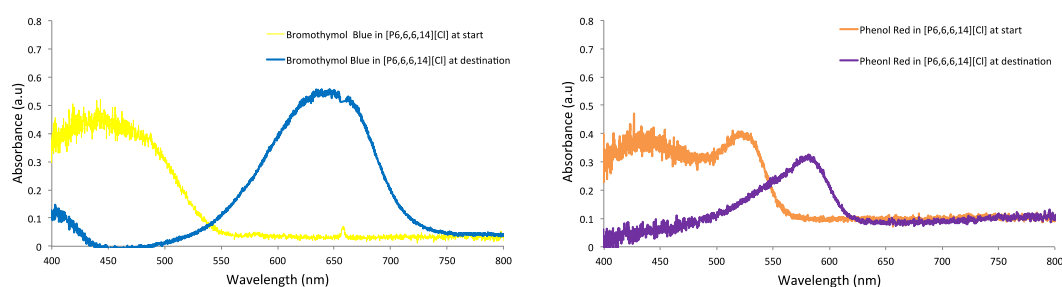


*Figure C.4 Absorbance spectra of  $[P_{6,6,6,14}][Cl]$  containing 4% (w/v) bromothymol blue (left) and 4% (w/v) phenol red (right), before and after being introduced in the channel containing  $10^{-2}$  M NaOH solution in the presence of 70  $\mu$ l of 0.005 M KBr. The spectra represents the colour of the  $[P_{6,6,6,14}][Cl]$  droplet containing the pH dye at the start and destination.*

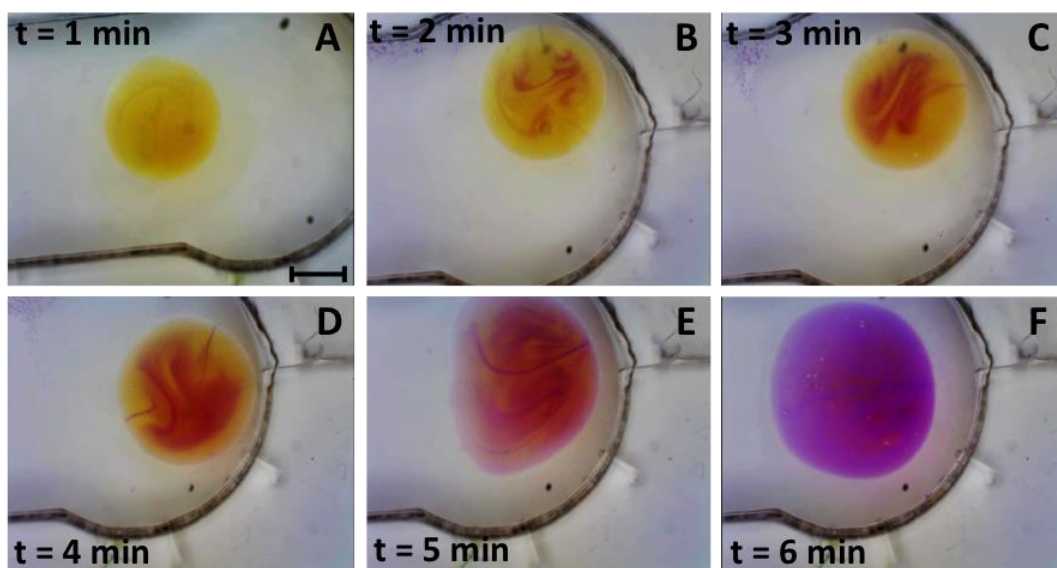


*Figure C.5 Selection of sequential snapshots from Video S7 showing the colour change of the phenol red containing  $[P_{6,6,6,14}][Cl]$  droplet upon reaching the source of KBr chemoattractant. The channels were filled with 0.01 M NaOH and 70  $\mu$ l of 0.005 M KBr solution was placed at the desired destination. Marangoni like flows can be clearly observed inside the droplet.*

In order to determine that such Marangoni like flows (**Figure C.5**) are only observed in the case when KBr, or KI solutions are used as chemoattractants, the dynamics of the colour change inside the  $[P_{6,6,6,14}][Cl]$  droplets containing the pH dyes (bromothymol blue and phenol red, respectively) were investigated in the presence and in the absence of chemoattractant (KBr). For this purpose, a phenol red containing  $[P_{6,6,6,14}][Cl]$  droplet was placed in a small circular container filled with  $10^{-2}$  M NaOH solution in the absence of any chemoattractant and the colour change was monitored over time (**Figure C.6**).

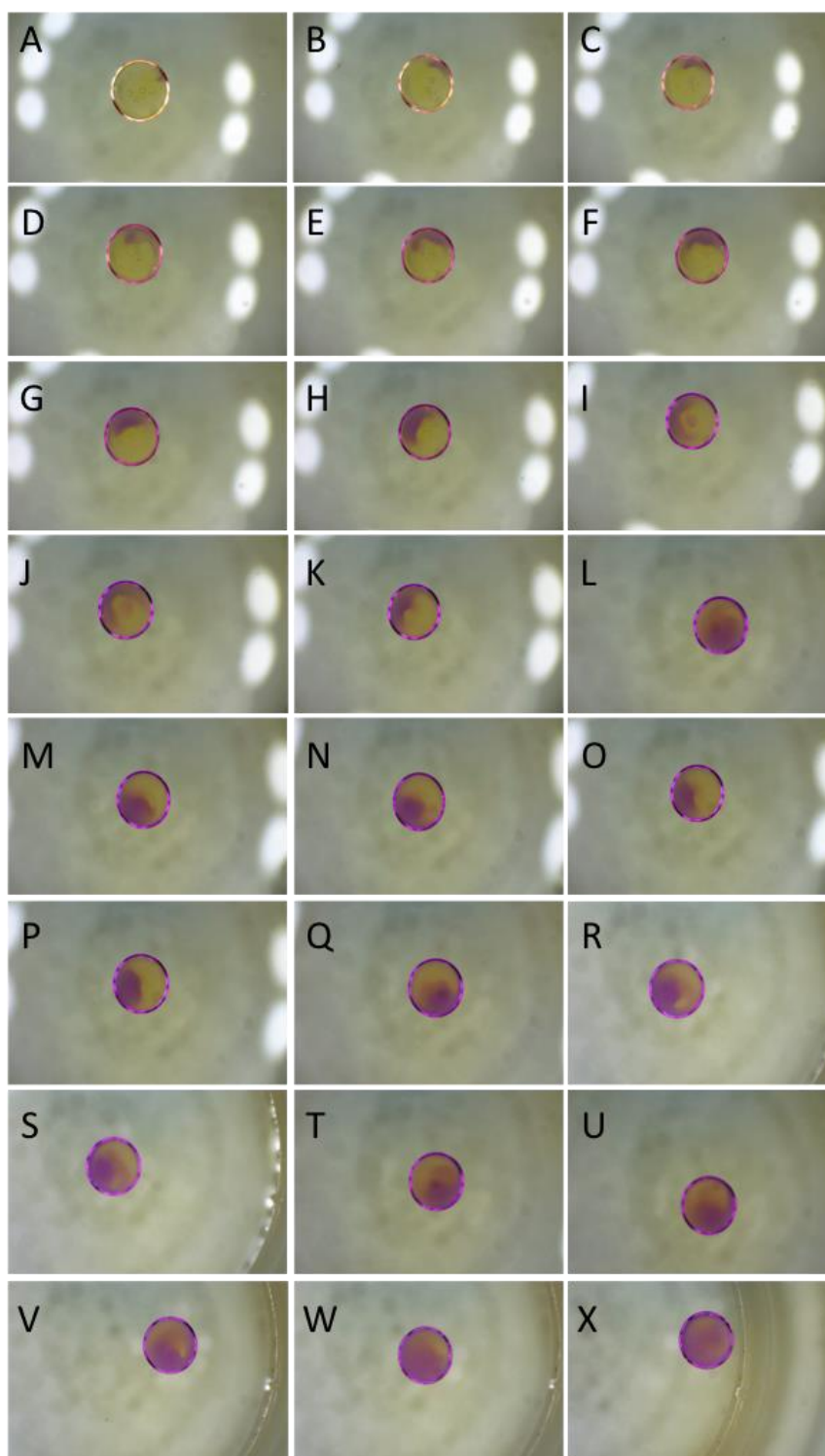
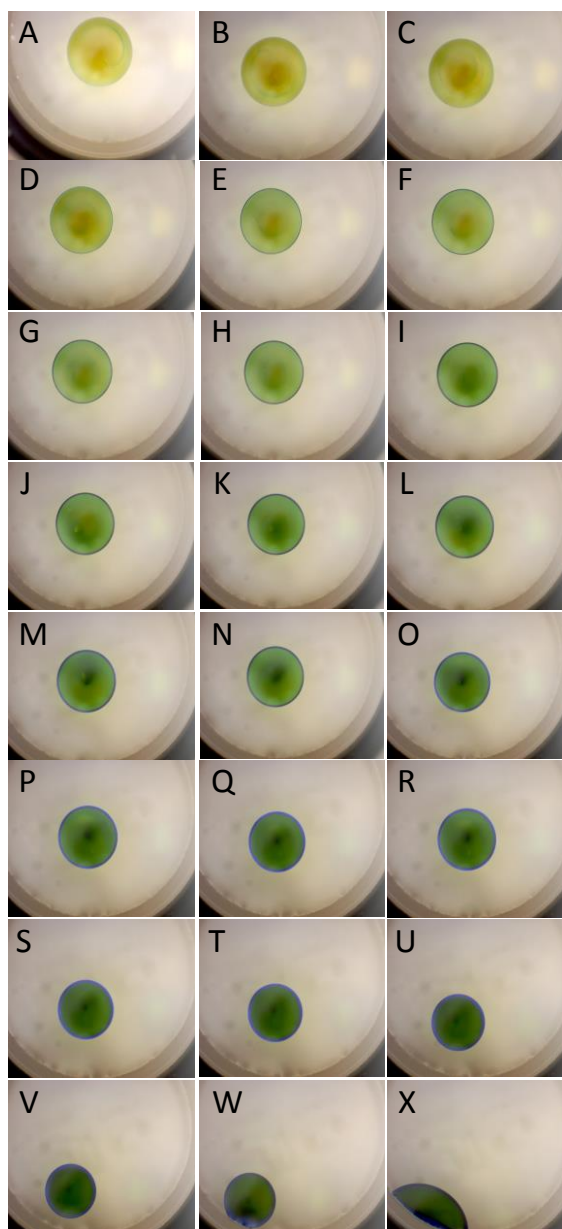
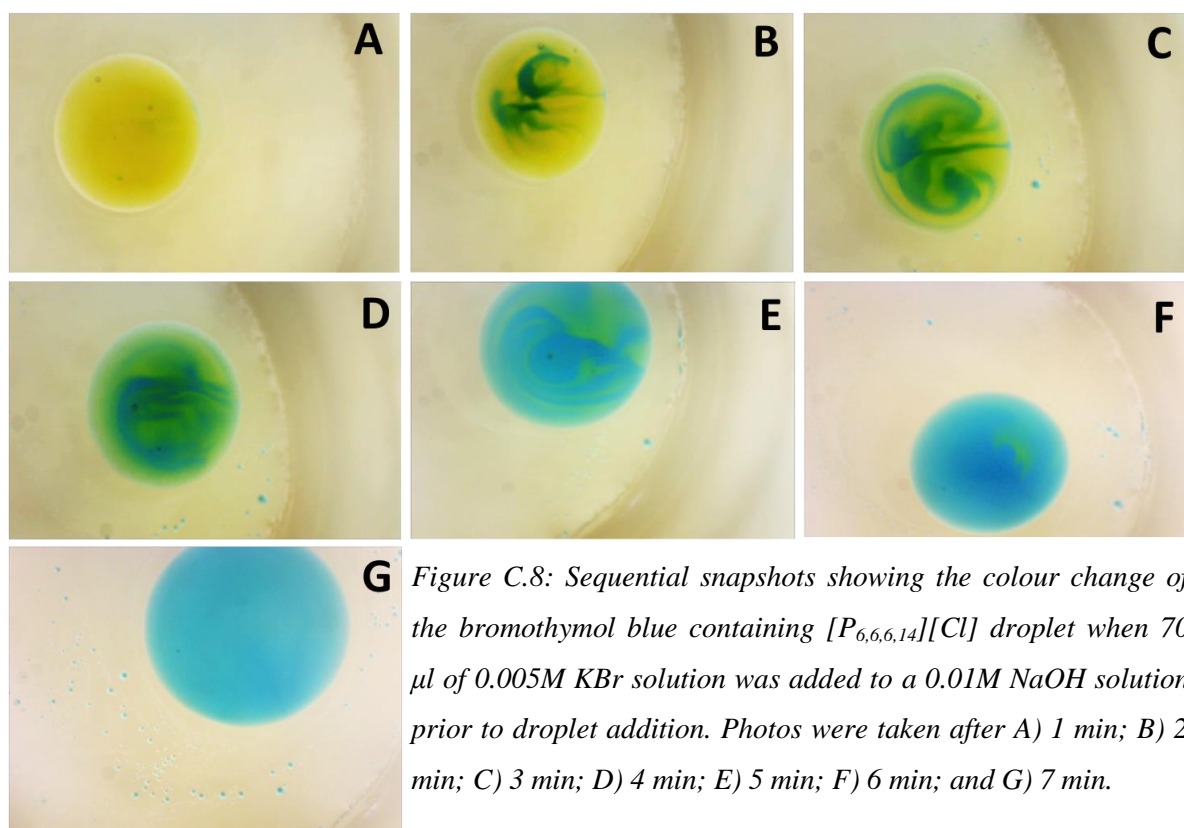


Figure C.6 Sequential snapshots showing the colour change of the phenol red containing  $[P_{6,6,6,14}][Cl]$  droplet when subject to 0.01 M NaOH solution in the absence of any chemoattractant. Photos were taken after A) 1 min; B) 2 min; C) 3 min; D) 4min; E) 5 min; F) 6 min; G) 7 min; H) 8 min; I) 9 min; J) 10 min; K) 11 min; L) 12 min; M) 13 min; N) 14 min; O) 15 min; P) 16 min; Q) 17 min; R) 18 min; S) 19 min; T) 20 min; U) 21min; V) 22 min; W) 23 min; and X) 24 min.

Similarly, a bromothymol blue containing  $[P_{6,6,6,14}][Cl]$  droplet was placed in a small circular container filled with  $10^{-2}$  M NaOH solution in the absence of any chemoattractant (**Figure C.7**) or when 70  $\mu$ l of 0.005M KBr solution was added prior to droplet addition (**Figure C.8**).



*Figure C.7 Sequential snapshots showing the colour change of the bromothymol blue containing  $[P_{6,6,6,14}][Cl]$  droplet when subjected to a 0.01 M NaOH solution in the absence of any chemoattractant. Photos were taken after A) 1 min; B) 2 min; C) 3 min; D) 4 min; E) 5 min; F) 6 min; G) 7 min; H) 8 min; I) 9 min; J) 10 min; K) 11 min; L) 12 min; M) 13 min; N) 14 min; O) 15 min; P) 16 min; Q) 17 min; R) 18 min; S) 19 min; T) 20 min; U) 21 min; V) 22 min; W) 23 min; and X) 24 min.*



It is clear that in the absence of additional chemoattractant, the colour of the droplet changes slowly due to diffusion of  $OH^-$  ions and no convectonal current or Marangoni flows are observed inside the droplet.

#### C.4 Damage Find and Repair

In order to chemotactically move the repairing droplet to the damage in the channel, a 60  $\mu$ l aliquot of the chemoattractant ( $10^{-2}$  M HCl solution which contained 1 % w/v sodium alginate and 50 % v/v 0.05 M KBr) was placed behind the damage in the channel. Once the IL droplet ( $[P_{6,6,6,14}][Cl]$  which contained 4 % w/v  $CaCl_2$ ) had been introduced in the T-shaped channel, it migrated towards the source. Upon reaching the damaged area, it attached to the walls of the channel and began to gelate, repairing the damage (**Figure C.8**, **Figure C.9** and **Figure C.10**, and **Video 6.8**).

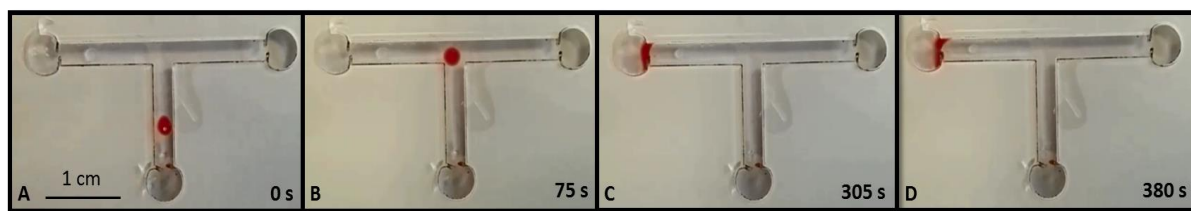


Figure C.9 Series of snapshots which demonstrate the IL droplet's ability to chemotactically find a damaged section of a channel and repair it. A – Depicts the introduction of the repairing droplet; B – Droplet migrating to source of damage; C – Droplet attaches itself to the walls of the channel; D – Droplet gels and forms a seal to repair the damage.

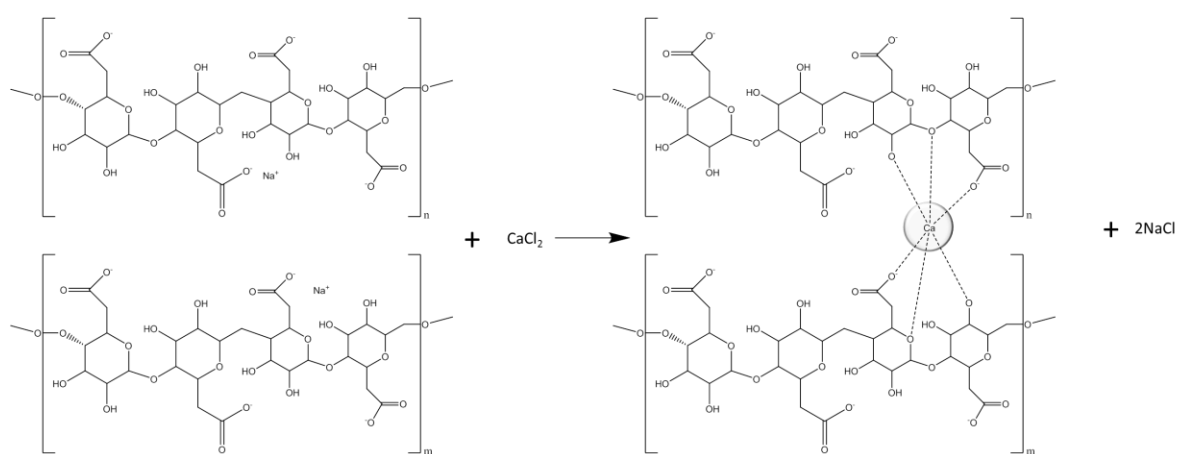


Figure C.10 Reaction scheme showing the crosslinking of sodium alginate chains by the  $\text{Ca}^{2+}$  ions.

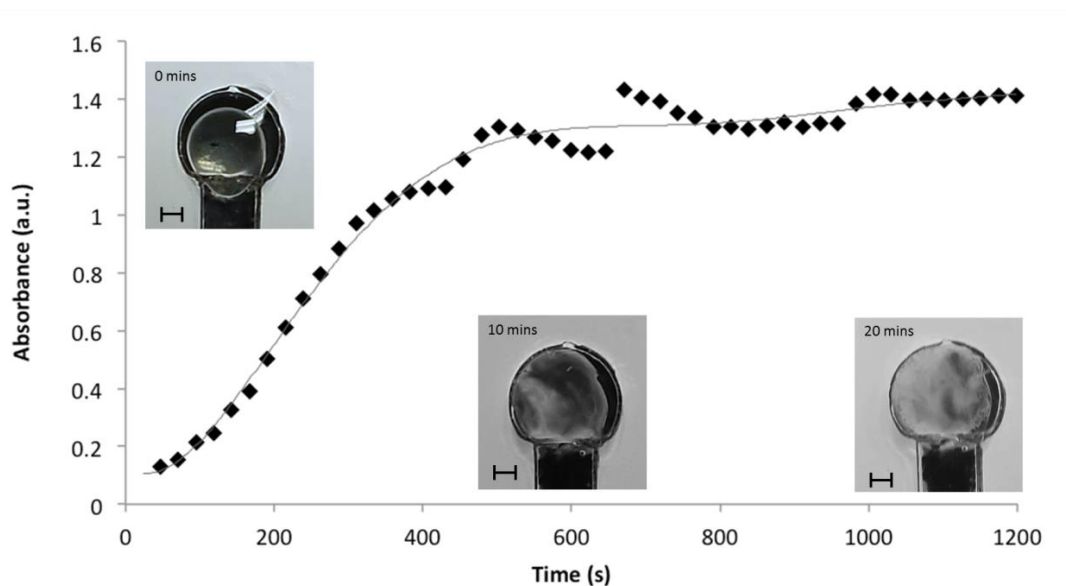


Figure C.11 Absorbance (at 700 nm) increase over time of the  $[P_{6,6,6,14}][Cl]$  droplet (containing 4 % w/v  $CaCl_2$ ) resting on a  $10^{-2}$  M NaOH solution after the addition of the chemoattractant (60  $\mu$ l aliquot of a  $10^{-2}$  M HCl solution which contained 1 % w/v sodium alginate and 50 % v/v 0.05 M KBr).

## C.5 Videos

**Video 6.1:** This video demonstrates the signaller ( $10^{-2}$  M  $Cu(NO_3)_2$ ) in  $[P_{6,6,6,14}][DCA]$  and seeking ( $10^{-2}$  M PADAP in  $[P_{6,6,6,14}][Cl]$ ) behaviour of the IL droplets used in this study. Initially the channels are filled with a solution of  $10^{-2}$  M NaOH, and the signaller droplet (which had a yellow colour) is then placed at the destination. After a few seconds ( $\sim 15$  s) the seeker droplet (which had an orange colour) is introduced into the system. The seeker droplet would then autonomously seek out and merge with the signaller droplet. Upon merging the contents of both droplets would react. This resulted in the droplet changing to a purple colour, indicating that the PADAP had complexed with the  $Cu^{2+}$  ions. For convenience the video has been sped up by a factor of 8.

**Video 6.2:** This video displays an IL droplet ( $[P_{6,6,6,14}][Cl]$  containing a small amount of 1-(methylamino)anthraquinone red dye) which is subjected simultaneously to two different concentrations of the same chemoattractant (HCl). In video S2 the channels were initially filled with a solution of  $10^{-2}$  M NaOH. At the left destination 30  $\mu$ l of a solution of 1 M HCl was added and at the right destination 30  $\mu$ l of a solution of  $10^{-2}$  M HCl was added. Once the droplet was added, this migrated towards the source of highest concentration (left). For convenience the video has been sped up by a factor of 8.

**Video 6.3:** This video shows an example of the  $[P_{6,6,6,14}][Cl]$  IL droplet (containing a small amount of 1-(methylamino)anthraquinone red dye) choosing between different halide salts. In this instance the channel were initially filled with a solution of  $10^{-2}$  M NaOH. At the left and right destinations, 30  $\mu$ l of  $10^{-1}$  M KF and KBr, respectively were added simultaneously. Once the droplet was introduced, it migrated towards the source of the KBr. For convenience the video has been sped up by a factor of 8.

**Video 6.4:** This video is an example of how the IL droplets in this study can be used to carry cargo, sense and report on the solution upon which they are travelling. In this case the channel was initially filled with a solution of  $10^{-2}$  M NaOH. At the destination 60  $\mu$ l of a solution of  $10^{-3}$  M KBr was added. The droplet ( $[P_{6,6,6,14}][Cl]$  containing 4 % (w/v) bromothymol blue) was then introduced to the fluidic network where upon it migrated to the source of the KBr and changed colour, which indicated the pH of the solution. For convenience the video has been sped up by a factor of 8.

**Video 6.5:** Similarly to Video S4, in this case the channel was initially filled with a solution of  $10^{-2}$  M NaOH. At the destination 60  $\mu$ l of a solution of  $10^{-2}$  M KBr was added. The droplet ( $[P_{6,6,6,14}][Cl]$  containing 4 % (w/v) phenol red) was then introduced to the fluidic network where upon it migrated to the source of the KBr and changed colour, which indicated the pH of the solution. For convenience the video has been sped up by a factor of 8.

**Video 6.6:** Similarly to Video S4 and Video S5, in this case the channel was initially filled with a solution of  $10^{-2}$  M NaOH. At the destination 60  $\mu$ l of a solution of  $10^{-1}$  M KBr was added. The droplet ( $[P_{6,6,6,14}][Cl]$  containing 4 % (w/v) phenol red) was then introduced to the fluidic network where upon it migrated to the source of the KBr and changed colour, which indicated the pH of the solution. For convenience the video has been sped up by a factor of 8.

**Video 6.7:** This video shows a close-up of the pH responsive droplets featured in Videos 6.4, 6.5 and 6.6. In this case the channel was initially filled with a solution of  $10^{-2}$  M NaOH. At the destination 70  $\mu$ l of a solution of  $5 \times 10^{-3}$  M KBr was added. The droplet ( $[P_{6,6,6,14}][Cl]$  containing 4 % (w/v) phenol red) was then introduced to the fluidic network where upon it migrated to the source of the KBr and changed colour, which indicated the pH of the solution.

**Video 6.8:** This video exhibits the IL droplet's ( $[P_{6,6,6,14}][Cl]$  which contained 4 % w/v  $CaCl_2$ ) ability to find and repair damage in a fluidic network. The channels in this example were initially filled with a solution of  $10^{-2}$  M NaOH. At the site of damage in the channel a 60  $\mu$ l aliquot of the chemoattractant ( $10^{-2}$  M HCl solution which contained 1 % w/v sodium alginate and 50 % v/v 0.05 M KBr) was added. Once the droplet was introduced it started to migrate towards the damage. Upon arrival it stuck to the walls and gelled. For convenience the video has been sped up by a factor of 8.

# Appendix D

---

## D.1 Figures

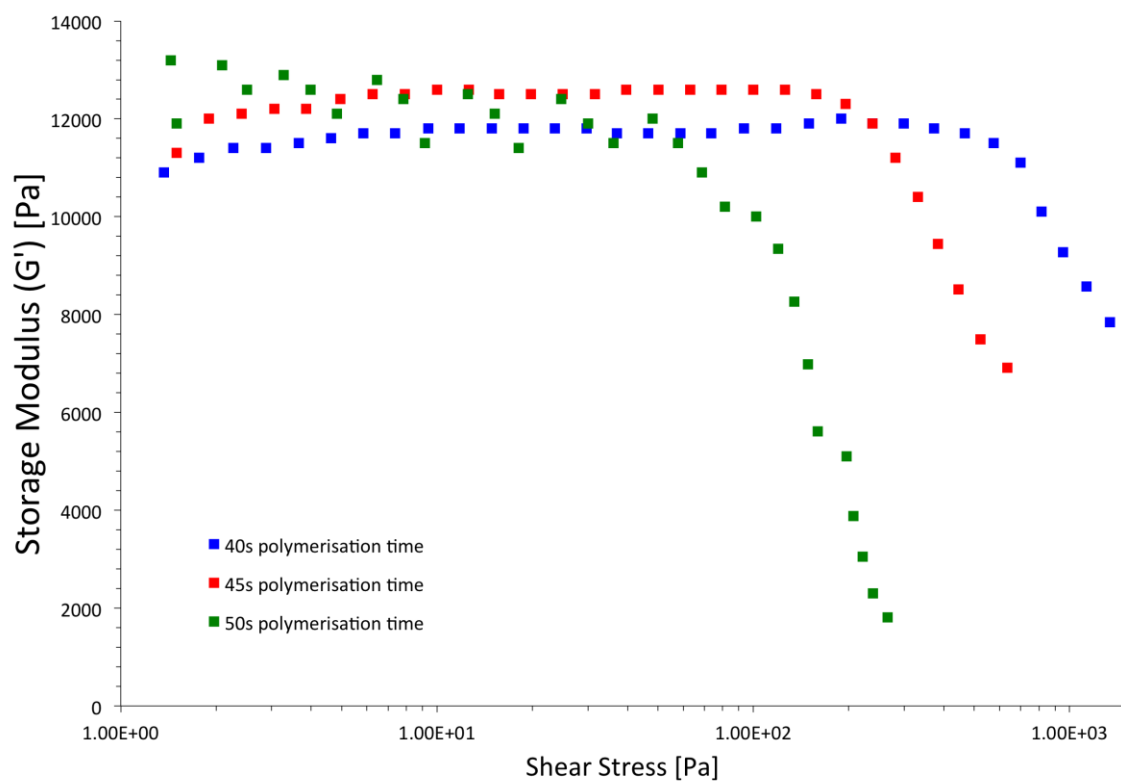


*Figure D.1 Storage moduli versus shear stress of the hydrated hydrogels polymerised during 40s, 45s and 50s of white light irradiation, respectively, using a strain amplitude sweep with a normal force of 1 N.*

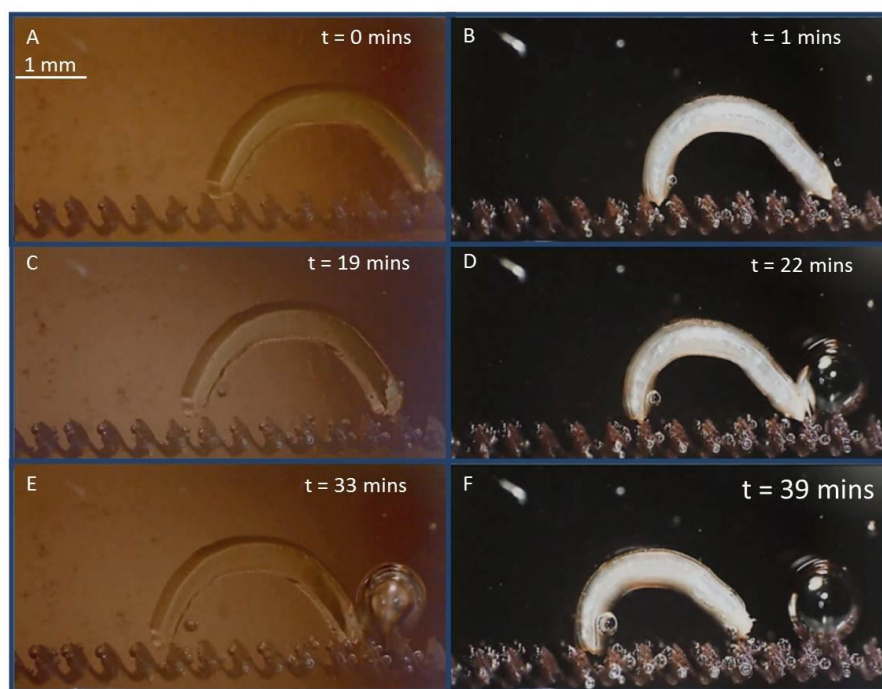


*Figure D.2 Series of snapshots showing the walking behaviour of the hydrogel (Video 7.2); A - shows the initial position of the hydrogel before any white irradiation; B, D and F show the contraction of the trailing leg during respective white light irradiation phases. C and E show how the swelling in the dark (after the respective white light irradiation phases) results in the forward leg being pushed over the ratchet.*

## **D.2 Videos**

[Video 7.1](#) demonstrates the observed locomotion of the p(NIPAAm-co-SP-co-AA) hydrogels. The ratcheted channels in this video are filled with deionised water. Once the hydrogel had been securely placed onto the ratchet, it was irradiated with white light ( $\sim 305$  kLux). After the trailing leg had been dragged across at least one of ratcheted steps, the light was removed. When the leading leg had been pushed over at least one of the ratchet steps the light was re-introduced. This was repeated until the walker moved out of frame, resulting in a walking motion across 5 ratchet steps. For convenience the speed of the video was increased by a factor of 64.

[Video 7.2](#) shows another example of the walking motion of a p(NIPAAm-*co*-SP-*co*-AA) hydrogel. The channel was again filled with DI water. Similarly to the above example, the walker was irradiated with white light ( $\sim 305$  kLux) until the trailing leg had been dragged across at least one of the walker steps. The white light was then removed and the walker was monitored in real time until the leading leg had been pushed across at least one of the ratchet steps. This was repeated until the walker got dislodged from the ratchet. The walker in this video completed three full cycles of white light irradiation and walked across 7 of the ratchet steps. For convenience the speed of the video was increased by a factor of 64.